



Bryce, Steven Alan (2014) *Regulation of the bioavailability of CCR7 ligands*. PhD thesis.

<http://theses.gla.ac.uk/5904/>

Copyright and moral rights for this work are retained by the author

A copy can be downloaded for personal non-commercial research or study, without prior permission or charge

This work cannot be reproduced or quoted extensively from without first obtaining permission in writing from the author

The content must not be changed in any way or sold commercially in any format or medium without the formal permission of the author

When referring to this work, full bibliographic details including the author, title, awarding institution and date of the thesis must be given

Enlighten:Theses  
<http://theses.gla.ac.uk/>  
theses@gl.a.ac.uk

# **Regulation of the Bioavailability of CCR7 Ligands**

**Steven Alan Bryce BSc.**



A thesis submitted to the College of Medicine, Veterinary and Life Sciences, University of Glasgow in fulfillment of the requirements for the degree of Doctor of Philosophy

September 2014

Institute of Infection, Immunity and Inflammation  
University of Glasgow  
120 University Place  
G12 8TA

# Contents

<b>DECLARATION</b>	<b>7</b>
<b>ACKNOWLEDGMENTS</b>	<b>8</b>
<b>ABSTRACT</b>	<b>11</b>
<b>LIST OF FIGURES</b>	<b>15</b>
<b>LIST OF TABLES</b>	<b>19</b>
<b>ABBREVIATIONS</b>	<b>20</b>
<b>1 INTRODUCTION</b>	<b>28</b>
1.1 GENERAL INTRODUCTION	28
1.2 LYMPH NODE STRUCTURE AND FUNCTION	32
1.3 THE CELLULAR ORCHESTRA OF THE LYMPH NODES	37
1.3.1 DCs	37
1.3.2 LYMPH NODE RESIDENT MACROPHAGES	41
1.4 MEDULLARY MACROPHAGES	43
1.5 INNATE-LIKE LYMPHOCYTES IN INTERFOLLICULAR REGIONS OF LYMPH NODES	45
1.5.1 $\gamma\delta$ T CELLS	45
1.5.2 INVARIANT NATURAL KILLER T (iNKT) CELLS	46
1.5.3 NK CELLS	47
1.6 LYMPH NODE DEVELOPMENT	48
1.7 ORGANISATION, STRUCTURE AND FUNCTION OF THE LYMPHATIC NETWORK	50
1.8 THE SPLEEN - STRUCTURE AND FUNCTION	54
1.9 THE SKIN	57
1.9.1 SKIN DCs	58
1.9.2 EPIDERMAL LANGERHANS CELLS	59
1.9.3 DERMAL DCs	61
1.9.4 SKIN RESIDENT T CELLS	62
1.10 CHEMOKINES	64
1.10.1 INFLAMMATORY AND HOMEOSTATIC CHEMOKINES	66
1.10.2 PROTEASE REGULATION OF CHEMOKINE FUNCTION	68

1.10.3	CHEMOKINE INTERACTIONS WITH GLYCOSAMINOGLYCANS (GAGs)	68
<b>1.11</b>	<b>CHEMOKINE RECEPTORS</b>	<b>70</b>
1.11.1	CHEMOKINE RECEPTOR/LIGAND INTERACTIONS AND SIGNALLING	72
<b>1.12</b>	<b>MECHANISMS OF CHEMOKINE-DRIVEN CELL MIGRATION</b>	<b>74</b>
<b>1.13</b>	<b>CCR7 AND CCR9: ARCHETYPICAL HOMEOSTATIC CHEMOKINE RECEPTORS.</b>	<b>79</b>
1.13.1	CCR7	79
1.13.2	CCR9	84
<b>1.14</b>	<b>THE ATYPICAL CHEMOKINE FAMILY</b>	<b>86</b>
1.14.1	D6	87
1.14.2	DUFFY ANTIGEN RECEPTOR FOR CHEMOKINES (DARC)	90
1.14.3	CXCR7	91
1.14.4	CCRL1	93
<b>1.15</b>	<b>AIMS</b>	<b>97</b>
<b>1.16</b>	<b>HYPOTHESES</b>	<b>98</b>
<b>2</b>	<b>MATERIALS AND METHODS</b>	<b>100</b>
<b>2.1</b>	<b>ANIMALS</b>	<b>100</b>
<b>2.2</b>	<b>GENOTYPING OF GENETICALLY-MODIFIED MICE</b>	<b>101</b>
<b>2.3</b>	<b>ANIMAL PROCEDURES</b>	<b>102</b>
2.3.1	INDUCTION OF SKIN INFLAMMATION	102
2.3.2	INJECTION OF CFA INTO THE EAR / FOOT PAD	102
2.3.3	PHOTO-CONVERSION OF KAEDE TRANSGENIC MICE	102
2.3.4	<i>IN VIVO</i> MACROPHAGE DEPLETION BY INJECTION OF CLODRONATED LIPOSOMES	103
2.3.5	ADOPTIVE TRANSFER OF SPLENOCYTES	104
<b>2.4</b>	<b>SAMPLE HANDLING AND PREPARATION</b>	<b>104</b>
2.4.1	ISOLATION OF LEUKOCYTES FROM LYMPHOID TISSUES	104
2.4.2	ISOLATION OF LEUKOCYTES FROM THE SKIN	105
2.4.3	SKIN CRAWL-OUT ASSAY	105
<b>2.5</b>	<b>SEPARATION OF LEUKOCYTES FROM HUMAN BUFFY COATS</b>	<b>106</b>
2.5.1	LEUKOCYTE ISOLATION FROM LYMPHOID TISSUES BY MACS BEAD SEPARATION	106
2.5.2	BIO-AVAILABLE CHEMOKINE QUANTIFICATION – PUNCH BIOPSIES	107
2.5.3	TISSUE EMBEDDING AND SECTIONING – FROZEN SECTIONS	107
<b>2.6</b>	<b>IMMUNOFLUORESCENCE STAINING – FROZEN SECTIONS</b>	<b>108</b>
<b>2.7</b>	<b>IMAGE J ANALYSIS OF LYMPH NODES</b>	<b>109</b>

2.7.1	STAINING OF CELLS FOR INJECTION INTO MICE	111
2.7.2	PREPARATION OF HOMOGENATES FOR ELISA / WESTERN BLOT ANALYSIS	111
2.7.3	QUANTIFICATION OF CHEMOKINE CONCENTRATIONS BY ELISA	111
<b>2.8</b>	<b>MOLECULAR METHODS</b>	<b>112</b>
2.8.1	ISOLATION OF RNA	112
<b>2.9</b>	<b>COMPLEMENTARY DNA (CDNA) SYNTHESIS</b>	<b>113</b>
<b>2.10</b>	<b>TAQMAN QRT-PCR</b>	<b>113</b>
<b>2.11</b>	<b>SDS-PAGE AND WESTERN BLOT ANALYSIS</b>	<b>114</b>
<b>2.12</b>	<b>GENERATION OF LEUKOCYTES FROM BONE MARROW</b>	<b>115</b>
2.12.1	GENERATION OF DCs USING GM-CSF	115
2.12.2	GENERATION OF DCs USING FLT3L	116
2.12.3	ACTIVATION OF DENDRITIC CELLS <i>IN VITRO</i>	116
2.12.4	GENERATION OF MACROPHAGES	116
<b>2.13</b>	<b>CHEMOKINE CLEAVAGE ASSAY</b>	<b>117</b>
2.13.1	STAINING OF LEUKOCYTES FOR FLOW CYTOMETRY ANALYSIS	117
2.13.2	INTRACELLULAR FLOW CYTOMETRY ANTIBODY STAINING	118
<b>2.14</b>	<b>FLUORESCENT CCL19 CHEMOKINE</b>	<b>122</b>
<b>2.15</b>	<b>CHEMOKINE UPTAKE ASSAY</b>	<b>122</b>
2.15.1	FLOW CYTOMETRY ANALYSIS	123
2.15.2	FLOW CYTOMETRY GATING STRATEGIES	123
<b>2.16</b>	<b>STATISTICAL ANALYSES.</b>	<b>125</b>
<b>3</b>	<b><u>THE ROLE OF CCRL1 IN COORDINATING DC MIGRATION</u></b>	<b>127</b>
<b>3.1</b>	<b>INTRODUCTION</b>	<b>127</b>
<b>3.2</b>	<b>WT AND CCRL1-DEFICIENT LYMPH NODE DC NUMBERS AT REST</b>	<b>127</b>
<b>3.3</b>	<b>DC MIGRATION IN RESPONSE TO CUTANEOUS APPLICATION OF FITC</b>	<b>129</b>
<b>3.4</b>	<b>DC ACCUMULATION IN SKIN-DRAINING LYMPH NODES AFTER SKIN INFLAMMATION</b>	<b>129</b>
<b>3.5</b>	<b>IS ARRIVAL OF DCs IN LYMPH NODES DELAYED IN CCRL1-DEFICIENT MICE?</b>	<b>133</b>
<b>3.6</b>	<b>DC MIGRATION USING KAEDE TRANSGENIC MICE</b>	<b>134</b>
<b>3.7</b>	<b>CCL19 RECEPTOR EXPRESSION ON LYMPH NODE CELLS DURING TPA AND FITC</b>	<b>135</b>
<b>3.8</b>	<b>DC MIGRATION DURING TPA AND FITC IS LARGELY DRIVEN BY CCR7</b>	<b>137</b>
<b>3.9</b>	<b>CFA-INDUCED SKIN INFLAMMATION</b>	<b>138</b>
<b>3.10</b>	<b>DCs IN RESTING SKIN</b>	<b>140</b>
<b>3.11</b>	<b>DC NUMBERS IN INFLAMED SKIN</b>	<b>141</b>

3.12	DC MIGRATION FROM THE SKIN – <i>EX VIVO</i> ANALYSIS	141
3.13	DYSREGULATION OF CCL19 AND CCL21 IN CCRL1-DEFICIENT SKIN.	142
3.14	CCL19 DELETION RESCUES DEFECTS IN DC MIGRATION IN CCRL1-DEFICIENT MICE.	144
3.15	EXPRESSION OF CCRL1 IN RESTING INGUINAL LYMPH NODES	145
3.16	CCRL1 EXPRESSION IN THE DORSAL SKIN AND EAR	147
3.17	SUMMARY	148
4	<u>CCRL1 AND CD169<sup>+</sup> MACROPHAGES AT THE SCS REGION OF THE LYMPH NODE</u>	179
<hr/>		
4.1	INTRODUCTION	179
4.2	THE LOCALISATION OF CD169 MACROPHAGES IN WT INGUINAL LYMPH NODES	179
4.3	CCRL1 IS EXPRESSED ADJACENT TO CD169 <sup>+</sup> MACROPHAGES	180
4.4	CD169 <sup>+</sup> MACROPHAGES EXPRESS CCL19 RECEPTORS, PROBABLY CCR7	180
4.5	CD169 <sup>+</sup> MACROPHAGE DISTRIBUTION AND NUMBER IN INGUINAL LYMPH NODES IS UNAFFECTED BY CCRL1 DEFICIENCY	181
4.6	EXPANSION OF CD169 <sup>+</sup> MACROPHAGES AND LYVE-1 <sup>+</sup> CELLS IN MESENTERIC LYMPH NODES OF CCRL1-DEFICIENT MICE	182
4.7	CCL19 RECEPTOR EXPRESSION ON CD169 <sup>+</sup> MACROPHAGES REVISITED	183
4.8	CHARACTERISATION OF NK, iNKT AND $\gamma\delta$ T CELLS IN MESENTERIC LYMPH NODES	185
4.9	CHARACTERISATION OF NK, iNKT AND $\gamma\delta$ T CELLS IN THE INGUINAL LYMPH NODE	186
4.10	CCRL1 EXPRESSION AND FUNCTION IN THE RESTING SPLEEN	187
4.11	THE ROLE OF CD169 <sup>+</sup> MACROPHAGES IN REGULATING LYMPHANGIOGENIC RESPONSES IN LYMPH NODES	190
4.11.1	CD169 MACROPHAGES CAN BE DEPLETED IN THE POPLITEAL LYMPH NODE BY ADMINISTRATION OF CLODRONATED LIPOSOMES INTO THE FOOTPAD	191
4.12	CD169 MACROPHAGES ARE REQUIRED FOR LYMPHATIC VESSEL EXPANSION DURING CFA-INDUCED INFLAMMATION IN THE LYMPH NODE.	192
4.13	SUMMARY	193
5	<u>LEUKOCYTE-MEDIATED C-TERMINAL TRUNCATION OF CHEMOKINES</u>	221
<hr/>		
5.1	INTRODUCTION	221
5.2	TRUNCATION OF FULL LENGTH CCL21 CHEMOKINE BY DCs <i>IN VITRO</i>	222

<b>5.3</b>	<b>CHEMOKINE TRUNCATION - NON-ACTIVATED VS. ACTIVATED DCs</b>	<b>223</b>
<b>5.4</b>	<b>CHEMOKINE TRUNCATION - GMCSF VS. FLT3-L MATURED BMDCs</b>	<b>223</b>
<b>5.5</b>	<b>CCL21 TRUNCATION BY HUMAN DCs</b>	<b>224</b>
<b>5.6</b>	<b>LEUKOCYTE-MEDIATED CHEMOKINE PROCESSING</b>	<b>225</b>
<b>5.7</b>	<b>CCL21 TRUNCATION BY LYMPH NODE CELLS</b>	<b>226</b>
<b>5.8</b>	<b>CCL21 TRUNCATION <i>IN VIVO</i></b>	<b>226</b>
<b>5.9</b>	<b>CCL21 TRUNCATION <i>IN VIVO</i> AFTER THE INDUCTION OF INFLAMMATION</b>	<b>227</b>
<b>5.10</b>	<b>TRUNCATION OF CCL21 CANNOT BE MEDIATED BY DC-CONDITIONED MEDIUM OR COMPETED BY CCL19</b>	<b>228</b>
<b>5.11</b>	<b>TRUNCATION OF OTHER CHEMOKINES WITH EXTENDED C-TERMINAL DOMAINS</b>	<b>228</b>
<b>5.12</b>	<b>SUMMARY</b>	<b>231</b>
<b>6</b>	<b><u>DISCUSSION</u></b>	<b><u>244</u></b>
<b>6.1</b>	<b>BASAL DC TRAFFICKING IN CCRL1-DEFICIENT MICE</b>	<b>245</b>
<b>6.2</b>	<b>THE ROLE OF CCRL1 IN REGULATING DC TRAFFICKING DURING INFLAMMATION</b>	<b>247</b>
<b>6.3</b>	<b>THE ROLE OF CCRL1 AT THE SCS</b>	<b>256</b>
<b>6.3.1</b>	<b>CD169<sup>+</sup> SCS MACROPHAGES</b>	<b>256</b>
<b>6.4</b>	<b>INNATE-LIKE LYMPHOCYTES</b>	<b>260</b>
<b>6.5</b>	<b>THE SPLEEN</b>	<b>261</b>
<b>6.6</b>	<b>MACROPHAGE DRIVEN LYMPHANGIOGENESIS</b>	<b>261</b>
<b>6.7</b>	<b>CHEMOKINE TRUNCATION BY DCs</b>	<b>262</b>
<b>6.8</b>	<b>LEUKOCYTE-MEDIATED CHEMOKINE TRUNCATION</b>	<b>264</b>
<b>6.9</b>	<b><i>IN VIVO</i> TRUNCATION</b>	<b>265</b>
<b>6.10</b>	<b>FUTURE DIRECTIONS</b>	<b>266</b>
<b>7</b>	<b><u>APPENDIX</u></b>	<b><u>269</u></b>

## **Declaration**

I hereby declare that this thesis is the result of my own work and has not been submitted in whole or in part elsewhere for any award. Any assistance and contribution by others to this work is duly acknowledged within the text.

---

Steven Alan Bryce, BSc.

## Acknowledgments

First, I would like to thank my supervisor Professor Rob Nibbs for allowing me to work in his lab. Rob has been instrumental in the successful completion of this thesis, even though he probably wondered if I would ever finish writing (I enjoyed it too much). Rob has provided great ideas and suggestions that have made this project the success that it is, and his extensive knowledge of the chemokine field and immunology as a whole has been invaluable. They say that a successful PhD depends a lot on the supervisor, and I can definitely say that Rob is an excellent supervisor. He gave me a break when most people wouldn't, and for that I am thankful. However, no one told me that he sometimes, particularly when caffeine or nicotine deprived, he behaves like a stropky adolescent boy. However, I am glad, as this made the time in the lab more fun...most of the time. I would also like to thank my other supervisor, Professor Gerry Graham for his input into the project, for his support over the years and for allowing me to work within the CRG. Both Rob and Gerry were supportive of my trip to Boston, and my other scientific endeavors (conference in Hawaii) and so I thank them both for these life-changing experiences. I must also thank Professor Andy Luster and Dr Shannon Bromley, both of whom made my time at MGH enjoyable and productive.

To past and present lab members. I would like to thank Elinor Anderson, AKA Smellinor, Elinor Rigby, Elinor Roosevelt, Eliespot...the list goes on. Ellie took me under her wing and was (unfortunately for her) my go-to person for everything relating to flow cytometry. On many an evening Elinor would come into work at midnight to find me almost crying/wrestling with the MACSQuant either because it was blocked or, on one night, when I dropped my samples. I know I have met a true friend for life and I wish you hadn't run away to Italy (without your ciao bella bag). But, when I lost Elinor, I gained Trish, who was as equally as fun to have around the lab. Trish and I, by all accounts, definitely come as a package. Since her arrival in Glasgow we have shared many laughs, upsets, some fall-outs and tears but through it all we are true friends for life. I cannot say enough nice things about Trish, but I will say one thing, POTATO. Ok, ...one more thing...RAGAAAAAN. Again, without Trish, this thesis

wouldn't be what it is today, and I'm sure she will agree that she may know my project more than I do as I talk about it, A LOT. My thanks extend to other members of the group, Chris Hansell (Rafikki- the wise monkey), Darren (Dazbo), Laura, Mairi Clarke (My lab mum), Catherine and Ross. I'm sure you all, at some point, have suffered me enthusiastically talking about my project but your knowledge and expertise have helped me enormously over the years. I would also like to thank my friends from the "other" chemokine group, namely Allison, Kenny and Kay, thanks for making work a fun place, even though my thesis-induced mood swings didn't always show off my fun side! To my office buddies over the years, Helen, Fabian, Carolyn and Laura, thank you for keeping me topped up in caffeine and for the laughs.

I would also like to thank my friends outside of work for keeping me sane and understanding the nature of big FACS experiments, whereby 7 pm probably means closer to 10 pm. Particularly, I would like to thank Scott, Bobby, Mark, Darren, Clare, Ashleigh, Katie and Derek. We have had many good times over the years, some of you even got married, and I look forward to many more good times, particularly in the pub after my VIVA. A special thanks goes to Derek, who was there from the beginning as my senior honors lab partner, and who has been a great support, particularly over the past year. I also want to thank Lisa, who sadly left me to live in sunny Valencia, you are one of my oldest friends and I can't wait to visit as a Dr! Finally, I would like to thank everyone in my life whoever inspired me to be hard working, dedicated and who have shown belief in me. This includes my primary and secondary teachers, particularly my standard grade biology teacher who was a fantastic woman. However, like Rob, she was very emotional, maybe I am the common denominator. I would also like to thank my family and extended family. My mum and dad have given me an excellent work ethos and have strived to give me the best start in life. They have been supportive in everything (most things) I do and for that I am forever thankful. I'm sure they will be the proudest parents on graduation day when they realise that all the time, money and effort they invested in me paid off, and that I achieved something that they probably felt was out of they're reach growing up. I would also like to thank my sister, who has been supportive to me growing up, and more recently. She has been gifted with two amazing children who I love

very much and look forward to seeing grow up and one day graduate themselves. I would like to thank my aunt Arlene and uncle Gary, who are like a second set of parents to me, I'm sure you'll both be proud of what I have achieved. Finally, I want to dedicate this thesis to a man, who sadly, passed away before he could see me complete this thesis. That man was my papa, who I miss every day and wish could watch me graduate. Generally, people declare the Love they have for their partner at this point, however, to break with tradition, to everyone I mentioned, I.LOVE.YOU!

## Abstract

The efficient functioning of the immune system is dependent on the coordinated movement and positioning of immune cells. These cells patrol the body and facilitate the clearance of pathogens, whilst maintaining self-tolerance and inducing adaptive immunity. The coordinated migration of cells into and within tissues is mediated by chemokines, a family of small chemotactic cytokines that are potent inducers of cellular movement. Chemokines and their cognate receptors have been shown to play key roles in health, and in a broad spectrum of diseases.

After their secretion, chemokines can be controlled by proteases and interactions with atypical chemokine receptors that structurally resemble conventional chemokine receptors but cannot couple to the signaling pathways that they use. Instead, they are thought to degrade, transport or buffer extracellular chemokines to regulate their access to cells bearing conventional chemokine receptors. However, their functions *in vivo* remain to be fully defined. CCRL1, a member of the atypical chemokine receptor family, binds to CCL19, CCL21 and CCL25 and is proposed to be a scavenger of these chemokines. Post-translational regulation of these chemokines is important because their interactions with cognate, conventional receptors CCR7 and CCR9, are critical for the development and functioning of the immune system. The work in this thesis primarily explores the importance of CCRL1 in regulating CCR7 ligands, but also considers the impact of protease-mediated ‘clipping’ on the function of CCL21 and other extended chemokines.

Whilst *in vitro* evidence, and a growing body of *in vivo* evidence, supports the idea that CCRL1 serves an important role in the chemokine control, the true biological function of CCRL1 remains unclear. Therefore, the principal aim of this thesis was to further our understanding of the biology of CCRL1, mainly through the characterisation of CCRL1-deficient mice. Firstly, the effect of CCRL1 deletion on dendritic cell (DC) migration from the skin was investigated. Four distinct subsets of migratory DCs were examined in skin-draining lymph nodes at steady state and after induction of cutaneous inflammation. Under

inflammatory conditions, skin-derived DCs were identified by FITC painting or by photoconverting the skin of Kaede transgenic mice. CCRL1 deficiency was found to result in a specific reduction in the abundance of Langerin<sup>+</sup> skin-derived DCs in inguinal lymph nodes at rest, and although the initial inflammation-driven arrival of DCs at skin-draining lymph nodes showed no requirement for CCRL1, DCs that took longer to reach these organs were substantially reduced in CCRL1-deficient mice. All DC subsets were affected, but overall it was epidermal Langerhans cells that showed the greatest requirement for CCRL1. Defective DC arrival at lymph nodes was accompanied by DC retention in resting and inflamed skin, and these cells struggled to leave CCRL1 deficient skin in *ex vivo* ‘crawl out’ assays. Further experiments demonstrated that, as expected, DC arrival at lymph nodes draining inflamed skin was heavily dependent on CCR7 in the models being used, and that increased levels of bioavailable CCL19 and CCL21 accompanied CCRL1 deficiency in inflamed skin. This suggested CCRL1 regulates chemokine to prevent DCs from becoming disorientated in the skin and failing to efficiently egress this tissue. I hypothesised that dysregulation of CCL19 rather than CCL21 may be particularly significant because of its greater diffusivity, and strikingly, inflammation-driven DC migration defects observed in CCRL1 deficient mice were completely reversed by genetic deletion of CCL19 in the same animals.

To place these findings in an anatomical context, expression of CCRL1 in skin and lymph node was explored using CCRL1<sup>+gfp</sup> ‘knock-in’ receptor mice and anti-CCRL1 antibodies. In skin, CCRL1 was abundantly expressed by keratinocytes, and found on lymphatic endothelial cells (LECs) that are traversed by migrating DC as they leave the skin. In lymph nodes draining the skin, LECs in the supcapsular sinus (SCS) were strongly CCRL1<sup>+</sup>. Although some leukocytes were found to express very low levels of eGFP in CCRL1<sup>+gfp</sup>, the data suggested that CCRL1-mediated scavenging of CCL19 by keratinocytes and LECs facilitates CCR7-driven DC migration from resting and inflamed skin.

CCRL1 expression in other secondary lymphoid tissues was examined and its role in regulating leukocyte populations residing in or around the SCS was explored. As in the inguinal lymph node, CCRL1 was restricted to the SCS LECs in other lymph nodes, such as the mesenteric lymph nodes that drains the

intestine. In the spleen, endothelial cells lining venules adjacent to the white pulp marginal zone specifically expressed CCRL1. The overall cellularity and microanatomy of lymph nodes and the spleen appeared normal in CCRL1-deficient mice, as was the recruitment of CCR7<sup>+</sup> cells into the spleen two hours after adoptive transfer. However, NK cells, iNKT cells and  $\gamma\delta$  T cells, which are thought to reside in intrafollicular regions, were less abundant in CCRL1-deficient inguinal and mesenteric lymph nodes, although they were present at normal frequency in the spleen. CD169<sup>+</sup> macrophages are intimately associated with CCRL1<sup>+</sup> endothelial cells in the spleen. CCRL1 deficiency had no clear impact on these cells in the inguinal lymph nodes, and only resulted in a small increase in the abundance of these cells in the spleen, without obviously affecting their position. Strikingly, however, in mesenteric lymph nodes, CD169<sup>+</sup> macrophages, and LECs with which they associate, were far more abundant when CCRL1 had been deleted and were aberrantly distributed throughout the lymph node parenchyma. The reason this phenotype is restricted to the mesenteric lymph node is unclear, but it might be related to the fact the intestine, unlike other non-lymphoid tissues, is an abundant source of CCL25. This, along with the immunological implications of these observations, requires further investigation.

There is a lot of evidence that macrophages regulate lymphangiogenesis. The close association between LECs and CD169<sup>+</sup> macrophages in lymph nodes, and the phenotype in CCRL1-deficient mesenteric lymph nodes, stimulated experiments to explore functional interactions between these cells. Inflammation in the footpad induced lymphangiogenesis in draining popliteal and inguinal lymph nodes. When clodronated liposomes were used to specifically deplete macrophages from the popliteal lymph node of WT mice, lymphangiogenesis appeared suppressed while it continued unabated in the inguinal lymph node where the CD169<sup>+</sup> macrophage population was intact. WT and CCRL1-deficient mice responded similarly, and although preliminary, these data suggest that CD169<sup>+</sup> macrophages play an important role in stimulating lymph node lymphangiogenesis.

In addition to the CCRL1 studies above, other mechanisms that might regulate chemokines after their secretion were explored. Work published at the beginning

of my PhD showed that CCL21, which carries an extended C-terminus that anchors it to the extracellular matrix, can be cleaved by bone marrow-derived DCs (BMDCs) to release a more freely diffusible version. These findings were reproduced here using *in vitro*-derived human or mouse DCs. DCs were far better at cleaving CCL21 than other leukocytes, and they could also cleave CCL2, a pro-inflammatory chemokine with an extended C-terminus. Interestingly, a truncated version of CCL21 was detected in mouse secondary lymphoid tissues. It was larger than the version generated by BMDCs *in vitro*, and the nature of its truncation is not clear, but this shows that CCL21 processing occurs *in vivo*. If this form of CCL21 is more diffusible than the full-length protein, then it might be more available for regulation by CCRL1. However, neither forms of CCL21 were more abundant in CCRL1-deficient secondary lymphoid tissues than equivalent tissues from WT mice.

CCR7 plays a critical role in directing DC egress from tissues, their entry into lymph nodes, and their movement within these tissues. The work presented in this thesis provides evidence of two mechanisms that regulate CCR7 ligands: CCRL1-mediated CCL19 scavenging and DC-mediated CCL21 cleavage. It reveals that, under certain circumstances, CCRL1 is critical for facilitating DC egress from peripheral tissues to the lymph nodes, and plays an indispensable role in regulating LECs and CD169<sup>+</sup> macrophages in lymph nodes. These studies extend our understanding of CCRL1 and the chemokine networks at work in lymph nodes and other tissues, and form the foundation on which to explore the immunological importance of the regulation of extracellular chemokines.

## List of Figures

FIGURE 1.1: THE STRUCTURE OF THE LYMPH NODE.....	33
FIGURE 1.2: THE SCS REGION OF THE LYMPH NODE.....	42
FIGURE 1.3 SCHEMATIC OF LYMPH NODE DEVELOPMENT. ....	49
FIGURE 1.4: POSSIBLE METHODS OF LYMPHATIC VESSEL EXPANSION DURING INFLAMMATION. ....	53
FIGURE 1.5: THE STRUCTURE OF THE SPLEEN.....	55
FIGURE 1.6: THE STRUCTURE AND DC COMPOSITION OF THE SKIN. ....	59
FIGURE 1.7: THE HUMAN CHEMOKINE NETWORK.....	65
FIGURE 1.8: HOMEOSTATIC, INFLAMMATORY AND ‘DUAL FUNCTION’ CHEMOKINES.....	67
FIGURE 1.9: SCHEMATIC OF A CHEMOKINE RECEPTOR.....	70
FIGURE 1.10: CHEMOKINE-MEDIATED LEUKOCYTE EXTRAVASATION FROM THE BLOOD.....	75
FIGURE 1.11: EXAMPLES OF LEUKOCYTE MOVEMENT BY HAPTOTAXIS AND HAPTOKINESIS.....	77
FIGURE 1.12: CLEAVAGE OF FULL-LENGTH CCL21 CHEMOKINE.....	83
FIGURE 1.13: MODEL OF CCRL1-MEDIATED CHEMOKINE INTERNALIZATION.....	94
FIGURE 2.1: PHOTOCONVERSION OF KAEDE TRANSGENIC MICE. ....	103
FIGURE 2.2: GATING STRATEGY FOR ANALYSIS OF FLOW CYTOMETRY DATA OF SKIN + LYMPH NODE CELLS. .....	124
FIGURE 3.1: MIGRATORY DCs ARE REDUCED IN THE SKIN-DRAINING LYMPH NODES OF CCRL1 KO MICE DURING STEADY STATE.....	150
FIGURE 3.2: CD24 AND CD205 IDENTIFY DISTINCT CELL SUBSETS AMONGST CD103 <sup>-</sup> LANGERIN <sup>-</sup> DCs IN SKIN-DRAINING LYMPH NODES.....	151
FIGURE 3.3: FITC <sup>+</sup> MIGRATORY DCs ARE REDUCED IN SKIN-DRAINING LYMPH NODES OF CCRL1 KO MICE AFTER CUTANEOUS FITC PAINTING.....	152
FIGURE 3.4: SKIN-DRAINING LYMPH NODES CONTAIN THE SAME NUMBERS OF MIGRATORY DCs AFTER A CONCOMITANT TPA + FITC PAINT ON THE DORSAL SKIN. ....	153
FIGURE 3.5: SKIN-DRAINING LYMPH NODES FROM CCRL1 KO MICE CONTAIN FEWER FITC <sup>+</sup> CD103 <sup>-</sup> LANGERIN <sup>-</sup> DCs AFTER A CONCOMITANT TPA + FITC PAINT ON THE DORSAL SKIN. ....	154
FIGURE 3.6: SKIN-DRAINING LYMPH NODES FROM CCRL1-DEFICIENT MICE CONTAIN FEWER MIGRATORY DCs THAN WT MICE IN THE TPA-24-FITC MODEL. ....	155
FIGURE 3.7: CCRL1 DEFICIENCY IS ASSOCIATED WITH A REDUCTION IN THE ABUNDANCE OF ALL FOUR MIGRATORY DC POPULATIONS IN THE INGUINAL LYMPH NODES IN THE TPA-24-FITC MODEL. ....	156
FIGURE 3.8: CCRL1 DEFICIENCY LEADS TO A REDUCTION IN LANGERHANS CELLS IN SKIN-DRAINING LYMPH NODES IN THE TPA-24-FITC MODEL. ....	157
FIGURE 3.9: EPCAM <sup>+</sup> CELLS ARE LESS ABUNDANT IN CCRL1 KO LYMPH NODES THAN IN WT LYMPH NODES IN THE TPA-24-FITC MODEL. ....	158
FIGURE 3.10: FITC <sup>+</sup> MIGRATORY DCs ARE ONLY REDUCED IN THE SKIN-DRAINING LYMPH NODES OF CCRL1 KO MICE 24 HOURS POST FITC PAINTING.....	159

FIGURE 3.11: LANGERHANS CELLS AND OTHER MIGRATORY DC SUBSETS ARE ONLY REDUCED IN THE SKIN-DRAINING LYMPH NODES OF CCRL1 KO MICE 24 HOURS POST FITC PAINTING.....	160
FIGURE 3.12: KAEDE RED <sup>+</sup> MIGRATORY DCs ARE REDUCED IN NUMBERS IN CCRL1 KO SKIN-DRAINING LYMPH NODES AFTER CUTANEOUS TPA PAINTING. ....	161
FIGURE 3.13: FLUORESCENT CCL19 TETRAMER BINDING TO LYMPH NODE CELLS.....	162
FIGURE 3.14: CCR7 IS ESSENTIAL FOR THE SUCCESSFUL MIGRATION OF SKIN DCs TO DRAINING LYMPH NODES AFTER TPA INDUCED INFLAMMATION.....	163
FIGURE 3.15: MIGRATORY DCs ARE REDUCED IN CERVICAL LYMPH NODES OF CCRL1 KO MICE AFTER CFA INJECTION INTO THE EAR. ....	164
FIGURE 3.16: SPECIFIC DC SUBSETS ARE REDUCED IN CERVICAL LYMPH NODES OF CCRL1 KO MICE AFTER CFA INJECTION INTO THE EAR. ....	165
FIGURE 3.17: CD103 <sup>+</sup> LANGERIN <sup>+</sup> DERMAL DCs ARE INCREASED IN THE SKIN OF CCRL1 KO MICE AT REST COMPARED WITH WT MICE. ....	166
FIGURE 3.18: THE PROPORTION OF DCs IN THE INFLAMED SKIN OF CCRL1 KO MICE IS INCREASED COMPARED WITH WTs (TPA-24-FITC PROTOCOL). ....	167
FIGURE 3.19: LANGERHANS CELLS ARE SPECIFICALLY RETAINED IN THE INFLAMED SKIN OF CCRL1 KO MICE (TPA-24-FITC MODEL). ....	168
FIGURE 3.20: DEFECTIVE DC DEPARTURE FROM CCRL1 KO SKIN. ....	169
FIGURE 3.21: CCL19 AND CCL21 PROTEIN IN RESTING AND INFLAMED INGUINAL LYMPH NODES.....	170
FIGURE 3.22: BIO-AVAILABLE CCL19 AND CCL21 LEVELS ARE INCREASED IN THE INFLAMED SKIN OF CCRL1 KO MICE.....	171
FIGURE 3.23: DELETION OF CCL19 RESCUES THE MIGRATORY DC DEFECT SEEN AT REST IN CCRL1 KO MICE.....	172
FIGURE 3.24: DELETION OF CCL19 RESCUES THE MIGRATORY DC DEFECTS SEEN IN CCRL1 KO MICE..	173
FIGURE 3.25: EGFP IS EXPRESSED ON LYVE-1+ LYMPHATIC ENDOTHELIAL CELLS AND CELLS ASSOCIATED WITH THESE VESSELS IN THE INGUINAL LYMPH NODES OF CCRL1 <sup>GFP/+</sup> MICE.....	174
FIGURE 3.26: CCRL1 PROTEIN IS EXPRESSED BY CELLS RESIDING AT THE SCS AND MEDULLARY REGIONS OF INGUINAL LYMPH NODES. ....	175
FIGURE 3.27: CCRL1-eGFP IS EXPRESSED BY HAIR FOLLICLES AND CELLS IN THE EPIDERMIS AND DERMIS. ....	176
FIGURE 3.28: CCRL1-eGFP IS EXPRESSED ON LYMPHATIC VESSELS AND APCs IN THE EAR.....	177
FIGURE 4.1: CD169 <sup>+</sup> MACROPHAGES ARE SITUATED IN THE SCS REGION OF THE LYMPH. ....	194
FIGURE 4.2: CCRL1 IS NOT EXPRESSED BY CD169 <sup>+</sup> SCS MACROPHAGES. ....	195
FIGURE 4.3: CD169 <sup>+</sup> MACROPHAGES EXPRESS CCL19 RECEPTORS. ....	196
FIGURE 4.4: CD169 <sup>+</sup> MACROPHAGE DISTRIBUTION AND ABUNDANCE IS NORMAL IN THE INGUINAL LYMPH NODES OF CCRL1-DEFICIENT MICE. ....	197
FIGURE 4.5: DELETION OF CCRL1 LEADS TO AN EXPANSION OF CD169 <sup>+</sup> MACROPHAGES AND LYVE-1 <sup>+</sup> LYMPHATIC VESSELS IN THE MESENTERIC LYMPH NODE.....	198
FIGURE 4.6: CCRL1 DEFICIENCY IS ASSOCIATED WITH AN INCREASE IN CD169 <sup>+</sup> MACROPHAGE ABUNDANCE IN THE MESENTERIC LYMPH NODE.....	199

FIGURE 4.7: CD169 <sup>+</sup> MACROPHAGES DO NOT EXPRESS CCL19 RECEPTORS OR CCR9.....	200
FIGURE 4.8: DELETION OF CCRL1 RESULTS IN FEWER $\gamma\delta$ T CELLS IN THE MESENTERIC LYMPH NODE.....	201
FIGURE 4.9: DELETION OF CCRL1 LEADS TO A REDUCTION IN NK1.1 <sup>+</sup> CCR6 <sup>-</sup> DX5 <sup>+</sup> NK CELLS IN THE MESENTERIC LYMPH NODE.....	202
FIGURE 4.10: DELETION OF CCRL1 LEADS TO A REDUCTION IN NK1.1 <sup>+</sup> CCR6 <sup>-</sup> DX5 <sup>+</sup> iNKT CELLS IN THE MESENTERIC LYMPH NODE.....	203
FIGURE 4.11: DELETION OF CCRL1 RESULTS IN FEWER $\gamma\delta$ T CELLS IN THE INGUINAL LYMPH NODE.....	204
FIGURE 4.12: DELETION OF CCRL1 LEADS TO A REDUCTION IN SUBSETS OF iNKT CELLS IN THE INGUINAL LYMPH NODE. ....	205
FIGURE 4.13: DELETION OF CCRL1 LEADS TO A REDUCTION IN NK1.1 <sup>+</sup> CCR6 <sup>-</sup> DX5 <sup>+</sup> NK CELLS IN THE INGUINAL LYMPH NODE.....	206
FIGURE 4.14: CCRL1 IS EXPRESSED ON SPLENIC VENULES. ....	207
FIGURE 4.15: ADOPTIVELY TRANSFERRED WT SPLENOCYTES LOCALISE COMPARABLY IN WT AND CCRL1- DEFICIENT SPLEENS. ....	208
FIGURE 4.16: THE PERCENTAGE OF CD169 MACROPHAGES IS INCREASED IN THE SPLEENS OF CCRL1- DEFICIENT MICE.....	209
FIGURE 4.17: DELETION OF CCRL1 DOES NOT AFFECT THE ABUNDANCE OF T CELLS OR B CELLS IN THE SPLEEN.....	210
FIGURE 4.18: LOSS OF CCRL1 DOES NOT AFFECT THE FREQUENCY OF DCs IN THE SPLEEN.....	211
FIGURE 4.19: THE PERCENTAGE OF NK CELLS AND iNKT CELLS IS UNAFFECTED BY LOSS OF CCRL1 IN THE SPLEEN.....	212
FIGURE 4.20: CD169 <sup>+</sup> MACROPHAGES ARE SENSITIVE TO LOCAL DEPLETION IN THE LYMPH NODE BY INJECTION OF CLODRONATED LIPOSOMES. ....	213
FIGURE 4.21: FLUORESCENTLY LABELED LIPOSOMES INJECTED INTO THE FOOTPAD ARE ACQUIRED BY CD169 <sup>+</sup> MACROPHAGES IN THE POPLITEAL LYMPH.....	214
FIGURE 4.22: CD169 <sup>+</sup> MACROPHAGES ARE ABSENT FROM POPLITEAL LYMPH NODES TWO WEEKS AFTER INJECTION WITH CLODRONATED LIPOSOMES INTO THE FOOTPAD.....	215
FIGURE 4.23: CFA INJECTION INTO THE FOOTPAD DRIVES LYMPHANGIOGENESIS IN WT AND CCRL1- DEFICIENT POPLITEAL LYMPH NODES. ....	216
FIGURE 4.24: CFA INJECTION INTO THE FOOTPAD DRIVES LYMPHANGIOGENESIS IN WT AND CCRL1- DEFICIENT INGUINAL LYMPH NODES. ....	217
FIGURE 4.25: CLODRONATED LIPOSOME AND CFA INJECTION INTO THE FOOTPAD INDUCES LYMPHANGIOGENESIS IN THE INGUINAL LYMPH NODES OF WT AND CCRL1-DEFICIENT MICE.....	218
FIGURE 4.26: MACROPHAGES ARE REQUIRED FOR LYMPHANGIOGENESIS IN THE POPLITEAL LYMPH NODE OF WT AND CCRL1-DEFICIENT MICE AFTER CFA INJECTION INTO THE FOOTPAD. ....	219
FIGURE 5.1: WT AND CCRL1-DEFICIENT BMDCs CLEAVE FULL LENGTH CCL21 TO PRODUCE A SOLUBLE CCL21 FRAGMENT. ....	232
FIGURE 5.2: UNACTIVATED AND LPS-MATURED BMDCs TRUNCATE FLCCCL21 TO THE SAME DEGREE. ..	233
FIGURE 5.3: FLT3L-MATURED BMDCs MEDIATE CCL21 TRUNCATION <i>IN VITRO</i> . ....	234

FIGURE 5.4: FLCCCL21 CHEMOKINE IS CLEAVED BY HUMAN DCs, AND THIS IS UNAFFECTED BY LPS ACTIVATION.....	235
FIGURE 5.5: FLCCCL21 CAN BE TRUNCATED BY DCs, T CELLS AND MACROPHAGES.....	236
FIGURE 5.6: TCCL21 IS GENERATED FROM FLCCCL21 BY CULTURE WITH CELLS FROM WT SECONDARY LYMPHOID TISSUES.....	237
FIGURE 5.7: TCCL21 IS FOUND IN THE SPLEEN, MESENTERIC AND AXILLARY LYMPH NODES OF WT AND CCRL1-DEFICIENT MICE AND ITS ABUNDANCE IS UNAFFECTED BY CCRL1-DEFICIENCY AT REST OR DURING SKIN INFLAMMATION. ....	238
FIGURE 5.8: CLEAVAGE OF CCL21 IS NOT MEDIATED BY CCR7 OR DC-CONDITIONED MEDIUM.....	239
FIGURE 5.9: THERE ARE TWO COMMERCIALY AVAILABLE MOUSE CCL2 CHEMOKINES WITH DIFFERENT MOLECULAR WEIGHTS. ....	240
FIGURE 5.10: THE AMINO ACID SEQUENCE OF FULL LENGTH MOUSE CCL25 AND RECOMBINANT MOUSE CCL25 FROM R&D SYSTEMS.....	241
FIGURE 5.11: BMDCs CLEAVE FULL LENGTH CCL2 BUT DCs AND MACROPHAGES ARE UNABLE TO CLEAVE CCL25.....	242
FIGURE 6.1. PROPOSED MECHANISM OF DC MIGRATION FROM THE RESTING SKIN OF WT AND CCRL1- DEFICIENT MICE. CCRL1 IS EXPRESSED BY KERATINOCYTES AND LECs AND COORDINATES THE MIGRATION OF DCs FROM THE SKIN TO THE LYMPH NODE. ....	254
FIGURE 6.2: PROPOSED MECHANISM OF CCRL1-GUIDED DC EXIT FROM THE SKIN DURING INFLAMMATION. CCRL1 IS EXPRESSED BY KERATINOCYTES AND LECs AND COORDINATES THE MIGRATION OF ALL DC SUBSETS FROM THE SKIN TO THE LYMPH NODE DURING INFLAMMATION. ....	255
FIGURE 7.1: LYVE-1 DISTRIBUTION IN WT MESENTERIC LYMPH NODES.....	269
FIGURE 7.2: LYVE-1 DISTRIBUTION IN CCRL1-DEFICIENT MESENTERIC LYMPH NODES.....	270
FIGURE 7.3: CD169 <sup>+</sup> MACROPHAGE DISTRIBUTION IN WT MESENTERIC LYMPH NODES.....	271
FIGURE 7.4: CD169 <sup>+</sup> MACROPHAGE DISTRIBUTION IN CCRL1-DEFICIENT LYMPH NODES. ....	272

## List of Tables

TABLE 1: ANTIBODIES FOR IMMUNOFLUORESCENT STAINING	110
TABLE 2: GENE PROBES FOR TAQMAN	114
TABLE 3: FACS ANTIBODIES	121

## Abbreviations

The following abbreviations are used in this thesis:

AF647	Alexafluor647
Ag	Antigen
$\alpha$ GalCer	$\alpha$ -galatosylceramide
AMPs	Antimicrobial peptides
AP-2	Adaptin-2
APC	Allophycocyanin
APCs	Antigen presenting cells
APRIL	A proliferation inducing ligand
BAFF	B cell activating factor
BM	Bone marrow
BMCs	Bone marrow cells
BMDCs	Bone marrow derived DCs
BMDMs	Bone marrow derived macrophages
C-terminal	Carboxy terminal
CCL	CC chemokine ligand
CCR	CC chemokine receptor
CD	Cluster of differentiation
cDC	Conventional dendritic cell
cDNA	Complementary DNA

CFA	Complete Freund's adjuvant
CHS	Contact hypersensitivity response
CMV	Cytomegalovirus
CNS	Central nervous system
CX <sub>3</sub> CL	CX <sub>3</sub> CL chemokine ligand
CX <sub>3</sub> CR	CX <sub>3</sub> CR chemokine receptor
CXCL	CXC chemokine ligand
CXCR	CXC chemokine receptor
Cy7	Cyanine 7 dye
DAMP	Danger associated molecular pattern
DARC	Duffy antigen receptor for chemokines
DC	Dendritic cell
dDCs	Dermal dendritic cells
DETCs	Dendritic epidermal T cells
DN	Double negative
DNA	Deoxyribonucleic acid
DSS	Dextran sodium sulphate
DTR	Diphtheria toxin receptor
EAE	Experimental autoimmune encephalomyelitis
EDTA	Ethylenediaminetetraacetic acid
eGFP	Enhanced green fluorescent protein
ELISA	Enzyme-linked immunosorbent assay
EpCAM	Epithelial cellular adhesion molecule
EST	Expressed sequence tags

FACS	Fluorescence activated cell sorting
FCS	Foetal calf serum
FDC	Follicular dendritic cell
FITC	Fluorescein isothiocyanate
fICCL21	Full length CCL21
Flt3L	Fms-like tyrosine kinase-3 ligand
fMLP	Formyl-Methionyl-Leucyl-Phenylalanine
FMO	Fluorescence minus one
FoxP3	Forkhead box P3
FRC	Fibroblast reticular cell
FSC	Forward scatter
IMMGEN	Immunological Genome Project
iNKT	Invariant natural killer T cell
GAG	Glycosaminoglycan
GC	Germinal centre
GDP	Guanosine diphosphate
GEF	Guanine nucleotide exchange factor
GFP	Green fluorescent protein
GM-CSF	Granulocyte macrophage-colony stimulating factor
GPCR	G-protein coupled receptor
GTP	Guanine triphosphate
HBSS	Hanks balanced salt solution
HEK	Human embryonic kidney

HEPES	4-(2-hydroxyethyl)-1-piperazineethanesulfonic acid
HEV	High endothelial venule
hi	High
I.P	Intraperitoneally
ICAM	Intracellular adhesion molecule
IELs	Intraepithelial lymphocytes
IFN	Interferon
Ig	Immunoglobulin
IL	interleukin
Immgen	Immunological Genome Project
IRES	Internal ribosome entry site
KGF	Keratinocyte growth factor
KO	Knock out
LECP	lymphatic endothelial cell progenitors
Lo	Low
LPS	Lipopolysaccharide
LT	Lymphotoxin
LTi's	Lymphoid tissue inducer cells
M cell	Microfold cell
Mins	Minutes
MGH	Massachusetts General Hospital
MLN	Mesenteric lymph node
MM	Medullary macrophage

MMM	Metalophilic macrophages
MMP	Matrix metalloproteinase
mRNA	Messenger RNA
MRC	Marginal reticular cell
MSM	Medullary sinus macrophage
MZM	Marginal zone macrophage
N-terminal	Amino-terminal
NK cells	Natural killer cells
PALS	Periarteriolar lymphoid sheaths
PBS	Phosphate buffered saline
pDC	Plasmacytoid dendritic cell
PE	Phcoerythrin
PerCP	Peridinin-chlorophyll-protein
<i>plt/plt</i>	Paucity of lymph node T cells
PP	Peyer's patch
PRR	Pattern recognition receptor
QPCR	Quantitative polymerase chain reaction
RALDH	Retinal dehydrogenase
RBCs	Red blood cells
RNA	Ribonucleic acid
RPM	Revolutions per minute
RPMI	Roswell Park Memorial Institute-1640 medium
RT	Room temperature
RT-PCR	Reverse transcriptase-polymerase chain reaction

S1P	Sphingosine-1-phosphate
SCS	Subcapsular sinus
Secs	Seconds
SEM	Standard error of the mean
Ser	Serine
Siglec	Sialic-acid-binding lectin
SHM	Somatic hypermutation
SSC	Side scatter
SSM	Subcapsular sinus macrophage
TAM	Tumour associated macrophage
TBM	Tingible body macrophage
tCCL21	Truncated CCL21
tCCL2	Truncated CCL2
TCR	T cell receptor
TEC	Thymic epithelial cell
T <sub>H</sub> 1	T helper 1 cell
T <sub>H</sub> 17	T helper 17 cell
T <sub>H</sub> 2	T helper 2 cell
Thr	Threonine
TLR	Toll-like receptor
TNF $\alpha$	Tumour necrosis factor alpha
TPA	12-O-tetradecanoylphorbol-13-acetate
TRANCE	TNF-related activation-induced cytokine
TRANCER	TNF-related activation-induced cytokine receptor

TRCM	Recirculating central memory T cells
Treg	Regulatory T cell
VEGF	Vascular endothelial growth factor
vs.	Versus
WT	Wild type
XCL	XC chemokine ligand
XCR	XC chemokine receptor

# Chapter One

## Introduction

# 1 Introduction

## 1.1 General Introduction

The immune system is composed of a complex array of cells, organs and cellular mediators that function to provide the host with protection against disease and infection. The immune system must protect against viral, bacterial and fungal pathogens that are hard-wired to circumvent many of the immune system's strategic defence mechanisms. It needs to do this whilst imposing minimal damage to the host itself. To add to this complexity, the immune system can fight tumours, repair wounds and clear dysfunctional cells but must also tolerate innocuous particles that enter the body. In the broadest sense, the immune system can be divided into innate and adaptive arms. The innate immune system is equipped to quickly recognise and respond to pathogenic insult and tissue damage through pattern recognition receptors (PRRs) encoded in the germline. It is populated by cells that have an inbuilt ability to control, destroy and clear pathogens and initiate and regulate processes of tissue repair. It provides fast immune protection against invading pathogens and helps to prevent their systemic dissemination. Often the innate response is insufficient to kill and clear the invading pathogen, and instead acts to control infection during the lag phase required for the establishment of the antigen-specific adaptive arm of the immune response. This typically develops 4-7 days after infection. The adaptive arm of the immune system is composed of a combination of highly specialised cells and components each of which is specific for a very limited range of antigens carried by the host or invading microorganisms. These antigen specific cells mature via a series of somatic mutations in their antigen-sensing receptors that equips them with high affinity receptors for a specific but highly limited repertoire of antigens.

The activation of adaptive immune cells requires their interaction with antigen presenting cells (APCs) that link the innate and adaptive arms of the immune system. This activation leads to the development of immune effector cells and molecules that regulate the cells of the innate immune system to shape their ability to fight pathogens and repair damaged tissues. It also leads to the

generation of memory cells that are capable of swift and robust responses should the host encounter the antigen again. These cells are instrumental in providing efficient protection from re-infection, and are critical cellular mediators of effective vaccination strategies. The power of the immune system provides protection from pathogens but needs to be carefully controlled to avoid tissue damage and autoimmunity. This is achieved by regulatory immune cells and immunosuppressive molecules that actively counteract the inappropriate activation of the immune system and ensure that homeostasis is restored after deployment of immune attack. The concerted activation and regulation of immune cells and immune mediators ensures that, in a healthy individual, pathogens are efficiently eliminated with minimal collateral damage.

To facilitate many of the aforementioned processes, leukocytes must be brought in contact with each other in lymphoid organs in order to propagate adaptive immune responses. These tissues are highly organised to provide a niche for immune cell development. All leukocytes originate in the bone marrow and then enter the blood. T cells then mature in the thymus whereas B cells mature in the bone marrow but undergo further maturation in the spleen. After their development and maturation, T cells and B cells localise in lymph nodes, the spleen and other secondary lymphoid tissues. These tissues provide a niche for the concentration and presentation of antigen and the interaction of APCs with antigen-specific T cells and B cells. Localisation of cells to these organs, and regions within them, is facilitated by guidance cues that orchestrate the spatial and temporal positioning of APCs and antigen specific T cells and B cells. These guidance cues are detected by appropriate surface receptors that translate the message via intracellular signalling pathways to initiate cell movement in a coordinated and directional manner, propelling receptor-bearing cells to particular locations. To ensure the correct homing of cells, peripheral tissues such as the skin and gut have a particular 'address' that attracts cells bearing the specific receptors for those molecules. The receptor repertoire of a leukocyte determines its homing properties and is a key aspect of its function.

Cells regulate their surface receptor expression in order to facilitate their movement to and from the periphery and also to guide them to specific microanatomic regions in lymphoid organs and other tissues. This receptor

switching along with discrete expression of chemotactic molecules within lymph nodes helps to establish distinct lymphoid microenvironments that contain specific populations of cells, such as the B cell follicles and T cell zones. It is essential that cells are able to properly sense directional cues and move appropriately in order to mount an adaptive immune response and so they must express the appropriate receptors at the appropriate time. As there are a multitude of small chemical mediators present in the lymph node directing the movement of various cell types, it can be appreciated why it is necessary that this complex system of locomotive cues be tightly regulated to prevent aberrant cellular movement and localisation.

After the recognition of antigen in lymphoid tissues, differentiated antigen specific T cells and B cells switch their surface receptors in order to move to other locations in the lymphoid tissue or to home to peripheral sites to perform effector functions. Subsequently, a small proportion of these cells will remain after the contraction of the effector T cell and B cell populations in order to form a pool of high affinity memory cells that are involved in protection against secondary infection. The localisation of these memory cells depends on expression of surface receptors for migratory cues. Some memory T cells transit through the blood and peripheral tissues patrolling the body, whereas others traffic through lymphoid tissues like naïve T cells. Similarly, antigen-specific B cells differentiate into plasma cells, switch their surface receptors to allow them to migrate to the bone marrow where they remain for extended periods of time producing high affinity antibodies. Alternatively, activated B cells can differentiate into memory B cells that are able to live for long periods of time circulating through secondary lymphoid tissues and that respond quickly upon secondary exposure to antigen. Plasma cells and memory B cells will produce high affinity antibodies as they have undergone somatic hypermutation (SHM) and affinity maturation, in structures called germinal centres that form within secondary lymphoid tissues.

Receptor switching and cellular homing must be tightly controlled in order to ensure the proper positioning of cells during development, homeostasis, immune surveillance, tolerance and memory. Chemokines are small, secreted proteins that play a critical role in directing leukocyte migration by interacting with

receptors that decorate leukocyte surfaces. Their function is subject to various levels of regulation that help ensure that leukocyte localisation is precisely controlled. A breakdown of this control can lead to aberrant cellular localisation. This thesis will investigate the role of an atypical chemokine receptor that is a member of a family of proteins that have been described as having the ability *in vitro* and *in vivo* to regulate chemokine abundance and localisation. In this introduction I will discuss the development and organisation of the immune system with a specific focus on chemokines and chemokine receptors and the key immunological roles these molecules play.

## **1.2 Lymph Node Structure and Function**

Lymph nodes and other secondary lymphoid tissues are essential for the concentration of immune cells and antigen in order to initiate and propagate adaptive immune responses<sup>1-5</sup>. The architecture and organisation of the lymph node is represented in (Figure 1.1).

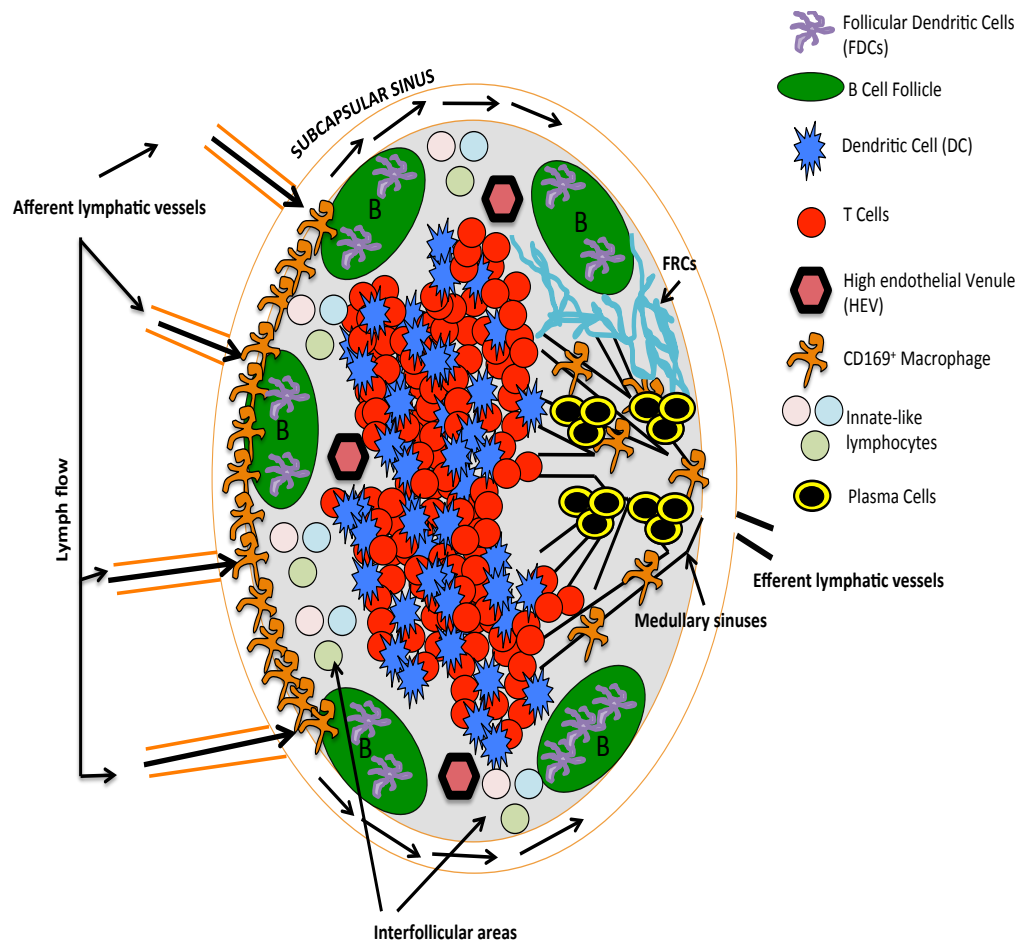


**Figure 1.1: The structure of the lymph node.**

The lymph node is surrounded by a fibrous capsule (shown in orange) overlying the subcapsular sinus (SCS) that is fed with lymph draining in via lymphatic vessels originating in peripheral tissues. Within the SCS region lies a specialised population of CD169<sup>+</sup> macrophages that sequester antigen and pathogen entering via the SCS. CD169<sup>+</sup> macrophages are also present in the medulla of lymph nodes, which is also home to populations of antibody-producing plasma cells. B cells are positioned within follicles that lie underneath the SCS. These follicles contain follicular dendritic cells (FDCs) that are involved in antigen presentation to B cells, and are sites where germinal centres develop. T cells are positioned in the medullary regions (paracortex) that are also home to antigen presenting cells including DCs. The regions between B cell follicles (interfollicular regions) are populated by DCs and T cells, but also contains populations of innate-like lymphocytes such as NK cells. Soluble antigen, immune complexes, pathogens and DCs arrive at the lymph node by way of the afferent lymphatic vessels whereas B cells and most T cells arrive via the HEVs. If a T cell does not encounter its cognate antigen it exits the lymph node via the efferent lymphatic vessels, which is also the route by which lymph leaves the lymph node. The efferent lymph often contains antibodies released by lymph node plasma cells and it eventually drains back into the blood at the thoracic duct

The lymph node is compartmentalised into specific zones to increase its efficiency in bringing together naïve T or B cells with appropriate APCs. B cells are located in B cell follicles that are situated underneath the SCS that is located just beneath the lymph node capsule. Under steady-state conditions these follicles contain naïve and memory B cells. T cells are located in a specialised lymph node compartment known as the T cell zone. Within this region are APCs, most importantly DCs, that present antigen to naïve T cells in order to induce tolerance or initiate adaptive immune responses. This compartmentalisation into B cell follicles and T cell zones is only possible due to the discrete expression of chemokines and other molecules within the B cell follicles and T cell zones. These cues only attract cells with the specific cognate receptors and thus help to establish lymph node compartmentalisation. This also occurs in the spleen, which is discussed in section 1.8, and other secondary lymphoid tissues such as Peyer's Patches (PP).

It is essential that antigen be delivered to the lymph node in a timely and efficient manner. To achieve this, lymphatic vessels draining from peripheral sites carry antigen-loaded APCs and soluble lymph-borne antigen to the lymph node. The passage of small lymph-borne molecules into the lymph node parenchyma occurs via a system of fibroblastic reticular cells (FRCs)<sup>6</sup> that form an interconnected network – the conduit system. Lymph node resident DCs are able to survey the contents of the conduits to acquire antigen and present it to T cells in the T cell zones. In order to bring together naïve T cells and antigen loaded DCs, the FRCs secrete small chemoattractant molecules<sup>7</sup>. Therefore, the FRCs act as a physical network on which T cells can migrate during their “random walk” behaviour when in search of their cognate antigen. Only low molecular weight molecules (<70kDa) can travel in the conduit system. Thus, antigen is excluded from entry to the T cell zone based on size, so the conduit system also acts as a form of lymph node filter. Chemokines can drain from inflamed tissues found upstream of the lymph node and then travel down the conduits and be presented on high endothelial venules (HEVs) and thus influence the entry of leukocytes to lymph nodes. Other small inflammatory mediators, such as cytokines like TNF $\alpha$ , can also enter lymph nodes from peripheral tissue via this route. Within the FRC-rich T cell zone, initiation of T cell responses occurs. During this time, important

decisions are being made. These decisions define the fate of the responding T cell – the balance between tolerance and immunity, migratory potential and the type of T cell that will be induced. These decisions are driven by the characteristics of the APCs and are thought to be influenced by the FRC network facilitating the concentration of soluble lymph-borne antigen that can be sampled by lymph node resident APCs<sup>8-11</sup>.

The conduit system extends into B cell follicles and delivers low molecular weight antigen that can be picked up by cognate B cells. B cell follicles lack FRCs but contain a distinct cell population termed FDCs that enwrap the conduits and are responsible for the attraction and retention of B cells by secreting B cell chemoattractant molecules. They are also important secretors of B cell activating and survival factors including B cell activating factor (BAFF), IL-6 and IL-1<sup>12</sup>. FDCs also play important roles in antigen acquisition and retention within B cell follicles<sup>13-15</sup>. They do so by acquiring immune complexes from non-cognate B cells via their complement receptors and recycling them on their surface for display to cognate B cells. In contrast to the FRC network that shuttles low molecular weight antigen from the SCS into the T cell area, FDCs do not extend to the SCS region. Instead they are positioned deep within follicles. The reason for this is unclear but it might ensure that they are protected from interactions with macrophages and DCs and so that opsonised antigen can be displayed on their surface for longer periods of time without being removed by phagocytes. The mechanisms underpinning the relay of larger antigens from the SCS to FDCs remain to be fully understood.

The SCS is a very important region within the lymph node and is home to a variety of immune cell types each with a specific function<sup>16</sup>. As this is the entry point for viruses, bacteria and antigen, it is essential that these pathogens are appropriately contained at this site. This job belongs to a specialised population of CD169<sup>+</sup> macrophages that are positioned between LECs on the floor of the SCS. These cells act to limit pathogen dissemination in lymph nodes whilst constantly sampling lymph arriving in the subcapsular sinus<sup>17</sup>. They are poorly phagocytic and instead antigen is captured and decorates the surface of these cells. It is thought that these macrophages constantly deliver antigen to B cells

moving within the underlying follicles<sup>17</sup> and these B cells may transport and deposit this antigen to FDCs<sup>18,19</sup>.

As mentioned previously, the antigen that arrives by way of the afferent lymphatics can be soluble, particulate, or cell-associated. Under steady state conditions, immature DCs in peripheral tissues constantly sample their immediate environment for “self antigen” and constitutively traffic by way of the lymphatic network to draining lymph nodes, and finally into T cell zones. Here they play an important role in deleting auto-reactive T cells, and so are important players in the maintenance of peripheral tolerance to self antigen<sup>20-22</sup>. DCs located at peripheral sites can also encounter foreign antigen and pathogen. In this case, they internalise antigen, become activated, and transit to draining lymph nodes. Collecting LECs express chemoattractant molecules that attract DCs into lymphatic vessels, and chemoattractants also drive the extravasation of DCs out of lymphatic vessels into the parenchyma on the lymph node. Once inside the lymph node, DCs must position themselves within the T cell zones in order to present their antigen payload to naïve T cells via their MHCII molecules (or MHCI when the DCs are capable of cross-presentation). Chemoattractant molecules largely orchestrate this behaviour and the FRC network facilitates DC migration within a lymph node and plays an important role in increasing DC-T cell “contacts”.

Unlike the entry of tissue-derived DCs that transit via the lymphatic system, the entry of lymphocytes into lymph nodes occurs mainly from the blood as it passes through HEVs that are present in the T cell zones of the lymph node and at the T/B boundary<sup>23</sup>. Extravasated lymphocytes are directed to specific regions of the lymph node by chemoattractant molecules that are specific for B cells and T cells. Lymphocytes that do not encounter their cognate antigen within 12-18 hours of entering the lymph node exit by way of the efferent lymphatics and then continue on their quest to encounter cognate antigen by moving from lymph and into the blood where they are carried to other secondary lymphoid tissues. Sphingosine-1-phosphate (S1P) regulates exit of both T and B cells. S1P is an extracellular ligand for a group of G-protein coupled receptors including S1PR1. S1PR1 drives the egress of lymphocytes from lymph nodes by way of the efferent lymphatics<sup>24,25</sup>. S1P levels are much lower in the lymph node compared

with the lymph and blood. S1PR1 on lymphocytes in the lymph and blood is desensitised by the high levels of S1P, and therefore these cells become unresponsive to S1P. Once they enter lymph nodes, their responsiveness to S1P is slowly re-established and eventually reaches a level at which lymphocytes become responsive to S1P in the lymph and then egress out of the lymph node into efferent lymphatics. This cycling between sensitisation and desensitisation allows lymphocytes to overcome retention signals they encounter in secondary lymphoid organs<sup>25</sup>.

### **1.3 The Cellular Orchestra of the Lymph Nodes**

After birth, all leukocytes originate in the bone marrow and mature in primary lymphoid organs such as the thymus for T cell maturation and the bone marrow for B cell maturation and all other leukocyte subsets. Lymph nodes and other secondary lymphoid tissues provide a niche for the concentration of mature lymphocytes and also many other leukocyte subsets each with specific functions. These leukocytes are unique in their ontogeny, function, location and mode of activation. I will next outline the functions of specific leukocyte subsets that are found in lymph nodes and which will be studied in this thesis.

#### **1.3.1 DCs**

Dendritic cells are a group of heterogeneous APCs that are highly efficient at activating or tolerising naive T cells and thus initiating adaptive immunity and peripheral tolerance, respectively. DCs can be defined based on their functionality but also on their development, activation and localisation. Classical DCs (cDCs) are so-called based on Ralph Steinman's first observations and characterisation of a cell he termed the dendritic cell in the late 1970s<sup>26,27</sup>. More recently, researchers have uncovered a new type of DC, the plasmacytoid DC (pDC). These DCs more closely resemble plasma cells in terms of their morphology and are potent secretors of type I interferons<sup>28,29</sup>. Both DC subsets are derived from common progenitors but perform distinct immunological functions. Another type of DC subset, FDCs, are found in B cell follicles, but these cells are not derived from hematopoietic stem cells like cDCs, but instead are of mesenchymal origin<sup>30-32</sup>. FDCs are non-migratory and make up the

stromal component of germinal centres (GCs)<sup>13,32-34</sup>. For the purposes of this thesis, I will not describe the role of FDCs further, however, the role of each of the other DC subsets mentioned above are outlined below.

### **1.3.1.1 Development of DCs**

In mice, all DCs except FDCs, develop from common myeloid progenitors in the bone marrow and all subsets share expression of the integrin molecule CD11c and MHC class II molecules. It is known that both pDCs and cDCs develop from haematopoietic stem cells that give rise to multipotent progenitors. These cells can then give rise to both common myeloid progenitor (CMP) cells and common lymphoid progenitor (CLP) cells. cDCs, on the whole, complete their differentiation in the periphery, although a small population of fully differentiated cDCs is present in the bone marrow. cDCs can be grouped into CD8 $\alpha$ <sup>+</sup> or CD8 $\alpha$ <sup>-</sup> cDCs and both subsets are capable of polarising T cells via secretion of factors such as IL-12<sup>22,35-37</sup>. However, only CD8 $\alpha$ <sup>+</sup> DCs possess the capacity to cross present exogenous antigen on MHC class I molecules and thus prime CD8<sup>+</sup> T cells, making them important in the initiation of adaptive immune responses to tumours and viruses<sup>38-46</sup>. As DCs have a high turnover rate and thus short life span, especially following activation, it is essential that DCs are constantly replenished in peripheral lymphoid tissues. The growth factor fms-like tyrosine kinase-3 ligand (Flt3L) is pivotal for the differentiation of pre-cDCs and pDCs, with Flt3L-deficient animals showing a deficiency in all DC subsets. Also, Flt3L injection into mice results in an expansion of both cDCs and pDCs. A decrease in cDC numbers in the spleen and other lymphoid tissues results in an increase in Flt3L in the blood and consequently an increase in the frequency and differentiation of pre-cDCs triggering a restoration of cDC numbers in these lymphoid tissues. In addition, under inflammatory conditions monocytes can also contribute to the DC populations in lymphoid tissues by differentiating into “inflammatory” DCs<sup>47,48</sup>.

### 1.3.1.2 Classical DCs

cDCs refers to all DCs that are not pDCs or FDCs. cDCs are positioned throughout the periphery in lymphoid and non-lymphoid tissues. Within non-lymphoid tissues such as the skin, lung and gut, they function to sense and respond to pathogenic insult as well as playing a role in tolerance<sup>20,49-51</sup>. They do so by internalising antigen and presenting it on MHC molecules whilst concomitantly migrating to draining lymph nodes<sup>52-55</sup>. Antigen is then presented to T cells in lymph nodes and this initiates adaptive immunity to pathogen or ignorance to self-antigen during tolerance. cDCs are sometimes referred to as professional APCs due to several key attributes. They have well evolved antigen capturing and processing capabilities and have the capacity to produce costimulatory molecules and cytokines. They also display a very efficient ability to migrate to lymph nodes and also to T cell zones of lymph nodes during homeostasis and inflammation. These characteristics endow DCs with superior T cell priming capabilities compared with other APCs and they have the ability to fully activate naïve T cells.

Immature cDCs home to sites of insult and injury guided by their expression of chemokine receptors that recognise inflammatory chemokines released by the damaged tissue. Once at the site of insult or injury, DCs sample their environment and acquire antigen. They can also be stimulated via their toll-like receptors (TLRs) by pathogen associated molecular patterns (PAMPs) and danger associated molecular patterns (DAMPs) which in combination with cytokines, increase DC activation and drives the expression of co-stimulatory molecules. After antigen acquisition and activation, these cells become less phagocytic, their morphology changes, and they increase their antigen presenting capabilities. cDCs have a high turnover rate in their immature state that is shortened by their activation<sup>56</sup>. This feature may act to limit the duration of antigen presentation and T cell responses to antigen.

Tissue-migratory cDCs are located in lymph nodes and migrate to these sites by way of the afferent lymphatics. These cells constitutively traffic from non-lymphoid tissues where they are loaded with antigen, and shuttle to T cell zones in lymph nodes for presentation of antigen to naïve T cells. This process can be

increased in response to tissue inflammation<sup>57,58</sup>. Under steady-state conditions, migratory cDCs are distinguished from lymph node resident DCs by their higher MHC-II expression. However, during inflammation, it is necessary to include other markers for the definitive segregation of migratory and resident DCs because resident DCs can upregulate their MHCII expression during inflammation.

Lymph node resident cDCs mature in secondary lymphoid tissue from precursor cells that enter the lymph node via HEVs, and spend their lives within these organs. CD8 $\alpha$ <sup>+</sup> DCs represent approximately 20-40% of lymph node resident cDCs<sup>37</sup>. These DCs, unlike CD8<sup>+</sup> T cells, express the CD8 $\alpha$  transcript and protein and not the CD8 $\beta$  protein. These CD8 $\alpha$ <sup>+</sup> DCs also express CD24, CD205, CD11c, MHCII, CD103 and CD45. The lymph node is also home to a population of DCs that express the integrin CD11b, but that lack CD8 expression. This DC subtype predominates and forms the largest proportion of the lymph node resident cDCs<sup>37</sup>. As mentioned previously, immature DCs are highly phagocytic and dendritic in morphology, which means they are excellent at capturing antigen that drains into the lymph node via the afferent lymphatic vessels. These DCs acquire antigen from the conduits, become activated, upregulate co stimulatory molecules and then activate naïve T cells<sup>37,59-61</sup>.

### **1.3.1.3 Plasmacytoid DCs**

Since their first characterisation in 1999<sup>62</sup>, our understanding of pDCs has increased substantially. First described as a rare subset of lymphocytes due to their similarity in morphology to plasma cells and their expression of B cell markers, such as B220, pDCs are now known to make up a rare population of DCs. In the absence of a pDC specific marker, it is conventional to identify these cells based on expression of markers such as CD11c, B220, PDCA-1, Siglec-H and Ly6C. They are morphologically and functionally distinct from conventional DCs. pDCs migrate into lymph nodes via HEVs facilitated by their constitutive expression of L-selectin and specific chemokine receptors<sup>63-65</sup>. Typically they account for 0.3-0.5% of cells in secondary lymphoid organs but show higher representation in the gut, blood and bone marrow<sup>29</sup>. The cardinal characteristic

attributed to pDCs is their ability to produce and secrete large amounts of IFN- $\alpha$  after viral infection and they are thought to be able to produce up to 1000-fold more IFN- $\alpha$  than any other cell type<sup>66</sup>. This is because pDCs express TLR7 and TLR9 allowing them to sense endosomal single stranded RNA and cytosine phosphate guanine (CpG)<sup>28,29,67</sup>. IFN- $\alpha$  has direct anti-viral effects and is a potent mediator of viral clearance. Furthermore, as IFN- $\alpha$  is a key inducer of cytotoxicity in NK cells and CD8<sup>+</sup> T cells, it provides a bridge between the innate and adaptive immune responses<sup>29,68-70</sup>.

### **1.3.2 Lymph Node Resident Macrophages**

Macrophages are found in all tissues of the body and each population of tissue-resident macrophages perform a specific function in their tissue of residence. Generally, a macrophage is considered to be highly phagocytic cell that is adapted and equipped to respond swiftly to pathogenic insult<sup>71,72</sup>. Based on intranodal location and the expression of certain cell surface markers, three subpopulations of macrophages can be identified in resting peripheral lymph nodes. These are referred to as subcapsular sinus macrophages (SSMs), medullary sinus macrophages (MSMs) and medullary cord macrophages (MCMs) These populations of cells are discussed in more detail later, but together they are essential for the recognition and transportation of lymph borne particulate antigen to B cells, T cells and DCs as well as the production of cytokines and chemokines. Collectively, these features contribute to innate and adaptive immune responses in the lymph node. CD169<sup>+</sup> macrophages can be easily identified on lymph node sections via immunohistochemical staining with anti-CD169 antibody. CD169 is also known as Siglec-1 and is a member of the sialic acid-binding lectin (Siglec) family<sup>73-76</sup>. CD169 is found not only on SCS macrophages, but also on medullary macrophages, bone-marrow macrophages and can be induced on inflammatory monocytes<sup>74</sup>.

#### **1.3.2.1 Subcapsular Sinus Macrophages**

A convergence of studies has led to important advances in our understanding of the role of lymph node macrophages during infection. In particular, it is now

clear that SCS macrophages are permissive to viral infection and are crucial in mounting anti-viral responses *in vivo*<sup>17,77</sup>. Depletion of macrophages with clodronated liposomes can lead to the systemic dissemination of virus and increased morbidity<sup>17,77</sup> emphasising the crucial role that they play in the containment of pathogen spread. Their function as lymph node “gate keepers” is facilitated by their positioning in these tissues. The roof of the SCS is composed of the type IV collagen-rich lymph node capsule, important for shielding the inside of the lymph node from the surrounding environment. The inside of the capsule is lined with LYVE-1<sup>+</sup> LECs (Figure 1.2). The floor of the SCS is also composed of a population of LYVE-1<sup>+</sup> LECs sandwiched between a dense upper layer of extracellular matrix and an underlying layer of marginal reticular cells (MRCs)<sup>78,79</sup>.

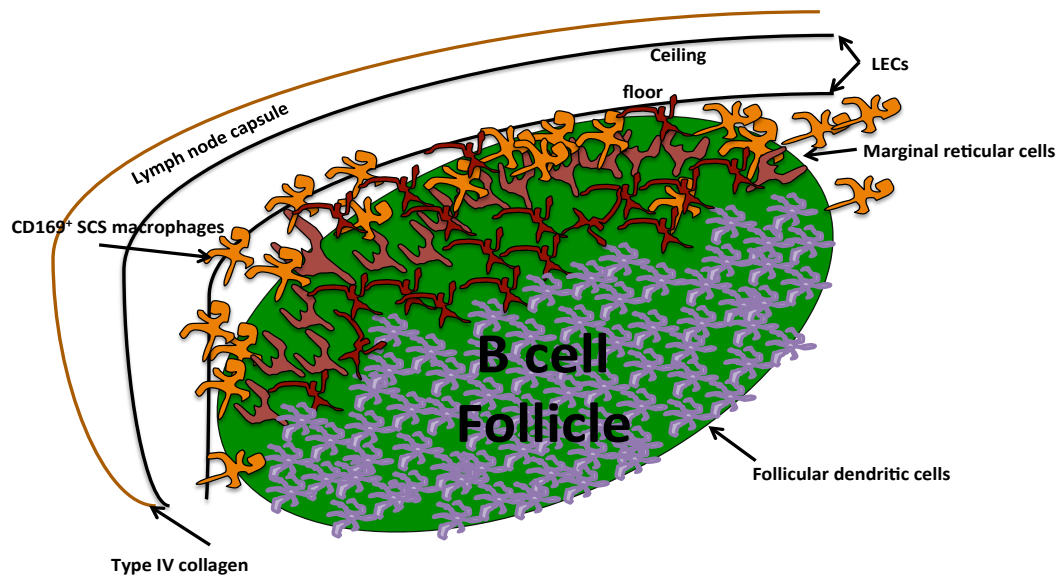


**Figure 1.2: The SCS region of the lymph node.**

The lymph node is surrounded by a fibrous capsule overlying the SCS. The SCS is composed of a type IV collagen with LECs decorating the ceiling and floor. Within the SCS region situated above marginal reticular cells and below LECs on the floor of the SCS lies a specialised population of CD169<sup>+</sup> macrophages. These cells are found above B cell follicles and in interfollicular regions and sequester antigen and pathogen entering via the SCS (see text for further details).

The SCS floor is lined with a highly specialised population of CD169<sup>+</sup> CD11b<sup>+</sup> F480<sup>-</sup> SCS macrophages. These macrophages form a dense layer of cells at this key barrier site<sup>17</sup>. SCS macrophages protrude across the lymphatic lining and

extend their cellular processes into the SCS to sample lymph, whilst remaining anchored to the lymphatic lining via their “tails”. These macrophages are poorly phagocytic, and have been described as being specialised in presenting particulate antigen to B cells. Lymph node resident B cells acquire antigen from SCS macrophages via complement receptors and Fc receptors<sup>17,18,80,81</sup>. CD169<sup>+</sup> SCS macrophages have been described as having a very poor capacity to internalise and degrade opsonised antigen and are also permissive to viral infection<sup>17,80,82</sup>. As well as augmenting B cell responses to pathogen, a recent study by Kastenmuller *et al*, eloquently exemplified the important relationship that exists between SCS macrophages and innate-like lymphocytes during the induction of innate immune responses in the lymph node. They showed that SCS macrophages, when activated by *Pseudomonas aeruginosa*, produce a cocktail of cytokines including inflammasome-generated IL-18. This in turn leads to the activation of a strategically positioned population of iNKT cells, CD8<sup>+</sup> T cells and  $\gamma\delta$ T cells lying in the interfollicular areas in close proximity to the SCS. These cells secrete IFN $\gamma$  that bestows CD169<sup>+</sup> macrophages with antimicrobial resistance<sup>83</sup>. Cellular interactions within the SCS/interfollicular region of the lymph node are very interesting. Innate-like T cells such as  $\gamma\delta$  T cells and iNKT cells<sup>19,83,84</sup> are of critical importance for viral protection and for limiting spread of pathogen throughout the lymph node and are positioned at these sites<sup>81</sup>.

#### **1.4 Medullary Macrophages**

Medullary sinuses are fluid-filled spaces that are lined by LECs that are patrolled by MSMs. These sinuses are linked to the SCS to form one continuous network of sinuses linking afferent and efferent lymphatic vessels. When visualised on lymph node sections, MSMs appear closely situated to LYVE-1<sup>+</sup> LECs often appearing as part of the sinus wall. In fact, macrophages residing within the medullary sinus are also reported to express LYVE1<sup>85-87</sup>, although this is still contentious. Medullary sinuses contain lymphocytes and small numbers of plasma cells that are egressing the lymph node. The medullary region of the lymph node represents a small portion of the lymph node during rest however upon peak of plasma cell response to infection this region increases in size. Furthermore, during the course of an immune response, cells such as DCs from

peripheral tissues enter this region carrying antigen and thus during infection this area is densely packed with cells<sup>88</sup>. The main role of the medulla is to clear pathogen and antigen from the lymph; to support the expansion of plasma cells; and then to facilitate the transport of antigen-specific antibodies by way of the efferent lymphatics<sup>89</sup>. MSMs are involved in phagocytosis and the clearance of lymph borne pathogenic material. They are distinguishable by their expression of CD169<sup>+</sup> and F480<sup>+</sup> as well as other markers such as SIGNR1, DC-SIGN, Mac1 and MARCO.

Medullary sinus macrophages also play a role in sensing and acquiring lipids, much like macrophages positioned throughout the periphery. Interestingly, in mesenteric lymph nodes, these macrophages play an important role in the clearance of short chain fatty acids. Indeed, in mice deficient in angiopoietin-like-4 (angptl4), which are unable to process and regulate short chain fatty acids, there is a massive expansion in the size of the mesenteric lymph nodes and they contain numerous lipid laden F480<sup>+</sup> macrophages and giant cells<sup>90</sup>. The interplay between the unique environment of the mesenteric lymph nodes and CD169<sup>+</sup> macrophages will be a theme that I explore in detail later in the Results chapters of this thesis.

The parenchymal regions between medullary sinuses are referred to as “medullary cords”. Within this site are macrophages, lymphocytes, DCs and often blood vessels. Medullary cord macrophages (MCMs) play an important role in the provision of trophic support to plasmablasts and plasma cells, and aid in the clearance of dying plasma cells. In rats, these macrophages are recognisable due to the presence of small lysosomes, and are distinct from medullary sinus macrophages by having homogenous vesicles and low acid phosphatase. MSMs and MCMs can also be distinguished based on their phagocytosing capabilities. After injection of labelled antigen, the major site of antigen localisation is in medullary regions whereas cortical regions are practically free from antigen. This probably represents the fact that MSMs are more efficient at capturing and internalising antigen compared with MCMs. Isolation of MCMs showed that they are major producers of **A P**roliferation-Inducing **L**igand (APRIL) within this region of the lymph node<sup>75,91</sup>.

Overall MCMs and MSMs appear to play distinct roles within the lymph node although their characterisation and distinction is not often clear. Better characterisation, including the identification of subset-specific markers would help the future identification and characterisation of each population.

## **1.5 Innate-like Lymphocytes in Interfollicular Regions of Lymph Nodes**

There are innate-like lymphocytes in lymph nodes that are found in interfollicular regions and that functionally interact with SCS macrophages. These cells are studied in this thesis in relation to deletion of CCRL1 at the SCS.

### **1.5.1 $\gamma\delta$ T cells**

$\gamma\delta$  T cells belong to a group of innate like T cells that contain  $\gamma\delta$  TcRs instead of  $\alpha\beta$  TcRs. They are found in secondary lymphoid organs and the blood where they constitute a relatively low percentage (3-5%) of total lymphocytes<sup>92</sup>. Strategically positioned at the lymph node subcapsular sinus and interfollicular regions (Figure 1.1), these cells are known to be an early source of innate IL-17 production in various autoimmune conditions such as rheumatoid arthritis<sup>93-95</sup>. This early source of IL-17 coupled with their production of IL-21, initiates responses mediated by conventional T<sub>H</sub>17 cells. They are not MHC restricted and do not require CD4 or CD8 co-receptors for antigen recognition. These cells are highly represented in mucosal and barrier tissues such as skin and the small intestine lamina propria<sup>96-98</sup>. They account for around 50% of total intraepithelial lymphocytes in the gut, and play an important role in gut immunology<sup>92</sup>.  $\gamma\delta$  T cells bridge the gap between innate and adaptive immune responses, which is why they are termed innate-like lymphocytes. Furthermore they express a limited repertoire of TCR V-region genes. They have been described as major players in the defence against *Staphylococcus aureus* (*S.aureus*) infection in the skin<sup>99</sup> as well as *Listeria monocytogenes* infection in the liver<sup>84</sup> and *Mycobacterium tuberculosis* (*M.tuberculosis*) infection in the lung<sup>100</sup>.

Some  $\gamma\delta$  T cell subsets have been shown to express MHCII molecules as well as co-stimulatory molecules such as CD28 and so they can act as antigen presenting

cells<sup>101,102</sup>. They have also been implicated in cross presentation of antigen to T cells<sup>103</sup>, in addition to promoting the cross presentation of DCs<sup>104,105</sup>. This highlights their role in bridging innate and adaptive immune responses.

### **1.5.2 Invariant Natural Killer T (iNKT) cells**

iNKT cells were first described as conventional T cells expressing NK cell markers that recognised CD1d restricted glycolipid antigens<sup>106-108</sup>. Similar to  $\gamma\delta$  T cells, iNKT cells have been described as a rich source of IL-17 associated with protection against infection and are also known to be positioned beneath the SCS and within interfollicular regions of lymph nodes<sup>109</sup> (Figure 1.1). iNKT cells are described as playing protective roles during microbial infection but have also been described as playing harmful roles in autoimmune diseases<sup>69,110,111</sup>. They have  $\alpha\beta$  TCRs that undergo somatic recombination and selection in the thymus. Unlike conventional T cells, iNKT cells respond very rapidly to danger signals and as such are said to be in a “poised effector state”. The lipid antigens for iNKT cells identified so far fall into two groups; ceramide-based glycolipids (glycosphingolipids) and glycerol based lipids (such as membrane phospholipids). The first, and best-described ligand for iNKT cells is  $\alpha$ -galatosylceramide ( $\alpha$ GalCer), a derivative from a marine sea sponge and a member of the ceramide-based glycolipids<sup>108,112</sup>. iNKT cells respond to  $\alpha$ GalCer presented in the context of CD1d molecules on the surface of APCs. This CD1d restriction allows these cells to be identified using lipid-loaded CD1d tetramers. They represent around 1-2% of lymphocytes in the mouse spleen and around 20-30% of leukocytes in the liver<sup>113-115</sup>. Within the liver they patrol liver sinusoids and on activation release a cocktail of pro-inflammatory cytokines. iNKT cells can be divided into  $T_H1$ - and  $T_H2$ -like cells depending on their secretory cytokine profile<sup>109,110,116</sup>. Within the liver and spleen,  $T_H1$  iNKT cells predominate and secrete IFN- $\gamma$  after activation<sup>117</sup>.  $T_H2$  iNKT cells are found in the lung and secrete IL-4, IL-9 and IL-13<sup>118</sup>. Finally, a population of  $T_H17$ -like iNKT cells predominate in the skin, lungs and peripheral lymph node<sup>119,120</sup>. They produce IL-17A and express the chemokine receptor CCR6. Within the liver, iNKT cells produce IL-4 and IFN- $\gamma$  in response to  $\alpha$ GalCer, and rapidly produce chemokines

that attract Gr1<sup>+</sup> CD11b<sup>+</sup> cells including neutrophils and monocyte-derived cells<sup>84,121</sup>.

### 1.5.3 NK cells

NK cells were originally discovered in the 1970s and characterised by their ability to kill tumour cells<sup>122</sup>. It is now clear that NK cells are equipped with an armoury capable of tackling more than just tumour cells. NK cells contribute to the innate immune defence against intracellular viruses such as cytomegaloviruses (CMV)<sup>123</sup>. They carry an array of receptors that have the capacity to sense and differentiate between normal and transformed cells as well as detecting virally-infected cells. NK cells are most abundant in the liver, blood and spleen although they are also present to a lesser extent in the lymph nodes<sup>123</sup>. NK cells are poised to defend by constitutively expressing IFN $\gamma$  transcript, although stimulation by type-I interferons IFN $\alpha$  and IFN $\beta$  or pro-inflammatory cytokines such as IL-12, IL-15 or IL-18 is needed for their full maturation. Activation of NK cells by these pro-inflammatory mediators induces the release of IFN $\gamma$  and perforin that is stored in granules. In many instances it is cDCs that are the source of pro-inflammatory mediators that activate the NK cell to produce IFN $\gamma$ . This IFN $\gamma$  then acts on the cDCs to increase their effector functions and so both cell types are involved in an amplification loop. Interestingly, a newly described partnership has been detailed between NK cells and CD169<sup>+</sup> macrophages. In this study it was shown that CD169<sup>+</sup> SCS macrophages are the primary mediators of NK cell activation in response to lymph-borne viral particles<sup>124</sup>. Furthermore these macrophages facilitate the accumulation of these NK cells at the SCS, and depletion of macrophages by administration of clodronated liposomes abolishes NK cell localisation at the SCS<sup>124</sup>. Thus, during infection, these macrophages are critical for the recruitment of NK cells and defence against virus. Understanding the relationship between CD169<sup>+</sup> macrophages, NK cells and  $\gamma\delta$  T cells within the SCS of the lymph node is therefore potentially very interesting.

## **1.6 Lymph Node Development**

As described above, the recruitment of cells to lymph nodes is largely driven by chemoattractants that direct the movement of leukocytes expressing the cognate receptors. Similarly, the development of lymph nodes depends on the discrete and controlled expression of chemotactic guidance cues that mobilise and coordinate the movement of the cells that initiate and drive lymph node development (Figure 1.3). Mice with defective lymph node development display aberrant adaptive immune responses demonstrating the importance of these organs in the immune system.

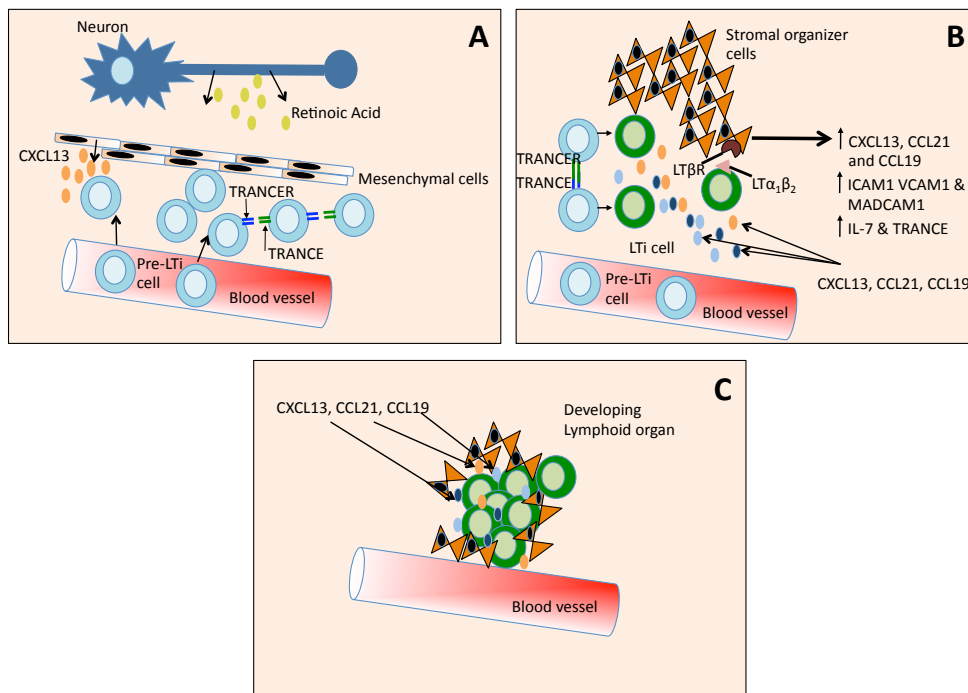


**Figure 1.3 Schematic of lymph node development.**

(A) Retinoic acid produced by neurons induces production of the chemokine CXCL13 in neighboring mesenchymal cells. CXCL13 is then detected by lymphoid tissue inducer (LTI) precursor cells and drives their egress from the blood and migration towards the mesenchymal cells. The clustering of LTI precursor cells promotes the ligation of the cytokine TRANCE with its receptor TRANCER and so signaling via TRANCER ensues. (B) TRANCE-TRANCER interactions induces the expression of lymphotoxin  $\alpha_1\beta_2$  on the LTI precursor cells resulting in their maturation into mature LTI's.  $LT\alpha_1\beta_2$  on LTI cells interacts with  $LT\beta R$  on stromal organizer cells. The stromal organizer cells then produce chemokines CXCL13, CCL19 and CCL21 as well as adhesion molecules ICAM1 and VCAM1. (C) Production of chemokines promotes the recruitment of more haematopoietic cells that then form a cluster. This cluster then matures and develops into a mature lymph node. Figure adapted from Van de Pavert and Mebius, 2010<sup>5</sup>.

In the embryo, lymph node development occurs at the same time as lymphatic vascularisation (which is described in Section 1.7). The systematic formation of lymph nodes occurs within a tight developmental window beginning with the development of the mesenteric lymph nodes at around embryonic day 9-10 (E9-E10). This is followed by the brachial lymph nodes at E13, axillary lymph nodes at E15, inguinal lymph nodes at E16, and finally the popliteal lymph nodes at E17<sup>125 126</sup>. Cytokines, including members of the TNF family of cytokines largely

drive this developmental process and TRANCE and IL-7 are particularly important players in lymph node organogenesis<sup>127,128</sup>. TRANCE (TNF-related activation-induced cytokine, also known as RANKL/OPGL/ODF or TNFSF11) along with its receptor TRANCE-R and TRAF-6, a key member of the TRANCE signalling pathway, are all required for the development of lymph nodes. In mice, deletion of either TRANCE, TRAF-6 or TRANCE-R results in a complete loss of lymph node development although Peyer's patches (PPs) and the spleen develop normally<sup>129,130,131</sup>. In the case of PP development, IL-7 replaces the function of TRANCE. TRANCE is expressed by pre lymphoid tissue inducer cells (pre LTi's) that are recruited to sites of lymph node development by the chemokine CXCL13 which is induced in mesenchymal cells by retinoic acid released by neurons at the site of lymph node development<sup>132</sup>. TRANCE promotes the survival and differentiation of pre-LTi's to mature lymphoid tissue inducer cells (LTis) and up-regulates the expression of  $LT\alpha_1\beta_2$  on the surface of these cells<sup>129,133</sup>. It interacts with  $LT\beta R$  on mesenchymal cells to trigger their differentiation and induce expression of chemoattractant molecules and cell adhesion molecules that are important for recruitment of LTi's<sup>133,134,135,136</sup>. Like TRANCE, IL-7 is also able to induce expression of  $LT\alpha_1\beta_2$  on LTi cells and plays a role in the development and expansion of LTi cells from common lymphoid progenitor cells<sup>130</sup>.

## **1.7 Organisation, Structure and Function of the Lymphatic Network**

I have outlined the development and architecture of lymph nodes, and the immunological importance of cells that reside within them. In order for lymph nodes to perform their function, antigen and APCs must be efficiently delivered from peripheral tissues. This job is performed by lymphatic vessels. The lymphatic system is a network of vessels comprised of small blind-ended capillaries and larger collecting vessels that drain from most soft tissues of the body. Lymphatic vessels can be found in all vascularised tissue in the body except brain and bone marrow. Primary/initial lymphatic vessels are principally involved in collecting tissue fluid. These vessels are composed of LECs containing button-like junctions<sup>137</sup>. Bodily movement such as breathing and

muscle contraction establishes lymph flow. This movement propels the fluid in a unidirectional fashion until it reaches larger collecting lymphatic vessels that contain a series of valves that prevent the backflow of lymph fluid. These vessels are often covered in smooth muscle cells, the contraction which also helps to propel lymph along the vessels.

Afferent lymph is a cocktail of protein, lipids, macromolecules, pathogens and pathogen-derived antigens as well as immune cells such as DCs. An important function of the lymphatic system in the intestine is the absorption of fatty acids. Lymph is filtered through a series of lymph nodes positioned throughout the lymphatic network. Most of the protein and lipids are recycled and returned to the venous circulation through the thoracic duct and finally back to circulation via the subclavian vein. However, one of the most important roles of the lymphatic network is to facilitate the migration of APCs from tissues to lymph node in order to present their antigen to lymphocytes. This migration of DCs is not a passive process but involves the adherence of DCs to the wall of initial and collecting lymphatic vessels before they are then carried by lymph flow in larger lymphatic vessels<sup>52</sup>. Soluble antigen, immune complexes, bacteria and viruses can also transit by way of the lymphatic system and enter draining lymph nodes via the conduit system<sup>6</sup>. In this way the lymphatic vasculature performs a dual immunological function. It acts a highway for cellular transport between peripheral lymph nodes and also as a courier system for the delivery of antigen and antigen bearing cells that drain from peripheral sites. Moreover, the lymphatic vasculature recycles tissue fluid and prevents lymphoedema.

The precise origins of LECs lining these vessels are still not fully understood but it is thought that they originate from endothelial cells in the cardinal vein around E8.5<sup>138</sup>. Blood vasculature develops from embryonic mesoderm in a process known as vasculogenesis. This early development involves a series of morphological and transcriptional changes to give functional specialisation. Lymphatic vasculature is derived from blood vasculature and the differentiation into LECs is thought to be initially driven by the transcription factor CoupTFII followed by expression of the transcription factor Sox18 at day E9.0<sup>139</sup>. Sox18 drives the expression of the transcription factor Prox1, considered to be the lymphatic cell lineage commitment “master switch”<sup>126,140-143</sup>. Subsequently,

these pre-committed cells go through a series of transcriptional changes. This involves the up regulation of various LEC genes and the down regulation of venous endothelial cell markers. The result is that cells then bud-off from the cardinal vein to form primitive structures termed “lymph sacs” and superficial lymphatic vessels<sup>141,144</sup>. Cells from these lymph sacs then migrate outwards and form new vessels. Cells exit the vein at various points in a dorsolateral fashion so that ultimately the lymphatic vasculature develops from anterior to posterior<sup>125,145</sup>. These early lymphatic vessels then undergo remodelling and will eventually give rise to the postnatal lymphatic network. However, differences exist in the development of the lymphatic system between species. In fish, the lymphatic system does not have valves or lymph nodes<sup>125,146</sup> whereas mammals do, while birds have more primitive lymphatic valves and lack lymph nodes<sup>147</sup>. Amphibians and reptiles have lymphatic hearts that pump lymph through the lymphatic vasculature whereas fish, birds and mammals largely rely on muscle contractions and movement for the flow of lymph, although larger vessels have smooth muscle layers that aid in lymph flow.

The formation of new LECs does not stop at birth, and inflammation and tumours can drive the formation of new lymphatic vessels, a process referred to as lymphangiogenesis<sup>85,148-150</sup>. The origins of new LECs remain unclear, and the dogma is that either new LECs occur from pre-existing lymphatic vessels or from progenitors emanating from the bone marrow. An emerging body of work also points to macrophages as major contributors to lymphangiogenesis (Figure 1.4)<sup>85,86,148,150,151</sup>. Macrophages are one of the most prominent cell types involved in the initiation, orchestration and propagation of chronic inflammation. As such, their presence is closely associated with the formation of new lymphatic vasculature. Lymphangiogenesis can be triggered by macrophage-derived inflammatory mediators including members of the vascular endothelial growth factor (VEGF) family, including VEGF-A, VEGF-B and VEGF-C<sup>147,152-154</sup>. VEGF-C operating through VEGFR3 plays a particularly prominent and specific role in lymphangiogenesis while other VEGF family members also stimulate blood vessel growth. Interestingly, as well as contributing to the formation of these vessels by secretion of inflammatory mediators, some reports suggest that

macrophages can also differentiate into lymphatic endothelial cell progenitors (LECP) <sup>155,156</sup> (Figure 1.4).

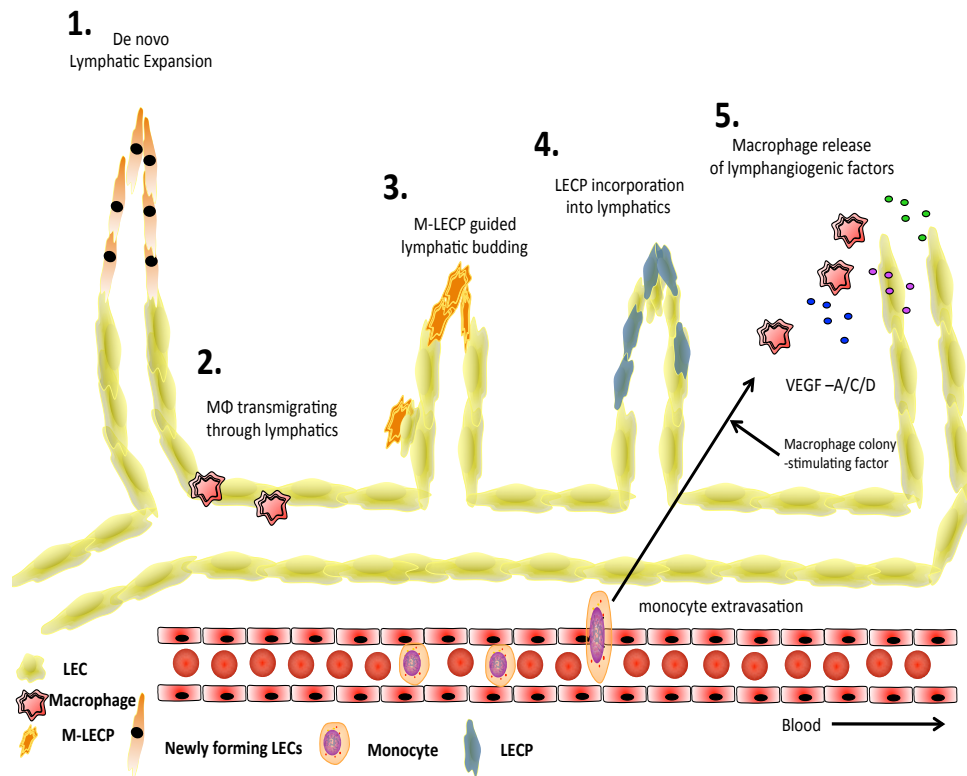


**Figure 1.4: Possible methods of lymphatic vessel expansion during inflammation.**

Lymphatic vessels are thought to expand in a variety of ways, one of which is de-novo expansion (1). The expansion of these vessels can be influenced by macrophages that lie in very close contact with them; such is the case for CD169<sup>+</sup> macrophages in peripheral lymph nodes. It is still unclear whether macrophages incorporate within newly forming lymphatic branches or if they are simply trafficking through these vessels (2). Macrophages secrete a variety of pro-lymphangiogenic factors such as VEGF-A/C and D (5) that support expansion of these vessels. M-LECP (3) and LECPs (4) can contribute to the expansion of lymphatic vessels by guiding the budding of newly forming branches and integrating within newly forming vessel walls (see text for further details).

Early LECPs are bone marrow-derived and express both lymphatic cell markers as well as myeloid markers <sup>156,157</sup>. These cells can, upon stimulation with inflammatory cytokine, differentiate into LECs. Evidence for this differentiation includes the upregulation of LEC markers such as Prox1 and LYVE-1 and the downregulation of stem cell or progenitor markers. LECPs can be derived from

many progenitor types, although several studies point to CD11b<sup>+</sup> monocytes as being the main source. Recently, macrophage lymphatic cell progenitor cells (M-LECPs) have been characterised by *in vivo* analyses and visualisation of cells expressing both myeloid/macrophage markers (CD11b) and lymphatic specific markers (LYVE-1, VEGFR-3 or Prox1). Thus, as M-LECPs express markers of both macrophages and LECs, the term ‘M-LECP’ refers to LECs that are macrophage and not monocyte/bone marrow progenitor derived<sup>85,87,148</sup>. Studies into macrophage driven lymphangiogenesis have been conducted in models of inflammation, including corneal injury and LPS-induced peritonitis<sup>158,159</sup> and M-LECP incorporation into nascent lymphatic vessels has been examined. During LPS-induced peritonitis, it is claimed that up to 80% of new LECs had an M-LECP origin<sup>158</sup>. Furthermore, in several cancer studies, there have been reports that tumour associated macrophages (TAM) positive for myeloid markers CD11b and F480, co-express the LEC marker LYVE-1 suggesting that they can become part of the lymphatic vessel walls<sup>87,160-162</sup>. However, further work is required to determine if these cells actually become components of the lymphatic vessel wall. Nevertheless, it is clear that macrophages are implicated as regulators of lymphangiogenesis. Moreover, it is tempting to speculate that, due to their close proximity to LECs in lymph nodes, macrophages may be important contributors to lymphangiogenesis and lymphatic endothelial cell phenotype in these organs. Conversely, it is conceivable that LECs could regulate the positioning and function of lymph node macrophages. Part of the experimental work described in this thesis explores the relationship between these two cell types.

## **1.8 The Spleen - Structure and Function**

Lymphoid organs such as the spleen and PPs have similarities to lymph nodes but differ in the method of antigen delivery. PPs contain specialised microfold cells (M cells) that sample antigen directly from the intestinal lumen and deliver this antigen to underlying APCs. These APCs then activate B cells and T cells that in turn travel to the mesenteric lymph nodes and the immune response is amplified. These T and plasma B cells then express receptors that home them to the small intestine via the thoracic duct and once in the intestine they perform their effector functions. The spleen is also unique in its architectural organisation

and route of antigen delivery. The spleen is separated into two regions, the red and white pulp with the white pulp architecture similar to B cell and T cell zones found in lymph nodes<sup>163</sup>.

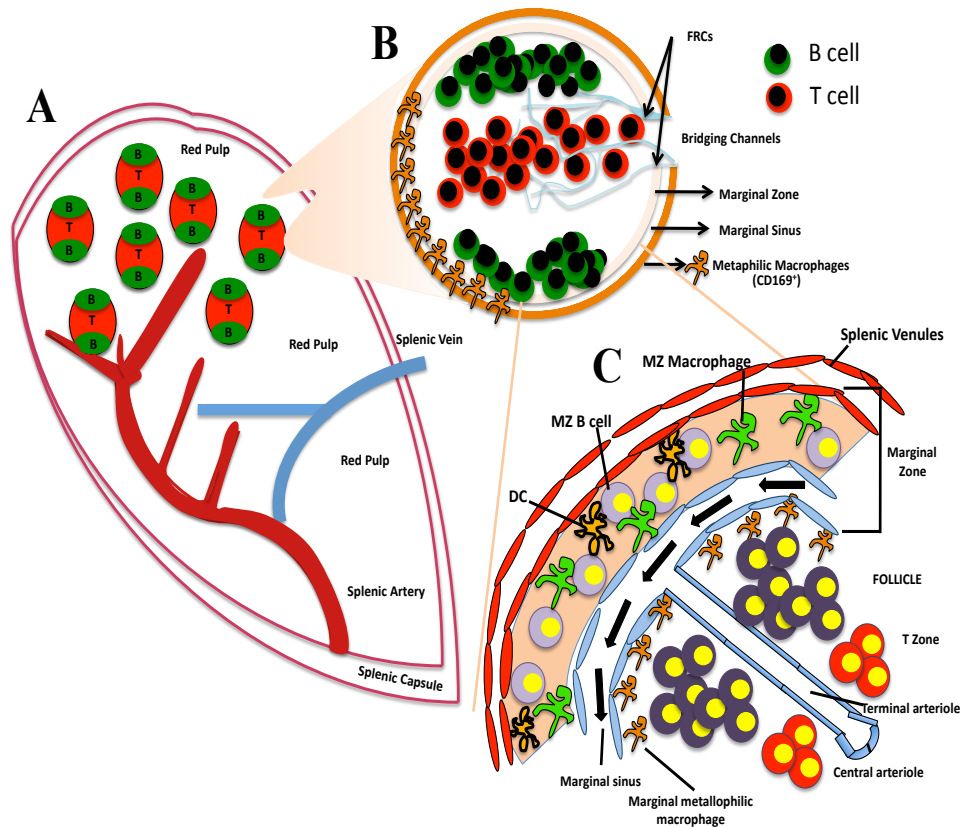


**Figure 1.5: The structure of the spleen.**

The spleen is anatomically distinct from the lymph node and is divided into red pulp and white pulp (A). White pulp harbours T cell and B cell populations and is encompassed by the marginal sinus and the marginal zone. Entry into the white pulp is facilitated by bridging channels as indicated (B). The marginal zone (C) surrounds the white pulp and contains a population of metallophilic CD169<sup>+</sup> macrophages that are functionally related to CD169<sup>+</sup> macrophages that line the SCS of lymph nodes (C). A second macrophage population called marginal metallophilic macrophages is found adjacent to the marginal sinus (see text for further details).

The spleen does not contain afferent lymphatic vessels or M cells for antigen delivery purposes and instead antigen is delivered via the blood that passes through the marginal sinus. Bridging channels, narrow corridors that extend between red pulp and white pulp, are thought to facilitate cellular entry into the white pulp from splenic venules (Figure 1.5 B). They are rich in FRCs that

produce the chemokine CCL21 and this guides CCR7<sup>+</sup> T cells into periarteriolar lymphoid sheaths (PALS). The red pulp contains a network of veins that bestows the spleen with important blood filtering capabilities. Within this region arterial blood is pumped in and arrives at splenic cords present in the red pulp. These cords are open-ended and are composed of reticular fibres and fibroblasts<sup>164</sup>. They are home to large populations of F480<sup>+</sup> macrophages that assist in the spleen's blood filtering capabilities, removing old erythrocytes and recycling iron<sup>165,166</sup>. Furthermore, by sequestering iron, these macrophages starve pathogens that depend on iron for growth. In addition to red pulp macrophages, the spleen is home to marginal zone macrophages (MZMs) and marginal metallophillic macrophages (MMMs) both of which reside near the marginal sinus at the edge of the white pulp (Figure 1.5 C). MZMs and MMMs can be distinguished by expression of SIGNR1 and CD169 respectively, and in many respects these macrophages are functionally similar to the lymph node macrophages discussed earlier (Section 1.3.2). Both MZMs and MMMs have roles in the capture of antigen, viruses and microbes from the blood. MZMs have also been shown to regulate retention of MZ B cells. MMMs have been shown to produce large amounts of type I interferon after viral infection<sup>167</sup>.

The white pulp is home to T and B cell compartments that are organised in a way that closely resembles the structure of lymph nodes. Splenic T cell zones are home to both CD8<sup>+</sup> and CD4<sup>+</sup> T cells as well as DCs and contain a network of FRCs upon which the T cells move<sup>164</sup>. Splenic B cell follicles mirror lymph node B cell follicles and contain a network of FDCs. As in lymph nodes, chemical guidance cues direct the movement and localisation of B cells and T cell in the splenic white pulp and are important for the establishment of discrete B cell and T cell zones.

Collectively, the lymphoid tissues described above help to contain the spread of pathogens and facilitate the propagation of adaptive immune responses. These tissues function by bringing together APCs, pathogen, immune complexes, antigen and effector cells to expel foreign bodies. However, immune responses to pathogens are often initiated in peripheral tissues where pathogen enters the host. These peripheral tissues contain a unique and highly specialised array of innate and adaptive immune cells that protect the host from pathogen and that are

critical for maintenance of self-tolerance. This thesis explores the role of immune cells present in the skin, and how these cells migrate to lymph nodes during homeostasis and inflammation.

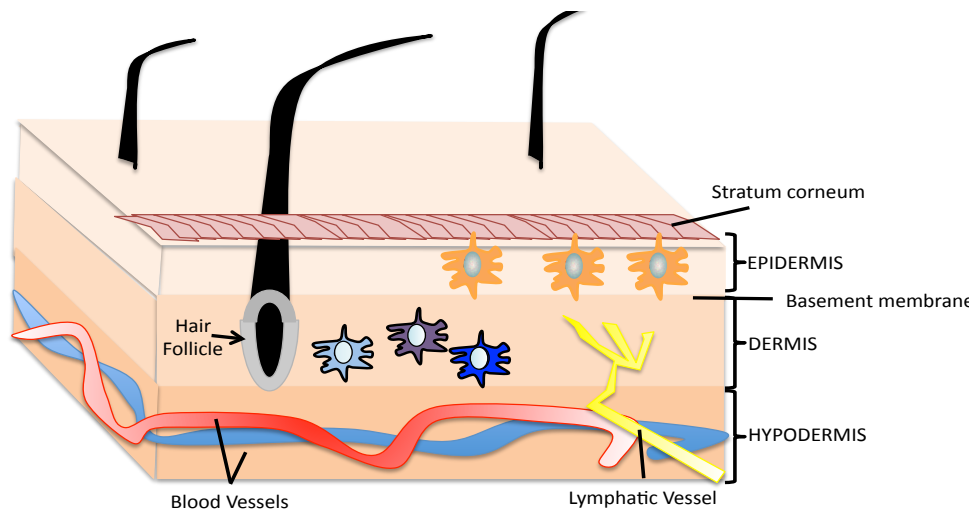
## 1.9 The Skin

The skin is the largest organ in the body and forms a key interface between the body and the external environment. As such, the skin needs to be equipped with an array of defense mechanisms to prevent infection and limit the spread of pathogens that breach this barrier site. Defending the body across the entirety of this large organ presents its own unique challenges and requires the interplay between immune sentinels, effector cells and non-immune mechanisms to protect against microbial, physical and chemical insult. The skin contains two main compartments, the epidermis and the dermis with each compartment harbouring distinct populations of leukocytes. The epidermis is primarily composed of keratinocytes and develops from ectoderm during embryonic development<sup>168,169</sup>. Keratinocytes provide structural support and act as scaffolding. They also produce chemoattractant molecules and help shape the response to exogenous antigen. Furthermore keratinocytes produce the stratum corneum that is present in the outer most layer of skin and which is water impermeable. Residing within the epidermis is a population of dendritic cells called Langerhans cells. During homeostasis, Langerhans cells are the only DC population present in the epidermis although other leukocytes, such as T cells, are present. Specialised intraepithelial lymphocytes (IELs) called dendritic epidermal T cells (DETCs) are localised in the epidermis<sup>97,170,171</sup>. Making up the majority of these cells in mice and humans are  $\gamma\delta$ T cells that contribute to the epidermal immune system and wound repair. Lying underneath the epidermis is the dermis, a sparsely populated tissue home to fibroblasts and a variety of immune cells including macrophages, T cells, NK cells and DCs. The dermal DC (dDC) populations within this location are more heterogeneous than those found in the epidermis<sup>172-174</sup>. All these distinct skin resident DC lineages are capable of migrating to lymph nodes to propagate peripheral tolerance to skin derived self-antigens and to initiate immune responses to exogenous pathogen-derived antigens. In the dermis, T cells are situated in very close proximity to postcapillary venules just

below the epidermal/dermal barrier. Memory T cells predominate with a roughly 50:50 mix of CD4 and CD8 T cells<sup>175,176</sup>.

### **1.9.1 Skin DCs**

Langerhans cells were considered to be the predominant dendritic cell type in the skin that transports antigen to draining lymph nodes. However, recently the complexity of the skin DC compartment has become apparent and multiple DC populations have been identified in the dermis (Figure 1.6). For the purposes of this thesis, I will describe skin resident DCs as being either Langerhans cells or dermal DCs (dDCs). Within this dDC population there exist different subsets that can be identified by flow cytometry using a combination of intracellular and surface markers.



CELL TYPE	SURFACE MARKERS	LOCATION
Langerhans cell	CD11c <sup>+</sup> MHCII <sup>hi</sup> Langerin <sup>+</sup> CD103 <sup>-</sup> CD11b <sup>+</sup> EpCAM <sup>+</sup> CD24 <sup>+</sup>	Epidermis
Dermal DC	CD11c <sup>+</sup> MHCII <sup>hi</sup> Langerin <sup>+</sup> CD103 <sup>+</sup>	Dermis
Dermal DC	CD11c <sup>+</sup> MHCII <sup>hi</sup> Langerin <sup>-</sup> CD103 <sup>+</sup>	Dermis
Dermal DC	CD11c <sup>+</sup> MHCII <sup>hi</sup> Langerin <sup>-</sup> CD103 <sup>-</sup>	Dermis

**Figure 1.6: The structure and DC composition of the skin.**

The skin is anatomically arranged into distinct compartments with the epidermis and the dermis forming the two main compartments. Within both the epidermis and the dermis are distinct populations of DCs, identifiable by their expression, or lack of expression, of various surface markers. Langerhans cells reside within the epidermis and express CD11c, MHCII, Langerin, CD11b, EpCAM, CD24 and lack CD103 expression. The dermis is home to four DC populations that all express CD11c and MHCII but that differ in their expression of Langerin and CD103.

### 1.9.2 Epidermal Langerhans Cells

Langerhans cell precursors first populate the epidermis at E18 and proliferate *in-situ*. They are among the first DCs to come into contact with exogenous antigen and pathogens. Unlike classical DCs, Langerhans cells are a self-renewing population of DCs that are radio-resistant. They are in direct contact with keratinocytes and extend their dendrites horizontally and vertically to increase their antigen capture capability. They are easily identifiable by their anatomic location, the presence of characteristic Birbeck granules, and because they are the only cell that expresses MHCII in the epidermis. Markers of Langerhans cells include CD11c, MHCII, EpCAM, Langerin and CD11b<sup>59,177,178</sup>. Notably Langerhans cells lack CD103 expression. This is important, as it is now known

that Langerin, once considered a Langerhans cell specific marker, is also expressed by other cutaneous DC populations. Therefore, during analysis by flow cytometry, lack of CD103 but expression of CD11c, Langerin and MHCII can identify a population of Langerhans cells. For the purposes of this thesis I identify Langerhans cells as being CD11c<sup>+</sup>, MHCII<sup>hi</sup>, Langerin<sup>+</sup> and CD103<sup>-</sup>.

Langerhans cells constitutively migrate from the skin to lymph nodes carrying self-antigen and thus are likely to be involved in the maintenance of peripheral tolerance. Similar to classical migratory DCs, Langerhans cells localise in T cell zones of lymph nodes and present their antigen on MHCII molecules. After topical application of chemical irritants, such as FITC, their migration from the skin is enhanced<sup>179</sup>. It remains to be elucidated whether Langerhans cells propagate or dampen immune responses. One group has reported that Langerhans cells are unable to generate a protective CD8<sup>+</sup> T cell response to HSV-1<sup>180</sup>, whilst others have shown by Langerhans cell depletion that they are required to prevent disproportionate contact hypersensitivity (CHS) responses indicating a role for Langerhans cells in tolerance<sup>181</sup>. However, Batf3<sup>-/-</sup> mice, that lack CD103<sup>+</sup> dermal DCs but retain Langerhans cells, develop normal CHS responses<sup>182</sup>. Other work using K5.mOVA mice, in which keratinocytes express a membrane form of OVA, Langerin<sup>+</sup> CD103<sup>+</sup> dermal DCs were reported to be the only skin DC subset able to cross present OVA *in vitro* and *in vivo*<sup>183</sup>. They were also described as the only skin DC population to transport keratinocyte antigen and present it to CD4<sup>+</sup> T cells. Furthermore, in adoptive transfer experiments, OVA-specific naïve T cells transferred into K5.mOVA mice were shown to differentiate into Treg-cells<sup>183</sup>. In bone marrow chimera experiments in which only radioresistant Langerhans cells or radiosensitive migratory dDCs expressing CD205 had access to the antigen, it has been deduced that Langerhans cells are as efficient as Langerin<sup>+</sup> dDCs at inducing Treg differentiation<sup>184</sup>. Taken together, these observations have made the field of skin-DC biology confusing, and further experiments are needed to clarify and distinguish between the roles of dermal DCs and Langerhans cells in adaptive immunity. Much of the contradiction and controversy regarding the role of Langerhans cells in immune responses has arisen due to earlier reports mistakenly identifying dDC populations as Langerhans cells. In 2007, Valladeau and Saeland described

Langerin as a Langerhans cell-specific marker<sup>185</sup>. This inspired the genetic engineering of Langerin-eGFP and Langerin-DTR mice for the study of Langerhans cells. Langerin-DTR mice contain a human diphtheria toxin receptor driven by the expression of the Langerin gene, that allows for the selective depletion of Langerin<sup>+</sup> cells after the injection of diphtheria toxin into these mice. Langerin-GFP mice express eGFP under the control of the Langerin promoter and so all Langerin<sup>+</sup> cells express eGFP. However, as mentioned previously, it is now understood that a population of dDCs also express Langerin. Moreover, Langerin is also expressed by DCs at other anatomical sites such as the spleen and the lung<sup>186</sup>. Therefore, conclusions drawn about epidermal Langerhans cells in publications utilising Langerin-GFP and Langerin-DTR mice strains must be treated with some caution.

The kinetics of Langerhans cell arrival at skin draining lymph nodes in response to cutaneous inflammation are well characterised. Typically, Langerhans cells arrive later than dDCs, and do not reach the lymph node until around 72 hours after the induction of inflammation<sup>187</sup>. This is probably due to the time that these cells need to cross the basement membrane and connective tissue that separates the epidermis from the dermis, and to migrate towards, and into, lymphatic vessels in the skin. In contrast dDCs are positioned in the dermis much closer to skin lymphatics therefore their journey time is much shorter<sup>187</sup>. During constitutive trafficking and also during inflammation Langerhans cells are guided from the skin to skin-draining lymph nodes by interacting with chemotactic cytokines released by lymphatic vessels<sup>54,188,189</sup>. These are discussed in more detail in Section 1.12.

### **1.9.3 Dermal DCs**

The dermis is home to a variety of DC subtypes, identifiable by their expression of surface markers. The most simplified classification of dDCs is based on Langerin expression along with CD11c and MHCII expression, which subdivides them into Langerin<sup>+</sup> dDCs and Langerin<sup>-</sup> dDCs. In contrast to Langerhans cells, Langerin<sup>+</sup> dDCs in adults are bone marrow-derived. Like Langerhans cells, Langerin<sup>+</sup> dDCs migrate to skin-draining lymph nodes constitutively and also in response to inflammation<sup>172,187,190</sup>. Typically, they arrive in the lymph node

around 18 hours after challenge<sup>187</sup>. They are also in a high state of flux and are constantly replaced by blood monocytes<sup>190</sup>. dDCs colonise particular microanatomical niches within the paracortical zones of the skin-draining lymph nodes. It is thought that both Langerin<sup>+</sup> and Langerin<sup>-</sup> dDCs migrate to draining lymph nodes after hapten sensitisation however, only Langerin<sup>+</sup> CD103<sup>+</sup> dDCs can cross present antigen to CD8<sup>+</sup> cytotoxic T cells<sup>191</sup>.

The dermis is also home to a population of pDCs that are rare in healthy skin but have been implicated in diseases such as psoriasis<sup>192</sup>. Skin pDCs, through their expression of TLR9, have been shown to respond to self-DNA released by dying cells and which is coupled to cathelicidin LL37<sup>193</sup>. This can result in the breakdown of tolerance to self-DNA and secretion of type I interferon by the pDCs and the consequent activation of the adaptive immune response. The current model of pDC involvement in psoriasis therefore is focused on this interaction of LL37 with self-DNA. The model proposes that skin trauma results in the release of self-DNA from dying/damaged cells that then couples to LL37. These LL37/self-DNA complexes are then acquired and taken up by pDCs that become activated via TLR9 to produce type-I interferon that subsequently activates autoreactive T cells in the skin. This activation of autoreactive T cells then propagates the development of psoriasis.

Collectively, these studies reveal the complexity of the DC network present in the skin that gives rise to a diverse range of immunological responses. These DCs are of paramount importance in maintaining peripheral tolerance to skin-derived self-antigens, and play a key role in the induction of protective immune responses to pathogens entering the skin. However, they can also be the driving force behind the propagation of immune pathologies in diseases such as psoriasis.

#### **1.9.4 Skin Resident T cells**

The skin is home to a large heterogeneous population of T cells and in humans contains around twice as many T cells as the blood. Skin resident T cells are thought to play an important role in skin immune homeostasis and pathology. Skin resident memory T cells are positioned in the epidermis and provide the

first line of defence against secondary antigen challenge. In the epidermis, CD8<sup>+</sup> αβ T cells predominate, most of which are memory cells, and these cells are in close contact with epidermal Langerhans cells.

The three main CD4<sup>+</sup> T helper cell subsets (T<sub>H</sub>1, T<sub>H</sub>2 and T<sub>H</sub>17) can be found in the skin during inflammation. T<sub>H</sub>1 cells are commonly associated with autoimmunity such as psoriasis<sup>194-196</sup> whereas T<sub>H</sub>2 cells are thought to be linked to allergic diseases such as atopic dermatitis<sup>197,198</sup>. However recently, characterization of T<sub>H</sub>17 cells have shown these cells to be involved in both aforementioned conditions challenging our understanding of the propagation of these diseases<sup>98,195,199</sup>. More recently, cutaneous CD4<sup>+</sup> memory T cells have been shown to be composed of recirculating memory T cells and a population of T cells that remain in the skin<sup>175</sup>. These T cell populations are phenotypically and functionally distinct from each other in terms of surface antigen expression, positioning and effector functions.

The skin is also home to populations of unconventional T cells, namely γδ T cells and iNKT cells. γδ T cells in the skin of mice perform a variety of functions, including negatively regulating skin cancer and inflammation<sup>98,200-202</sup>. However less is known about the role of these unconventional T cells in humans. It is known that in patients with melanoma, leprosy, psoriasis and cutaneous leishmaniasis that the number of γδ T cells is increased, suggesting that these cells may be involved in these skin conditions. Additional roles for these cells include wound repair and the secretion of growth factors, such as keratinocyte growth factor (KGF). They also contribute to microbial defense by producing antimicrobial peptides (AMPs), including cathelicidins<sup>171</sup>. iNKT cells were first described in the plaques of human psoriasis patients<sup>203</sup>. Although in normal skin keratinocytes express very low levels of CD1d molecules, in the plaques of psoriasis patients expression of CD1d is significantly increased<sup>204</sup>. This would suggest that self-derived glycolipid antigen can be presented in the context of CD1d molecules to iNKT cells that in turn could activate neighbouring keratinocytes. In this way iNKT cells might contribute to pathology in psoriasis. During infection it has been proposed that iNKT cells are specialised in recognising bacterial-derived glycolipids. In this context, iNKT cells may

function as immune sentinels and play a protective role in the skin against microbial colonisation. Collectively it is clear that both conventional and unconventional skin resident T cells play an important role in the defence of the skin against pathogen dissemination but also in mediating pathologies that arise in various skin conditions.

This section of the introduction has explored the structure and function of secondary lymphoid tissues, particularly the lymph node, and described the different leukocyte populations that are present in the skin. Throughout, it is clear that the migration of leukocytes between, and within, these tissues, is a fundamental process critical for the correct functioning of the immune system. In the next section, I explore key molecules involved in directing cell migration, namely the chemokine family.

## **1.10 Chemokines**

Chemokines are small, secreted chemotactic cytokines that mediate their effects via G protein-coupled receptors (GPCRs). They play an important role in immune homeostasis<sup>135</sup>, inflammation<sup>205</sup>, embryogenesis<sup>206</sup> and cancer metastasis<sup>207</sup>. They are instrumental in driving lymphoid tissue compartmentalisation, regulating the localisation of cells, and directing the migration of leukocytes into and within lymphoid tissues. Chemokines regulate the development of the immune system, and play a central role in driving innate immune responses, adaptive immune responses, tolerance and memory. The chemokines identified to date fall within one of four sub-families (CC, CXC, XC and CX3C) defined by positional variations of conserved cysteine residues (Figure 1.7). Chemokine proteins have a highly conserved secondary structure although they can vary considerably in amino acid sequence<sup>208</sup>. The primordial function of chemokines was probably to regulate embryogenesis and stem cell migration. Modern day vertebrates have evolved to possess over 40 chemokines and 18 chemokine receptors, and there is a high degree of promiscuity amongst chemokines and their receptors<sup>209</sup>. There is considerable variation between species. For example, chemokines CCL12, CCL6 and CCL9 are found in mice but not in humans whereas CCL3L1, CCL23, CCL18, CCL13 and CXCL8 are found in humans but not in mice. Chemokines can be broadly classified into two

groups depending on whether they play a role in basal homeostatic cellular trafficking or are induced in response to inflammatory stimuli and regulate cell migration during inflammation. However, it is now becoming clear that there exists some crossover within this over-simplified classification<sup>210</sup>. Notably however, chemokine and chemokine receptor promiscuity exists primarily within the inflammatory group of chemokines and chemokine receptors (Figure 1.8). Chemokines usually activate signal transduction after binding their cognate receptors, but some chemokines are natural chemokine receptor antagonists (Figure 1.8 B), and this can be introduced into a chemokine after protease mediated clipping (Section 1.10.2)

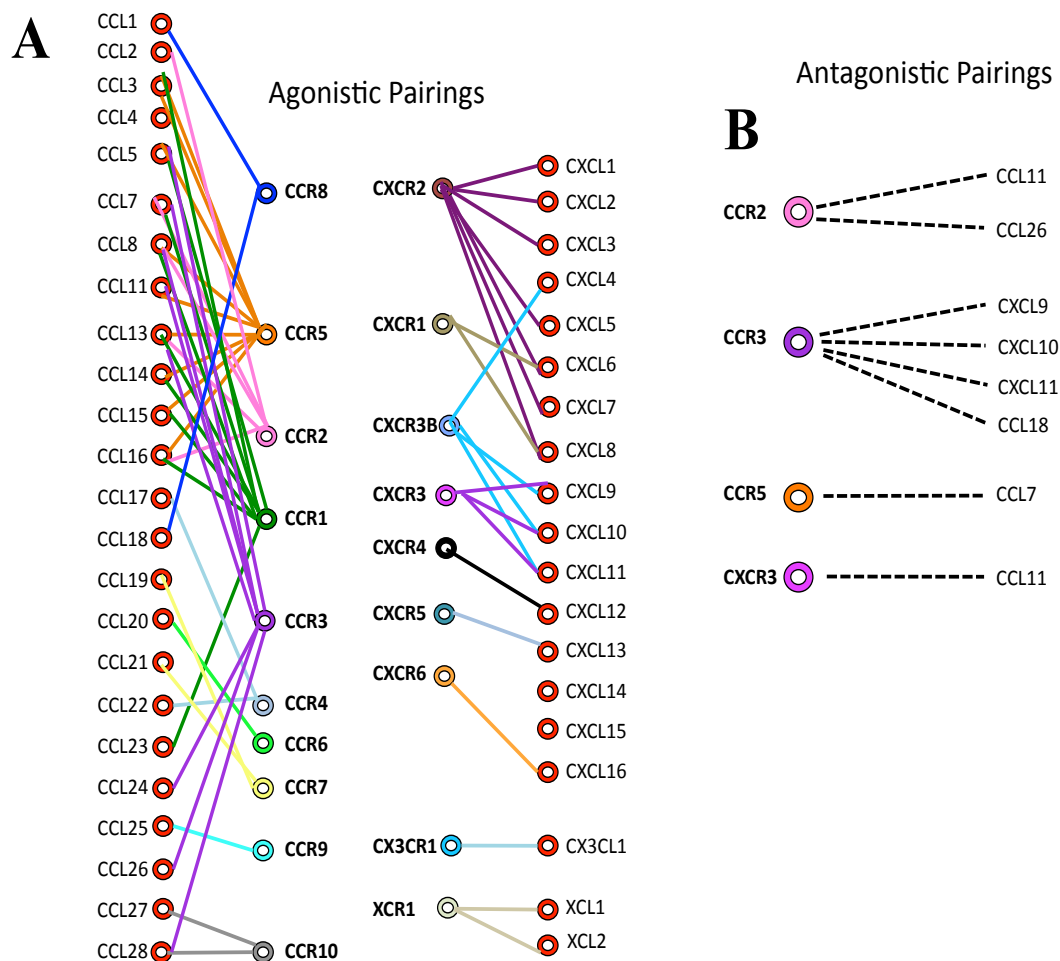


**Figure 1.7: The human chemokine network.**

Human chemokines receptors and their corresponding chemokines are grouped according to their agonistic binding patterns (A) and their antagonistic pairings (B). There are four subfamilies of chemokines CC, CXC, C and CX<sub>3</sub>C chemokines, each of which are shown. The diagram above was adapted from Rot *et al*, Annual Reviews of Immunology 2004<sup>210</sup>.

### **1.10.1 Inflammatory and Homeostatic Chemokines**

Inflammatory chemokines (Figure 1.8) recruit leukocyte effector cells to specific areas of pathogen invasion, inflammation and tissue damage. Generally, inflammatory chemokines are not normally expressed at significant levels during basal conditions although ‘inflammatory’ chemokines that bind to CCR2 have been demonstrated to drive bone formation and monocyte release from bone marrow at rest<sup>211,212</sup>. Upon inflammation, inflammatory chemokines are abundantly produced by leukocytes and tissue cells that participate in the inflammatory response. Inflammatory chemokine receptors and chemokines are generally considered to be promiscuous, with each receptor capable of binding many chemokines and each chemokine acting as a ligand for many receptors. CCL5 is an example of a versatile inflammatory chemokine able to act on at least three chemokine receptors (CCR1, CCR3 and CCR5).



These chemokine/receptor pairings are of particular relevance to this thesis and their function within the immune system will be discussed in depth later in this Introduction.

It is becoming increasingly clear that some chemokines are able to function as both homeostatic and inflammatory chemokines and as such are termed ‘dual function’ chemokines (Figure 1.8). These chemokines play a role in the localization and homing of cells during homeostasis but are also upregulated in certain contexts during inflammation to facilitate cellular migration. In fact, the classification of chemokines as ‘inflammatory’ or ‘homeostatic’, while useful in pinpointing the dominant context in which individual chemokines operate, is somewhat archaic and it is possible that most chemokines contribute to a greater or lesser extent to homeostatic and inflammatory leukocyte trafficking.

### **1.10.2 Protease Regulation of Chemokine Function**

Chemokines can be cleaved by several means to give rise to smaller truncated versions of full-length chemokine. Protease clipping of chemokine N-terminus can produce chemokines with increased, decreased or unchanged activity for their cognate receptor. Furthermore, chemokine clipping can lead to the introduction of antagonist activity or alter receptor specificity. In the case of CCL4, proteolytic cleavage of two N-terminal residues by CD26 influences how the resulting chemokine fragment interacts with chemokine receptors CCR1 and CCR2, however CCL4/CCR5 interactions are unaffected<sup>213,214</sup>. Many chemokines are secreted and soluble, but CXCL16 and CX3CL1 are expressed in membrane bound forms, anchored in the plasma membrane via mucin-like stalks. It is understood that proteases can cleave these chemokines so they can be shed from the cell surface allowing them to behave like soluble chemokines and inducing chemotaxis in responding leukocytes instead of cellular adhesion.

### **1.10.3 Chemokine Interactions with Glycosaminoglycans (GAGs)**

Generally, in order for chemokines to mediate their biological function, they must be secreted and then diffuse from their source in order to be sensed by leukocytes. To perform such a task, chemokines must be soluble and remain in this state. However, chemokines are known to interact with sulphated sugars

known as glycosaminoglycans (GAGs)<sup>215-220</sup>. These sugars include chondroitin sulphate and heparan sulphate, both of which are expressed on the surface of most cells. GAGs decorate the surface of cell walls and the extracellular matrix and it is here that they bind chemokine. Due to the diverse array of binding motifs that chemokines use for GAG binding, there exists a degree of specificity of GAG molecules for binding to chemokine<sup>221</sup>. These sulphated sugar molecules are involved in the immobilisation and presentation of chemokines. It has also been suggested that GAG molecules may be involved in the transcytosis of chemokine from basal to apical endothelial cell surfaces<sup>222</sup>. As yet, it is still unclear as to the nature of chemokine signalling via GPCRs when they are coupled to GAGs. However, as haptotaxis, haptokinesis and extravasation do not occur efficiently without GAG immobilisation of chemokine, it can be inferred that chemokines can signal when bound to GAG molecules.

The importance of GAG molecules to the functionality of chemokines has been exemplified by studies looking at mutated chemokines disrupted specifically at GAG binding domains. These chemokines have been shown to lack function *in vivo*<sup>218,223</sup>. Chemokine mobilisation and immobilisation mediated by GAGs could also be a key mechanism by which chemokine is either 'seen' or 'unseen' by leukocytes. Uncoupling of chemokine from GAGs could reveal a previously unseen chemokine to leukocytes in the direct microenvironment. However, detachment of chemokines from GAGs could remove chemokine from immobilised locations, causing the chemokine to dissipate from this localised site and thus interacting leukocytes are no longer able to sense it. It is known that for the rolling adhesion of leukocytes along endothelial cell surfaces and their subsequent diapedesis, chemokine immobilisation on GAGs is necessary (a process discussed in more depth later (Section 1.12)). This has been shown experimentally whereby leukocytes were shown to display a more rapid degree of integrin activation and adhesion in response to immobilised chemokine on the surface of endothelial cells compared with soluble chemokine. This also explains how leukocytes are able to sense chemokine in the vasculature, without the chemokine being washed away by the blood.

## 1.11 Chemokine Receptors

The specific effects that chemokines exert on a cell are mediated through their interactions with their cognate receptors<sup>209,210,224</sup>, which are 7-transmembrane spanning GPCRs (Figure 1.9), They are part of the rhodopsin family of GPCRs, the largest of the five GPCR families described.

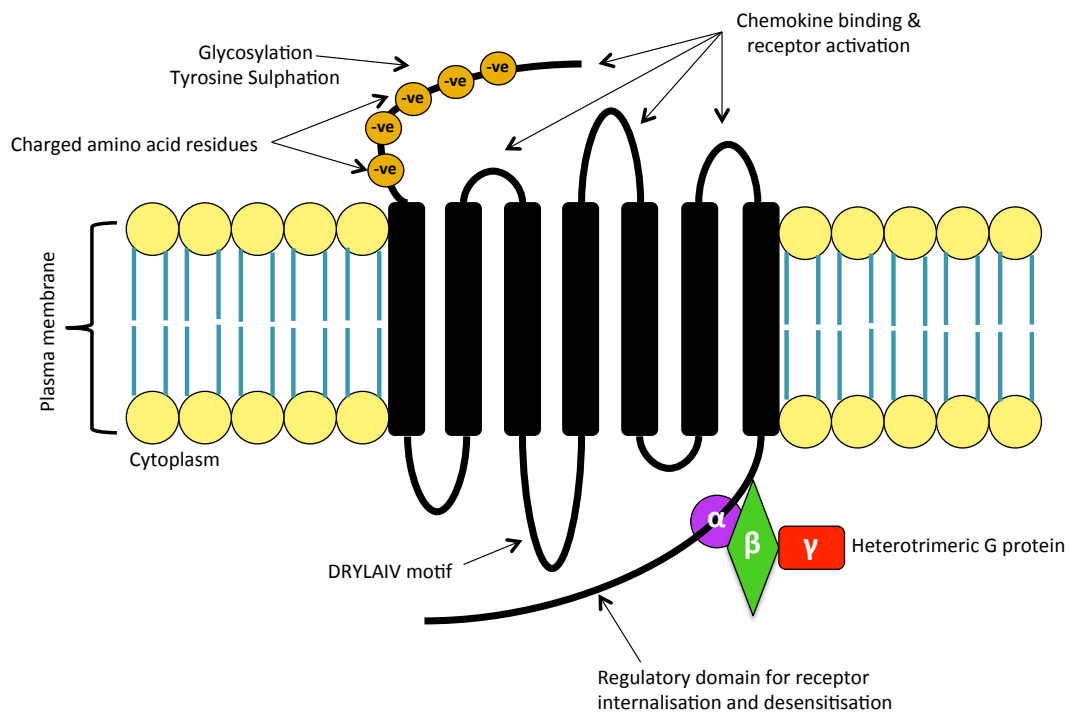


**Figure 1.9: Schematic of a chemokine receptor.**

Chemokine receptors are 7-transmembrane proteins that contain a canonical DRYLAIV motif in the second intracellular loop that aids coupling to heterotrimeric G proteins. Chemokine binding occurs via the four extracellular domains and induces intracellular signaling mediated with heterotrimeric G proteins. Glycosylation and tyrosine sulphation of the N-terminus of the receptor increases the negative charge in this region and aids in interactions with positively charged regions of the chemokine.

To date there have been 18 chemokine receptors characterised; 1 CX3C chemokine receptor (CX3CR1), 1 XC chemokine receptor (XCR1), 6 CXC chemokine receptors (CXCR1-CXCR6), and 10 CC chemokine receptors (CCR1 to CCR10) (Figure 1.7). The receptors are named according to the subfamily of

chemokines they bind (thus CCR chemokine receptors bind CC chemokines and so forth) and numbered according to when they were discovered. We generally think of chemokine receptors being faithful to their corresponding subfamily of chemokine ligand, that is to say that CC chemokine receptors bind only CC chemokines and so on<sup>209</sup>. However, this is not strictly true for all of the chemokine receptors, and we now understand that there is some degree of cross-family interaction and that some chemokine receptors are not faithful within their own chemokine family. For example, CCR3 can bind agonistically to CCL5, 7, 11, 13 15, 24 and 26 but can also bind antagonistically to CCL8, CXCL9, 10 and 11 (Figure 1.7).

Chemokines receptors are typically around 350 amino acids long with three extracellular and three intracellular hydrophilic loops, along with an intracellular carboxy terminus which contains important serine (ser) and threonine (thr) residues that are important for desensitisation and internalisation of the receptor<sup>225-227</sup> (Figure 1.9). A disulphide bond forms between the first two extracellular loops of the chemokine receptor and between loop 3 and the N-terminal tail. The extracellular N-terminal region of the chemokine receptor, which is rich in charged amino acid residues and sulphated tyrosines, is important for tethering its chemokine ligand to allow it to engage chemokine to engage transmembrane domains with its N-terminus (Figure 1.9). This leads to a conformational change in the receptor that initiates signal transduction. The intracellular loops couple to the signal transduction machinery of the cells and the DRYLAIV amino acid motif in the second intracellular loop of the receptor is of particular importance in this process and perpetuates coupling of the activated receptor to heterotrimeric G-proteins<sup>228-230</sup>.

As mentioned previously, chemokine receptors are often promiscuous with regards to the ligands they bind, with many of the pro-inflammatory chemokine receptors binding to more than one chemokine ligand (Figure 1.7). In contrast, receptors for homeostatic chemokines are restricted to one or two chemokines. This has led to the suggestion of chemokine receptor redundancy within the inflammatory chemokine receptor network. Others argue that the ability of chemokine receptors to bind many ligands is a selective advantage to the host and is a result of evolutionary pressure from pathogens, many of which have the

capability to disrupt components of the pro-inflammatory chemokine networks. Therefore, by having chemokine receptors that bind to multiple ligands and ligands that bind multiple receptors, robust responses to pathogens are ensured and the attraction of effector cells is maintained in order to mediate pathogen clearance.

Chemokine receptors and other GPCRs have been shown to homo and hetero-oligomerise: for example CCR5 homo-oligomerises, and CCR2 and CCR5 hetero-oligomerise. This is thought to influence the signalling events that proceed after ligand binding and can affect the strength of signalling. Interestingly, some atypical chemokine receptors have been shown to hetero-oligomerise with classical chemokine receptors and the significance of this pairing will be discussed later in this thesis.

### **1.11.1 Chemokine Receptor/Ligand Interactions and Signalling**

Chemokines are known foremost for their capacity to induce cell migration. Indeed chemokines were named because of their ability to induce chemotaxis *in vivo*: **chemotactic cytokines**. However this is an over simplification of their role and does not fully explain the multitude of effects that chemokines can impose on cells. Downstream effects after chemokine receptor/ligand interactions include integrin activation, adhesion, migration, cell survival and respiratory burst<sup>231-233</sup>. All of these effects are achieved by intracellular signalling after chemokine ligand binding to GPCRs. Directed cellular migration requires actin polymerisation which induces cellular polarity within the cell whereby the cell adopts a “leading edge” known as a pseudopod and a “tail” known as a uropod<sup>234-236</sup>. Chemokine receptor signalling ultimately results in the rearrangement and remodelling of the cytoskeleton of the responding cell that accounts for the induction of cellular motility and the morphological changes of the cell. Intracellular signalling induces cellular polarisation whereby the cell clusters its chemokine receptors at a leading edge and simultaneously reorganises adhesion molecules such as ICAM-1 and ICAM-3 to a trailing edge<sup>237</sup>. Further work on the dynamics of pseudopod establishment has revealed that pseudopods are not formed specifically during chemotaxis, but are also present during chemokinesis, or random cell movement<sup>238</sup>. It has been shown that should the

chemokine gradient a cell is sensing be reversed, the cell then re-establishes its pseudopod to the tail region, or maintains its current pseudopod but completes a U-turn to sense the new established gradient. This idea displays the idea that pseudopods are specialised structures involved in the sensing of chemokine gradients by leukocytes. This dynamic process of cytoskeletal remodelling and motility is mediated by small GTPases including RhoA and Rac<sup>239</sup>.

Both chemokine and chemoattractant receptors use heterotrimeric G-proteins in order to transduce signals intracellularly. These G-proteins are comprised of  $\alpha$ ,  $\beta$ , and  $\gamma$  subunits.  $G\alpha$  subunits can exist both as trimeric complexes with  $G\beta\gamma$  or as free entities independent of  $\beta$  and  $\gamma$  subunits. G-protein coupled chemokine receptor activation by chemokine ligand results in a conformational change in the receptor. The GPCR acts as a guanine nucleotide exchange factor (GEF) for  $G\alpha$  subunits, which release GDP, binds GTP and activates downstream signalling cascades<sup>240-242</sup>. However, it is probably the free  $\beta\gamma$  heterodimer that mediates much of the downstream signalling after GPCR activation<sup>243</sup>.

Upon chemokine receptor ligation with its cognate chemokine ligand, the receptor/ligand complex is usually internalised<sup>244,245</sup>. Under basal homeostatic conditions chemokine receptors undergo internalisation and degradation/recycling, however chemokine binding induces a greater degree of internalisation and intracellular trafficking of the receptor. Receptor down-modulation results in a reduction in the expression of chemokine receptors on the cell surface and is a well-characterised process seen across the GPCR superfamily. The method by which the receptor undergoes internalisation can take two forms: clathrin-mediated endocytosis or lipid raft caveolae-dependent internalisation. While some chemokine receptors may utilise one form of internalisation, others can take advantage of both pathways, and the cellular background is likely to influence the route of internalisation taken by a particular receptor. Binding of chemokine to the receptor induces phosphorylation of ser-thr residues in the intracellular C-terminal tail of the receptor and this leads to the inhibition of G-protein coupling and consequently receptor desensitisation<sup>246</sup>. Additionally, the phosphorylation of these ser and thr residues is an important step for the recruitment of  $\beta$ -arrestin.  $\beta$ -arrestins link the receptor to adaptin-2

(AP-2)<sup>247</sup>, which facilitate the internalisation of the receptor via association with clathrin and clathrin-coated pits. These clathrin-coated pits ‘pinch off’ to form clathrin-coated vesicles that enter the early endosomal compartment inside the cell. Evidence shows that  $\beta$ -arrestins may also mediate intracellular trafficking of the receptor, and it is now emerging that  $\beta$ -arrestins acts as a scaffold for the activation of intracellular signalling events from the internalised receptor/ligand complexes<sup>248</sup>. Clathrin-independent methods of internalisation have also been described and include lipid rafts and caveolae structures, which are rich in cholesterol. Caveolae mediated chemokine internalisation has been described for chemokine receptors CCR2, CCR4 and CCR5 as well as for some atypical chemokine receptors<sup>245,249-251</sup>.

## **1.12 Mechanisms of Chemokine-Driven Cell Migration**

Leukocyte egress from the blood and entry into tissues is dependent on chemokines and chemokine receptors. The migration of cells from the blood is considered to be a multistep process involving selectins, integrins and chemokines working in unison to facilitate the egress of leukocytes from the blood and entry into the tissues.

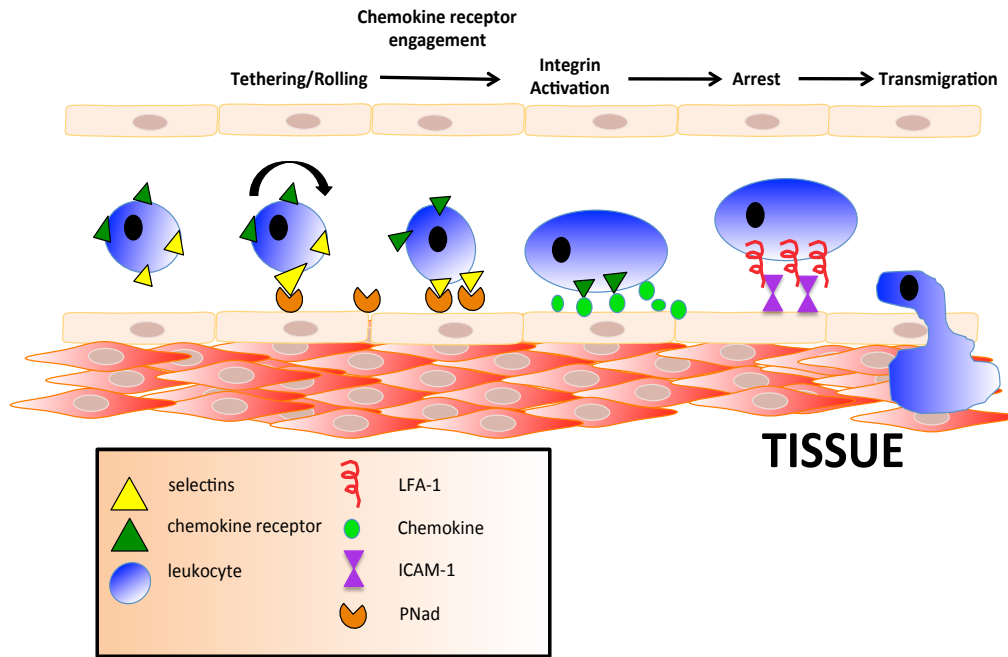


**Figure 1.10: Chemokine-mediated leukocyte extravasation from the blood.**

The multi-step rolling, adhesion and egress of leukocytes from the blood involves selectins, chemokines, integrins and cell adhesion molecules. Selectin expression on the leukocyte promotes tethering and rolling of the leukocyte along the wall of the blood vessel by interacting with peripheral node addressin (PNAd, CD34). Chemokine receptors on the leukocyte recognise their chemokine ligand presented via glycosaminoglycan molecules (GAGs) such as heparan sulphate. This leads to the activation of integrin molecules on the leukocyte such as LFA-1 that then interact with cell adhesion molecules on the endothelial cell surface such as ICAM-1. This results in the firm adhesion of the leukocyte to the wall of the blood vessel. After the arrest of the leukocyte, it then squeezes through tight cell junctions in a process known as transendothelial migration.

First, leukocytes begin rolling on the surface of the activated blood endothelium, a process governed by the expression of selectins expressed on the leukocytes. These selectins bind with low affinity to CD34 on the surface of the blood endothelium<sup>252-255</sup> slowing down the passage of the leukocyte through the blood (Figure 1.10). Cytokines can drive the expression of integrins on the surface of the leukocytes whilst at the same time driving the expression of integrin ligands on endothelial cells. Thus, cytokines help to induce the correct surface receptor repertoire on leukocytes and endothelial cells to support the tethering and slowing down of leukocytes. Integrin binding results in a high affinity interaction

that further slows down the leukocyte (Figure 1.10). Chemokines are expressed by blood endothelial cells and are presented to the leukocyte bound to GAG molecules. Once the leukocyte senses the chemokine it results in a conformational change in the structure of integrin molecules expressed by the leukocyte giving them a higher affinity for their ligand which is a prerequisite for firm adhesion and tissue entry<sup>254,256-258</sup>. The final stage involves the transmigration of the leukocyte between endothelial cells (paracellular) (Figure 1.10). Alternatively, and more rarely, the leukocyte can migrate through the endothelial cells, a process referred to as transcellular migration.

The importance of chemokines in facilitating integrin activation is exemplified by inhibition of chemokine receptor signalling via treatment with pertussis toxin and also from the analysis of chemokine receptor deficient mice. The inhibition or loss of chemokine receptor signalling results in a failure of integrin activation and so cells do not extravasate<sup>259,260</sup>. Once cells extravasate, they have to migrate through a 3-dimensional environment of interstitial matrix, such as that found in the parenchyma of secondary lymphoid tissues or the dermis of the skin. This migration is largely driven by chemokines though other chemoattractants such as leukotrienes also play an important role<sup>261</sup>. The migration of leukocytes in these environments is much more dynamic than that described for leukocyte extravasation in the blood (Figure 1.10). In the aforementioned scenario, leukocytes firmly adhere to blood endothelium, whereas in tissues such as lymph nodes, leukocytes loosely adhere to FRCs and move in a variety of ways in response to chemokines. Chemokines are the main orchestrators of cell movement in lymph nodes and help to establish B cell follicles and T cell zones. To establish distinct lymph node compartments that contain rapidly moving lymphocytes that do not mix, the lymph node is enriched with FRCs and FDCs that form a 3D matrix promoting the movement of T cells and B cells, respectively. Homeostatic chemokines such as CCL21 are immobilised on the lymph node FRCs and their associated extracellular matrix, by interacting with GAG molecules. These immobilised chemokines trigger the random or directed movement of lymphocytes.

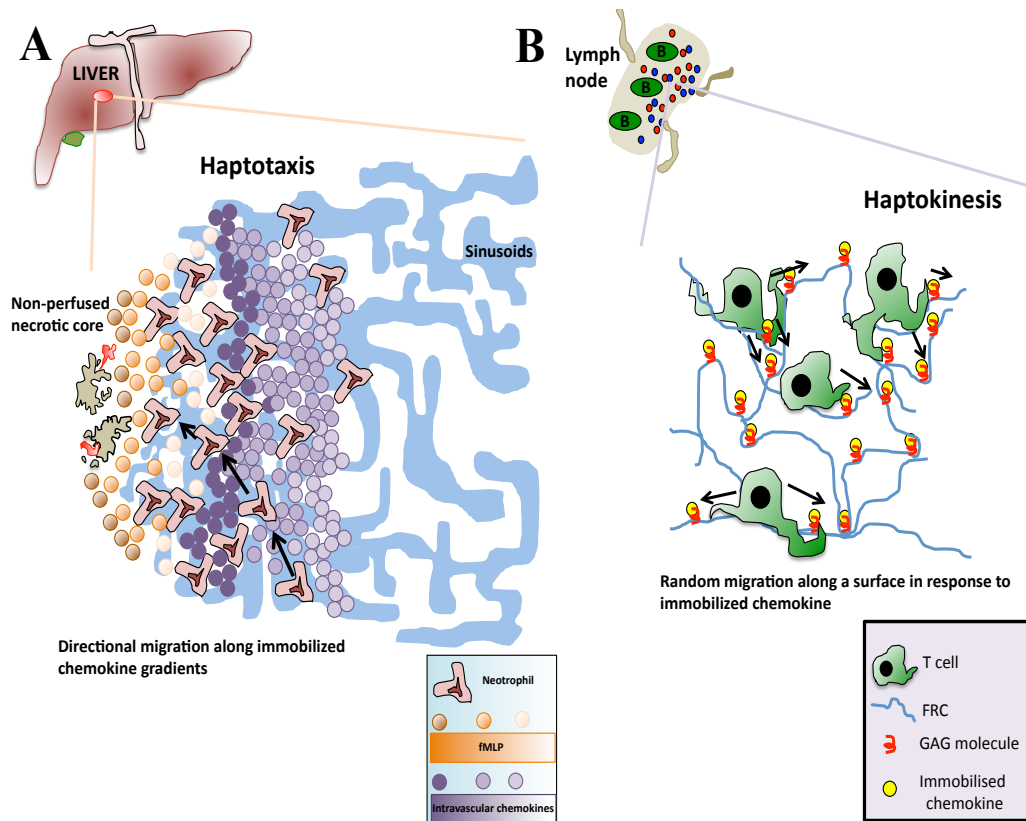


**Figure 1.11: Examples of leukocyte movement by haptotaxis and haptokinesis.**

(A) During a model of sterile liver injury, a gradient of CXCL2 guides neutrophils to the site of injury. The CXCL2 gradient stops around 150 $\mu$ m from the necrotic core and is replaced by a gradient of formyl-methionyl-leucyl-phenylalanine (fMLP) that is probably released by dying cells. Therefore, CXCR2<sup>+</sup> neutrophils switch to formylated peptide receptor 1 (FPR1)-guided attraction in order to cluster around the damaged focus. Neutrophils adhere to and migrate in the vasculature in a chemokine directed fashion, therefore neutrophils are said to migrate haptotactically in this model<sup>262</sup>. (B) CCL19 and CCL21 in lymph nodes elicit an increase in T cell motility without the presence of concentration gradient. In this case, T cells randomly move along FRCs by haptokinesis<sup>263</sup>.

Histological and intravital microscopy analysis has shown that T cells, B cells and DCs migrate along the lymph node stromal scaffolding, suggesting that these cells preferentially use stromal cells as guidance tracks for their migration within a lymph node<sup>164,263,264</sup>. Further analysis by intravital microscopy has shown that migratory behaviour within the lymph node can quickly change. For example, it has been shown that CD8 T cells swarm towards recently activated DCs and CD4 T cells suggesting a rapidly changing chemokine gradient is responsible in

orchestrating this behaviour<sup>265</sup>. In this scenario, it is unlikely that immobilised chemokine is driving the movement of CD8 T cells and it is more likely that cells use a combination of both soluble and immobilised chemokines to drive their migration. Cells can move in response to chemokine by either haptotaxis, haptokinesis or chemotaxis (Figure 1.11). Haptotaxis refers to the directed movement of cells and involves integrin-mediated attachment of cells to surfaces. It has recently been shown that neutrophils in the liver microvasculature sense intravascular chemokine gradients and migrate by haptotaxis towards a site of sterile hepatic injury (Figure 1.11 A). In this model of chemically induced sterile liver injury, CXCR2<sup>+</sup> neutrophils sense intravascular gradients of CXCL2 and migrate to the injury zone. Once neutrophils approach the site of necrosis, they then sense formylated peptides (fMLPs) that are released directly by the injury site using FPR1. Interpretation of fMLPs and chemokines drives neutrophil recruitment to injury sites in a haptotactic manner. The concept of haptotaxis has also been demonstrated for DC migration in the dermis. In this scenario, gradients of CCL21 promote haptotactic movement towards lymphatic vessels<sup>266</sup>. In a similar study using two-photon intravital microscopy, neutrophil swarming in the skin was shown to be driven by chemotaxis which is driven by leukotriene expression<sup>267</sup>. Chemotaxis is the directed movement of cells along a soluble chemokine gradient that does not involve integrin mediated cellular adhesion but instead involves the protrusive flowing of the actin cytoskeleton. Haptokinesis refers to the random movement of cells along a surface and involves integrin-mediated attachment of cells to surfaces. In lymph nodes, T cells and DCs have been shown to move along FRCs by haptokinesis (Figure 1.11 B). Interestingly, a study by Sixt and colleagues has shown how DCs are able to incorporate both chemotaxis and haptokinetic movements by sensing immobilised CCL21 for movement and using soluble CCL21 gradients to steer their migration<sup>268</sup>. The importance of these findings will be discussed later in this thesis when considering the function of CCR7 (Section 1.13.1).

## **1.13 CCR7 and CCR9: archetypical homeostatic chemokine receptors.**

The chemoattractant properties of chemokines were first discovered by the description of neutrophil migration in a chemotaxis assay using IL-8 (now renamed CXCL8)<sup>269</sup>. Since then the importance of chemokine-driven migration has been well described by many others. Central to this thesis are the chemokines CCL19, CCL21 and CCL25. CCL19 and CCL21 are ligands for the CCR7 receptor while CCL25 operates through CCR9. All three of these chemokines bind to CCRL1, the atypical chemokine receptor that is the principal focus of this thesis.

### **1.13.1 CCR7**

CCR7 exerts its function by interacting with CCL19 and CCL21 and is important for the homeostatic recruitment of leukocytes to secondary lymphoid organs. Naïve T cells and B cells are programmed to continually migrate between secondary lymphoid organs in a process that is largely driven by CCR7 interacting with CCL21 produced in lymphoid tissues and anchored to the surface of HEVs. Tissue-derived migratory DCs also require CCR7 to enter lymphatic vessels, and to traverse the floor of the SCS from the lymph into the lymph node parenchyma. Although both CCL19 and CCL21 bind to CCR7, CCL21 is sufficient, in the absence of CCL19, to drive DC migration and entry into lymph nodes and the recruitment of lymphocytes from the blood<sup>270</sup>. Once in the SCS, DCs migrate along gradients of CCL21 produced by FRCs, and thus DCs are guided into the T cell zones of lymph nodes. CCR7<sup>+</sup> T cells also sense immobilised CCL21 produced by FRCs and migrate from HEVs to localise in the T cell zones. Once brought together in the T cell zone, activated DCs carrying the appropriate antigen interact with T cells to propagate adaptive immune responses. Although both CCL19 and CCL21 bind to CCR7 with similar affinity, one study has shown that CCL19 is able to provide survival signals to T cells but CCL21 does not<sup>271</sup>. Other experiments have shown that DCs will preferentially migrate towards bound CCL21 if presented with equal amounts of CCL19 and CCL21<sup>272</sup>. Therefore, both chemokines bind to CCR7

and induce unique responses suggesting that both CCL19 and CCL21 are required to support normal T cell migration, localisation and survival.

Early work using CCR7-deficient mice exemplified the importance of CCR7 in driving leukocyte migration to lymphoid tissues by showing that loss of CCR7 reduced T cell entry into lymph nodes, and to a lesser degree, B cell entry into these organs<sup>88</sup>. As a consequence, these mice have reduced lymph node cellularity and abnormal lymph node architecture with the absence of clearly defined B cell follicles and T cells zones. Recent work has shown that CCR7-dependent DC migration also controls lymph node size and structure. In this study the authors showed that DCs mainly enter lymph nodes by transmigrating through the floor of the SCS whereas naïve T cells in the lymph mainly enter via medullary sinuses. DCs when migrating via the SCS induce local changes in the structure of the lymphatic vessels and promote the entry of T cells via this site in a CCR7-dependent manner<sup>53</sup>. This phenomenon is lost when CCR7 is absent on DCs. In the same study, the authors showed the dependence on CCR7-mediated signaling by DCs and T cells for directed migration into T cell zones. WT and CCR7-deficient mice contain comparable numbers of DCs in their peripheral non-lymphoid organs however numbers of migratory DCs within lymph nodes of CCR7-deficient mice is dramatically reduced. This indicates that CCR7 plays no appreciative role in the recruitment of DC progenitors to peripheral sites such as skin and mucosa but is required to drive the migration of semi-mature DCs from these sites to lymph nodes. Loss of CCR7 results in enhanced immune responses in these animals that is attributed to the aberrant positioning of FoxP3<sup>+</sup> Tregs in the lymph node<sup>273</sup>. The importance of CCL21 guidance cues in mediating DC: T cell contacts has also been exemplified by the loss of CCR7. Studies in CCR7-deficient mice show that these mice have reduced DC motility of around 50%, and around a 30% reduction in velocity with a similar result noted for T cells<sup>274</sup>. For CD4<sup>+</sup> T cells, intranodal motility of these cells is reduced in the absence of CCR7 signaling either by deletion of the receptor itself or its ligands. *plt/plt* mice were used to explore the impact that loss of CCL19 and CCL21 has on CCR7<sup>+</sup> leukocyte migration to lymph nodes and their movement within these organs. *plt/plt* (paucity of lymph node T cells) mice harbour a spontaneous deletion of CCL19 and CCL21a (CCL21-ser) in secondary lymphoid organs while CCL21b

(CCL21-leu) found in non-lymphoid tissues, remains intact<sup>275-277</sup>. Adoptive transfer of WT CD4<sup>+</sup> T cells along with systemic administration of CCL21 restored T cell motility in the lymph nodes of *plt/plt* mice<sup>274</sup>. *plt/plt* mice also show reduced numbers of T cells and DCs in lymph nodes and models using skin sensitisation have shown that DCs display defective trafficking to skin draining lymph nodes.

Similar to the lymph node, chemokines CCL19 and CCL21 dominate in the spleen and control the movement of lymphocytes. This is exemplified by loss of these chemokines in *plt/plt* mice that leads to defective accumulation of T lymphocytes in the white pulp<sup>277</sup>. In a similar fashion to the way in which cells transmigrate from blood into tissues, cells traversing the marginal zone do so in an active fashion involving integrins and chemokines. The marginal zone is a unique and interesting environment containing narrow corridors that extend between red pulp and white pulp and that are thought to facilitate cellular entry into the white pulp from splenic venules (Section 1.8). These bridging channels are rich in FRCs and these cells have been shown to secrete CCL21. This chemokine therefore is proposed to guide CCR7<sup>+</sup> cells into PALS<sup>164</sup>.

CCR7 and CCL21 are fundamental to the development and function of the thymus<sup>278-280</sup>. The thymus is a primary lymphoid tissue involved in the development of thymocytes into mature T cells. The expression of CCL21 within the thymus is widespread and found in both the cortex and medullary regions. CCR7 is expressed by double negative thymocytes (CD4<sup>-</sup> CD8<sup>-</sup>) and single positive thymocytes (CD4<sup>+</sup> CD8<sup>-</sup> or CD4<sup>-</sup> CD8<sup>+</sup>) and guides these cells through both regions of the thymus. Early thymic precursors and late stage thymocytes depend on CCR7 for their migration and as such CCR7 functions to control multiple stages of thymocyte development<sup>280,281</sup>. Multiple models involving single gene KO and multiple gene KOs have shown that CCR7, CCR9 and CXCR4 work in synchrony to drive the migration of bone marrow derived thymic precursors to the thymus<sup>278,280,282-284</sup>. Inside the thymus, CCR7 is important for the outward migration from the corticomedullary junction of double negative 2 thymocytes (lineage<sup>-</sup>, CD44<sup>+</sup>, CD25<sup>+</sup>, and CD117<sup>+</sup>) to the cortex<sup>281</sup>. This was shown in *plt/plt* mice and CCR7-deficient mice with both mouse strains displaying an accumulation of double negative 2 and double

negative 3 (lineage<sup>-</sup>, CD44<sup>-</sup> and CD25<sup>+</sup>) cells at the corticomedullary junction. Together, studies using these mice have shown that CCR7-deficient and *plt/plt* mice show abnormal thymus morphology and that CCR7-deficient mice display low numbers of thymocytes<sup>275,279,285</sup>. Studies conducted in CCR7-deficient mice have also shown that these mice also develop spontaneous autoimmunity<sup>286</sup>. It can be appreciated that as CCR7 plays such a critical role in guiding developing thymocytes throughout the entirety of the thymus that deletion of CCR7 would have a profound impact on the generation of conventional T cells, Tregs and deletion of autoreactive T cells.

Recently, the interaction between CCL21 and CCR7 was shown to be more complex than once thought. CCL21 is extended at the C terminus and highly charged residues within this region facilitate chemokine interactions with heparin sulphate molecules and GAGs that decorate the surface of cells. In contrast, CCL19 lacks a C terminus extension and as such is an obligate soluble chemokine. Both CCL21 and CCL19 are capable of binding to CCR7 to induce cellular movement. However, Schumann and colleagues reported in 2010 via a series of *ex vivo* and *in vitro* experiments that CCL21, can, upon culturing with mature DCs, become truncated to produce a smaller soluble fragment that retains its capacity to induce chemotaxis in CCR7<sup>+</sup> cells<sup>268</sup> and behaves in a manner similar to that of CCL19 (Figure 1.12).

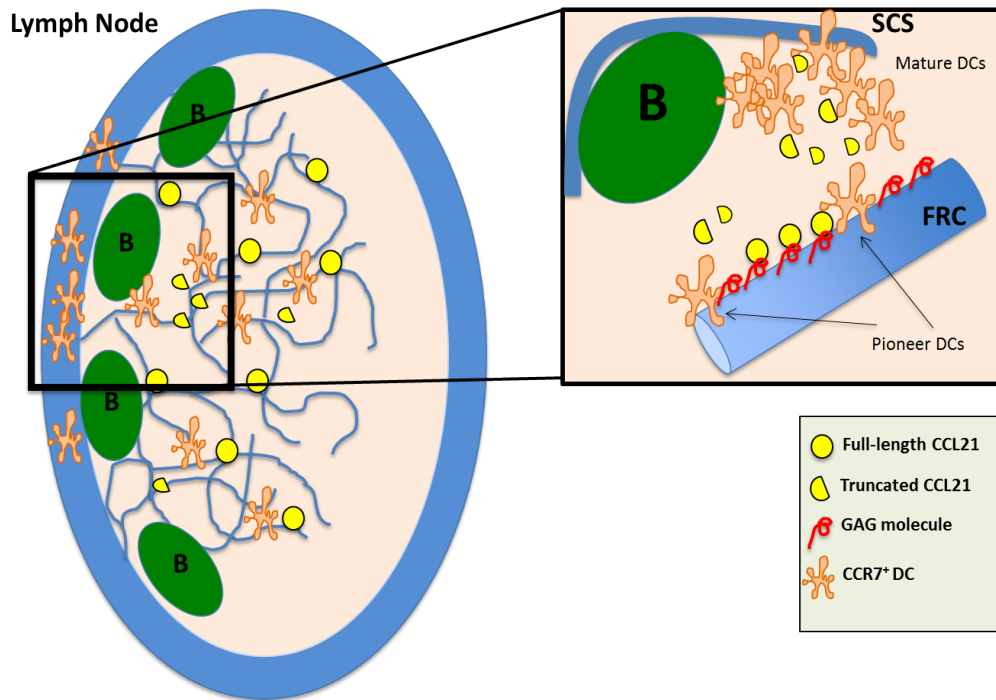


**Figure 1.12: Cleavage of full-length CCL21 chemokine.**

The above diagram is a proposed model of the significance of DC mediated cleavage of CCL21 chemokine *in vivo*. DCs entering a lymph node recognise immobilised fCCL21 that decorates the surface of FRCs. DCs then move along FRCs via haptokinesis. These DCs are termed ‘pioneer’ DCs. Pioneer DCs then cleave the C-terminus of CCL21 to create a soluble CCL21 fragment that diffuses from its site of production. Soluble CCL21 steers the movement of DCs that subsequently enter the lymph node by inducing the chemotactic movement of these cells. The soluble fragment also attracts mature DCs entering the lymph node by way of the SCS lymphatics.

In this study, the authors show that DCs carry an as yet unknown protease that has the capacity to cleave the C-terminus of CCL21 and create a soluble CCL21 fragment. From their observations made *in vitro*, the authors suggest what may occur mechanistically *in vivo*. They hypothesise that soluble CCL21 diffuses from the source inside the lymph node and attracts responding mature DCs into the lymph node parenchyma and migration towards the T cell zone (Figure 1.12). In this study they were also able to show that DCs sense CCL21 and move via haptokinesis but then their movement becomes directional upon sensing of truncated soluble CCL21 generated by other DCs. This sensing of truncated CCL21 (tCCL21) along with the recognition of immobilised CCL21 causes the

DCs to move via haptokinesis but with the tCCL21 fragment steering the direction of DC migration. This paper detailed for the first time the ability of haptokinetic and chemotactic movement to occur within the same system. The results from this study open up the possibility that other C-terminally extended chemokines may be cleaved to produce a chemotactically active fragment from a normally immobilised haptotactic or haptokinetic chemokine. This is a theme I will explore later in the Results chapters of this thesis.

### 1.13.2 CCR9

Parallels can be drawn between the roles described for CCR7 and what is known about CCR9. Like CCR7, CCR9 directs the migration of leukocytes to and from discrete immune compartments. Specifically, CCR9 is important in the intestinal immune system and drives the migration of leukocytes to the small intestine. CCR9 is also involved in the maturation and positioning of thymocytes.

CCR9 is expressed on thymocytes at various stages throughout their maturation. CCR9<sup>+</sup> thymocytes are guided through the thymus by recognising CCL25, the only known ligand for CCR9, which is produced by thymic epithelial cells (TECs)<sup>287</sup>. It is known that CCR9 specifically drives the migration of thymocyte progenitors from the bone marrow as well as driving DN thymocytes from the cortex to the medulla<sup>278,287,288</sup>.

Both CCR9 and CCR7 are important for the migration of pDCs<sup>20,289-293</sup>. It has been shown that CCR7 is upregulated on pDCs following activation with TLR ligands and this facilitates their extravasation into lymph nodes via HEVs. This has been demonstrated in CCR7-deficient mice in which experiments have shown that irrespective of activation state, CCR7 null pDCs have a reduced propensity to localise in secondary lymph nodes, whereas their homing to bone marrow and spleen is unaffected. CCR9<sup>+</sup> pDCs migrate to the small intestine during homeostasis and inflammation<sup>289</sup>. In CCR9 deficient animals, the number of pDCs in the lamina propria of the small intestine is reduced, whereas the number of pDCs in secondary lymphoid organs is unaffected<sup>289</sup>. Almost all pDCs express high levels of CCR9 and this drives their constitutive trafficking. Further experiments involving adoptive transfer of WT and CCR9-deficient pDCs has

also revealed a role for CCR9 in the recruitment of pDCs from the blood to the small intestine<sup>289</sup>. CCR9<sup>+</sup> pDCs reportedly have tolerogenic properties. It was shown by two separate groups that CCR9<sup>+</sup> pDCs are able to induce the generation of IL-10 secreting Tregs from naïve T cells. Furthermore, Hadeiba et al. describe a role for CCR9<sup>+</sup> pDCs in reducing the severity of graft versus host disease by suppressing the generation of IL-17 producing T cells<sup>20</sup>.

T cells that encounter antigen in lymph nodes undergo a series of reprogramming events during which they change their homing properties by changing their chemokine receptor and integrin expression. Imprinting of cells within lymph nodes is unique to the specific lymph nodes in which the cell resides. The mesenteric lymph node has a unique microenvironment and is home to a specialised population of DCs that allows for the imprinting of gut homing receptors upon T cells<sup>294,295</sup>. The continual migration of leukocytes to and from the small intestine lamina propria is of paramount importance to efficient immune surveillance and also for the induction of tolerance towards commensal bacteria and food antigens. DCs and macrophages within the small intestine lamina propria continuously sample and uptake antigen from the intestinal lumen. DCs then use CCR7 to travel from the small intestine lamina propria via the afferent lymphatic vessels to arrive at the MLN where they present their antigen to T cells<sup>296</sup>. T cells recognise the antigen via their cognate TcRs and become activated. The imprinting of small intestine lamina propria homing receptors can only occur via the interaction of T cells with specialised retinoic acid producing DCs<sup>297-299</sup>. These DCs are able to induce the expression of CCR9 and the integrin  $\alpha_4\beta_7$  on the T cell by releasing retinoic acid, a vitamin A metabolite. These DCs are equipped with the ability to induce these receptors by high expression of retinal dehydrogenase (RALDH), an enzyme that converts dietary vitamin A to retinoic acid. Both CCR9, via interactions with CCL25, and  $\alpha_4\beta_7$ , via interaction with MAdCAM-1, home the T cell to the small intestine lamina propria. Compared to WT animals,  $\beta_7$ -deficient mice and CCR9 deficient mice contain reduced numbers of T cells in the small intestine lamina propria<sup>287,300</sup>. Finally, retinoic acid is also required for driving CCR9 and CCR10 expression on IgA secreting plasmablasts which drive the migration of these cells to the small intestine lamina propria (CCR9) and large intestine (CCR10)<sup>301</sup>. It

has been shown that vitamin A-deficient mice lacked intestinal IgA-secreting cells and that retinoic acid is required for the homing of these cells and for their ability to secrete IgA<sup>301</sup>. Therefore taken collectively, these reports illustrate the importance of the mesenteric lymph node microenvironment in shaping the repertoire of surface receptors, that homes leukocytes to the small intestine lamina propria.

This body of work shows how both CCR7 and CCR9 driven processes are of fundamental importance to the development and homeostasis of the immune system and play key roles in the induction of adaptive immunity.

### **1.14 The Atypical Chemokine Receptor Family**

I have described how chemokines are important regulators of leukocyte migration *in vivo* and as a consequence how they act as key components of the immune system. As such chemokines and their receptors must be tightly controlled at transcriptional, translational and post-translational levels to prevent aberrant localisation and recruitment of leukocytes. Over the past 10-15 years it has become increasingly clear that a separate group of receptors, known as atypical chemokine receptors, function in a non-classical way to 'conventional' chemokine receptors and play a role in regulating chemokines and their receptors. At present, atypical chemokine receptors include Duffy Antigen Receptor for Chemokines (DARC), D6, CXCR7, and CCRL1 (also known as CCX-CKR). CRAM (chemokine receptor on activated macrophages) may represent an additional member to this family of receptors but controversy exists over its ability to bind to CCL19. Therefore, for the purposes of this thesis, I will describe only the functions of DARC, D6, CXCR7 and CCRL1.

Collectively, atypical chemokine receptors structurally resemble conventional chemokine receptors but are unique in their function. Although not all uniform in terms of the mechanisms by which they function, it is known that they do not initiate classical chemokine receptor signalling upon ligand binding. It has been proposed that they may function to exert post-translational control over chemokines, and possibly regulate co-expressed conventional chemokine receptors. Evidence has supported the view that some of the atypical chemokine

receptors, such as D6, are chemokine scavengers, able to internalise and degrade large quantities of extracellular chemokine by continuously cycling to and from the cell surface whilst resisting chemokine-induced receptor desensitisation. Other atypical chemokine receptors, such as DARC, appear to act to buffer chemokine levels *in vivo* and may be involved in transporting chemokines across microanatomical barriers such as endothelial cell layers lining blood vessels. Therefore, this family of atypical chemokine receptors is able to mediate post-translational control of extracellular chemokines in different ways. This thesis will examine the control of the chemokine ligands for CCR7 and CCR9 by the atypical chemokine receptor CCRL1. First, the other members of the atypical chemokine family are discussed.

### **1.14.1 D6**

D6 belongs to the atypical chemokine receptor family due to its ability to scavenge large quantities of chemokine whilst showing an inability to become desensitised. Furthermore, D6 does not activate classical signalling pathways after chemokine binding. The first characterisation of D6 expression was from Northern blot analysis showing that human placenta has the highest expression of D6 in humans<sup>302</sup>. It subsequently emerged that this was due to its strong expression by fetal trophoblasts<sup>303</sup>. D6 has also been shown to be expressed by lymphatic vessels in human skin, lung and gut and by lymph node afferent lymphatics, although D6 expression is absent from lymphatic vessels in other organs<sup>304-308</sup>. D6 expression has also been reported on human pDCs, B cells, cDCs, macrophages and mast cells<sup>309,310</sup>.

D6 is currently thought to function as a chemokine scavenger that binds, internalises and degrades 12 inflammatory CC chemokine ligands in humans (CCL3, CCL3L1, CCL4, CCL4L1, CCL5, CCL7, CCL8, CCL11, CCL13, CCL14, CCL17, and CCL22)<sup>302,311-313</sup>. This is thought to help dampen and resolve inflammatory responses by controlling leukocyte migration. Mouse D6 has more limited ligand specificity<sup>314,315</sup>. Work carried out on transfected cell lines has shown that over time D6 can remove large quantities of inflammatory CC chemokines from the extracellular milieu by rapid constitutive internalisation and degradation<sup>316</sup>. Experiments have also shown that after internalisation,

chemokines are dislodged from D6 and targeted for degradation, while the receptor can recycle and be re-expressed on the cell surface for further chemokine binding, a process driven in a ligand-independent manner<sup>317</sup>.

The absence of a reliable D6 antibody has hampered attempts to characterise D6 expression in mice. However, D6 mRNA is readily detectable in the lung, liver and placenta of the mouse<sup>303,315</sup>, and data from the Immunological Genome Project (Immgen, [www.immgen.org](http://www.immgen.org)) and from work done by Malhotra *et al* has described D6 expression on mouse lymph node LECs<sup>318</sup>. In addition, fluorescent chemokine uptake assays have been used to show expression of functional D6 protein by innate-like B cells and at low levels by some other leukocyte subsets<sup>314,319,320</sup>.

Due to the expression of D6 on LECs in barrier tissues, it has been implicated as a key regulator of inflammatory chemokine at these sites. It has been reported that D6 functions on these cells to sequester excess inflammatory chemokine from the lymphatic surface in order to promote tissue flow and the proper egress of leukocytes from peripheral sites<sup>306,321,322</sup>. In the absence of D6, leukocytes are held up in lymph nodes and surrounding skin lymphatic vessels due to presentation of excess inflammatory chemokine by LECs and this leads to lymphatic congestion. As a consequence, DCs from peripheral sites such as the skin are hindered in their ability to localise in secondary lymph nodes leading to defective initiation of adaptive immune responses<sup>306</sup>.

Although D6 is described as an inflammatory chemokine scavenging receptor, D6-deficient mice have some phenotypes at rest. D6 is expressed on innate like B cells including body cavity B1 B cells and MZ B cells in the spleen. In D6-deficient mice at rest the numbers of B1 cells is reduced compared with WT animals<sup>314</sup>. Furthermore, D6-deficient mice have lower levels of circulating class-switched antibodies specific for phosphorylcholine which are generated from innate-like B cells<sup>314</sup>. Rather than loss of chemokine scavenging, these defects are probably linked to the observation that B1 cells have an increased responsiveness to CXCL13, a chemokine that drives the localisation and migration of CXCR5<sup>+</sup> B1 cells. The reason for this increased responsiveness is unclear but the data suggest that D6 is able to suppress the activity of co-

expressed conventional chemokine receptors. In addition, D6-deficient mice display defects in inflammatory monocyte egress from the bone marrow as well as producing monocytes phenotypically distinct from WT counterparts<sup>323</sup>. The migration of Ly6C<sup>hi</sup> monocytes from the bone marrow is enhanced in D6-deficient mice and this is probably due to dysregulation of CCR2 chemokine ligands<sup>323</sup>. Inflammatory monocytes express high levels of CCR2 and this is important for their release into the blood<sup>212</sup>.

Induction of inflammatory responses in D6-deficient mice has demonstrated the reduced capacity of these animals to resolve inflammation. In many of these studies levels of D6 associated chemokines are elevated in the inflamed tissues of D6-deficient mice. D6-deficient mice have an increased susceptibility to gut and skin tumours<sup>324,325</sup>. Furthermore, D6 has been described as a key player in resolving cutaneous inflammation induced by topical application of phorbol esters or by CFA injection, with D6-deficient animals displaying an enhanced pathology compared to WT counterparts<sup>304,326,327</sup>. Transgenic expression of D6 in keratinocytes conferred an increase in protection against cutaneous inflammation and inflammation-driven papilloma formation. Collectively, these studies highlight the crucial role D6 plays at barrier sites in terms of controlling the levels of inflammatory chemokine and, as a consequence, inflammation and tumour formation<sup>326</sup>. Research has also shown that D6-deficient mice are more susceptible to *M.tuberculosis*<sup>328</sup> with aberrant leukocyte accumulation in the lungs, mediastinal lymph nodes, kidneys and liver ultimately leading to an increase in mortality. However, loss of D6 did not affect bacterial load. D6-deficient mice are more sensitive to liver damage after carbon tetrachloride-induced acute liver damage and have an exaggerated DC and eosinophil infiltrate during models of allergic lung inflammation<sup>329,330</sup>. D6-deficient mice carrying D6-deficient pups are more susceptible than WT counterparts to undergo inflammation-associated miscarriage induced by LPS or antibodies against phospholipids<sup>331</sup>. It has also been shown that fetal D6 aids the survival of mouse embryos transferred into allogenic hosts<sup>303</sup>.

In many of the aforementioned studies, levels of D6-binding chemokines were elevated in the inflamed tissues of D6-deficient mice compared with WT mice. This would support the idea that D6 functions as a chemokine scavenger to

restrict the recruitment of inflammatory leukocytes. As levels of D6 are often elevated in inflamed tissues, it is possible that D6 is induced to help resolve inflammation by controlling chemokine-driven leukocyte migration.

### **1.14.2 Duffy Antigen Receptor for Chemokines (DARC)**

Originally described in the 1950s as the molecular determinant of the Duffy blood group antigen, DARC was further classified in the 1990's as a receptor for inflammatory chemokines. There are three major polymorphisms in humans that give rise to the Duffy blood groups. DARC is present on erythrocytes and is known to be the cellular entry point for the malarial parasite *Plasmodium Vivax* (*P.vivax*)<sup>332</sup>. It is thought that this has driven the emergence of the DARC null phenotype, which is particularly prevalent amongst the sub-Saharan African population. Individuals with this phenotype possess a mutation in the promoter of both their alleles that disrupts a binding site for the GATA-1 transcription factor<sup>333</sup>. The result is the loss of DARC specifically from erythrocytes, although expression remains on other cells. These individuals are protected from infection from *P.vivax*. Interestingly, they also display benign neutropenia<sup>334-336</sup>. Therefore, DARC may control the bioavailability or biodistribution of DARC-binding chemokines to regulate the dynamics of neutrophil generation and/or departure from the bone marrow.

DARC, similar to other atypical chemokine receptors, plays an important role in chemokine homeostasis. DARC is able to bind some, but not all, inflammatory chemokines including those from both CC and CXC subfamilies. Its expression is confined to red blood cells (RBCs), venular endothelial cells and Purkinje cells in the brain as well as kidney and lung endothelial cells. It is positioned at sites of high leukocyte extravasation, such as HEVs and post capillary venules<sup>337-339</sup>. As the levels of DARC on red blood cells are approximately 15nmol per litre of human blood, and even higher in mice, the capacity of these cells to bind chemokines is substantial.

The lack of the DRYLAIV motif in the second cytoplasmic loop renders the receptor 'silent'<sup>338</sup> and no detectable signalling has been reported to be induced upon chemokine binding to DARC. It is postulated that DARC on RBCs acts as a

chemokine ‘sink’ sequestering available chemokine and altering chemokine concentrations in the blood<sup>339</sup>. Evidence supports the idea that DARC also acts as a chemokine buffer in the blood by holding chemokine in a bound state on the surface of RBCs during inflammation. When inflammation subsides and plasma chemokine levels are reduced by DARC-independent mechanisms, DARC-bound chemokines are released ensuring that leukocyte recruitment is robust and targeted by preventing chemokine-induced receptor down-regulation on leukocytes.

On endothelial cells, DARC appears to support chemokine activity, and in transfection models, DARC was shown to be essential for the optimum migration of leukocytes<sup>340</sup>. This phenomenon can be explained by transcytosis. It is thought that DARC on endothelial cells binds and internalises chemokine, and then the chemokine/receptor complex is transported to the opposite side of the cell where the chemokine is presented to leukocytes<sup>251</sup>. This discovery has further added to the complexity of the chemokine networks and their regulation, and has challenged our thoughts of how atypical chemokine receptors function to control chemokines.

### **1.14.3 CXCR7**

Another chemokine receptor grouped alongside the ‘atypical receptors’ is CXCR7 (formerly known as RDC1). Until the discovery of CXCR7, it was thought that CXCR4 and CXCL12 formed a monogamous relationship, partly because the phenotypes of mice deficient for one or other of these genes were so similar. In fact, CXCR7 has a stronger affinity for CXCL12 than the classical signalling receptor CXCR4 and also has the ability to bind to CXCL11, a chemokine that operates through CXCR3<sup>341</sup>. Studies conducted in CXCR7-deficient mice have shown that it is critical for heart formation during embryogenesis and indeed most CXCR7-deficient mice die within a few days of birth due to cardiac defects including thickened semilunar valves and ventricular septal defects<sup>341,342</sup>. CXCR7 is able to homodimerise and heterodimerise with CXCR4<sup>343</sup> and in its heterodimeric form CXCR7 is able to regulate the subcellular localisation of CXCR4 to modulate biological effects mediated by CXCL12 engagement with CXCR4<sup>344</sup>.

CXCR7 transcripts are detectable in many tissues of adult mice although it is not yet known if this correlates with protein expression. Protein expression has been found in mouse fetal liver cells<sup>341</sup> and studies conducted using knock in reporter mice describe expression in osteocytes<sup>345</sup>. CXCR7 has also been shown to be up regulated in tumours and emerging neovasculature<sup>346,347</sup>. Furthermore, CXCR7 has been described to play a role in stem cell localisation<sup>348</sup>, tumour cell migration<sup>349</sup> and the regulation of CXCL12-induced leukocyte migration<sup>344</sup>. There still remains a debate over whether CXCR7 should be grouped alongside the atypical chemokine receptors. Indeed it has been shown that CXCR7 can induce increased cellular adhesion as well as promoting cell proliferation<sup>341</sup>. CXCR7 has been reported to activate MAP kinases through  $\beta$ -arrestins after ligand binding, suggesting that it may be better placed alongside the classical chemokine receptors.

The first described role for CXCR7 *in vivo* comes from studies conducted in zebrafish, in which investigators highlighted a key role for this receptor in embryogenesis<sup>125,350,351</sup>. Two CXCR7 genes are constitutively expressed in various tissues during embryogenesis in fish. The receptor is expressed in facial motor neurons and also in the lateral line<sup>352</sup>. Collective cell migration along the lateral line requires CXCR7 and CXCR4 to work in synchrony to direct the proper migration of cells<sup>350</sup>. At the leading edge, CXCR4 facilitates cell migration whereas CXCR7 is expressed on trailing cells and ensures these cells lose sensitivity to CXCL12. This partnership ensures the proper deposition of cells along the lateral line that eventually give rise to neuromasts which are mechanoreceptive organs. In this system it has been proposed that CXCR7 functions to control CXCR4 signalling and regulation.

In the embryo, CXCR4 and CXCL12 are also critical for neuronal development and progenitor cell survival. Within this system, CXCR7 is expressed alongside CXCR4 and is crucial for the migration of interneurons<sup>349,353</sup>. As mentioned previously, chemokine receptor desensitisation can limit the migration of cells and prevent aberrant responses to chemokines. It is proposed that CXCR7 functions in neuronal development to prevent the desensitisation of CXCR4 by regulating CXCL12 abundance and thus cells retain responsiveness to

CXCL12<sup>354</sup>. However, in another related study it was reported that CXCR7 and CXCR4 transmit distinct signals that are required for optimal migration<sup>355</sup>.

CXCR7 is expressed by tumour cells, especially in lymphomas and sarcomas<sup>341,346,356,357</sup>. Additionally, CXCR7 immunoreactivity has been reported in multiple human neoplasms including liver, thyroid, breast, cervix, colon pancreas, gall bladder and lung. There is strong anti-CXCR7 immunoreactivity on tumour vasculature however the role of CXCR7 at this site is not fully understood. *In vitro* studies as well as mouse models have identified CXCR7 as an important mediator of tumour cell proliferation, survival and metastasis<sup>346,355,356</sup>.

#### **1.14.4 CCRL1**

Compared with the other atypical chemokine receptors, CCRL1 is less well characterised. In 2000 a novel human chemokine receptor was identified by Gosling and colleagues from analysis of databases of expressed sequence tags (EST)<sup>358</sup> and named ChemoCentryx Chemokine Receptor (CCX-CKR) in reference to the company that first discovered it. CCRL1 shares some homology to other CC chemokine receptors, particularly CCR7 and CCR9. Human and mouse CCRL1 has a high affinity for homeostatic chemokines CCL25, CCL19 and CCL21<sup>359</sup> (half-maximal inhibitory concentration (IC<sub>50</sub> of 10-20nM)). Human CXCL13 also binds to human CCRL1 albeit with much lower affinity (IC<sub>50</sub> >100nM). Based on *in vitro* studies describing the ligand specificity of CCRL1, and *in vivo* studies describing increased CCL21 protein in CCRL1-deficient animals during inflammation, it is hypothesised that CCRL1 functions *in vivo* by scavenging extracellular CCL19, CCL21 and CCL25. Similar to the role of D6, it is possible that CCRL1, after chemokine binding, targets CCL19, CCL21 and CCL25 for degradation whilst consequently recycling to the cell surface for further chemokine binding (Figure 1.13).

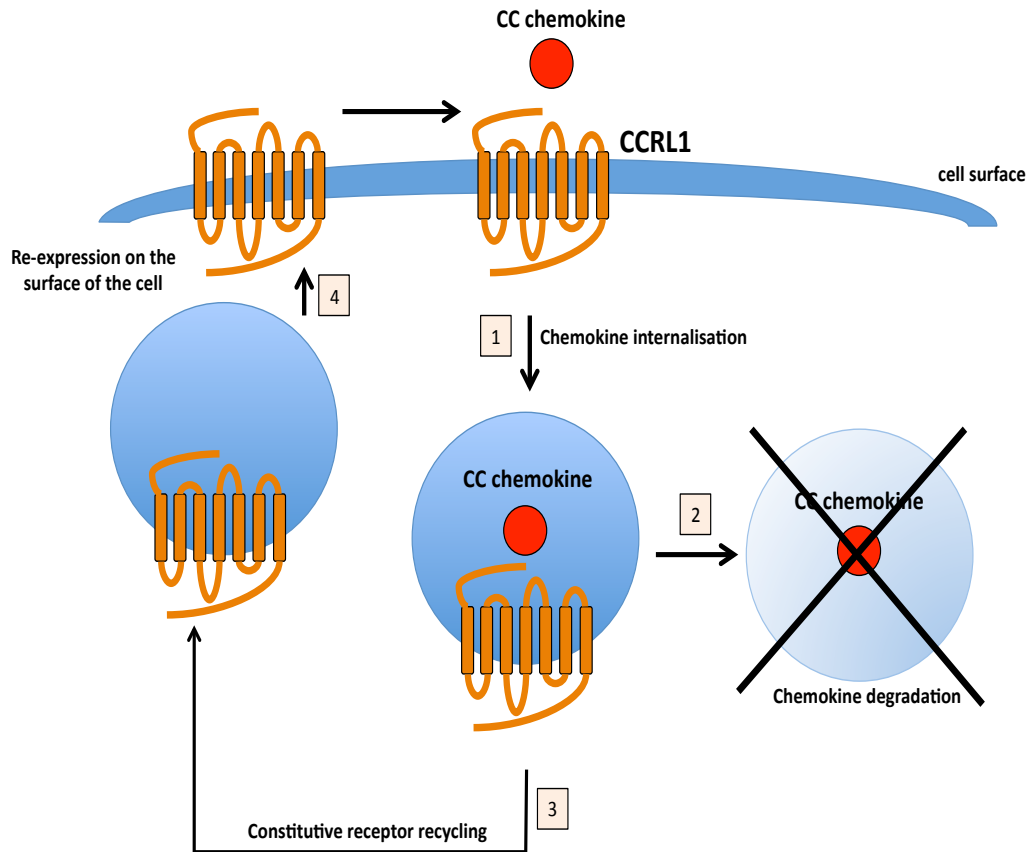


**Figure 1.13: Model of CCRL1-mediated chemokine internalization.**

The atypical chemokine receptor CCRL1 binds to CCL19, CCL21 and CCL25 chemokines but fails to initiate classical intracellular chemokine signaling cascades. It is proposed that CCRL1 constitutively traffics to and from the cell surface targeting chemokine ligand for degradation. However, direct evidence for this mechanism of action is currently lacking.

Following on from early expression studies, more recently Heinzl and colleagues have expanded understanding of where CCRL1 is expressed *in vivo* by generating CCRL1-eGFP reporter mice<sup>360</sup>. These mice were generated by replacing part of the coding sequence of CCRL1 with GFP. They therefore express GFP under the control of the CCRL1 promoter and so GFP identifies cells that have an active CCRL1 promoter. The group reported expression of GFP on cortical thymic epithelial cells, cells in the subcapsular region of secondary lymphoid organs, and keratinocytes in the skin. However, they did not report expression of GFP in heart tissue (which is reported to express high levels of CCRL1 transcripts using molecular techniques<sup>358,359</sup>) nor did they find

expression on CD45<sup>+</sup> leukocytes as determined by flow cytometry analysis, although data from the ImmGen Project ([www.immgen.org](http://www.immgen.org)) shows germinal centre B cells express CCRL1 transcript. The GFP<sup>+</sup> cells in the SCS of secondary lymph nodes are thought to be LECs, and according to microarray studies, these cells have been shown to express CCRL1 transcripts<sup>318</sup>. It is also notable that GFP<sup>+</sup> cells in the intestine also appear to be lymphatic vessel-like structures.

Thus far, the understanding of the biological functions exerted by CCRL1 *in vivo* are somewhat limited. CCRL1 does not appear to play a role in the embryonic development of the mouse as we and others have generated CCRL1-deficient mice and detect no obvious developmental abnormalities. Despite binding to CCL19 and CCL21, there are no dramatic changes in lymph node cellularity although it is reported that CCRL1-deficient mice contain fewer migratory DCs in skin-draining lymph nodes at rest<sup>360</sup>. This finding is interesting, because as discussed in section (Section 1.13.1), migratory DCs rely on CCL21/CCR7 for their steady-state migration from the periphery to draining lymph nodes and to traverse the floor of the SCS. Expression of CCRL1 in the skin and at the SCS could function to control biodistribution and bioavailability of CCL19 and CCL21 to provide optimal chemokine signals to CCR7<sup>+</sup> DCs although direct evidence of this is lacking.

Unsurprisingly due to the chemokines bound by CCRL1, deletion of the receptor is reported to have an effect on the adaptive immune response. One group has studied the impact of loss of CCRL1 expression on the development of experimental autoimmune encephalomyelitis (EAE) in mice and reported that these animals develop a more rapid onset of central nervous system (CNS) pathology. This was associated with elevated serum levels of CCL21<sup>361</sup>. In the same study they found elevated levels of both CCL19 and CCL21 in the lymph nodes of these mice. Interestingly however, the earlier onset of autoimmunity was attributed not to increased activation of T cells in the lymph node but as a result of aberrant T<sub>H</sub>17 generation in the spleen. CCRL1-deficient mice had elevated expression of IL-23 transcripts in the spleen, a cytokine is known to drive the expansion of T<sub>H</sub>17 cells. The mechanisms underpinning this enhanced T<sub>H</sub>17 response in CCRL1-deficient mice during EAE remain to be elucidated.

During the course of my PhD studies, the same group also described a role for CCRL1 in fine-tuning the behavior and migration of thymic precursors to the developing thymus<sup>362</sup>. They showed that CCRL1-deficient mice displayed abnormal thymocyte localisation and abundance leading to loss of central tolerance, and this predisposes them to autoimmunity, with aged CCRL1-deficient mice spontaneously developing a Sjogren's-like autoimmune disease. However, studies conducted on homozygote CCRL1-GFP reporter mice (which lack CCRL1 expression) did not find thymic defects. The reasons behind these discrepancies remains to be resolved in future investigations and the impact of CCRL1 deficiency on thymic function remains a controversial issue.

Other reports point to potential roles of CCRL1 in the protection against the formation breast cancer<sup>363</sup>. Interestingly, it appears that disease free-survival of patients is associated with high co-expression of CCRL1, D6 and DARC<sup>363</sup>. This is an interesting example of atypical chemokine receptors working in synergy, and may hint to the importance that lies in co-expression of atypical chemokine receptors within the same tissue.

## 1.15 AIMS

The chemokine family is critically important for the proper migration of cells throughout development and during the course of immune homeostasis, inflammation and the induction of adaptive immune responses. Due to its ligand specificity, CCRL1 could broadly impact the immune system in areas such as development and immune function. CCRL1 is already emerging as a regulator of adaptive immune responses with key papers published in recent years detailing its role in adaptive immunity.

Therefore, based on previous studies and on going investigations within the lab, I focused my investigations on characterising the impact of CCRL1 deficiency on the mouse immune system. As one of the principal roles of CCL21 is to direct DC migration from the periphery, I sought to examine in detail the role of CCRL1 in coordinating DC migration to peripheral lymph nodes. I explored the impact of CCRL1 deletion on DC migration during inflammation using contact sensitisation assays and models of cutaneous inflammation. It was anticipated that these investigations would enhance our understanding of how CCRL1 coordinates DC migration and may explain why CCRL1-deficient mice have aberrant adaptive immune responses.

I also set out to explore the binding of CCRL1 to post-translationally modified chemokines. A report by Schumann and colleagues published at the beginning of my thesis reported that CCL21 could be proteolytically cleaved by mature DCs to produce a chemotactically active truncated, soluble fragment of CCL21. The enhanced diffusivity of this version of CCL21 might make it be particularly important target for putative regulation by CCRL1. I was interested in understanding the mechanism of this truncation and also to explore if DCs and other leukocytes interact with other C-terminally extended chemokines to produce shortened truncated forms.

I also focused on understanding interactions between cells residing at the SCS region of the lymph node and interfollicular regions. The SCS is home to CCRL1-expressing cells and I hypothesised that CCRL1 may affect the interactions, numbers and positioning of cells residing within or near the SCS.

Therefore, I characterised cells present within or near the SCS at rest and also during inflammation. These studies developed my interest in the significance of interactions between lymph node LECs and SCS macrophages. I investigated this by examining the expansion of lymphatic cells that occurs during inflammation and the role that SCS macrophages play in lymphangiogenic process. I was also interested to see how loss of CCRL1 expression affects expansion of these cells.

## **1.16 Hypotheses**

Based on the discussions above, the following hypotheses were formulated:

- 1) CCRL1-mediated regulation of CCL19 and/or CCL21 regulates the migration of DCs to lymph nodes during inflammation.
- 2) Leukocytes can cleave immobilised chemokines to release soluble versions that are regulated by CCRL1 and other atypical chemokine receptors.
- 3) CCRL1 regulates leukocyte abundance and distribution in the subcapsular and interfollicular regions of lymph nodes.
- 4) SCS macrophages control lymphangiogenic responses in lymph nodes during inflammation.

Progress was made in addressing each of these hypotheses, however, over the course of the experimental work, some projects developed more successfully and formed the principle focus of my efforts. These studies are described in Chapters 3-5. All work was conducted at the University of Glasgow, except for studies using CCR7-deficient mice, which were undertaken by myself at MGH, Harvard Medical School, Boston, MA. During my time at MGH I also learned how to utilise kaede transgenic mice for cellular migration studies.

The results are discussed in depth in the Discussion section (Chapter 6) where I link the different arms of this project and present a comprehensive picture of our current understanding of the function of the atypical chemokine receptor CCRL1.

# Chapter Two

## Materials and Methods

## 2 Materials and Methods

### 2.1 Animals

CCRL1-deficient mice were generated in Professor Rob Nibbs's lab as described elsewhere<sup>364</sup>. These animals were bred and maintained under specific pathogen free conditions (SPF) at the Beatson Research Facility located in the University of Glasgow. Wild-type C57B/6J (WT) mice were bought in from Harlan and housed at the Beatson for all experiments.

D6-deficient mice were generated by others<sup>304</sup> and bred on a C57B/6J background at the Beatson Institute for Cancer Research, Glasgow, under SPF conditions.

Kaede transgenic mice were obtained from Dr. Osami Kanagawa<sup>365</sup> (RIKEN Institute), rederived at Taconic, and then bred at Massachusetts General Hospital (MGH).

CCR7-deficient mice on a C57B/6J background were obtained from the Jackson Laboratory, and were housed at MGH under SPF microisolator environment. Strain name: B6.129P2(C)-Ccr7tm1Rfor/J, stock number: 006621.

CCR7 KO kaede transgenic mice on a C57B/6J background were generated in the Luster lab and housed at MGH under an SPF microisolator environment.

CCRL1-deficient kaede transgenic mice were generated in our lab by crossing C57Bl6 CCRL1-deficient mice with C57Bl6 kaede transgenic WT mice in order to produce mice with the desired genotype. These mice were then housed at the CRF, Glasgow, under SPF conditions.

CCRL1<sup>+/*gfp*</sup> transgenic mice were a kind gift Thomas Boehm<sup>360</sup>. CCL19-deficient mice on a C57B/6J background were a kind gift from Sanjiv Luther<sup>271</sup> (Universite de Lausanne). CCRL1-deficient x CCL19-deficient mice were generated in our lab and maintained on a C57B/6J background.

All procedures were conducted in accordance with the UK Home Office regulations and they were designed in order to comply with the necessary project

and personal licenses and had received ethical approval from the University of Glasgow ethics committee. The institutional care and use committee at MGH approved all animal studies conducted at MGH. Male animals were used throughout and typically animals were used at 6-10 weeks of age, and age matched within all experiments. Animals were sacrificed by CO<sub>2</sub> asphyxiation or cervical dislocation, as appropriate.

## **2.2 Genotyping of Genetically-Modified Mice**

When genotyping was required, tail-tips were removed using a scalpel blade by CRF staff then stored in 1.5mL eppendorfs at 4°C. Tail tips were incubated in 1.5mL eppendorf tubes at 55°C in 100 µl lysis buffer (5mM EDTA, 0.1mg/mL Proteinase K, 0.2% SDS, 100mM Tris.HCl, 200mM NaCl) for 5 hours on a heating block with gentle shaking. Tubes were then heated to 95°C for 5 minutes before 500µl of distilled water was added. Tubes were then centrifuged at 13,000 rpm for 5 minutes in a microcentrifuge to remove cellular debris. The genomic DNA-containing supernatant was used in a standard PCR reaction. 45µl of Prealiquoted ABgene PCR master mix “Reddymix” (Applied Biosystems) was used to carry out the PCR reaction. For each tailtip sample, 2.5µl of the primer mix along with 2.5µl of the template genomic DNA was added to each tube of the Reddymix. The three components were mixed using a pipette, pulsed using a microcentrifuge and then transferred to a PTC-200 Peltier Thermal Cycler (MJ research). The PCR products for each sample were then electrophorised for 1.5hours at 100V on a 2% agarose gel containing 10µl SYBR safe (Invitrogen). In order to assess the product size of each sample, 10µl of HyperLadder I (Bioline) was added to a well in the gel and the size of the sample PCR product compared to the various sized bands. DNA in the gel was visualised using a UV transilluminator.

Kaede mice were genotyped by harvesting peripheral blood from tail veins. After red blood cell lysis, cells were stained with Viaprobe, resuspended in FACS buffer and analysed by flow cytometry for kaede green positivity.

## **2.3 Animal Procedures**

### **2.3.1 Induction of Skin Inflammation**

Mice were shaved on the lower back 24 hours prior to administration of topical irritants. The mice were then treated with 12-O-tetradecanoylphorbol-13-acetate (TPA - Invitrogen) that was suspended at a concentration of 50 $\mu$ M in acetone. 150 $\mu$ l of the 50 $\mu$ M TPA was applied to the dorsal skin using a p200 pipette. Mice were then challenged dorsally 24 hours later with 150 $\mu$ l of fluorescent isothiocyanate isomer I (FITC - Sigma) and sacrificed 24, 72, 96, 120 and 144 hours later for analysis by RT-QPCR, Western Blot, Immunohistochemistry, flow cytometry and ELISA. In some experiments, TPA&FITC were painted together and tissues harvested 24 hours later.

### **2.3.2 Injection of CFA Into the Ear / Foot Pad**

Complete Freund's Adjuvant (CFA) (MD Bioscience) at 4mg/mL was added to an equal amount of PBS (1:1) and emulsified using a tissue homogeniser to create a paste. 50 $\mu$ l was injected intra-dermally into the ear to induce skin inflammation.

Alternatively, 50 $\mu$ L of a 4mg/mL CFA emulsion was injected into the paw of mice with and without pre-administration of clodronated liposomes in order to induce lymphatic vessel expansion in popliteal and inguinal lymph nodes.

### **2.3.3 Photo-conversion of Kaede Transgenic Mice**

Kaede transgenic mice were shaved on the lower back skin, anaesthetised and then the dorsal skin was exposed for 5 minutes to a U.V light (420 nm) using a Bluewave LED visible light-curing unit (Dymax Figure 2.1). The light unit was equipped with a 420 nm filter (Andover). In order to ensure consistency between photo-conversions, the light was placed at a distance of 7 cm above the dorsal flank and held in place with a stand clamp. As was reported in the literature, exposure to violet light does not affect leukocyte proliferation, induce IL-1 $\beta$

mRNA expression or affected leukocyte chemotaxis towards the chemokine CCL21<sup>365</sup>.

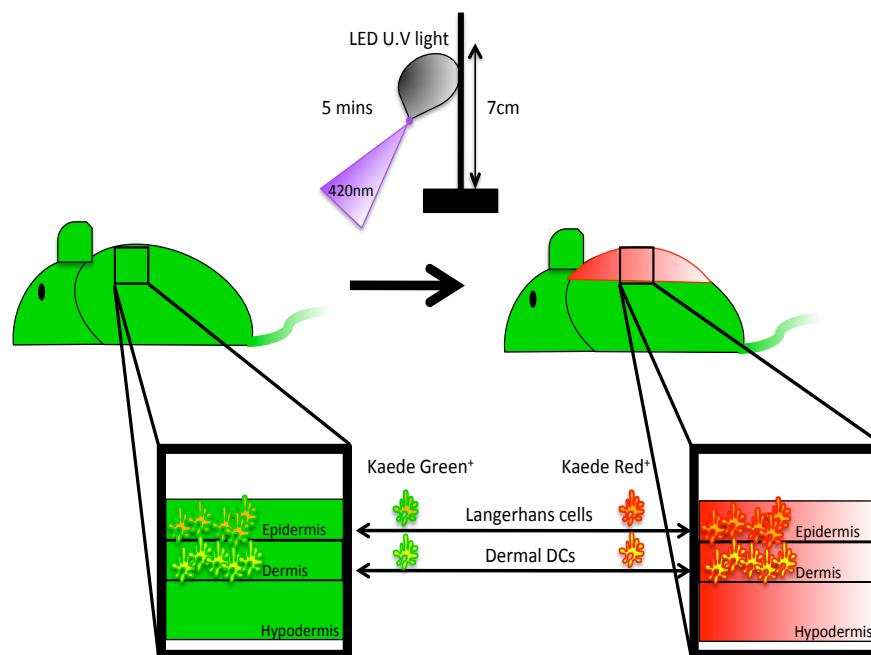


**Figure 2.1: Photoconversion of kaede transgenic mice.**

Kaede transgenic mice express kaede green protein under the control of the  $\beta$ -actin promoter. Upon flashing the skin with an ultraviolet light for 5 minutes, kaede green cells residing in the exposed back skin switch to expressing kaede red protein. This is an irreversible switch from green to red.

### **2.3.4 *In vivo* Macrophage Depletion by Injection of Clodronated Liposomes**

Macrophages were depleted *in vivo* using clodronated liposomes (Encapsula Nano Sciences). Mice were injected into the hind paw with 30 $\mu$ l of 5mg/mL clodronated liposomes buffered at pH 7.4, and then left for different periods of time, up to a maximum of two weeks, after which draining popliteal lymph nodes and inguinal lymph nodes were harvested for analysis. Control mice were injected with 30 $\mu$ l of PBS or 30 $\mu$ l of 5mg/mL control Fluoroliposomes (Encapsula Nano Sciences). Fluoroliposomes contain a PE dye instead of clodronate and allow the cells that engulf and internalise the liposomes to be identified and tracked.

### **2.3.5 Adoptive Transfer of Splenocytes**

Spleens were harvested from WT mice, single cell suspensions made by mashing the spleens through 70µm filters (BD Bioscience) and red blood cells depleted by incubating samples with 5mL of red blood cell lysis buffer (Sigma) for 5 minutes at room temperature (RT). Cells were then washed in 40mL of complete RPMI medium (CRM) containing 10% fetal calf serum (FCS), 5% L-glutamine and 5% penicillin/streptomycin, centrifuged at 400g for 5 minutes and cells resuspended in CRM. Splenocytes were incubated with 2.5mM CellTracker™ Red (CMTPX) (Invitrogen) for 30 minutes at 37°C in CRM. Cells were washed in 10mL of CRM, centrifuged at 400g for 5 minutes and adjusted to 10<sup>7</sup> cells/mL in PBS. 100µl of labeled splenocytes were then injected intravenously into the tail vein of WT and CCRL1-deficient mice. 1 or 2 hours after injection, spleens were harvested, snap frozen in OCT compound and stored at -80°C for subsequent analysis.

## **2.4 Sample Handling and Preparation**

### **2.4.1 Isolation of Leukocytes from Lymphoid Tissues**

Peripheral lymph nodes were harvested, placed into ice-cold complete-RPMI media (CRM), mechanically disrupted using a surgical blade (Swann-Morton) and incubated in 1.5mL eppendorf tubes at 37°C with 1mL of 1mg/mL Collagenase D (Roche) in HBSS (Invitrogen) for 45 minutes with gentle agitation. Collagenase D is needed in order to retrieve DC populations that adhere to fibroreticular surfaces.

Spleens were harvested into tubes containing ice-cold CRM, cut into 5mm<sup>2</sup> chunks using scissors, and placed in 1.5mL eppendorf tubes. To this was added 1mL of 1mg/mL collagenase D (Roche) in HBSS (Invitrogen). Spleens were incubated for 45 minutes, with gentle agitation at 37°C.

Peripheral lymph nodes and spleens were then passed through 70µm filters (BD Bioscience) and homogenised using a 1mL syringe plunger and washed through

with CRM to give a single cell suspension. For spleen, an additional step in the preparation of the samples was undertaken in which red blood cells were lysed by adding 4mL of red blood cell lysis buffer (Sigma) to the samples and then incubating for 5 minutes at RT. Samples were then flooded with 20mL of CRM, vortexed and then centrifuged at 400g for 5 minutes. Resulting cell pellets were then further analysed.

### **2.4.2 Isolation of Leukocytes from the Skin**

Shaven mouse dorsal skin was harvested from mice and stored in 5mL of CRM and placed on ice. The skin was cut into ~5mm<sup>2</sup> pieces using surgical dissection scissors and incubated in 7mL RPMI-1640 containing 1mg/mL Collagenase D (Roche) 0.5mg/mL Dispase (Sigma) and 0.05mg/mL DNase I (Invitrogen) for 1.75 hours. 3mL of fresh media containing the aforementioned enzymes was added after 30 minutes and then after 1 hour. The skin and supernatant were passed through a 70µm filter (BD bioscience) using a 2mL syringe plunger (BD bioscience) and flushed through with CRM. The flow-through was collected in a 50mL Falcon tube (BD Bioscience) and centrifuged at 400g for 5 minutes. The resulting pellet was then washed with fresh RPMI-1640 media, centrifuged at 400g for 5 minutes, the supernatant discarded and the cell pellet re-suspended in chilled fresh RPMI-1640 and stored at 4°C for subsequent analysis.

### **2.4.3 Skin Crawl-out Assay**

Shaved skin was excised from the backs of mice. Adhering fat and connective tissue was gently scraped away using a scalpel, and the skin cultured in 6 well tissue culture plates (Costar) containing CRM supplemented with 20ng/mL granulocyte colony stimulating factor (GM-CSF) (Peprotech). Skin was cultured for 72 hours to allow DCs to migrate and collect in the media. After 48 hours, 3mL of fresh CRM was added. Cells that had crawled out the skin and into the media were harvested by centrifuging the CRM for 5 min at 400g. At the same time, the skin that remained was digested as described previously (Section 2.4.2), and the resulting single cell suspension stained with the appropriate FACS antibodies. Skin crawl out cells were stained with the same panel of antibodies.

Total skin crawl out cells as well as total cells remaining in the skin were analysed by flow cytometry.

## **2.5 Separation of Leukocytes from Human Buffy Coats**

Peripheral blood mononuclear cells (PBMCs) were purified from buffy coats by first diluting the blood 1:2 in PBS. Approximately 10mL of diluted blood was layered on top of Histopaque 1077 (Sigma) at room temperature, and then centrifuged at 400g for 20 minutes, also at RT. The mononuclear cell layer was then carefully removed using a 10mL pipette and transferred into a 15mL Falcon tube. The cells were washed in 10mL of chilled PBS with 2% FCS, followed by centrifugation at 4°C for 5 minutes at 200g. This procedure was repeated until all cells from the same sample were pooled into a single tube. The number of cells was enumerated using a haemocytometer. Cells were diluted to the desired concentration and cultured at 37°C in 5% CO<sub>2</sub> with the addition of cytokines and TLR agonists as described.

### **2.5.1 Leukocyte isolation from Lymphoid Tissues by MACS**

#### **Bead Separation**

This experimental technique is used to isolate particular cell subsets from a mixed cell population by the use of magnetic bead conjugated antibodies. Single cell suspensions of total lymph node cells were prepared as described previously (Section 2.4). Anti-CD90.2 or anti-CD19 coated microbeads (Miltenyi) were used to separate T cells and B cells respectively. Single cell suspensions were incubated in CRM containing microbeads as per manufacturers instruction. Briefly, cells up to a maximum of  $1 \times 10^7$  cells were suspended in 40µl of MACS buffer (2nM EDTA, 0.5% BSA in PBS) and to this was added 10µl of antibody coated microbeads for 30 minutes at 4°C to allow binding to surface antigen. Cell suspensions were washed by centrifugation at 400g, re-suspended in 500µl of cold MACS buffer, transferred to an LS column (Miltenyi) and placed on a magnetic MACS separator (Miltenyi). The magnetically labelled cells were

added to the column. The negative fraction (the effluent) was allowed to flow through the column whilst the positive fraction (magnetically labelled B cells or T cells) adhered to the walls of the column – Positive selection. Adherent Cells were washed three times using MACS buffer as per manufacturer's instructions to ensure only positive selected cells remained. After the negatively selected cells had passed through the column, ice-cold MACS buffer was added to the column, the column removed from the magnet, and the plunger depressed slowly to elute the positive fraction. Collected cells eluted from the column were then placed on ice for subsequent analysis. Cells from the effluent were kept for analysis by flow cytometry to show specific depletion of the positively selected cells from the negative fraction.

### **2.5.2 Bio-available Chemokine Quantification – Punch Biopsies**

Dorsal skin was excised from mice and pinned out onto a cork dissection board using needle syringes. Biopsies of ~5mm in diameter were obtained by cutting the skin with a punch biopsy blade (Stiefel). A total of 10 biopsies/ portion of skin / mouse were retrieved. The biopsies were placed in a 1.5mL eppendorf tube containing 400µl of PBS containing protease inhibitor cocktail (Sigma) and incubated on a rotator for 5 hours at 4°C to allow chemokine to leach from the skin samples. After incubation, the tubes were centrifuged for 1 minute at room temperature at 10,000xg in order to pellet the skin and allow the supernatant to be harvested. Supernatants were then stored at -80°C for future analysis by ELISA.

### **2.5.3 Tissue Embedding and Sectioning – Frozen Sections**

For frozen sections, tissues were harvested into cryomoulds (VWR) containing Tissue-Tek OCT Compound (Sakura), snap frozen in liquid nitrogen, and stored in the -80°C for subsequent sectioning. Samples were cut using a cryostat machine (Thermo Scientific) to a thickness of 8-10µm and mounted onto poly-L-lysine microscope slides (VWR). For each slide, serial sections were made so that each slide contained three tissue sections. Sections were then fixed by

placing them in ice-cold acetone for 20 minutes in the -20°C freezer. Samples were stored at -80°C for subsequent immunofluorescent staining.

## **2.6 Immunofluorescence Staining – Frozen sections**

Frozen tissue sections were brought to RT by placing the slides on tissue paper and thawing for 20 minutes. A wax ring was then drawn around each tissue section using a wax pen (Vector Labs). Sections were then blocked with block solution (PBS containing 1% BSA (Sigma) and 10% donkey serum (Sigma)). The serum used for the blocking step was dependent upon the species in which the secondary antibody was raised. Therefore, when primary antibodies raised in a rabbit were used, the blocking solution would contain rabbit serum. Whenever the secondary antibody was raised in a goat, donkey serum was used instead of goat serum as goat serum leads to a high degree of non-specific staining. Donkey serum provides a good reduction in non-specific staining across a variety of different species. Sections were blocked by adding 100µl of the block solution to each section and incubating for 20 minutes at RT, after which the block solution was gently removed by tapping the slide onto tissue paper. Residual block solution remained on the slide and to this was added 100µl of antibody cocktail containing the appropriate antibodies diluted to the correct dilution in PBS. Antibody staining was carried out at RT in the dark for 2 hours or alternatively at 4°C overnight in a staining chamber depending upon the antibodies used. The tissue sections were then washed once in PBS containing 0.05% tween-20 (PBST) (Invitrogen), allowed to dry, and then stained with DAPI nuclear stain (Vector Laboratories). It was noted that Vectashield hard-set mounting medium with DAPI led to auto-fluorescence therefore we used the soft set mounting medium with DAPI and sealed the slide with a cover slip and clear nail varnish. Sections were then immediately visualised using a Zeiss Axio Imager fluorescent microscope (Zeiss).

## **2.7 Image J analysis of Lymph Nodes**

Whole images of lymph nodes were generated by confocal microscopy using the tiling program software (Zeiss). Digital images were analysed using NIH ImageJ software. A CD169 or LYVE-1 'score' was quantified for each individual lymph node and represented as a percentage of the total lymph node area (CD169-positive area/whole lymph node area or LYVE-1-positive area/whole lymph node area). The mean lymph node scores were calculated and represented in a graph.

<b>Ag/Ab</b>	<b>Expression</b>	<b>Supplier</b>	<b>Conc<sup>n</sup></b>	<b>Species/ Fluorophore</b>
<b>LYVE-1</b>	Lymphatic endothelial cells Macrophages	R & D	1:200	Purified monoclonal Rat IgG2A
<b>CCRL1 (CCX- CKR)</b>	Undefined – as part of project	Santa Cruz	1:50	Purified goat polyclonal IgG
<b>CD169</b>	Macrophages	AbD Serotec	1:200	Rat IgG2A – FITC Rat IgG2A- AF647
<b>B220</b>	B cells pDCs	eBioscience	1:200	Rat IgG2a AF647
<b>CD3</b>	T cells	eBioscience	1:200	Rat IgG2B e450 Rat IgG3 FITC
<b>CD11b</b>	Macrophages Monocytes DC subsets Neutrophils Langerhans cells	eBioscience	1:200	Rat IgG2B eFluor 660
<b>EpCAM</b>	Langerhans cells DCs T cells	eBioscience	1:100	Rat IgG2a APC
<b>MHCII</b>	Antigen presenting cells	eBioscience	1:200	Rat IgG2a eFluor 450 FITC
<b>IgD</b>	B cells	eBioscience	1:200	Rat IgG2a eFluor 450

**Table 1: Antibodies for immunofluorescent staining**

### **2.7.1 Staining of Cells for Injection into Mice**

B and T cells were isolated from mouse spleens as described previously (Section 2.5.1). Splenocytes were isolated from WT spleens as described previously. Cells were re-suspended at  $5 \times 10^6$  cells/mL in PBS containing 5% FCS and cultured at 37°C in 5% CO<sub>2</sub>. Carboxyfluorescein succinimidyl ester (CFSE) (Invitrogen) was diluted from a 5mM stock solution to a concentration of 10µM and added to an equal volume of cell suspension. Cells were then mixed with the CFSE and cultured for 30 minutes. For CMTPIX staining, the dye freely passes through the cell membrane and is then converted into a cell-impermeable form. For staining, a stock solution of 10mM was prepared by dissolving the lyophilized product in 7.3µl Dimethyl Sulfoxide (DMSO) (Sigma). A working concentration of 10µM was prepared in serum free RPMI and added to an equal volume of cell suspension. After mixing, the cells were cultured for 30 minutes at 37°C, 5% CO<sub>2</sub>. After culturing the cells with the appropriate dye, they were washed once in CRM and re-suspended in PBS for injection.

### **2.7.2 Preparation of Homogenates for ELISA / Western Blot**

#### **Analysis**

The tissue of interest was immersed in Tissue Protein Extraction Reagent (T-PER) (Thermo Scientific) containing complete, mini, EDTA-free protease inhibitor cocktail tablet (Roche) diluted 1:3 in distilled water. A steel bead (Qiagen) was then added into the eppendorf and the samples placed into a Tissuelyser LT homogeniser (Qiagen) for 7minutes to homogenise the tissue. After this time, tissue debris and the steel bead were excluded from the sample by centrifuging at 10000g for 5 minutes and the resulting supernatant harvested for further analysis or stored at -20°C.

### **2.7.3 Quantification of Chemokine Concentrations by ELISA**

Chemokine protein levels were detected by using DuoSet ELISA kits (R&D Systems). To detect CCL19 or CCL21, ELISA plates (Corning) were coated with 100µl of anti-CCL19 (2ug/mL R&D systems) or annti-CCL21 (4ug/mL R&D

systems) capture antibodies overnight at RT. Plates were then washed three times with PBS Tween (0.05%) before blocking with 300µl of reagent diluent (PBS/10%BSA) for 2 hours at RT. The plates were again washed 3 times with PBS Tween (0.05%) and incubated for 2 hours with serially diluted recombinant chemokine standards (R&D systems) in triplicate to allow for extrapolation of chemokine concentrations as per manufacturer's instructions. At the same time, 100µl of samples, in duplicate, were also added to the plate for 2 hours for assessment of chemokine protein concentrations. Plates were then washed 3 times with PBS Tween (0.05%), and incubated with specific biotinylated detection antibodies (100ng/mL of anti-CCL19 (R&D Systems) or (50ng/mL of anti-CCL21 (R&D Systems) for 2 hours in reagent diluent at RT. Plates were washed and incubated with 100µl of streptavidin horseradish-peroxidase (1/200 dilution (R&D systems) for 20 minutes at RT. Following a final series of washes with PBS Tween, plates were developed using tetramethylbenzidine (TMB) enzyme substrate (KPL), and the reaction stopped after 20 minutes by addition of sulphuric acid stop solution (R&D Systems). Plates were then read using a Sunrise microplate absorbance reader (Tecan) using Magellan software (Tecan). Samples concentrations were determined by extrapolating data from the standard curve and by using Magellan software.

## **2.8 Molecular Methods**

### **2.8.1 Isolation of RNA**

Mouse tissues were dissected into cryovials, snap frozen in liquid nitrogen, and stored at -80°C for subsequent analysis. Tissue was allowed to thaw at R.T, then 500µl of TRIZOL (Invitrogen) was added along with a stainless steel bead (Qiagen) and the samples were disrupted using a TissueLyser LT machine (Qiagen). Samples were placed in the LT machine for a total of 7 minutes at 4°C. Samples were centrifuged and the supernatant harvested and then stored at -80°C or further processed using an Rneasy mini kit (Qiagen) as per manufacturer's instructions.

## **2.9 Complementary DNA (cDNA) Synthesis**

Reverse transcription was carried out using an AffinityScript Multiple Temperature cDNA Synthesis Kit (Agilent) as per manufacturer's guidelines. Briefly, 300ng-5µg of starting RNA for each sample was made up to 14.7µl by the addition of nuclease-free water and 1µl of oligo(dT) primer (0.5µg/µl). Samples were then incubated in a PTC-200 Peltier Thermal Cycler at 65°C for 5 minutes and then 21°C for 10 minutes. These temperatures facilitate the removal of secondary structures in the RNA and allow the annealing of primers to the RNA, respectively. Next, a mastermix of the following components was made; 1µl of AffinityScript Multiple Temperature reverse transcriptase, 1X AffinityScript RT buffer, 2mM dNTP mix and 20U RNase Block Ribonuclease Inhibitor. 4.3µl of the mastermix was added to each sample. Samples were incubated at 42°C for 5 minutes in order to initiate the reaction and then 55°C for 1 hour and 70°C for 15 minutes (to extend the products and terminate the reaction respectively). After synthesis of the cDNA products, samples were usually used immediately for RT-QPCR analyses, or stored at -20°C for future analyses.

## **2.10 TaqMan QRT-PCR**

Complimentary DNA (cDNA) samples were prepared as previously described. Each cDNA sample was assayed in triplicate in either a 96 well plate or a 384 well plate. For each reaction, two controls were employed; no reverse transcriptase (-RT) control and no template control (NTC). NTC samples contained nuclease free water. All primers and TaqMan probes were purchased from Applied Biosystems. Those chosen generated products that spanned exon-exon boundaries to avoid amplification from contaminating genomic DNA. Gene expression was normalised to TATA box binding protein (Tbp) and gene expression changes calculated using the  $2^{-\Delta\Delta C_t}$  method.

Target Gene	Abbreviation	Assay ID	Amplicon length (B.Ps)
<b>Chemokine (C-C motif) receptor-like 1</b>	CCRL1	Mm02620636_s1	146
<b>Chemokine (C-C motif) ligand 19</b>	CCL19	Mm00839967_g1	79
<b>Chemokine (C-C motif) ligand 21</b>	CCL21	Mm03646971_gH	91
<b>Chemokine (C-C motif) receptor 7</b>	CCR7	Mm01301785_m1	78
<b>TATA box binding protein</b>	Tbp	Mm00446973_m1	73

**Table 2: Gene probes for TaqMan**

## 2.11 SDS-PAGE and Western Blot Analysis

Samples were either prepared from lymphoid tissue homogenates or from cell supernatants as described previously (Section 2.7.2). 20µl of sample was mixed with 5µl of x4 concentration loading buffer (Thermo Scientific) and 2.5µl of NuPAGE SDS sample reducing agent (Invitrogen). Each sample was incubated at 90°C for 10 minutes to ensure all proteins in the samples were in a linear form. Samples were centrifuged at 10,000 rpm in a microcentrifuge for 15 seconds, and 20µl of each sample was loaded into a pre-cast 4-12% Bis-Tris acrylamide gel (Invitrogen). In order to assess the size of the protein band, 10 µl of Novex Sharp pre-stained Protein Standard (Novex) was added to a well in the gel. The standards consist of 12 proteins ranging from 3.5 – 250 kDa in size, each with their own unique colour. Samples were electrophoresed in MOPS or MES running buffer (Invitrogen) at 200V for 30 minutes. Proteins were transferred onto a nitrocellulose membrane (Whatman) using NuPAGE transfer buffer (Invitrogen) with 20% (v/v) methanol for 1hour at 100V.

Following transfer, the membrane was washed using distilled water and then blocked overnight at 4°C (or for 2 hours at RT.) in PBST with 10% non-fat milk

protein (Marvel). Primary antibodies (anti-CCL19, anti-CCL21, anti-CCL25 and anti-CCL2 (R&D Systems) were added at 1:1000 dilution in 5% Marvel overnight at 4°C or in 5% Marvel for 2 hours at RT. Membranes were then washed 3x in PBST, 5 minutes per wash. Next, horseradish peroxidase (HRP)-conjugated secondary antibody was added at a concentration of 1:5000 in PBST containing 5% Marvel for 1 hour at R.T. Membranes were then washed three times in PBST, 5 minutes per wash. Bound HRP was then detected by chemiluminescence with addition of either West-Pico or SuperSignal West-Femto (Thermo Scientific) developing agents. For both detection methods equal volumes of solution A and solution B were pre-mixed in a bijoux tube and then 1mL of this solution was added to the nitrocellulose membrane and sealed within a plastic sandwich bag. The membrane was incubated for 1 minute and then excess solution poured off. Finally, membranes were placed within a fresh sandwich bag and then visualised by exposing the membrane to KODAK X-ray film. X-ray films were developed using an X-ray film processor.

## **2.12 Generation of Leukocytes from Bone Marrow**

### **2.12.1 Generation of DCs using GM-CSF**

Mice were sacrificed and femur bones extracted by cutting through connective tissue to free them from adhering soft tissue and muscle. The femurs were cut at both ends using scissors and to one end of the bone, RPMI medium was injected allowing the bone marrow to flush out of the other extremity. The bone marrow was mashed using the plunger of a 1mL syringe, passed through a 70µM filter and the suspension centrifuged at 400g for 5 minutes to obtain a cell pellet. This pellet was re-suspended in 5mL of CRM and cells counted using a haemocytometer. The bone marrow cells (BMCs) were then re-suspended to  $3 \times 10^6$  cells/mL in CRM, and 1mL of this suspension was added to 9mL of CRM supplemented with GM-CSF at a concentration of 40ng/mL. Cells were cultured on ultra-low adherence Petri dishes (Corning) for 7 days with 20% of the media being replaced on day 3 and 5 with fresh GM-CSF supplemented CRM.

### **2.12.2 Generation of DCs using Flt3L**

CHO-Flt3L cells were a kind gift from Dr Simon Milling, University of Glasgow. These cells were cultured in T75 flasks in CRM, and cells were harvested twice weekly upon reaching 70-80% confluence and conditioned media (CM) containing Flt3L was harvested typically every 3 days. CM was filtered through a 0.2µm pore filter syringe. The amount of Flt3L in CM was determined by ELISA as per manufacturers instructions (R&D Systems). Isolation of bone marrow was conducted in the same way as described previously.  $3 \times 10^6$  BMCs were cultured in CRM supplemented with 10% CM. Cells were cultured for a total of 9 days and on day 5 20% of the media was substituted with fresh CM.

### **2.12.3 Activation of Dendritic Cells *in vitro***

Bone marrow generated dendritic cells (BMDCs) ( $3 \times 10^6$ ) matured by either GM-CSF or Flt3L were activated *in vitro* by the addition of TLR agonists. On day 7 of culture for GM-CSF matured DCs and on day 9 for Flt3L matured DCs, 200ng of the TLR4 agonist *Escherichia coli* lipopolysaccharide (LPS) (Sigma) or 200ng of the TLR 7 agonist R848 (Enzo life science) was added to the 10mL cultures for 48 hours to induce activation. Cells cultured without LPS/R848 were supplemented with fresh medium at this time and then cultured for 48 hours. Non-adherent cells were analysed by flow cytometry to assess the purity of the DC population as well as their activation status.

### **2.12.4 Generation of Macrophages**

BMCs were isolated from femurs as in Section 2.12.1. BMCs were adjusted to a concentration of  $3 \times 10^6$ /mL in CRM. 1mL of this cell suspension was added to a 60mm petri dish along with 9mL of CRM containing 40ng/mL M-CSF (Peprotech). BMCs were cultured for 7 days with 20% of the media being replaced on day 3 with fresh M-CSF (40ng/mL) in CRM. Non-adherent cells were harvested and discarded and adherent cells harvested by adding ice cold PBS/1mM EDTA for ~ 5 minutes and then scraping the bottom of the petri dish

using cell scrapers (Costar). The adherent cells were analysed by staining cells with antibodies against F480 and CD11c and analysing by flow cytometry. CD11c<sup>-</sup> F480<sup>+</sup> cells were considered to be macrophages.

## **2.13 Chemokine Cleavage Assay**

1x10<sup>5</sup> leukocytes were cultured in flat-bottomed 96-well tissue culture plates (Costar) at 37°C in 5% CO<sub>2</sub> in 100µl of CRM containing 150ng of CCL21, CCL19, CCL25 or CCL2 (R&D Systems) to assess DC mediated chemokine cleavage. Depending on the experiment, the DCs were cultured with the chemokines for 2, 4, 6, 8 or 16 hours. The plates were spun down at 400g for 5 minutes, the supernatants harvested and stored at -20°C for future analyses.

### **2.13.1 Staining of Leukocytes for Flow Cytometry Analysis**

Up to 4 x 10<sup>6</sup> cells in FACS buffer (PBS, 1%FCS, 0.02% sodium azide and 5nM EDTA) were aliquotted into FACS tubes (BD Bioscience) and centrifuged at 400g for 5 minutes. Cells were re-suspended in 100µl of FACS buffer containing anti-mouse CD16/CD32 monoclonal antibody (Fc block) diluted at 1:100 (BD bioscience) for 15 minutes at 4°C to prevent non-specific binding of antibodies to Fc receptors. The cells were then centrifuged at 400g for 5 minutes, the supernatant aspirated and then stained with the antibody cocktail of interest. A list of antibodies used for the specific surface markers of interest is listed in (Table 3). All antibodies were used at 1:200 with the exception of CCR9 (1:50), CD169 (1:50), MHCII (1:400) and Langerin (1:100). In order to exclude dead cells during data analysis, the cells were treated with either Viaprobe (Invitrogen) or fixable viability dye AF780 (eBioscience). 7µl Viaprobe was added directly to the stained cells 15 minutes prior to running the cells through the flow cytometer. Prior to staining with fixable viability dye, cells were washed with PBS to remove any residual foetal calf serum from the FACS buffer as this interferes with cell staining by the fixable viability dye. 100µl of fixable viability dye was added to the cells at 1:1000 dilution for 30 minutes at 4°C in the dark. Cells were then centrifuged at 400g for 5 minutes washed in PBS and then re-suspended in FACS buffer for subsequent analysis by flow cytometry.

### **2.13.2 Intracellular Flow Cytometry Antibody Staining**

Cells were isolated, stained with antibodies against surface antigens as described in (Section 2.13.1), and labelled with fixable viability dye. Cells were permeabilised using a commercial permeabilisation kit (FixPerm kit (BD Bioscience)). Briefly, cells were incubated in 100µl of cytofix / cytoperm (BD) in order to fix and permeabilise the cells. Cells were washed twice in permwash (BD), and the intracellular antibody was added at the correct dilution in permwash (BD) for 30 minutes at 4°C in the dark. Cells were washed twice in 500µl of permwash (BD) and re-suspended in FACS buffer for analysis by flow cytometry.

<b>Antibody Target</b>	<b>Notes</b>	<b>Expression</b>	<b>Suppliers</b>	<b>Conjugate Dyes</b>
<b>CD11c</b>	Integrin Involved in phagocytosis Component of complement receptor 4 (CR4)	DCs, Macrophages	BD Biosciences	PE, PeCy7 PERCP APC
<b>CD11b</b>	Integrin, adhesion molecule Involved in phagocytosis Component of complement receptor 3 (CR3)	Macrophages, Granulocytes DCs NK cells B cells	eBioscience	E450 AF660 PE
<b>MHCII</b>	Antigen presentation	Antigen presenting cells	eBioscience	E450 PeCy7
<b>CD86</b>	Co-stimulatory molecule	Antigen presenting cells	BD Biosciences	PE
<b>CD8a</b>	TCR co-receptor	DCs and T cells	BD Biosciences	PECy7 PE
<b>CD103</b>	Intestinal and skin homing	DCs, T cells, intraepithelial lymphocytes	eBioscience	APC
<b>Langerin (CD207)</b>	Type II transmembrane, C-type lectin receptor	DCs, Langerhans cells	BD Biosciences	PE
<b>CD24</b>	Cell adhesion molecule.	DCs, B cells Granulocytes	eBioscience	PERCP

<b>Antibody Target</b>	<b>Notes</b>	<b>Expression</b>	<b>Suppliers</b>	<b>Conjugate Dyes</b>
<b>CD205/ DEC-205</b>	C-type lectin.	DCs, Langerhans cells pDCs NK cells	eBioscience	PECy7
<b>NK1.1</b>	NK cell receptor NK cell activation	NK cells, iNKT cells	Biolegend	PECy7 PERCP- Cy5.5
<b>CD3</b>	TCR signaling complex	T cells	eBioscience	FITC e450 PERCP
<b>CD4</b>	TCR co-receptor	T cells, DCs	BD Biosciences	Pacific blue APC
<b>CD19</b>	BCR co-receptor	B cells	eBioscience	E450
<b>B220</b>	Protein Tyrosine phosphatase	B cells, NK cells	eBioscience	PECy7 AF647
<b>LY6C</b>	Glcoprotein T cell activation	Monocytes Macrophages Granulocytes T cell subsets	BD Biosciences	FITC APC
<b>LY6G</b>	Leukocyte migration	Neutrophils	eBioscience	APC FITC
<b>GR1</b>	Leukocyte migration	Granulocytes		APC
<b><math>\gamma\delta</math> TCR</b>	T cell signaling	$\gamma\delta$ T cells	Biolegend	PERCP- Cy5.5 PE
<b><math>\alpha\beta</math> TCR</b>	T cell signaling	$\alpha\beta$ T cells	Biolegend	APC

<b>Antibody Target</b>	<b>Notes</b>	<b>Expression</b>	<b>Suppliers</b>	<b>Conjugate Dyes</b>
<b>DX5</b>	Adhesion and migration	NK cells, NK T cells	BD Biosciences	PE FITC
<b>F480</b>	Glycoprotein	Macrophages	eBioscience	PECy7 e450
<b>CD127</b>	Interleukin 7 receptor	T cells	eBioscience	AF647
<b>CD169/ MOMA1/ Sialoadhesin</b>	I-type lectin. Binds sialic acid	Macrophages	AbD- Serotech Biolegend	PE FITC AF647
<b>CD44</b>	Adhesion molecule Leukocte activation marker	Activated T cells	eBioscience	PERCP FITC PE e450
<b>CD45</b>	Common leukocyte antigen	Leukocytes	eBioscience BD Biosciences	PERCP FITC, PE e450
<b>EpCAM</b>	Adhesion molecule	Langerhans cells	eBioscience	APC
<b>LYVE-1</b>	Type 1 membrane glycoprotein	Lymphatic vessels Macrophages	BD Biosciences R&D	Purified FITC
<b>CD1c</b>	Human glycolipid Antigen presentation	Human DCs	eBioscience	PE
<b>CCR6</b>	Chemokine Receptor	iNKT cells B cells DCs	Biolegend	Brilliant Violet 421

**Table 3: FACS Antibodies**

## 2.14 Fluorescent CCL19 Chemokine

Almac chemically synthesise fluorescently labeled human chemokines with site specific labeled tags. The synthesis of the chemokines is such that high purity chemokines are produced with precise amino acid sequences. Human CCL19 is commercially available from Almac and is selectively labeled with an AlexaFluor 647 (AF647) tag on the C terminus. This chemokine was used throughout this project, along with unlabeled human CCL19 for competition assays. The amino acid sequences of both chemokines are shown below.

**CCL19<sup>AF647</sup>**      **GTNDAEDCCL SVTQKPIPGY IVRNFHYLLI KDGCRVPAVV**  
**FTTLRGRQLC APPDQPWVER IIQRLQRTSA KMKRRSSK (AF647®-NH2)**

**CCL19**              **GTNDAEDCCL SVTQKPIPGY IVRNFHYLLI KDGCRVPAVV**  
**FTTLRGRQLC APPDQPWVER IIQRLQRTSA KMKRRSS**

The AF647 dye was incorporated at the indicated position at a molar ratio of 1:1 dye:chemokine. Labelling of CCL19 at the C-terminus leaves the N-terminus, which is important for its biological function, unmodified.

## 2.15 Chemokine Uptake Assay

Single cell suspensions were prepared as discussed previously (Section 2.4) and cells re-suspended in CRM for staining. Functional chemokine receptor expression was assessed by incubating cells with 200ng/mL of AlexaFluor-tagged recombinant chemokine (Almac) for 1 hour at 37°C in CRM. After 1 hour, cells are washed in fresh CRM, centrifuged for 5 minutes at 400g and then re-suspended in antibody cocktail as described in (section 1.15.1). To define specific uptake of the chemokine during analysis, control samples were incubated with fluorescently tagged chemokine along with x10 molar excess of unlabelled recombinant chemokine. In the case of receptor identification using CCL19<sup>AF647</sup> uptake, cells were cultured with CCL19<sup>AF647</sup> and x10 molar excess of unlabelled CCL19. As both the unlabelled CCL19 and CCL19<sup>AF647</sup> share the same binding affinities for their cognate receptors, a x10 molar excess of CCL19 should compete for binding to CCR7 and so the uptake of CCL19<sup>AF647</sup> will be

reduced in these samples compared with samples not containing a x10 molar excess of unlabelled CCL19. Non-specific uptake of CCL19<sup>AF647</sup> (by pinocytosis for example) will not be competed by excess unlabelled CCL19.

### **2.15.1 Flow Cytometry Analysis**

Stained cells were analysed using a MACSQuant Flow cytometer (Miltenyi) or an LSRII (BD) and then data analysed using FlowJo software (Treestar Inc). During acquisition, different cell population parameters were determined using single stained cells or single stained beads (BD Bioscience). A single stained population was used to input the correct 'compensation' parameters on the machine, and adjust for 'bleeding' of certain fluorophores into other channels due to spectral overlap. Throughout all experiments, fluorescence minus one (FMO) controls were employed. FMOs are stained samples that lack only one of the antibody stains from the antibody cocktail of stains. For example, a FITC FMO sample will be stained with all other antibodies conjugated to their corresponding fluorescent dyes apart from the FITC conjugated antibody. During FlowJo analysis, FMO samples aid the correct drawing of gates.

### **2.15.2 Flow Cytometry Gating Strategies**

For all flow cytometry samples analysed by FlowJo, cells were pre-gated using physical properties and viability before gating for particular surface markers. Thus, "Cells" were first identified based upon forward scatter (FSC) and side scatter (SSC) with anything below a certain size was deemed to be too small to be a cell. The events lying out with the "Cells" gate probably represent cellular debris or red blood cells in samples not treated with RBC lysis buffer. After gating on "Cells", the samples were then assessed for viability by either using Viaprobe or Fixable viability dye. Cells positive for either Viaprobe or viability dye are dead, and so only cells that are negative are selected for subsequent analysis. Finally, cell doublets and higher order aggregates were excluded by plotting FSC area against FSC height. Any cells lying out with the "singlets" gate were excluded leaving only live single cells for subsequent analysis. After this pre-gating strategy, cells were analysed for specific markers depending upon the particular experiment being undertaken. The gating strategy for skin is shown

in (Figure 2.2 A-C) and compared with lymph node (Figure 2.2 D-F). The enzymatic digestion of the skin is different to that of the lymph node and involves a “cocktail” of various enzymes. As such there is a greater amount of cell death, and skin digests yield a higher proportion of debris.

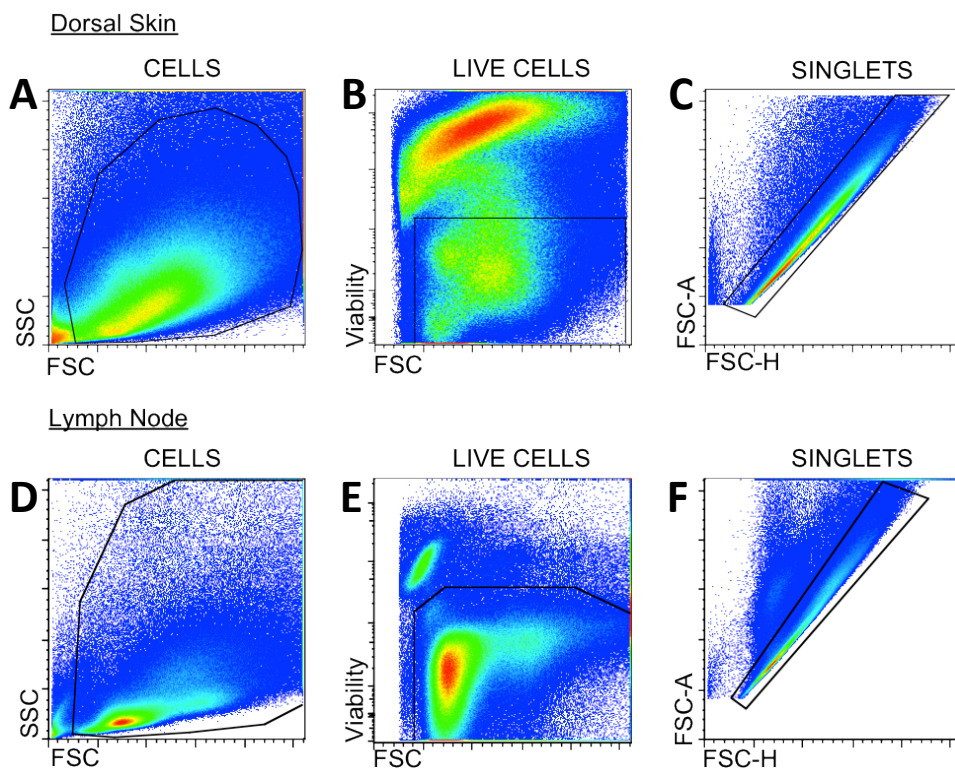


**Figure 2.2: Gating strategy for analysis of flow cytometry data of skin + lymph node cells.**

Single cell suspensions were made from dorsal skins (A-C) and lymph nodes (D-F). Cells were stained for surface markers and with the live/dead discrimination dye. First cells were identified and cellular debris excluded based on forward scatter and side scatter (A+D). Next, dead cells were identified as being positive for the viability dye and also excluded (B+E). Finally, doublets were excluded based on their FSC-A vs. FSC-H characteristics as shown (C+F). The resulting singlet population was further analysed by gating for particular antibody-stained leukocyte populations, depending on the particular experiment.

## **2.16 Statistical Analyses.**

In all graphs, data are shown as the mean + standard error of the mean (SEM), as indicated in the figure legends. Comparisons between groups were analysed by unpaired two-tailed Student's t test, one way ANOVA or two-way ANOVA with Bonferroni or Tukey's post-test as appropriate, and as indicated in the figure legends. Values of  $p < 0.05$  were considered to be statistically significant. Throughout, any significance with a p value of 0.05 to 0.001 is denoted by \*, of 0.01 to 0.001 by \*\*, and of below 0.001 as \*\*\*. All statistical analyses were performed using PRISM software (GraphPad Software, Inc).

# Chapter Three

## The Role of CCRL1 in Coordinating the Migration of DCs

## 3 The Role of CCRL1 in Coordinating DC Migration

### 3.1 Introduction

Chemokines are of fundamental importance to the orchestration of leukocyte migration and positioning. It is proposed that the atypical chemokine receptor CCRL1 is an important regulator of homeostatic CC chemokines that may fine-tune the migratory behaviour of leukocytes, including DCs. Interestingly, investigations using CCRL1<sup>gfp/+</sup> reporter mice have thus far shown that CCRL1 is expressed in the skin and SCS of peripheral lymph nodes. Therefore, the expression of CCRL1 *in vivo* would suggest that it is ideally placed to play a role in controlling the levels of CCR7-associated chemokine ligands CCL19 and CCL21 at sites to regulate CCR7-directed DC migration. DCs largely depend on CCR7 for their migration from the periphery to the lymph node, as well as for their ability to traverse the floor of the SCS. Thus, to explore the role of CCRL1 at these sites, I compared the migratory behavior of distinct skin-derived DC populations in WT and CCRL1-deficient mice. This body of work extends a previous report by Henzel and colleagues who have previously described a defect in basal DC migration<sup>360</sup> and sheds new light on the migration of DC subsets out of inflamed skin and their appearance at draining lymph nodes. Furthermore, this work describes the role of CCRL1 in the skin, which, at the point of writing this thesis, had not been described in the available literature.

### 3.2 WT and CCRL1-deficient Lymph Node DC Numbers at Rest

Henzel and colleagues described a reduction in CD11c<sup>+</sup> MHCII<sup>hi</sup> DCs in the skin-draining lymph nodes of CCRL1-deficient mice at rest<sup>360</sup>. Therefore, my initial focus was to quantify the total number of DCs in skin-draining inguinal lymph nodes of WT and CCRL1-deficient mice, and to subset them further based on various markers. At rest, the total cellularity of WT and CCRL1-deficient skin-draining lymph nodes was comparable (Figure 3.1 A). Migratory DCs were identified as CD11c<sup>+</sup> MHCII<sup>hi</sup> cells and lymph node resident DCs as CD11c<sup>+</sup> MHCII<sup>int</sup> (Figure 3.1 B). Within these populations there are several subtypes of

DCs, and certain markers can delineate skin-derived dermal and epidermal DCs as well as lymph node resident DCs. Epidermal Langerhans cells were defined as CD11c<sup>+</sup> MHCII<sup>hi</sup> CD103<sup>-</sup> Langerin<sup>+</sup> (Figure 3.1 D). Other skin-derived DCs in the CD11c<sup>+</sup> MHCII<sup>hi</sup> population include CD103<sup>+</sup> Langerin<sup>+</sup> dermal DCs, CD103<sup>+</sup> Langerin<sup>-</sup> dermal DCs and a heterogeneous CD103<sup>-</sup> Langerin<sup>-</sup> DC population (Figure 3.1 D). As shown in (Figure 3.1 C), and in contrast to Heinzel *et al*, there were no statistically significant differences in the total number of CD11c<sup>+</sup> MHCII<sup>hi</sup> migratory DCs or CD11c<sup>+</sup> MHCII<sup>int</sup> resident DCs in skin draining inguinal lymph nodes, although there was a clear trend towards lower numbers of migratory DCs in CCRL1-deficient lymph nodes at rest. However, analysis of DC subsets within the CD11c<sup>+</sup> MHCII<sup>hi</sup> population revealed a decrease in the total number of Langerhans cells (CD103<sup>-</sup> Langerin<sup>+</sup>) as well as CD103<sup>+</sup> Langerin<sup>+</sup> dermal DCs in the lymph nodes of CCRL1-deficient mice (Figure 3.1 E). The remaining two skin DC populations (CD103<sup>-</sup> Langerin<sup>-</sup> and CD103<sup>+</sup> Langerin<sup>-</sup>) were unaffected by loss of CCRL1 and their numbers in CCRL1-deficient lymph nodes were similar to that of WT mice (Figure 3.1 E). Thus, CCRL1 is required to establish normal levels of specific subsets of migratory DCs in inguinal lymph nodes during steady-state conditions.

The four populations of skin-derived DCs in inguinal lymph nodes express markers such as CD24 and CD205 that can identify further sub-populations in WT mice<sup>35,174</sup>. The large majority of CD103<sup>+</sup> Langerin<sup>+</sup>, CD103<sup>-</sup> Langerin<sup>+</sup> and CD103<sup>+</sup> Langerin<sup>-</sup> migratory CD11c<sup>+</sup> MHCII<sup>hi</sup> DCs expressed similar levels of surface CD205 and CD24 (Figure 3.2 A-B). However, within the CD11c<sup>+</sup> MHCII<sup>hi</sup> CD103<sup>-</sup> Langerin<sup>-</sup> population variation in CD24 or CD205 expression identified three subsets. While compared to WTs all three subsets appeared less abundant in CCRL1-deficient inguinal lymph nodes, there were no statistically significant differences (Figure 3.2 C). Collectively, these results suggest that loss of CCRL1 results in a defect in specific skin-derived DC subsets at rest that is consistent with defective migration from the skin.

### **3.3 DC Migration in Response to Cutaneous Application of FITC**

Having characterised DC subsets in resting inguinal lymph nodes, numbers of skin-derived DCs in the inguinal lymph nodes 24 hours after topical application of FITC were calculated in WT and CCRL1-deficient mice. FITC painting labels skin-resident DCs and also induces DC mobilisation and migration out of the skin. Unfortunately, when analysing the data, it became apparent that the channel designated to CD11c had not been appropriately compensated when calibrating the machine. However, from the flow cytometry plots and previous experience of analysing these cells (Figure 3.1 B), it is clear where to draw the migratory DC gate based on high MHCII expression alone. MHCII<sup>hi</sup> cells are almost exclusively migratory DCs. Thus, CD11b<sup>+</sup> MHCII<sup>hi</sup> cells were gated (Figure 3.3 A-B). In order to draw FITC gates, samples from mice that received an acetone paint in place of FITC were gated on first (Figure 3.3 C). This gate was then applied to the FITC painted samples (Figure 3.3 A-B) for assessment of the FITC positivity of CD11b<sup>+</sup> MHCII<sup>hi</sup> cells. CD11b<sup>+</sup> MHCII<sup>hi</sup> FITC<sup>+</sup> cells were enumerated (Figure 3.3 D). This showed that CCRL1-deficient mice had reduced numbers of CD11b<sup>+</sup> MHCII<sup>hi</sup> FITC<sup>+</sup> migratory DCs in the skin draining inguinal lymph nodes. As the FITC is a tool for labeling migratory skin DCs, these data would again be consistent with defective DC migration from the skin.

### **3.4 DC Accumulation in Skin-Draining Lymph Nodes After Skin inflammation**

Having characterised DC migration both at rest and after topical application of FITC, investigations were carried out to examine the migration of DCs from inflamed skin. To explore this, models of non-invasive skin inflammation by application of TPA were adopted. A single application of TPA induces a mild inflammatory response in the skin characterised by the rapid recruitment of neutrophils, followed by T cells and monocytes and which is typically resolved 4-5 days later. After TPA painting, FITC was immediately applied to the inflamed skins in order to label skin DCs. Inflammation activates DCs and drives their expression of CCR7. Furthermore, inflammation will also drive the

expression of chemokines, therefore, I was interested to see whether resting phenotypes and phenotypes observed during FITC painting alone were present, exaggerated or lost after a more pronounced inflammatory insult. By concomitantly painting the back skin with TPA and FITC I was able to identify those cells that had migrated to the skin-draining lymph node from the skin. Throughout this thesis the phrase 'TPA+FITC' will be used to denote when TPA and FITC are applied together at the same time.

First, total number of cells in the skin draining inguinal lymph nodes of WT and CCRL1-deficient mice was enumerated and no difference was found in the total lymph node cellularity (Figure 3.4 A). In addition, no differences in either CD11c<sup>+</sup> MHCII<sup>hi</sup> migratory DCs (Figure 3.4 B-C) or FITC<sup>+</sup> migratory DCs were apparent (Figure 3.4 D-E) and there was no difference in the total number of CD11c<sup>+</sup> MHCII<sup>int</sup> resident DCs (Figure 3.4 B-C). Of note, the number of CD11c<sup>+</sup> MHCII<sup>hi</sup> migratory DCs was around 15 times higher for WT and 25 times higher for CCRL1-deficient mice after TPA+FITC compared with resting lymph nodes (Figure 3.1 C, Figure 3.4 C). This shows that the TPA+FITC model induces rapid mobilisation of DCs from the skin. Within the CD11c<sup>+</sup> MHCII<sup>hi</sup> FITC<sup>+</sup> skin-derived migratory DC population, various subsets were identified based on CD103 and Langerin expression as before. Three dominant populations of DCs could be identified; CD103<sup>+</sup> Langerin<sup>+</sup>, CD103<sup>+</sup> Langerin<sup>-</sup> and CD103<sup>-</sup> Langerin<sup>-</sup> (Figure 3.5 A-B). There were few Langerhans cells (CD103<sup>-</sup> Langerin<sup>+</sup>) presumably because these cells have not had sufficient time to migrate from the epidermis to the lymph node. It is known that these cells have delayed kinetics with regards to egress from the skin and arrival in lymph nodes after inflammation<sup>187</sup>. Of the three populations of FITC<sup>+</sup> DCs present in the lymph node, only the CD11c<sup>+</sup> MHCII<sup>hi</sup> FITC<sup>+</sup> CD103<sup>+</sup> Langerin<sup>-</sup> cells were significantly reduced in the lymph nodes of CCRL1-deficient mice compared with WT animals (Figure 3.5 E).

In summary, these initial experiments demonstrate that:

1. Langerhans cells are reduced in CCRL1-deficient skin draining lymph nodes at rest.

2. Fewer migratory DCs are present in the skin-draining lymph nodes of CCRL1-deficient mice 24 hours after FITC painting.
3. Combined TPA + FITC painting results in only one subset of skin-derived DCs (CD103<sup>+</sup> Langerin<sup>-</sup> DCs) being reduced in abundance in the skin-draining lymph nodes of CCRL1-deficient mice.

Taken together, it seemed unlikely that the DC phenotype seen during FITC painting was a result of the absence of DCs in the skin, because there were a large number of skin-derived migratory DCs in both WT and CCRL1-deficient skin-draining lymph nodes in the TPA + FITC model.

24 hours after painting with TPA and FITC on the same day, FITC<sup>+</sup> Langerhans cells were virtually absent from the lymph nodes of WT and CCRL1-deficient mice. This was presumably because they had insufficient time to migrate from the epidermis to the lymph nodes. By adjusting the model, we hoped that it would be possible to enumerate Langerhans cells in skin-draining lymph nodes. To this end, a 24 hour period was placed between the TPA and FITC applications and skin-draining lymph nodes harvested 24 hours later. It was anticipated that this model might label Langerhans cells en route to skin-draining lymph nodes, and that proved to be the case (see below). To distinguish this experimental approach from others used previously, it will be referred to as TPA-24-FITC hereafter.

As in other models of skin inflammation, there was no difference in total lymph node cellularity between WT and CCRL1-deficient mice in this new experimental set up (Figure 3.6 A). Without gating FITC<sup>+</sup> cells, when the number of CD11c<sup>+</sup> MHCII<sup>hi</sup> DCs in the inguinal lymph nodes was enumerated, it was clear that there was a significant reduction in these cells in the inguinal lymph nodes of CCRL1-deficient mice compared with WT mice (Figure 3.6 B-C). This is in stark contrast to the results from the TPA+FITC model in which lymph nodes were analysed 24 hours after a concomitant TPA/FITC application. More CD11c<sup>+</sup> MHCII<sup>hi</sup> DCs are present in the inguinal lymph node in the TPA+FITC model than are present in the TPA-24-FITC model, but their numbers are unaffected by CCRL1-deficiency. When compared to the TPA+FITC model, there was a ~60% reduction in the number of migratory DCs (CD11c<sup>+</sup> MHCII<sup>hi</sup>)

in the inguinal lymph nodes of CCRL1-deficient mice compared with only a ~20% reduction in the number of these cells in WT mice during the TPA-24-FITC model (Figure 3.4 C, Figure 3.6 C). These data suggested that either a greater proportion of migratory DCs die in the lymph nodes of CCRL1-deficient mice between the two harvest time points used in the TPA+FITC and TPA-24-FITC models, or that in the TPA-24-FITC model fewer DCs depart the skin of CCRL1-deficient animals.

Indeed, the latter view was supported when the number of CD11c<sup>+</sup> MHCII<sup>hi</sup> cells that were FITC<sup>+</sup> were enumerated, as these cells were significantly reduced in the lymph nodes of CCRL1-deficient mice (Figure 3.6 E). Compared to the TPA+FITC model, a larger proportion of CD11c<sup>+</sup> MHCII<sup>hi</sup> cells are FITC<sup>-</sup> presumably because they have left the skin before the application of FITC. Many of these cells will have departed the skin immediately after TPA painting when, according to results from the previous experiment, they leave comparably in WT and CCRL1-deficient mice (Figure 3.4).

Next, in the context of the TPA-24-FITC model, FITC<sup>+</sup> migratory DCs were analysed for CD103 and Langerin expression by flow cytometry (Figure 3.7 A). Four DC sub-populations could be readily identified and strikingly all were significantly less abundant in the skin-draining inguinal lymph nodes of CCRL1-deficient mice than WT mice (Figure 3.7 A-E). Notably, a large population of Langerhans cells (CD103<sup>-</sup> Langerin<sup>+</sup>) was consistently found in the inguinal lymph nodes in the TPA-24-FITC model (Figure 3.7 A and D). This is in contrast to previous data from TPA + FITC co-application (Figure 3.5). Consistent with them being Langerhans cells, virtually all the CD11c<sup>+</sup> MHCII<sup>hi</sup> Langerin<sup>+</sup> CD103<sup>-</sup> cells expressed CD24, and when these cells were enumerated they were significantly reduced in the skin-draining lymph nodes of CCRL1-deficient mice in the TPA-24-FITC model (Figure 3.8 A-B). To confirm these observations, a new panel of antibodies was employed that identified Langerhans cells based on their expression of other markers. In the new antibody cocktail Langerhans cells were identified as being CD11c<sup>+</sup> CD103<sup>-</sup> EpCAM<sup>+</sup> CD11b<sup>+</sup> and FITC-positivity was used to demonstrate that they had migrated from the skin after FITC application. By using this staining combination, a population of cells was identifiable with the surface phenotype of Langerhans cells (Figure 3.8 C).

In agreement with previous observations in the TPA-24-FITC model, these cells were less abundant in CCRL1-deficient skin-draining lymph nodes than WT counterparts (Figure 3.8 D). Moreover, this reduction in EpCAM<sup>+</sup> cells was also evident when analysing inguinal lymph nodes by immunofluorescent staining (Figure 3.9 A-B).

Collectively, these data show that whilst the initial wave of DCs driven from the skin by TPA appear relatively unaffected by loss of CCRL1, those leaving at later time points require CCRL1 for optimal migration to the skin-draining lymph nodes.

### **3.5 Is Arrival of DCs in Lymph Nodes Delayed in CCRL1-Deficient Mice?**

Having described how populations of DCs are reduced in the skin-draining lymph nodes of CCRL1-deficient mice during a model of skin inflammation, investigations were undertaken to determine if this reduction reflects a delay in DC migration from the skin. If this were the case, we might expect to see an increased wave of DC migration in CCRL1-deficient mice relative to WT mice at a later time point. Thus, in the same TPA-24-FITC model, skin-draining lymph nodes were harvested 24, 72, 120 and 144 hours after FITC application. For each of the time points, CD11c<sup>+</sup> MHCII<sup>int</sup> ‘resident’ DCs and CD11c<sup>+</sup> MHCII<sup>hi</sup> DCs ‘migratory’ DCs were identified. Within the migratory DC population, FITC<sup>+</sup> DCs were identified (Figure 3.10 A). The total number of resident DCs at each time point is the same between WT and CCRL1-deficient mice and their abundance appears to stay constant across the time points (Figure 3.10 B). FITC<sup>+</sup> migratory DCs were abundant in WT skin-draining lymph nodes 24 hours after FITC application but their numbers tail off substantially at later time points (Figure 3.10 C). Only at the 24-hour time point is there a difference in the total number of FITC<sup>+</sup> migratory DCs between WT and CCRL1-deficient mice. At each harvest time point, the FITC<sup>+</sup> migratory DCs were divided into four populations based on CD103 and Langerin expression (Figure 3.11 A). Langerhans cells showed a specific influx to skin-draining lymph nodes 24 hours and 120 hours after FITC painting (Figure 3.11 A). However, the total number of Langerhans cells was only significantly different between WT and CCRL1-

deficient mice at the 24-hour time point (Figure 3.11 B). The total numbers of CD103<sup>+</sup> Langerin<sup>+</sup>, CD103<sup>+</sup> Langerin<sup>-</sup> and CD103<sup>-</sup> Langerin<sup>-</sup> dermal DCs were all reduced in skin-draining lymph nodes from CCRL1-deficient mice compared with WT mice but only at the 24 hour time point (Figure 3.11 C-E). Thus, there appears to be a specific window in which CCRL1 controls the abundance of skin-derived DCs in draining inguinal lymph nodes.

### **3.6 DC Migration Using Kaede Transgenic Mice**

In the previous experiments, FITC was included as a way of identifying DCs in the lymph node that were present in the skin at the time of FITC application. However, free-flowing FITC could conceivably travel to the skin draining lymph nodes and may be acquired by lymph node resident DCs. If these cells were to up-regulate their MHCII they would resemble migratory DCs, and this would make interpretation of results difficult. To address this potential criticism, kaede transgenic mice were obtained and crossed with CCRL1-deficient mice, therefore creating kaede<sup>+</sup> CCRL1-deficient mice. Kaede mice carry a photoconvertible fluorescent protein in all their cells and are a useful tool for quantifying and tracking cell migration from one compartment to another. The background to kaede transgenic mice and photoconversion within these mice is described in the Methods and Materials section of this thesis.

The experiment was set up as in the TPA-24-FITC model, except that instead of FITC painting, mice were flashed with a U.V light on the dorsal skin to induce photo conversion from green to red in the TPA-treated skin. As the FITC had been dissolved in acetone, mice were also painted with acetone at this point to mimic any effects that this solvent may have on driving skin inflammation. The results from this experiment were in agreement with the results from the TPA-24-FITC experiment. Specifically, the total number of CD11c<sup>+</sup> MHCII<sup>hi</sup> kaede red<sup>+</sup> migratory DCs was significantly reduced in the lymph nodes in the CCRL1-deficient background (Figure 3.12 B). Moreover, virtually all kaede red<sup>+</sup> cells in the skin-draining lymph nodes were CD11c<sup>+</sup> MHCII<sup>hi</sup>. Therefore, these cells are the predominant cell population to migrate from the skin to the lymph nodes in this model. As controls, unconverted kaede mice were used throughout these experiments (Figure 3.12 C).

The results from this experiment provided further evidence that the phenotype described earlier is a result of a failure of skin-resident DCs to depart the skin during inflammation rather than the result of lymph node resident DCs acquiring FITC antigen and up-regulating surface MHCII expression. Furthermore, it gave confidence that the method by which DC migration was characterised by labeling with FITC was appropriate and sensitive enough to make reasonable conclusions about the origins of DCs present in skin-draining lymph nodes. Additionally, the use of kaede mice also answers other criticisms, such as that previous observations were due to differential antigen uptake by CCRL1-deficient and WT DCs. As kaede conversion does not involve the acquisition of antigen then any possible defect in antigen uptake by CCRL1-deficient DCs would not affect the conversion of DCs from kaede-green to kaede-red.

In summary, by using a variety of different approaches it is clear that the absence of CCRL1 can result in a reduction in the number of migratory DCs present in skin-draining lymph nodes after the induction of cutaneous inflammation.

### **3.7 CCL19 Receptor Expression on Lymph Node Cells During TPA and FITC**

To date, CCRL1 has been described as having an expression pattern that is restricted to keratinocytes in the skin and LECs in the lymph node with no evidence for expression on leukocytes<sup>360</sup>. Therefore, to confirm these findings, an experiment was designed to test for expression of CCL19 receptors on DCs, the cell type that displays aberrant migration from the skin at rest and during inflammation. By using WT and CCRL1-deficient cells from the lymph node, it is possible to test for the expression of CCR7 and CCRL1 on these cells and thus conclude whether CCRL1 is expressed by leukocytes including DCs in the lymph node.

Commonly for analysis by flow cytometry anti-CCR7 antibody would be used to identify cells expressing this chemokine receptor. However, anti-CCR7 antibodies from different suppliers conjugated to different fluorphores were tested and none were sensitive enough to reliably detect CCR7 expression on cells, including T cells that are known to express high levels of CCR7 (data not

shown). Our lab has developed a method of detecting chemokine receptor expression by labeling cells with fluorescently tagged chemokine or chemokine tetramers<sup>319</sup>. This assay can be performed at 4°C to look for surface receptor expression or at 37°C to look at functional chemokine receptor expression by fluorescent chemokine uptake and internalisation. As the only known receptors for CCL19 are CCR7 and CCRL1, we can, by comparing WT and CCRL1-deficient cells, demonstrate CCR7 expression using these types of assays. To this end, CCL19 surface receptors were detected by culturing WT and CCRL1-deficient cells in the presence of CCL19 tetramers conjugated to the fluorophore PE and culturing them at 4°C. The method for this assay is outlined in the Materials and Methods section to this thesis. First, the surface expression of CCL19 receptors on CD11c<sup>+</sup> MHCII<sup>hi</sup> FITC<sup>+</sup> cells and CD11c<sup>+</sup> MHCII<sup>hi</sup> FITC<sup>-</sup> cells was assessed (Figure 3.13 A). Virtually all these cells in these populations were CCL19 receptor positive and there was no difference in expression between WT and CCRL1-deficient FITC<sup>+</sup> or FITC<sup>-</sup> migratory DCs (Figure 3.13 A). Similarly, no difference in CCL19 receptor expression was found between WT and CCRL1-deficient CD11c<sup>+</sup> MHCII<sup>int</sup> resident DCs and 65-70% of these cells were CCL19 receptor positive (Figure 3.13 B). Other populations identified include CD11c<sup>+</sup> MHCII<sup>-</sup> cells (Figure 3.13 C), CD11c<sup>-</sup> MHCII<sup>-</sup> cells (Figure 3.13 D) and CD11c<sup>-</sup> MHCII<sup>hi</sup> cells (Figure 3.13 E). Although these cells are not definitively identified using other markers, the CD11c low MHCII<sup>-</sup> population is probably mainly composed of T cells consistent with their expression of surface CCL19 receptors (CCR7) (Figure 3.13 D). CD11c<sup>-</sup> MHCII<sup>+</sup> cells in the lymph node will mainly be B cells and ~10% of these cells were able to detectably bind the CCL19 tetramers. All non-DC subsets did not display differential CCL19 binding between WT and CCRL1-deficient mice.

Collectively, these data confirm that migratory DCs express CCL19 receptors and that loss of CCRL1 expression does not affect the level of CCL19 receptor expression by any of the cell subsets examined. CCR7 is in all likelihood the receptor entirely responsible for CCL19<sup>PE</sup> binding in these assays. The data also indicate that lymph node leukocytes do not detectably express functional CCRL1, consistent with previous reports using CCRL1<sup>+/*gfp*</sup> mice<sup>360</sup>, and that

CCRL1 deficiency does not lead to a detectable change in the surface expression of CCR7.

### **3.8 DC Migration During TPA and FITC is Largely Driven by CCR7**

It is widely reported in the literature that CCR7 propels DCs towards peripheral lymph nodes during insult, injury and inflammation, as well as during basal homeostatic conditions<sup>54,189</sup>. This is true for the migration of DCs from the skin in a variety of models<sup>52,54,58,366,367</sup>. Having confirmed that CD11c<sup>+</sup> MHCII<sup>hi</sup> migratory DCs in inguinal lymph nodes express high levels of surface CCL19 receptors that we can infer are CCR7, I next set out to prove that CCR7 specifically propels the migration of these DCs from the skin to lymph node during the TPA-24-FITC model. To do so, I repeated the TPA-24-FITC model in WT and CCR7-deficient mice. Strikingly, CD11c<sup>+</sup> MHCII<sup>hi</sup> FITC<sup>+</sup> migratory DCs were virtually absent from the skin-draining inguinal lymph nodes of CCR7-deficient mice but were readably detectable in WT counterparts (Figure 3.14 A-B).

To confirm this result, kaede<sup>+</sup> CCR7-deficient mice were utilised and compared with WT kaede<sup>+</sup> cells that retain CCR7 expression. These mice were painted on the back skin with TPA, left for 24 hours and then photoconverted. As with previous experiments using kaede mice (Figure 3.12) acetone was applied to the skin at the same time as the photoconversion. The total number of CD11c<sup>+</sup> MHCII<sup>hi</sup> kaede red<sup>+</sup> cells in the skin-draining inguinal lymph nodes was then assessed 24 hours later (Figure 3.14 C-D). In agreement with data from the TPA-24-FITC model, skin-derived kaede red<sup>+</sup> migratory DCs were virtually absent from the lymph nodes of CCR7-deficient mice yet were abundant in the inguinal lymph nodes of kaede mice that retained CCR7 (Figure 3.14 D). Interestingly, in both experiments depicted in Figure 3.14, there were clearly some migratory DCs present in the lymph node of CCR7-deficient mice, albeit kaede red<sup>-</sup>, suggesting that some steady-state migration of these cells from the skin is occurring in a CCR7-independent manner. Alternatively, resident DCs may

upregulate MHCII expression in CCR7-deficient mice leading to their classification as “migratory DCs”.

Taken together, the data show that the migration of DCs from the skin in response to TPA-induced skin inflammation is critically dependent on CCR7 and this is regulated by CCRL1.

### **3.9 CFA-Induced Skin Inflammation**

In order to investigate whether the defect in DC migration from inflamed skin was reproducible in another model of cutaneous inflammation, I assessed DC accumulation in lymph nodes after subcutaneous injection of CFA into the ear skin. As in the TPA model, ears were painted with FITC 24 hours after CFA injection to label DCs in the skin, and the draining cervical lymph nodes were harvested 24 hours later.

First, the total cellularity of WT and CCRL1-deficient cervical lymph nodes was assessed and no difference was found between the strains (Figure 3.15 A). Next, total numbers of CD11c<sup>+</sup> MHCII<sup>hi</sup> migratory DCs was enumerated (Figure 3.15 B-C). As before, the absolute numbers of migratory DCs was reduced in CCRL1-deficient cervical lymph nodes (Figure 3.15 C). These migratory DCs were further characterised based on their expression of CD103, Langerin and CD24 as well as their FITC positivity. First they were separated as before based on CD103 and Langerin expression (Figure 3.16 A-B). Although Langerin<sup>-</sup> DCs were readily detectable in both strains, Langerin<sup>+</sup> DCs were rare in WT lymph nodes and virtually absent from CCRL1-deficient nodes. In fact, the relatively low expression of CD24 by Langerin<sup>+</sup> CD103<sup>-</sup> DCs suggested that these may be Langerin<sup>-</sup> CD103<sup>-</sup> DCs contaminating the Langerin<sup>+</sup> CD103<sup>-</sup> gate. Within these populations, cells were further characterised by assessing their CD24 expression and FITC positivity (Figure 3.16 A-B). CD24 expression was high on most CD103<sup>+</sup> DCs while Langerin<sup>-</sup> CD103<sup>-</sup> DCs were uniformly CD24 low. This contrasts with observations made on resting inguinal lymph nodes where CD24<sup>+</sup> and CD24<sup>-</sup> subsets were clearly identifiable amongst Langerin<sup>-</sup> CD103<sup>-</sup> DCs (Figure 3.2). Absolute numbers of CD103<sup>-</sup> Langerin<sup>+</sup> FITC<sup>+</sup> and CD103<sup>-</sup> Langerin<sup>-</sup> FITC<sup>+</sup> migratory DCs were significantly reduced in the cervical lymph

nodes of CCRL1-deficient mice compared to WT counterparts (Figure 3.16 C). CD103<sup>+</sup> Langerin<sup>+</sup> FITC<sup>+</sup> and CD103<sup>-</sup> Langerin<sup>-</sup> FITC<sup>+</sup> DCs also appear to be reduced in CCRL1-deficient mice but this failed to achieve statistical significance (Figure 3.16 C). Results from this model are in general agreement with previous data in that there is defective accumulation of DC populations in draining lymph nodes after the induction of cutaneous inflammation.

Thus, under certain circumstances migratory DC abundance in skin-draining lymph nodes is substantially reduced in CCRL1-deficient mice. There are several hypotheses that might explain these observations:

- 1) There are fewer DCs in the skin of CCRL1-deficient mice.
- 2) There is a defect in DC departure from the skin of CCRL1-deficient mice.
- 3) DCs have defective entry into skin-draining lymph nodes in CCRL1-deficient mice.

As shown by others, and confirmed here, DC migration from the skin to skin-draining lymph nodes is coordinated by CCR7. CCR7<sup>+</sup> epidermal and dermal DCs move into dermal lymphatic vessels under the direction of CCL21 expressed by LECs<sup>52,57,366</sup>. They are carried in these vessels to skin-draining lymph nodes. CCRL1 has previously been shown to be expressed in the epidermis of CCRL1<sup>gfp/+</sup> reporter mice. Therefore, due to the ligand specificity of CCRL1 it is reasonable to assume this atypical chemokine receptor may be important for the coordinated egress of DCs out of the skin via lymphatic vessels. CCRL1 is also reportedly expressed by cells in the SCS of the lymph node, and deletion of CCRL1 may affect the ability of DCs to traverse the floor of the SCS. To explore DC migration across the SCS is technically demanding, and is an area of CCRL1 biology that was under investigation by others in the field. Their work has recently been published<sup>368</sup> and will be discussed in the Discussion section.

My investigations into DC abundance in the lymph nodes led me to focus on DC numbers in the skin and their departure from the skin in order to relate these findings to their underrepresentation in skin-draining lymph nodes.

### 3.10 DCs in Resting Skin

To investigate DCs in resting skin, the back skin of WT and CCRL1-deficient mice was excised and DC subsets examined by flow cytometry. The data are represented as percentages of total live cells rather than as a total cell count due to the variability in cell isolation from the digests and the variability in cell death between samples and experiments. This is because digestion of the back skin requires an enzyme digestion mix containing dispase, collagenase and DNase whereas lymph node digestion involves only collagenase. The incubation with skin digestion cocktail therefore leads to less cell viability (Figure 2.2).

The initial aim was to ascertain if there were any obvious differences in the size of the leukocyte compartment of the skin. To do so, the percentage of CD45<sup>+</sup> leukocytes in the single cell skin suspensions was determined (Figure 3.17 A). The percentage of CD45<sup>+</sup> leukocytes in CCRL1-deficient animals was comparable to WT controls. Therefore loss of CCRL1 does not result in a gross change in leukocyte abundance in the skin.

Next, CD11c<sup>+</sup> MHCII<sup>+</sup> DCs were identified by flow cytometry and their proportions enumerated. There was no difference in the proportion of these cells as a percentage of total live cells (Figure 3.17 B-C). This population of cells was then split up into four DC subsets based on CD103 and Langerin expression. Interestingly, the CD103<sup>+</sup> Langerin<sup>+</sup> DC population showed an increase in the skin of CCRL1-deficient mice, although the other three populations showed comparable proportions between WT and CCRL1-deficient mice (Figure 3.17 D-G).

Thus, the percentage of dermal CD11c<sup>+</sup> MHCII<sup>+</sup> CD103<sup>+</sup> Langerin<sup>+</sup> DCs in the skins of resting CCRL1-deficient mice is increased and this coincides with a decrease in these cells in the skin-draining inguinal lymph nodes at rest (Figure 3.1). Interestingly, the percentage of Langerhans cells in the skin was not increased in CCRL1-deficient mice even though numbers of these cells are reduced in resting inguinal lymph nodes (Figure 3.1). This indicates that at rest, Langerhans cells are unaffected by loss of CCRL1 in the skin but may be affected by loss of CCRL1 at other anatomical or cellular locations, such as at the SCS. Alternatively, defective departure from the skin may lead to changes in

the dynamics of the skin Langerhans cell population such that the number of these cells remains constant.

### **3.11 DC Numbers in Inflamed Skin**

To investigate DC numbers in the skin during inflammation, single cell suspensions were prepared from WT and CCRL1-deficient skin that had been treated according to the TPA-24-FITC protocol. To ensure that skins of WT and CCRL1-deficient mice do not contain different amounts of leukocytes during TPA inflammation, skin samples were stained with antibodies against CD45 and the percentage of CD45<sup>+</sup> cells amongst live cells was calculated. The percentage of live cells in the skin preparations was also calculated to confirm that TPA-driven inflammation does not result in differences in cell viability between the two strains. Both the percentage of CD45<sup>+</sup> cells in the live cell gate and the percentage of total live cells in the skin preparations were comparable between WT and CCRL1-deficient mice (Figure 3.18 A, B and C). Next, the percentage of DCs in the live cell gate was enumerated. Interestingly, there was a higher percentage of CD11c<sup>+</sup> MHCII<sup>hi</sup> DCs in the skin of CCRL1-deficient mice than WT mice (Figure 3.18 D-E). Upon sub-dividing these cells based on CD103 and Langerin expression, it was clear that CD103<sup>+</sup> DCs were virtually absent from inflamed skin in contrast to their abundance (~45%) in resting skin (Figure 3.18 and Figure 3.19). Furthermore, there was a significant increase in percentage of CD103<sup>-</sup> Langerin<sup>+</sup> DCs (Langerhans cells) in CCRL1-deficient skin compared with WT skin (Figure 3.19 A-B). The percentages of CD103<sup>+</sup> Langerin<sup>+</sup>, CD103<sup>+</sup> Langerin<sup>-</sup> and CD103<sup>-</sup> Langerin<sup>-</sup> dermal DCs were all unaffected by CCRL1 deficiency (Figure 3.19 C-E). Therefore, during TPA-driven skin inflammation, Langerhans cells appear to be specifically retained in the skin of CCRL1-deficient mice. It is notable that these cells were previously shown to be less abundant in the skin-draining lymph nodes of CCRL1-deficient mice in the same TPA-24-FITC model of skin inflammation.

### **3.12 DC Migration From the Skin – *ex vivo* Analysis**

To further examine DC departure from the skin, skin ‘crawl out’ assays were performed. These *in vitro* assays are widely used to look at emigration of cells

from the skin. Without cannulating the skin draining lymphatic vessels and collecting the DCs in the lymph, something which is very technically demanding, this is an effective way to specifically examine the ability of DCs to enter dermal lymphatic vessels, a key step in their migration to skin-draining inguinal lymph nodes. To perform this experiment, dorsal skin was excised from WT and CCRL1-deficient mice, and the number of DCs that accumulate in the culture media over a period of three days was quantified. Cells in the skin after this incubation period were also enumerated. Interestingly, after 3 days in culture, the number of skin DCs that had emigrated from CCRL1-deficient skin and collected in the medium was significantly reduced compared to WT counterparts (Figure 3.20 A-B). Conversely, the number of DCs that remain in CCRL1-deficient skin after 3 days of culture was significantly higher than those found in WT skin (Figure 3.20 C and D).

Next, in order to further phenotype crawl-out DCs, cells were stained with anti-EpCAM antibody (Figure 3.20 E). As cells migrating out of the skin are very scarce, it is not advisable to stain them for Langerin expression as Langerin staining involves an intracellular staining step and during this procedure many cells are lost. The number of CD11c<sup>+</sup> EpCAM<sup>+</sup> cells were enumerated as a percentage of total CD45<sup>+</sup> crawl out cells. The percentage of CD11c<sup>+</sup> EpCAM<sup>+</sup> DCs was significantly reduced in the culture medium collected from CCRL1-deficient skin explant cultures (Figure 3.20 F). This population of cells express two Langerhans markers, EpCAM and CD11c. Therefore, from my previous *in vivo* DC migration models during skin inflammation and from this *ex vivo* skin crawl out assay, these data show that Langerhans cells appear to be particularly prone to defective migration from the skin when CCRL1 is absent.

### **3.13 Dysregulation of CCL19 and CCL21 in CCRL1-Deficient Skin.**

Next, the mechanisms responsible for defective DC migration in CCRL1-deficient mice were explored. It was hypothesised that CCRL1 deficiency would lead to dysregulation of CCL19 and CCL21, and that this would result in the disorientation of CCR7<sup>+</sup> DCs to interfere with their migration out of the skin. To

examine this, CCL19 and CCL21 protein levels were quantified in WT and CCRL1-deficient skin by ELISA.

We had access to lymph node lysates from *plt/plt* and CCL19-deficient mice, so in the first instance, these samples were used to ensure that the CCL19/CCL21 detection methodologies were suitably specific. Thus, lysates were prepared from WT and CCRL1-deficient inguinal lymph nodes and compared with *plt/plt* and CCL19-deficient samples in ELISAs (Figure 3.21). Inguinal lymph node lysates were also prepared from animals treated according to the TPA-24-FITC protocol.

CCL19 and CCL21 were readily detectable in all WT and CCRL1-deficient lymph nodes, and reassuringly both chemokines could not be detected in lymph nodes from *plt/plt* mice, and CCL19 was undetectable in CCL19-deficient lymph nodes (Figure 3.21 A-B). Thus the ELISAs being used show exquisite sensitivity for the chemokines they were designed to detect.

Having confirmed the sensitivity and specificity of the ELISAs, CCL19 and CCL21 levels were quantified in the inguinal lymph nodes of WT and CCRL1-deficient mice at rest and after the TPA-24-FITC model. Although there was a slight increase in both CCL19 and CCL21 in the resting lymph nodes of CCRL1-deficient mice, this did not reach statistical significance (Figure 3.21 A-B). In the TPA-24-FITC model, no differences in the levels of CCL19 were found (Figure 3.21 C) but surprisingly levels of CCL21 chemokine were significantly reduced in the inguinal lymph nodes of CCRL1-deficient mice (Figure 3.21 D).

Next, samples were prepared from the skin. As the function of CCRL1 may be to control bio-available post-translational chemokine it was necessary to quantify the levels of bio-available chemokine rather than total protein. Thus, rather than preparing skin lysates, punch biopsies were taken from resting WT and CCRL1-deficient back skins and levels of bio-available CCL19 and CCL21 that had leached from the skin into culture media over a period of 5 hours was quantified. No detectable differences in levels of CCL19 or CCL21 were detected in the resting back skin of WT and CCRL1-deficient mice (Figure 3.22 A-B). However, levels of bio-available CCL19 and CCL21 were both significantly increased in the skins of CCRL1-deficient mice treated according to the TPA-24-

FITC protocol compared to equivalently treated WT mice (Figure 3.22 A-B). These data support the concept that CCRL1 acts as a scavenger for CCL19 and CCL21 and it is possible that an increase in bio-available CCL19 and CCL21 protein in CCRL1-deficient mice could contribute to the altered migration of CCR7<sup>+</sup> DCs from the skin of these animals.

### **3.14 CCL19 Deletion Rescues Defects in DC Migration in CCRL1-Deficient Mice.**

Next, investigations to determine whether this increase in bioavailable CCL19 or CCL21 predisposes CCRL1-deficient mice to defective DC migration to lymph nodes. To do this, I planned to cross CCRL1-deficient mice with mice deficient in one or more of the chemokines that it is known to regulate. CCL21-deficient mice have not been generated and *plt/plt* mice, as described in the Introduction to this thesis, show serious defects in cellular migration, containing fewer T cells and DCs in their lymph nodes as well as displaying aberrant DC migration during FITC painting. Thus, they are not ideal for the investigations as defects caused by CCRL1 deficiency may be masked by those caused by the *plt* mutation. Importantly, to my knowledge, CCL19 is reported to be largely redundant with regards to guiding the egress of DCs from the skin<sup>270</sup>. However, as CCL19 is a very soluble chemokine, I reasoned that compared with CCL21, CCL19 may be more prone to dynamic regulation by CCRL1. Thus, I decided to cross CCL19-deficient mice with CCRL1-deficient animals to allow me to explore the role of CCL19 in the aberrant migration of DCs to skin-draining lymph nodes in CCRL1-deficient mice during TPA-induced skin inflammation. CCL19-deficient mice (retaining CCRL1 expression) were included as controls throughout.

TPA-induced inflammation was undertaken as before according to the TPA-24-FITC mode in WT, CCL19-deficient, CCRL1-deficient and CCL19+CCRL1 double deficient mice. Total lymph node cellularity was determined and DCs enumerated as before. There were no differences in total lymph node cellularity between the four strains (Figure 3.23 A). In agreement with my previous studies, the total number of CD11c<sup>+</sup> MHCII<sup>hi</sup> and CD11c<sup>+</sup> MHCII<sup>hi</sup> FITC<sup>+</sup> migratory

DCs was reduced in the skin-draining inguinal lymph nodes of CCRL1-deficient mice compared to WT mice (Figure 3.23 B-C). There was no difference between WT and CCL19-deficient mice with regards to total number of migratory DCs or FITC<sup>+</sup> migratory DCs in skin-draining lymph nodes, in agreement with reports in the literature that CCL19 is dispensable for DC migration from the periphery to lymph nodes<sup>270,276</sup>. Strikingly however, the reduced DC migration seen in CCRL1-deficient mice was rescued when CCL19 was absent (Figure 3.23 B and C). As before, specific skin DC populations were identified by their differential expression of CD103 and Langerin (Figure 3.24 A). The reduction in the total number of FITC<sup>+</sup> cells in the CD103<sup>-</sup> Langerin<sup>+</sup>, CD103<sup>+</sup> Langerin<sup>+</sup> and CD103<sup>-</sup> Langerin<sup>-</sup> DC populations seen in the skin-draining lymph nodes of CCRL1-deficient mice was rescued by loss of CCL19 (Figure 3.24 B, D and E). ANOVA analysis of data on FITC<sup>+</sup> CD103<sup>+</sup> Langerin<sup>-</sup> DCs failed to reveal a statistically significant difference between WT and CCRL1-deficient mice, despite a clear trend towards CCRL1-deficient lymph nodes containing fewer of these cells. This was lost when CCL19 was absent (Figure 3.24 C). The number of DCs in each of the four populations was unaffected by the loss of CCL19 alone, with the total numbers of these DCs in CCL19-deficient mice comparable to WT counterparts.

Therefore, collectively these data show that deletion of CCRL1 results in defective migration of skin DCs to skin-draining lymph nodes and this defect is largely dependent on CCL19. Thus, it appears that CCRL1-mediated regulation of CCL19 in inflamed skin plays a key role in facilitating the migration of skin DCs to draining lymph nodes.

### **3.15 Expression of CCRL1 in Resting Inguinal Lymph Nodes**

Finally, I explored in more detail where CCRL1 is expressed in skin and lymph nodes. eGFP expression was first investigated in the inguinal lymph nodes of CCRL1<sup>gfp/+</sup> mice. Lymph nodes were excised, frozen, sectioned and stained with antibodies. As Heinzel *et al* had seen eGFP in the SCS region of the inguinal lymph nodes<sup>360</sup>, anti-LYVE-1 antibody was used, as this should identify LECs lining the SCS. WT ‘non-eGFP’ mice were used as controls throughout to confirm true eGFP positivity. Strong eGFP signal was present in the SCS region

of the lymph node that largely co-localised with LYVE-1 staining (Figure 3.25 A). From these data, it would suggest that CCRL1 is expressed by LECs lining lymphatic vessels in the SCS of secondary lymph nodes. Within the SCS, there are also cells present that express eGFP but do not stain for LYVE-1. In the medullary region of the lymph node, LYVE-1<sup>+</sup> lymphatic vessels again showed eGFP expression (Figure 3.25 B). As in the SCS, eGFP<sup>+</sup> cells not expressing LYVE-1 were found in the medulla (Figure 3.25 B). These cells were closely associated with lymphatic vessels. As expected, eGFP expression was absent from both the SCS and the medulla of WT mice lymph nodes (Figure 3.25 C and D). Further analysis of eGFP cells in the inguinal lymph nodes of CCRL1<sup>+/*gfp*</sup> mice by flow cytometry revealed a small population of CD45<sup>+</sup> leukocytes that express CD11b and that also weakly express eGFP (Figure 3.25 E). This population was absent from WT mice, confirming the specificity of the eGFP reporter. Therefore, there is a very small population of CD45<sup>+</sup> leukocytes in inguinal lymph nodes that express the myeloid marker CD11b and that are eGFP<sup>+</sup> in CCRL1<sup>+/*gfp*</sup> mice.

As eGFP expression in knock-in mice does not always correlate with protein expression, I next focused on staining lymph node sections with CCRL1 antibody. By using this approach, CCRL1 protein could clearly be detected in the SCS of the lymph node. However, CCRL1 was not uniformly expressed within the subcapsular region of the inguinal lymph node and there were regions that did not express CCRL1 and regions that did (Figure 3.26 left hand panel). CCRL1 staining was absent from CCRL1-deficient control samples (Figure 3.26 right-hand panel). The interdigitating pattern of expression seen in WT lymph nodes is very interesting. This expression pattern would suggest that a subset of LECs express CCRL1 and precisely why the lymph node should adopt such a mosaic-like expression on these cells is something currently being examined by others and myself in the lab. CCRL1<sup>+</sup> cells were also found in non-SCS regions of the lymph node. Co-staining with LYVE-1 and CCRL1 was, at the time, not possible due to both antibodies being raised in the same species leading to cross-reactivity. With the commercial availability of directly conjugated LYVE-1 antibodies that work on frozen sections, this type of analysis is now possible and would be helpful in correlating the results from the CCRL1<sup>+/*gfp*</sup> mice. However,

without such analysis of LYVE-1 cells that demarcate medullary regions, we can speculate that the red CCRL1<sup>+</sup> cells in non-SCS regions probably correspond with eGFP<sup>+</sup> cells previously seen in the medullary regions of CCRL1<sup>+gfp</sup> mice.

### 3.16 CCRL1 Expression in the Dorsal Skin and Ear

Next, eGFP expression and CCRL1 protein expression was investigated in the skin of CCRL1<sup>+gfp</sup> and WT (eGFP negative) mice respectively. Although the primary focus in most experiments described in this chapter was to explore DC migration from dorsal skin, in one experiment I have investigated DC migration from the ear after CFA injection (Figure 3.8). As the ear is anatomically different from the back skin, it was important to investigate CCRL1 expression within the ear so as to draw appropriate conclusions with regards to CCRL1 guidance of DC egress from ear skin as well as back skin.

First, CCRL1-eGFP expression was investigated in the dorsal skin of CCRL1<sup>+gfp</sup> and CCRL1<sup>gfp/gfp</sup> mice. In agreement with reports from Heinzl and colleagues, eGFP expression was localised to keratinocytes in the epidermis and hair follicles in both CCRL1<sup>+gfp</sup> and CCRL1<sup>gfp/gfp</sup> mice (Figure 3.27 B-C). eGFP signal was absent from WT control mice (Figure 3.27 A). Interestingly, eGFP signal was also detectable in cells in the dermis of both CCRL1<sup>+gfp</sup> and CCRL1<sup>gfp/gfp</sup> skin (Figure 3.27 A-C).

To analyse CCRL1 protein expression, CCRL1<sup>+gfp</sup> ear samples were stained with anti-CCRL1 antibody. eGFP expression was uniform across the full length of the epidermis and this correlated with staining using the anti-CCRL1 antibody. Also, cells positive for anti-CCRL1 antibody staining also expressed eGFP in the dermis (Figure 3.27 D).

To further characterise the CCRL1<sup>+</sup> cells found in the dermis, ear samples from CCRL1<sup>+gfp</sup> mice were stained with antibodies against LYVE-1, CD45, CD11b and MHCII. eGFP was found to colocalise with LYVE1 staining (Figure 3.28 A). Therefore, as well as LYVE-1<sup>+</sup> vessels in the lymph node, CCRL1 is also expressed by LYVE-1<sup>+</sup> cells in the skin. These cells are likely LECs, and this is supported by the morphology of the CCRL1<sup>+</sup> LYVE-1<sup>+</sup> structures in the dermis.

Next, CCRL1<sup>+gfp</sup> ear skin was stained with antibodies against MHCII, CD45 and CD11b. From these data, it can be concluded that there are leukocytes (CD45<sup>+</sup>) of the myeloid lineage (CD11b<sup>+</sup>) capable of presenting antigen (MHCII<sup>+</sup>) that express eGFP in CCRL1<sup>+gfp</sup> skin (Figure 3.28 B). WT control samples were used to show the absence of eGFP expression in these samples (Figure 3.28 C). These eGFP<sup>+</sup> cells express markers shared with the eGFP<sup>+</sup> cells that I previously identified in inguinal lymph nodes (Figure 3.25 E). These cells were found to be CD11b<sup>+</sup>, which is a marker of cells from the myeloid lineage. This cell lineage includes cells such as monocytes, DCs and macrophages. As CD11b does not identify any specific myeloid cell population, eGFP<sup>+</sup> cells in the skin were analysed by flow cytometry for expression of CD11c and MHCII, common markers of DCs. As I have described defects in the ability of DCs to migrate from the skin in CCRL1-deficient mice, it seemed conceivable that these cells express CCRL1. Gating cells first on CD11c and MHCII expression identified DCs in the skin that were then analysed for eGFP expression. In CCRL1<sup>+gfp</sup> mice, a population of eGFP<sup>+</sup> DCs was identifiable by flow cytometry and this population of cells was absent in WT counterparts. eGFP<sup>+</sup> DCs accounted for ~10% of the total CD11c<sup>+</sup> MHCII<sup>+</sup> DC population in CCRL1<sup>+gfp</sup> mice.

Taken together, these data show CCRL1 is expressed in the epidermis of the skin, hair follicles and cells residing in the dermis. Further analysis of dermal cells revealed that eGFP expression in the dermis of CCRL1<sup>+gfp</sup> mice is confined to LYVE-1<sup>+</sup> LECs and CD45<sup>+</sup> CD11b<sup>+</sup> MHCII<sup>+</sup> APCs. Flow cytometry revealed that subsets of CD11c<sup>+</sup> MHCII<sup>+</sup> DCs express eGFP in CCRL1<sup>+gfp</sup> mice.

### 3.17 Summary

Based on the data presented in this chapter, I conclude that:

1. At rest, distinct subsets of skin-derived migratory DCs are less abundant in the inguinal lymph node of CCRL1-deficient mice than WT animals.
2. CCR7 drives the migration of DCs to skin-draining lymph nodes during TPA-induced skin inflammation.
3. CCRL1 is required to maintain DC arrival at skin-draining lymph nodes after the induction of cutaneous inflammation with TPA and CFA.

4. CCRL1 aids the egress of DCs from TPA-inflamed skin, and from skin explants.
5. CCRL1 regulates the levels of bioavailable CCL19 and CCL21 in the skin during TPA-induced inflammation.
6. The absence of CCL19 corrects the defect in DC arrival at inguinal lymph nodes seen in TPA-inflamed CCRL1-deficient mice.
7. CCRL1 is expressed by keratinocytes, LECs in the SCS and dermis, a subset of CD11b<sup>+</sup> myeloid cells in the lymph node; and a small population of DCs in the skin.

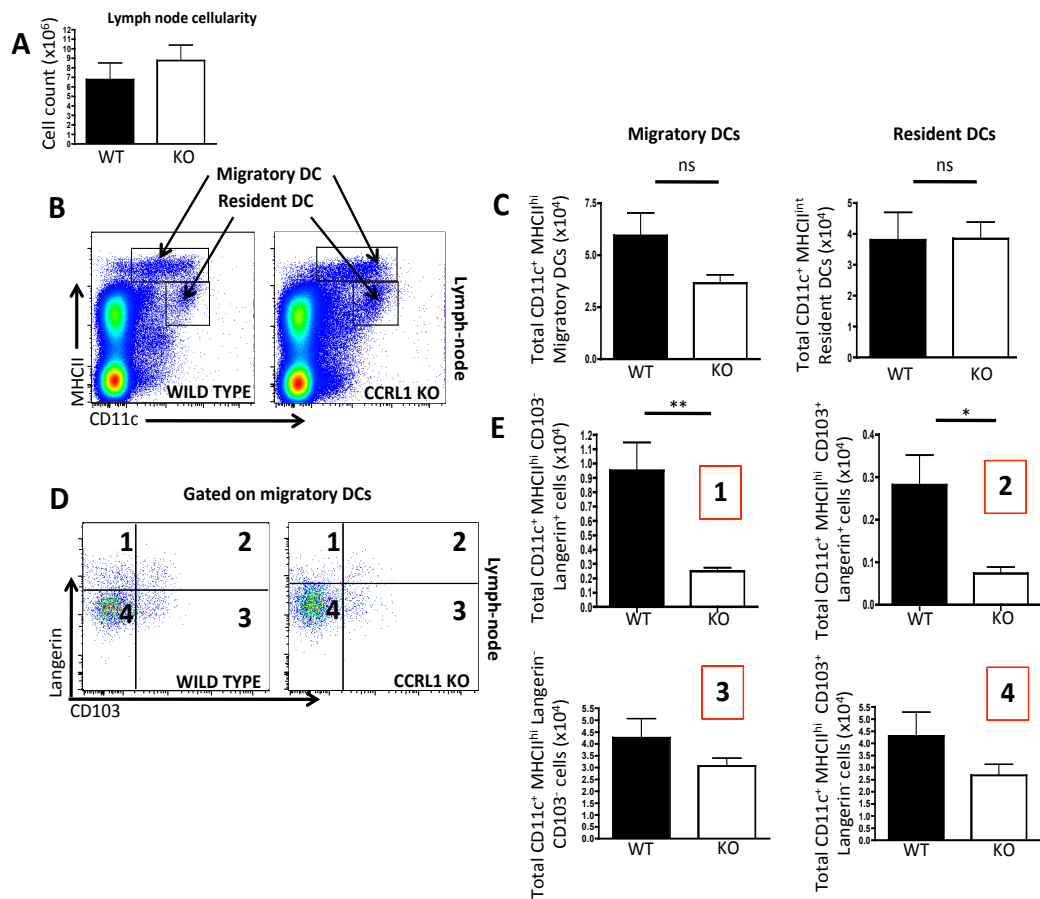


**Figure 3.1: Migratory DCs are reduced in the skin-draining lymph nodes of CCRL1 KO mice during steady state.**

(A) Total number of cells retrieved from WT and CCRL1 KO inguinal lymph nodes. (B) Representative flow cytometry plots of cells in skin-draining lymph nodes of WT (left) and CCRL1-deficient (right) during steady state gated for migratory and resident DCs. (C) Total number of CD11c<sup>+</sup> MHCII<sup>hi</sup> “migratory DCs” and CD11c<sup>+</sup> MHCII<sup>int</sup> “resident DCs”. (D) CD11c<sup>+</sup> MHCII<sup>hi</sup> migratory DCs subdivided based upon CD103 and Langerin expression. (E) Total number of cells in each DC sub-population. Data are representative of one out of three independent experiments with at least 3 mice per group. Data in graphs are presented as mean + SEM and were analysed using a Student’s t-test with \* p < 0.05 \*\* p < 0.01.

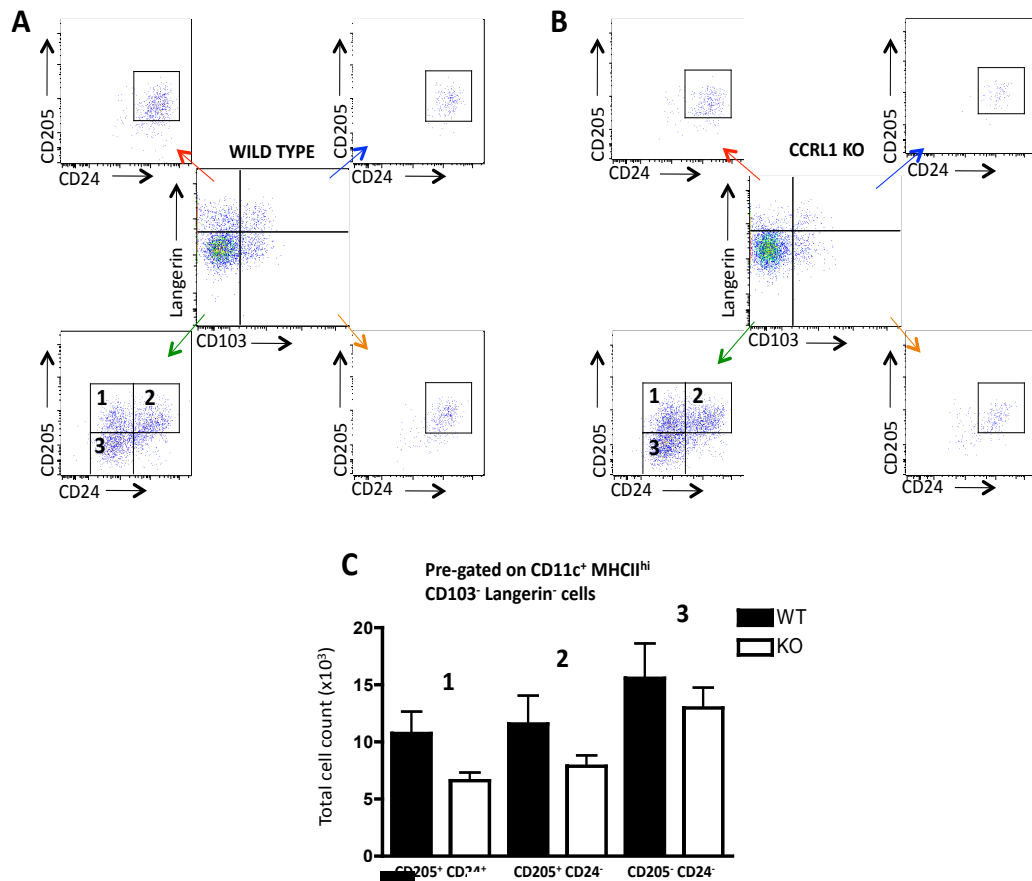


**Figure 3.2: CD24 and CD205 identify distinct cell subsets amongst CD103<sup>-</sup> Langerin<sup>-</sup> DCs in skin-draining lymph nodes.**

Single cell suspensions from resting WT and CCRL1 KO inguinal lymph nodes were prepared and incubated with antibodies to identify specific populations of DCs. WT (A) and CCRL1 KO (B) CD11c<sup>+</sup> MHCII<sup>hi</sup> lymph node cells separated according to CD103 and Langerin expression (central dotplot). CD205 and CD24 expression on each of these four populations of cells is shown in the four satellite dotplots. (C) The total number of each of the different DC populations within the CD103<sup>-</sup> Langerin<sup>-</sup> gate. Data are representative of 4 mice per genotype and the mean + SEM is shown. Data were analysed using one-way ANOVA and Tukey's post test. No statistically significant differences were found between WT and KO samples for each DC population.

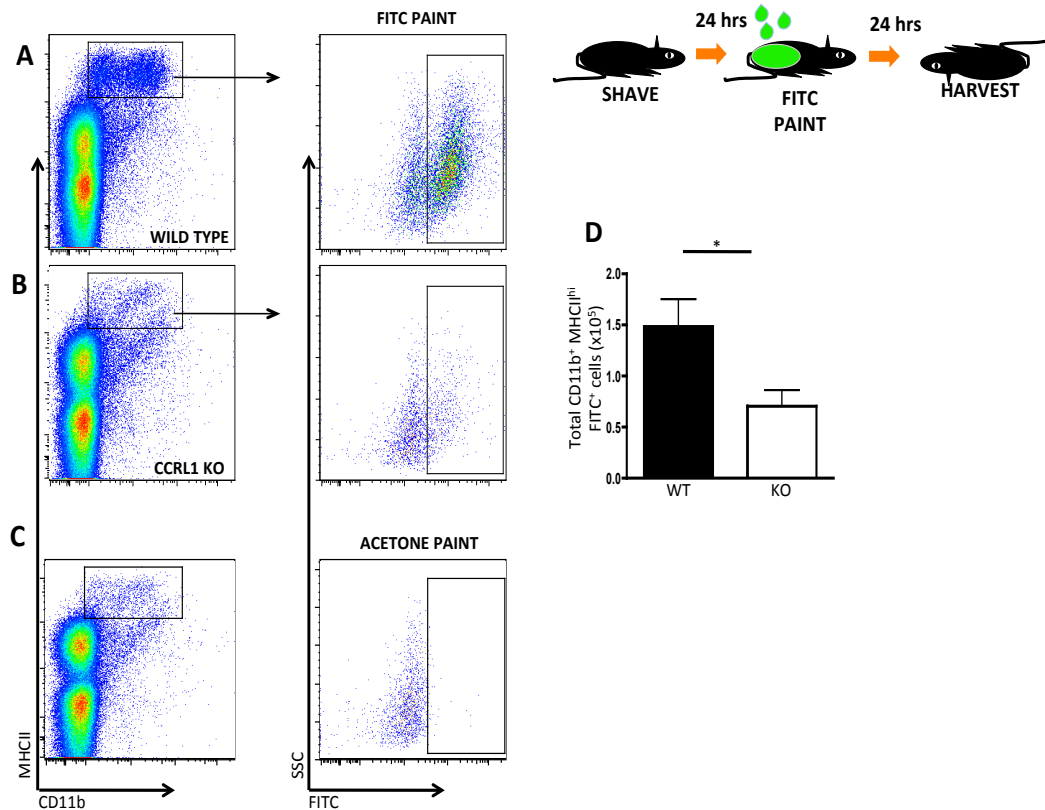


**Figure 3.3: FITC<sup>+</sup> migratory DCs are reduced in skin-draining lymph nodes of CCRL1 KO mice after cutaneous FITC painting.**

WT and CCRL1 KO mice were shaved, topically painted with FITC in acetone, or acetone alone. 24 hours later skin-draining inguinal lymph nodes were harvested and single cell suspensions prepared. The cell suspensions were incubated with antibodies against CD11b and MHCII. CD11b<sup>+</sup> MHCII<sup>hi</sup> DCs were identified in WT (A) and CCRL1 KO samples (B) and then, within both samples, FITC uptake was determined (right hand panels). FITC positive cells were determined by drawing gates on mice receiving acetone paints instead of FITC (C). The total number of CD11b<sup>+</sup> MHCII<sup>hi</sup> FITC<sup>+</sup> DCs are shown in (D). Data are representative of 4 WT mice and 5 CCRL1-deficient mice. Data in graphs are presented as the mean + SEM and were analysed using a Student's t-test with  $p < 0.05^*$ .

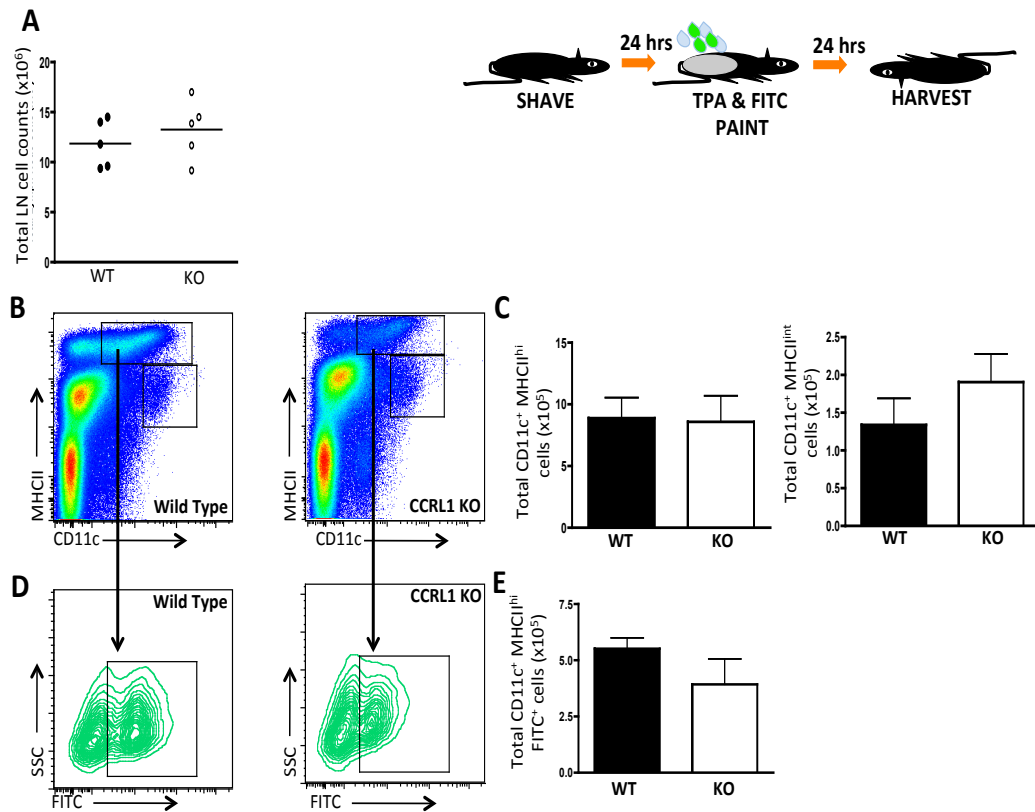


**Figure 3.4: Skin-draining lymph nodes contain the same numbers of migratory DCs after a concomitant TPA + FITC paint on the dorsal skin.**

WT and CCRL1 KO mice were shaved on the dorsal skin, left for 24 hours then concomitantly painted with TPA and FITC to induce skin inflammation and DC migration. 24 hours after TPA and FITC painting, the skin-draining inguinal lymph nodes were excised and single cell suspensions made and total cellularity determined (A). Cells were assessed for CD11c and MHCII expression by flow cytometry (B). The total number of migratory CD11c<sup>+</sup> MHCII<sup>hi</sup> DCs and CD11c<sup>+</sup> MHCII<sup>int</sup> resident DCs was enumerated and is shown in (C). Next, the number of FITC<sup>+</sup> cells amongst WT and CCRL1 KO migratory DCs was determined (D) by drawing gates based on cells from mice receiving acetone in place of FITC. The total number of CD11c<sup>+</sup> MHCII<sup>hi</sup> FITC<sup>+</sup> DCs is represented in (E). Data in graphs C and E are presented as mean + SEM. In A, the mean is indicated by the line amongst the individual data points. Data are from 5 mice per group and were analysed using a Student's t-test, and no statistically significant differences found in the total lymph node cellularity or in any of the DC populations.

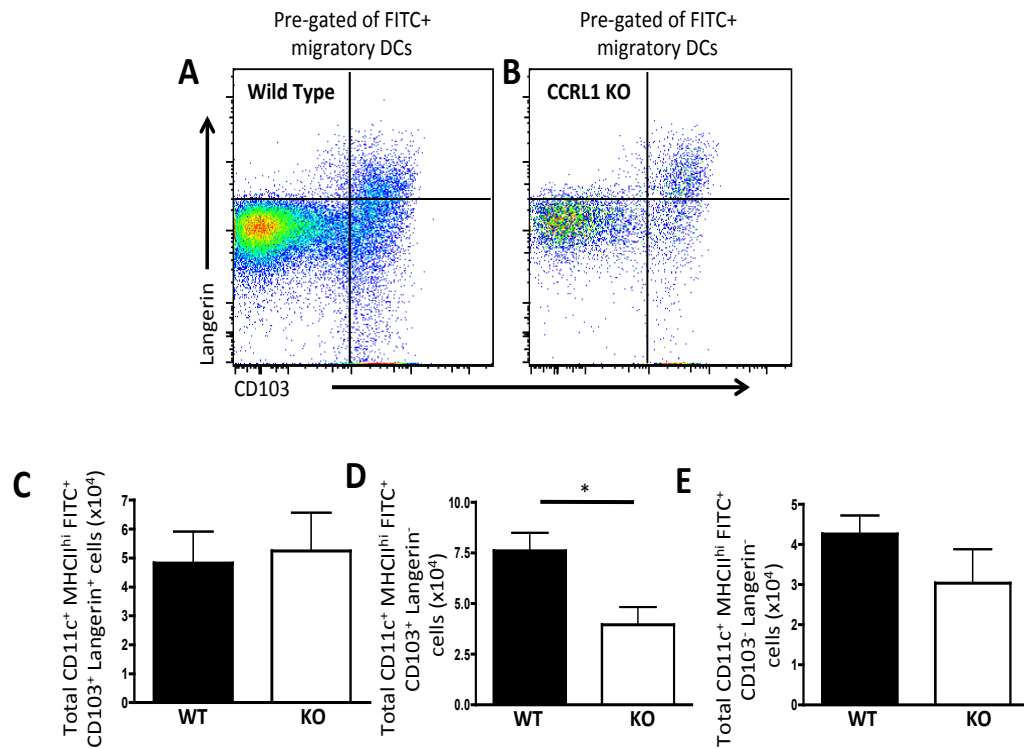


**Figure 3.5: Skin-draining lymph nodes from CCRL1 KO mice contain fewer FITC<sup>+</sup> CD103<sup>-</sup> Langerin<sup>+</sup> DCs after a concomitant TPA + FITC paint on the dorsal skin.**

WT and CCRL KO migratory DCs (CD11c<sup>+</sup> MHCII<sup>hi</sup> FITC<sup>+</sup>) were subdivided into different skin-derived migratory populations. Three populations of DCs were identified after staining with Langerin and CD103 in both WT and CCRL1-deficient samples (A). Each of these three populations was quantified (C-E). Data in graphs are presented as mean + SEM from 5 mice per genotype and were analysed using a Student's t-test with p<0.05\*.

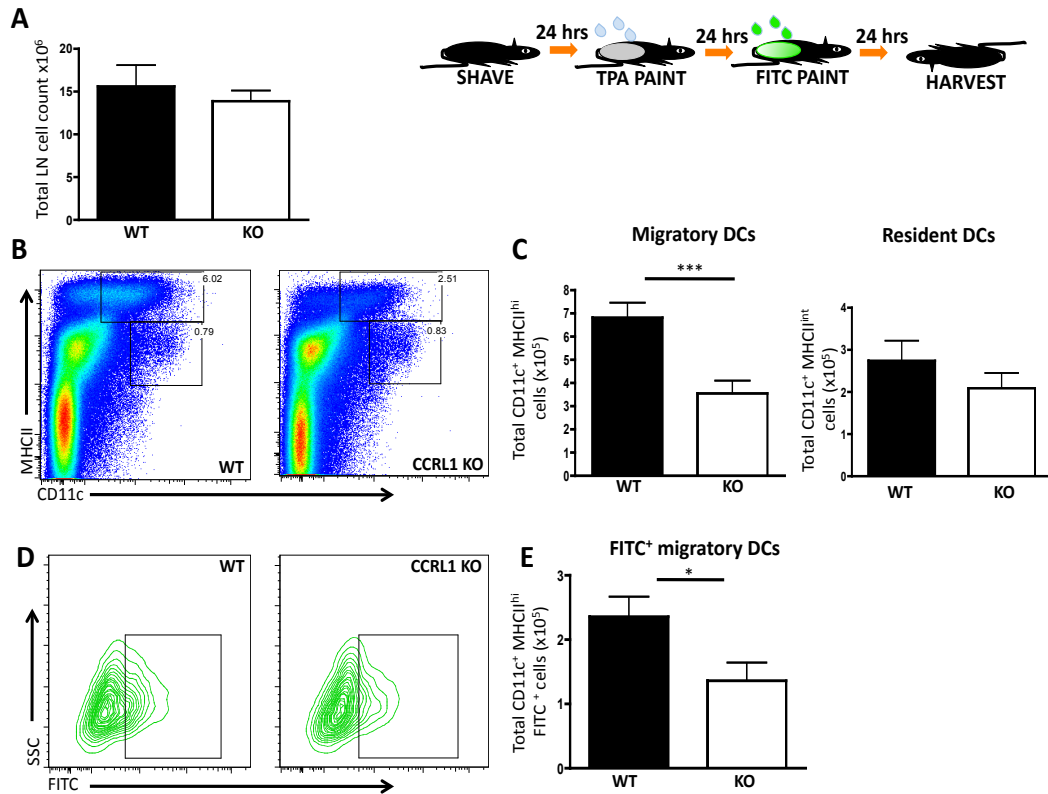


**Figure 3.6: Skin-draining lymph nodes from CCRL1-deficient mice contain fewer migratory DCs than WT mice in the TPA-24-FITC model.**

The dorsal skin of WT and CCRL KO mice was shaved, painted 24 hours later with TPA, and 24 hours after that with FITC. 24 hours after FITC painting the skin-draining inguinal lymph nodes were excised and single cell suspensions prepared for analysis by flow cytometry. Firstly total lymph node cells were enumerated (A). Next cells were stained for different surface markers, namely CD11c and MHCII to reveal DCs (B) and the total number of migratory DCs and resident DCs was then enumerated (C). These CD11c<sup>+</sup> MHCII<sup>hi</sup> migratory DCs were then assessed for FITC positivity by drawing gates based on mice that received acetone paints instead of FITC (D) and the total number of FITC<sup>+</sup> migratory DCs enumerated (E). Data are from 14 WT mice and 13 CCRL1 KO mice from 2 independent experiments. Data in graphs are presented as the mean + SEM and were analysed using a Student's t-test with p<0.05\* and p<0.001\*\*\*.

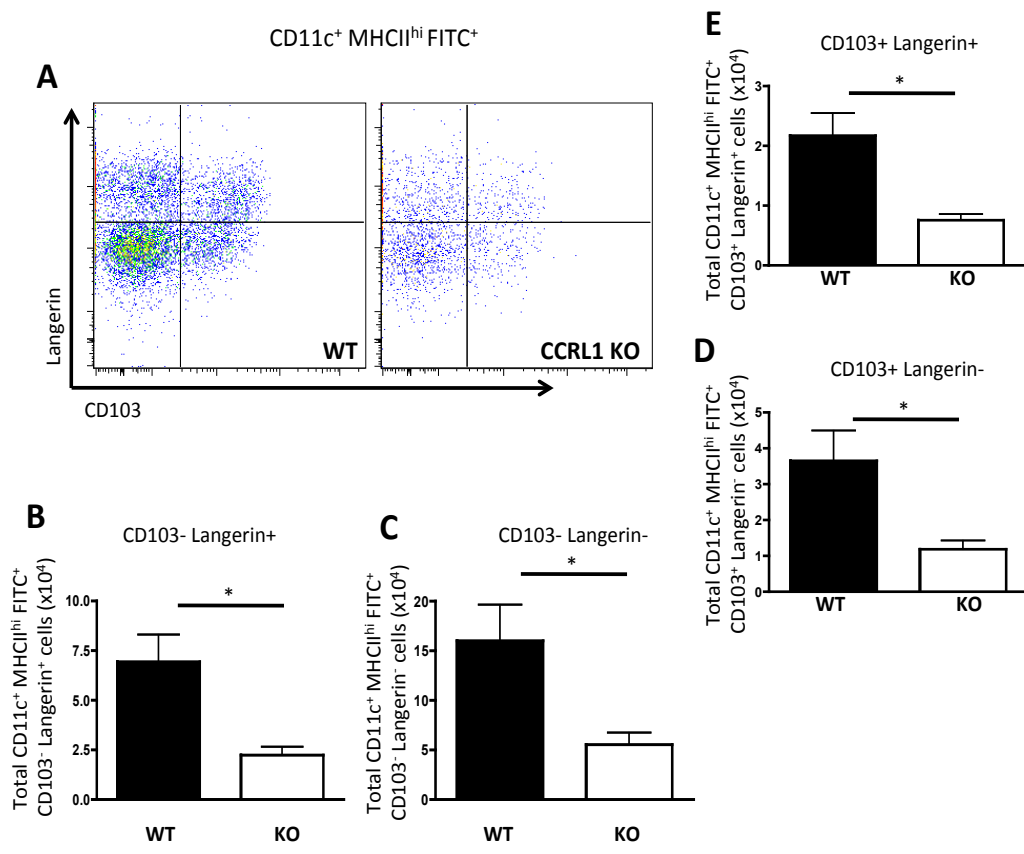


**Figure 3.7: CCRL1 deficiency is associated with a reduction in the abundance of all four migratory DC populations in the inguinal lymph nodes in the TPA-24-FITC model.**

The dorsal skin of WT and CCRL1 KO mice was shaved, painted 24 hours later with TPA, and 24 hours after that with FITC. 24 hours after FITC painting the skin-draining inguinal lymph nodes were excised and single cell suspensions prepared for analysis by flow cytometry. After pre-gating on FITC<sup>+</sup> Migratory DCs (CD11c<sup>+</sup> MHCII<sup>hi</sup> FITC<sup>+</sup>), cells were then separated by differential CD103 and Langerin expression to reveal four DC populations (A). The total number of each of these four DC populations is represented in (B, C, D and E). Data are representative of 5-7 mice per group from 3 independent experiments. Data in graphs are presented as mean + SEM and were analysed using a Student's t-test with p<0.05\*.

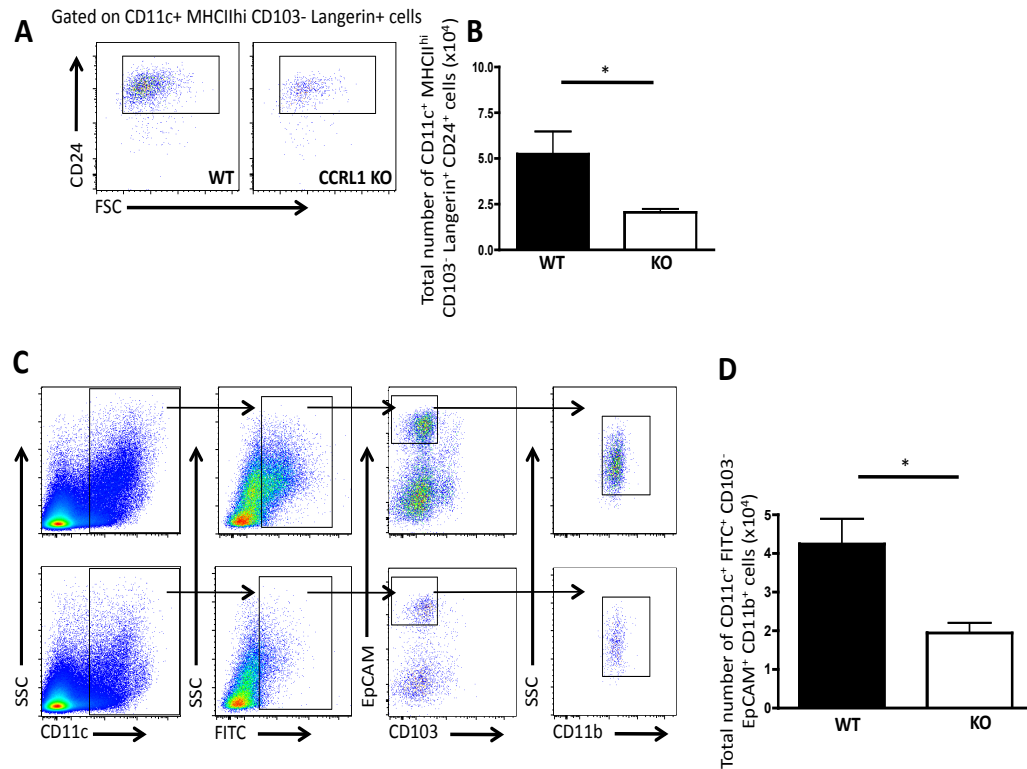


**Figure 3.8: CCRL1 deficiency leads to a reduction in Langerhans cells in skin-draining lymph nodes in the TPA-24-FITC model.**

The dorsal skin of WT and CCRL1 KO mice was shaved, painted 24 hours later with TPA, and 24 hours after that with FITC. 24 hours after FITC painting the skin-draining inguinal lymph nodes were excised and single cell suspensions prepared for analysis by flow cytometry. After pre-gating on CD11c<sup>+</sup> MHCII<sup>hi</sup> CD103<sup>-</sup> Langerin<sup>+</sup> Langerhans cells, DCs were then assessed for CD24 expression (A) and the total number of CD24 expressing Langerhans cells represented in (B). To confirm the identity of these cells as Langerhans cells, the same samples were stained for alternative antibodies against different antigens. DCs were first identified as being CD11c<sup>+</sup> and FITC<sup>+</sup>. FITC positivity was determined by drawing gates on samples from mice receiving only carrier (acetone) instead of FITC. Within the DC population, CD103<sup>-</sup> EpCAM<sup>+</sup> CD11b<sup>+</sup> cells were identified (C) and the total number of these cells in WT and CCRL1 KO inguinal lymph nodes was enumerated (D). Data are representative of 4-7 mice per group from 3 independent experiments. Data in graphs are presented as mean + SEM, and were analysed using a Student's t-test with  $p < 0.05^*$ .

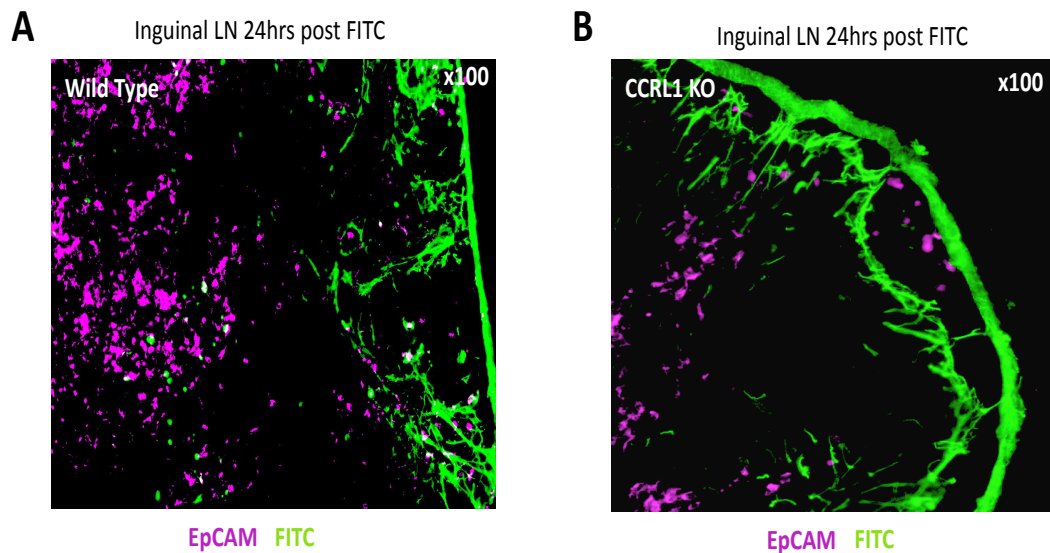


**Figure 3.9: EpCAM<sup>+</sup> cells are less abundant in CCRL1 KO lymph nodes than in WT lymph nodes in the TPA-24-FITC model.**

The dorsal skin of WT and CCRL1 KO mice was shaved, painted 24 hours later with TPA, and 24 hours after that with FITC. 24 hours after FITC painting the skin-draining inguinal lymph nodes were excised and snap frozen. 8-10 $\mu$ m frozen sections were cut using a cryotome and stained with anti-EpCAM antibody. WT inguinal lymph nodes (A) and CCRL1 KO inguinal lymph nodes (B) are shown at x100 magnification. Purple cells represent those cells that are EpCAM<sup>+</sup> and green staining represents unbound FITC present in the lymph node. Images are representative of 5 mice per genotype. EpCAM<sup>+</sup> cells are not obviously green due to the intensity of unbound FITC present in the lymph node. The strong fluorescent signal from unbound FITC swamps the FITC signal from EpCAM<sup>+</sup> cells thus, giving the impression that the EpCAM<sup>+</sup> cells are negative for FITC.

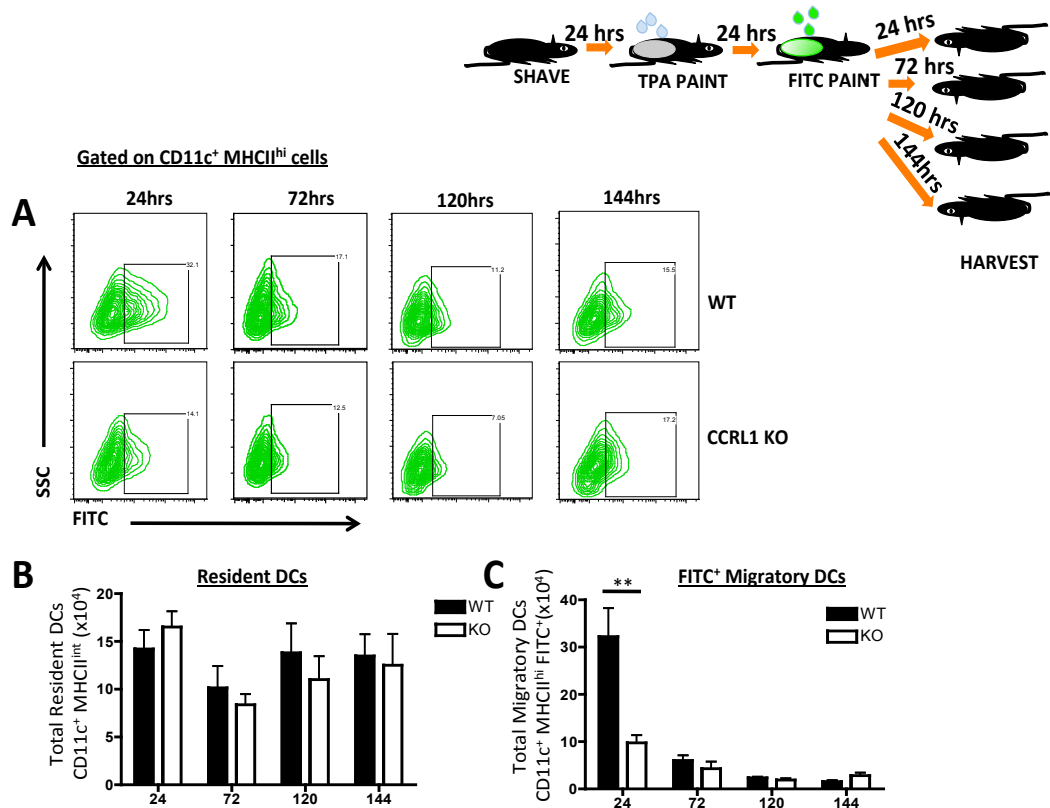


**Figure 3.10: FITC<sup>+</sup> migratory DCs are only reduced in the skin-draining lymph nodes of CCRL1 KO mice 24 hours post FITC painting.**

WT and CCRL1 KO mice were shaved on the dorsal flank and painted with TPA and FITC. The skin-draining inguinal lymph nodes were excised at various time points as indicated (A) and single cell suspensions made. Cells were gated for CD11c<sup>+</sup> MHCII<sup>int</sup> ‘Resident DCs’ and CD11c<sup>+</sup> MHCII<sup>hi</sup> FITC<sup>+</sup> ‘Migratory DCs’. The total number of each of these DC populations is represented in (B and C). Data are representative of 3-6 mice per group from 2 independent experiments. Data are represented as the mean + SEM, and they were analysed using two-way ANOVA and Bonferoni post test with  $p < 0.01^{**}$ .

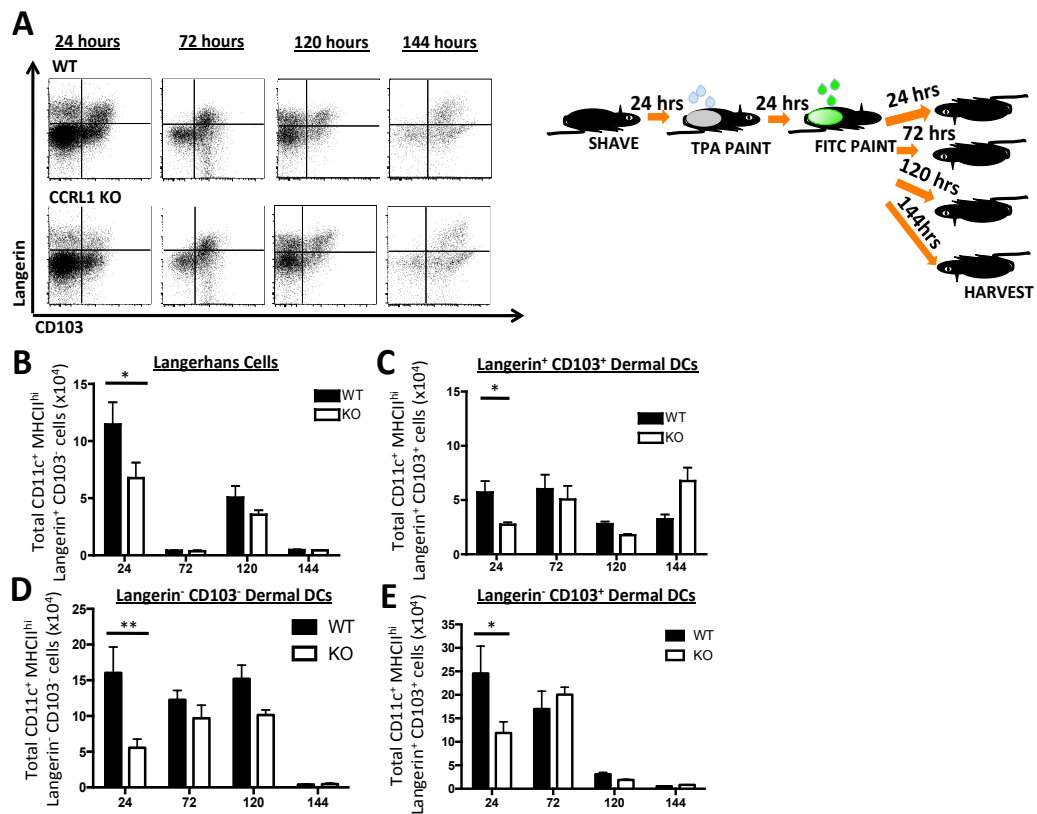


**Figure 3.11: Langerhans cells and other migratory DC subsets are only reduced in the skin-draining lymph nodes of CCRL1 KO mice 24 hours post FITC painting.**

WT and CCRL1 KO mice were shaved on the dorsal flank and painted with TPA and 24 hours later with FITC. The skin-draining inguinal lymph nodes were excised at various time-points as indicated and single cell suspensions prepared for analysis by flow cytometry. Cells were pre-gated for CD11c<sup>+</sup> MHCII<sup>hi</sup> FITC<sup>+</sup> ‘Migratory DCs’ and then separated into 4 populations based on expression of CD103 and Langerin (A). The total number of Langerhans cells (B) CD103<sup>+</sup> Langerin<sup>+</sup> dermal DCs (C) CD103<sup>-</sup> Langerin<sup>-</sup> dermal DCs (D) and CD103<sup>+</sup> Langerin<sup>-</sup> dermal DCs (E) were calculated. Data are representative of 3-6 mice per group from 2 independent experiments. Data are represented as the mean + SEM and were analysed using two-way ANOVA and Bonferoni post test with p<0.05\* and p<0.01\*\*.

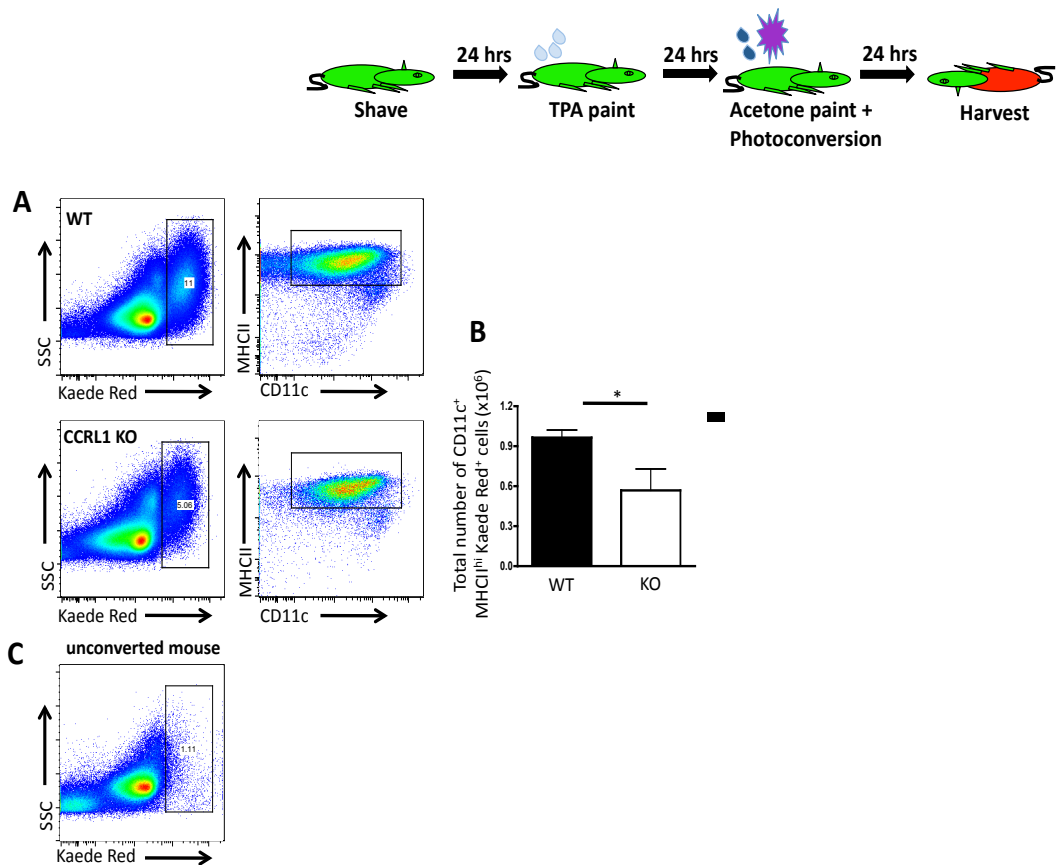


**Figure 3.12: Kaede Red<sup>+</sup> migratory DCs are reduced in numbers in CCRL1 KO skin-draining lymph nodes after cutaneous TPA painting.**

WT and CCRL1 KO mice were shaved on the dorsal flank, left for 24 hours then painted with TPA and 24 hours later photoconverted on the dorsal skin. 24 hours after photoconversion the skin-draining inguinal lymph nodes were excised and single cell suspensions prepared for analysis by flow cytometry. Cells were stained for antibodies against CD11c and MHCII to identify DCs (A) and the total number of kaede red<sup>+</sup> migratory DCs then enumerated (B). An unconverted kaede mouse was used as a control to allow for the gating of kaede red<sup>+</sup> cells (C). Data are representative of 5 kaede mice and 5 CCRL1 KO kaede<sup>+</sup> mice from 2 independent experiments. Graphs show the mean + SEM and data were analysed using Student's t-test with  $p < 0.05^*$ .

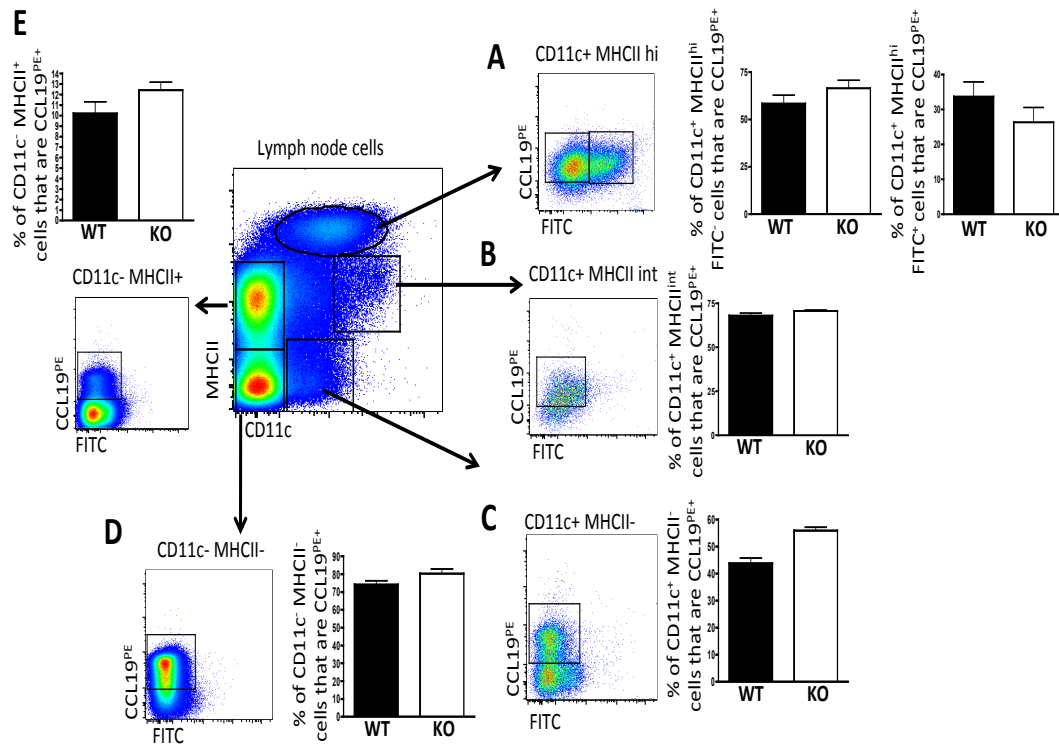


**Figure 3.13: Fluorescent CCL19 tetramer binding to lymph node cells.**

The dorsal skin of WT and CCRL1 KO mice was shaved, painted 24 hours later with TPA, and 24 hours after that with FITC. 24 hours after FITC painting the skin-draining inguinal lymph nodes were excised and single cell suspensions prepared for analysis by flow cytometry. To assess expression of surface CCL19 receptors on various lymph node cell populations in WT and CCRL1 KO mice, cells were incubated at 4°C with CCL19<sup>PE</sup> tetramers. Several different cell populations were identified based on levels of expression of CD11c and MHCII and the percentage of cells positive for CCL19<sup>PE</sup> binding was calculated. (A) CD11c<sup>+</sup> MHCII<sup>hi</sup> (B) CD11c<sup>+</sup> MHCII<sup>int</sup> (C) CD11c<sup>+</sup> MHCII<sup>-</sup> (D) CD11c<sup>-</sup> MHCII<sup>-</sup> (E) CD11c<sup>-</sup> MHCII<sup>+</sup> cells were identified. As a control, cells were exposed to streptavidin PE alone (without CCL19-biotin) in order to allow gates to be drawn to identify CCL19-PE<sup>+</sup> positive cells. Data are representative of the mean + SEM from 4 mice per group from 1 experiment.

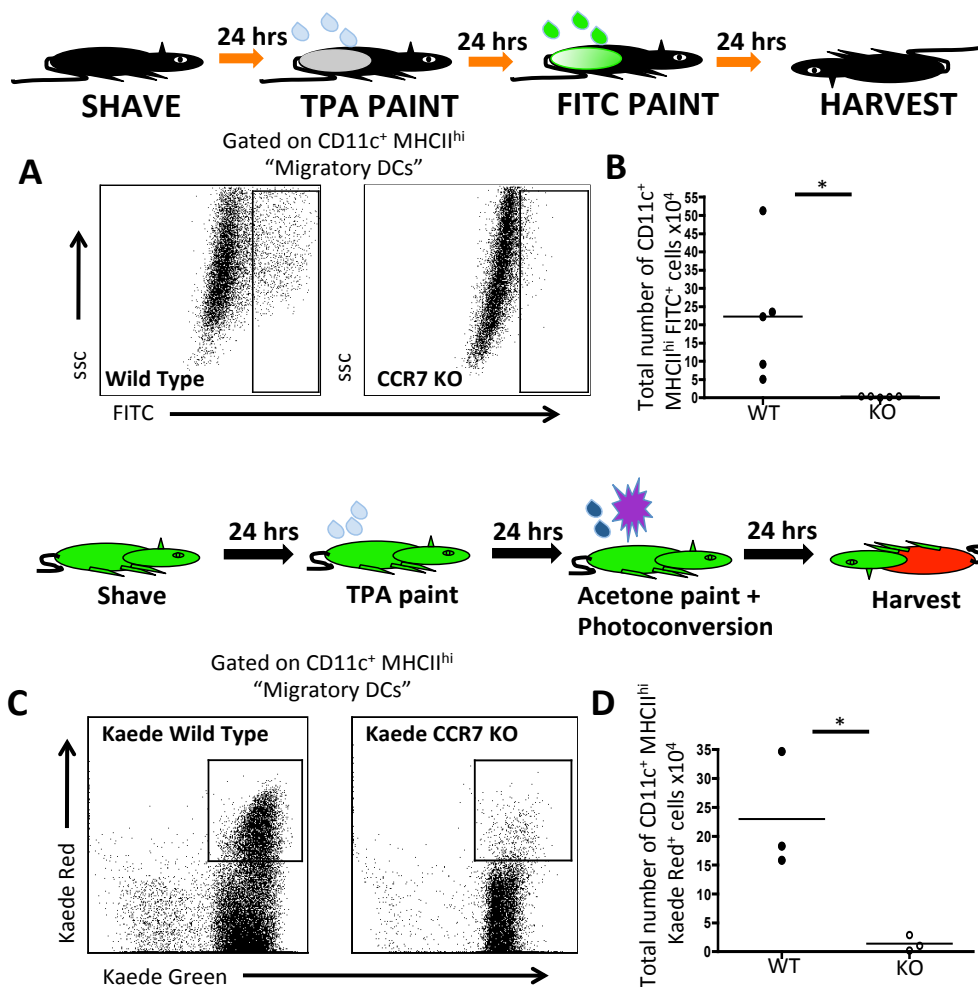


**Figure 3.14: CCR7 is essential for the successful migration of skin DCs to draining lymph nodes after TPA induced inflammation.**

(A-B) Dorsal skin of mice was shaved, TPA was applied 24 hours later, and FITC 24 hours after that. Representative flow cytometry plots of WT (left panel) and CCR7 KO (right panel) skin draining inguinal lymph nodes 24h post FITC paint for CD11c<sup>+</sup> MHCII<sup>hi</sup> FITC<sup>+</sup> migratory DCs. (B) Total number of CD11c<sup>+</sup> MHCII<sup>hi</sup> FITC<sup>+</sup> DCs in skin draining lymph nodes of WT and CCR7 KO mice after FITC painting. Data are representative of the mean from 1 of 2 independent experiments with at least 5 mice per genotype. \* p < 0.05 (Student's t-test). (C-D) Dorsal skin of kaede WT and kaede CCR7 KO mice was shaved and TPA was applied 24 hours later. 24 hours later skin was photoconverted using U.V light. Representative flow cytometry plots of kaede WT (left panel) and kaede CCR7 KO (right panel) skin draining inguinal lymph nodes 24 hours post photoconversion for CD11c<sup>+</sup> MHCII<sup>hi</sup> kaede green<sup>+</sup> kaede red<sup>+</sup> migratory DCs. (D) Total number of CD11c<sup>+</sup> MHCII<sup>hi</sup> kaede green<sup>+</sup> kaede red<sup>+</sup> migratory DCs in skin draining lymph nodes of kaede WT and kaede CCR7 KO mice after photo conversion. Data from individual mice are shown as circles with the mean represented as a line. Results are from 1 of 2 independent experiments with 3 mice per genotype. \*p<0.05 (Student's t-test).

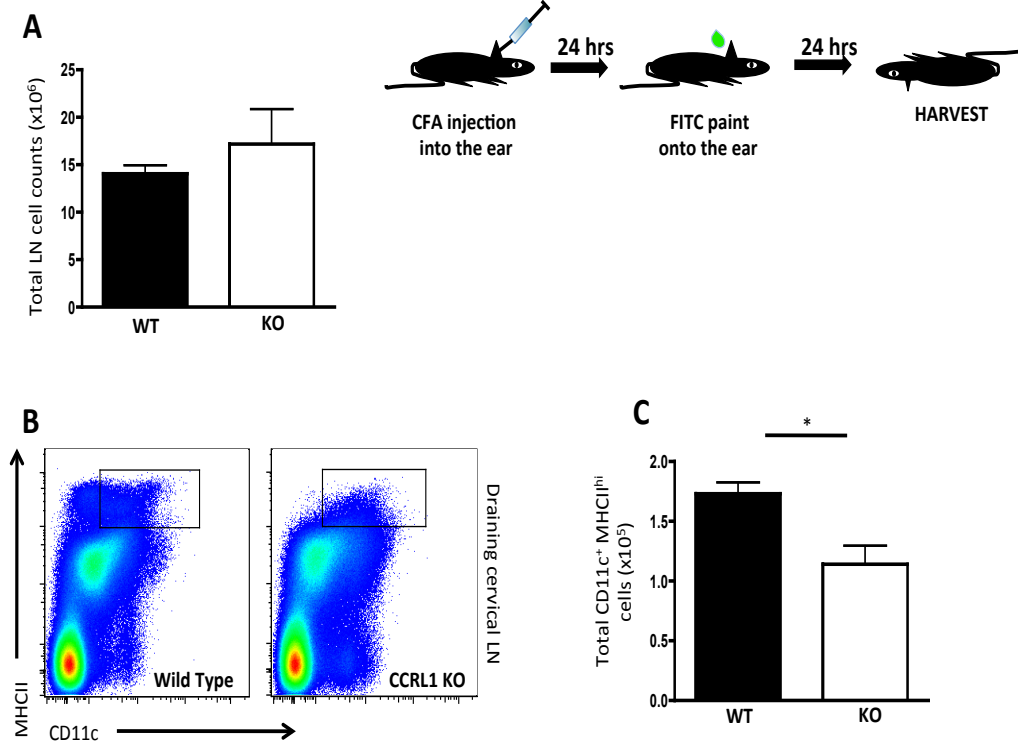


**Figure 3.15: Migratory DCs are reduced in cervical lymph nodes of CCRL1 KO mice after CFA injection into the ear.**

One ear of WT and CCRL1 KO mice were injected with CFA and then 24 hours later, ears were painted with FITC. 24 hours later draining cervical lymph nodes were excised and single cell suspensions prepared for analysis by flow cytometry. First, total lymph node cells were enumerated (A). Migratory DCs were then identified by staining with antibodies against CD11c and MHCII (B) and the total number of CD11c<sup>+</sup> MHCII<sup>hi</sup> migratory DCs calculated (C). Data are represented as the mean + SEM with 4-5 mice per group, and were analysed using Student's t-test with  $p < 0.05^*$ .

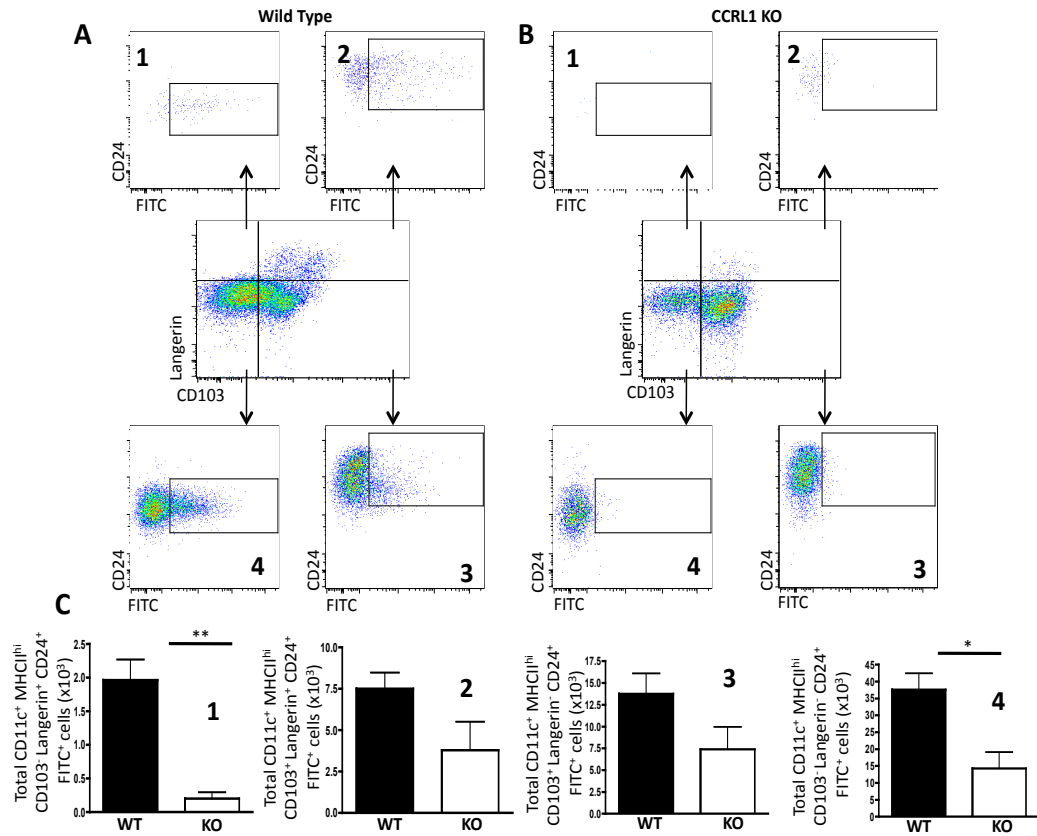


**Figure 3.16: Specific DC subsets are reduced in cervical lymph nodes of CCRL1 KO mice after CFA injection into the ear.**

CFA was injected into the right ear of WT and CCRL1 KO mice that were and 24 hours later the same ear was painted with FITC and 24 hours after that draining cervical lymph nodes were harvested. Single cell suspensions were prepared and stained with a panel of antibodies for analysis by flow cytometry. After pre-gating on CD11c<sup>+</sup> MHCII<sup>hi</sup> DCs, cells from WT and CCRL1 KO lymph nodes were interrogated for CD103, Langerin, CD24 and FITC expression (A) and (B). The total number of cells in each DC population was determined (C). Data are represented as the mean + SEM with n = 4-5 mice per group. Data was analysed using a Student's t-test with p<0.05\* and p<0.01\*\*.

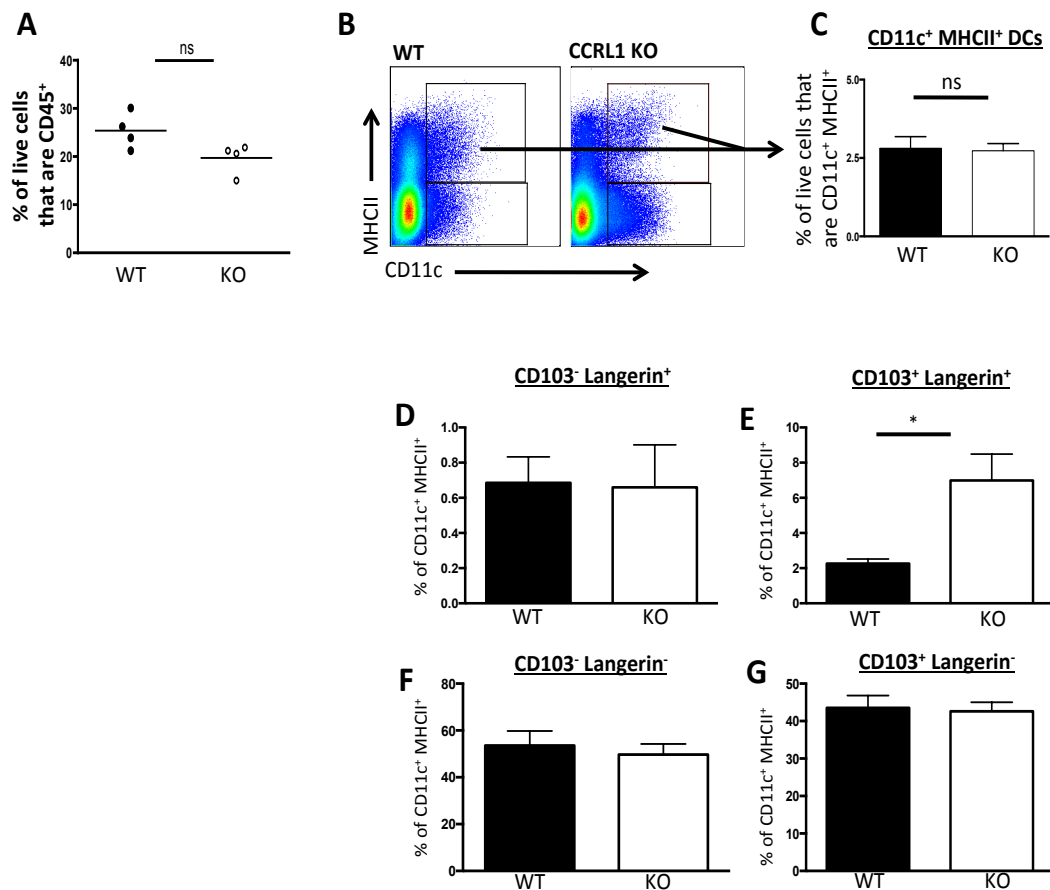


**Figure 3.17: CD103<sup>+</sup> Langerin<sup>+</sup> dermal DCs are increased in the skin of CCRL1 KO mice at rest compared with WT mice.**

Resting dorsal skin from WT and CCRL1 KO mice was harvested, enzymatically digested, and single cell suspensions prepared for analysis by flow cytometry. The percentage of CD45<sup>+</sup> leukocytes was quantified (A). The percentage of CD11c<sup>+</sup> MHCII<sup>+</sup> DCs was calculated (B and C). DCs were then analysed for CD103 and Langerin expression to reveal four DC subsets. The percentage of Langerhans cells (D), CD103<sup>+</sup> dermal DCs (E), CD103<sup>-</sup> Langerin<sup>-</sup> dermal DCs (F), and CD103<sup>+</sup> Langerin<sup>-</sup> dermal DCs (G) in the CD11c<sup>+</sup> MHCII<sup>hi</sup> population was calculated. Data are represented as the mean + SEM from 1 of 2 independent experiments with at least 4 mice per group. Data were analysed using Student's t-test with p<0.05\* and ns = not significant.

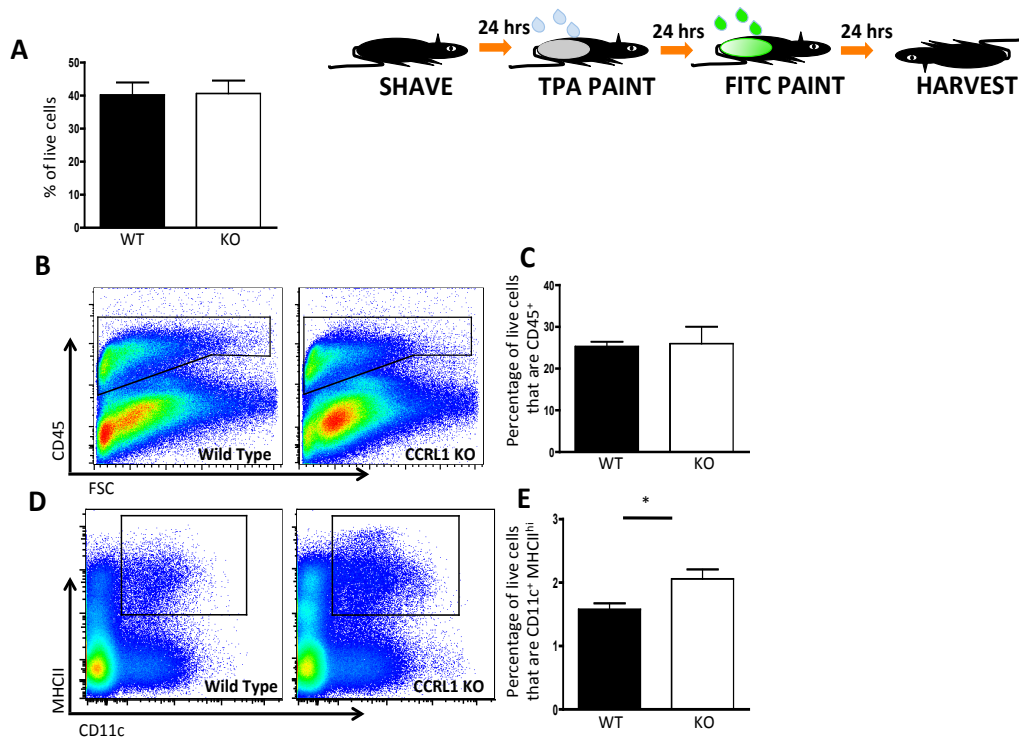


**Figure 3.18: The proportion of DCs in the inflamed skin of CCRL1 KO mice is increased compared with WTs (TPA-24-FITC protocol).**

WT and CCRL1 KO mice were shaved on the dorsal flank, left for 24 hours then painted with TPA and 24 hours later painted with FITC. 24 hours after FITC painting the back skin was excised and single cell suspensions prepared for analysis by flow cytometry. First, the percentage of live cells was quantified (A). The number of CD45<sup>+</sup> leukocytes was enumerated (B and C). To assess the number of DCs present in the skin, samples were stained for CD11c and MHCII (D) and the percentage of CD11c<sup>+</sup> MHCII<sup>+</sup> DCs calculated (E). Data are representative of the mean + SEM from 1 of 2 independent experiments with 4 mice per group. Data were analysed using Student's t-test with  $p < 0.05^*$ .

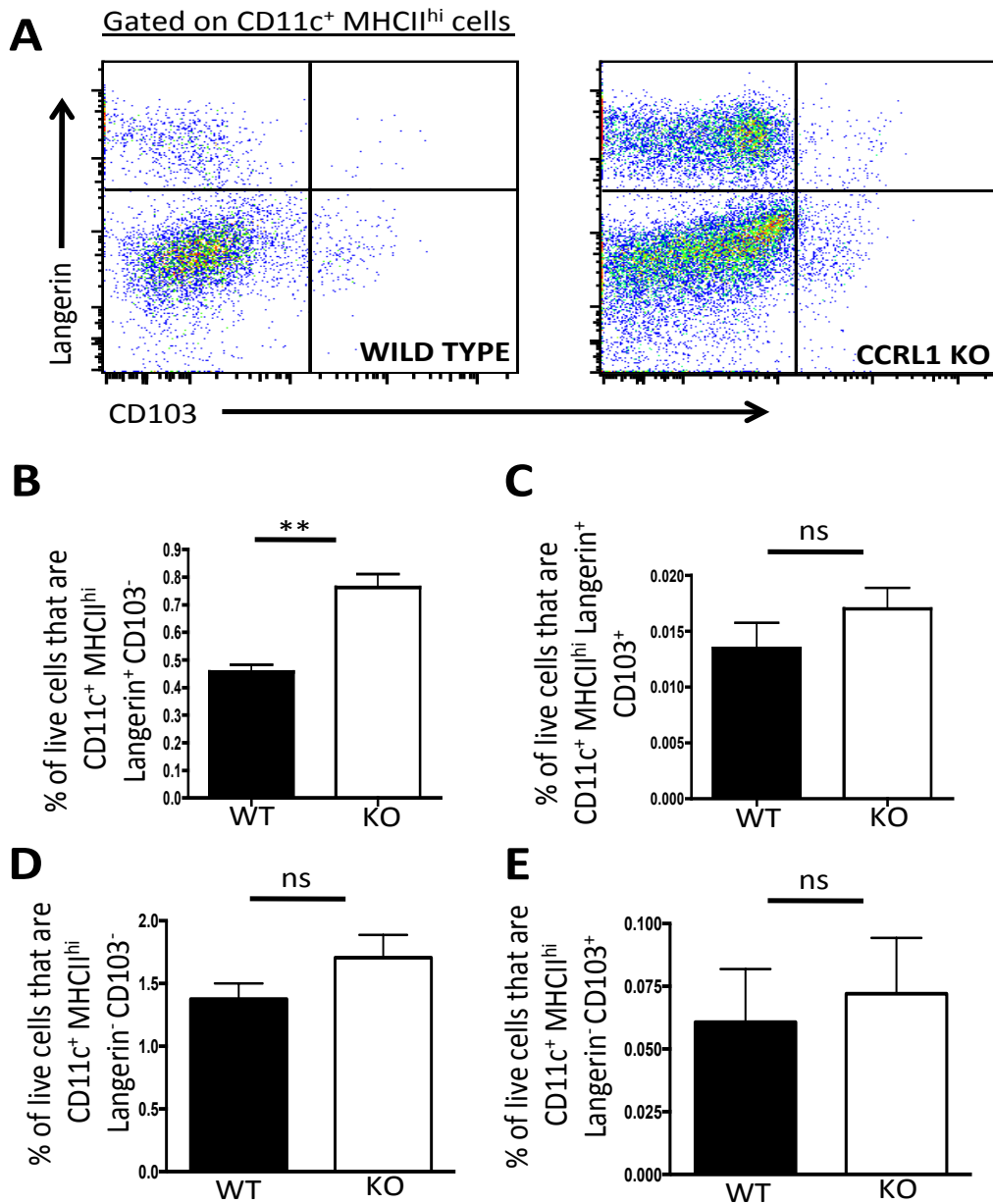


**Figure 3.19: Langerhans cells are specifically retained in the inflamed skin of CCRL1 KO mice (TPA-24-FITC model).**

WT and CCRL1 KO mice were shaved on the dorsal flank, left for 24 hours, painted with TPA, and 24 hours later painted with FITC. 24 hours after FITC painting, the back skin was excised and single cell suspensions prepared for analysis by flow cytometry. After pre-gating for CD11c<sup>+</sup> MHCII<sup>hi</sup> migratory DCs, cells were analysed for CD103 and Langerin expression to reveal four populations of skin DCs (A). The percentage of each DC population was calculated and is represented (B-E). Data are representative of the mean + SEM from 1 of 2 independent experiments with 4 mice per group. Data were analysed using Student's t-test with  $p < 0.01$  \*\* and ns = not significant.

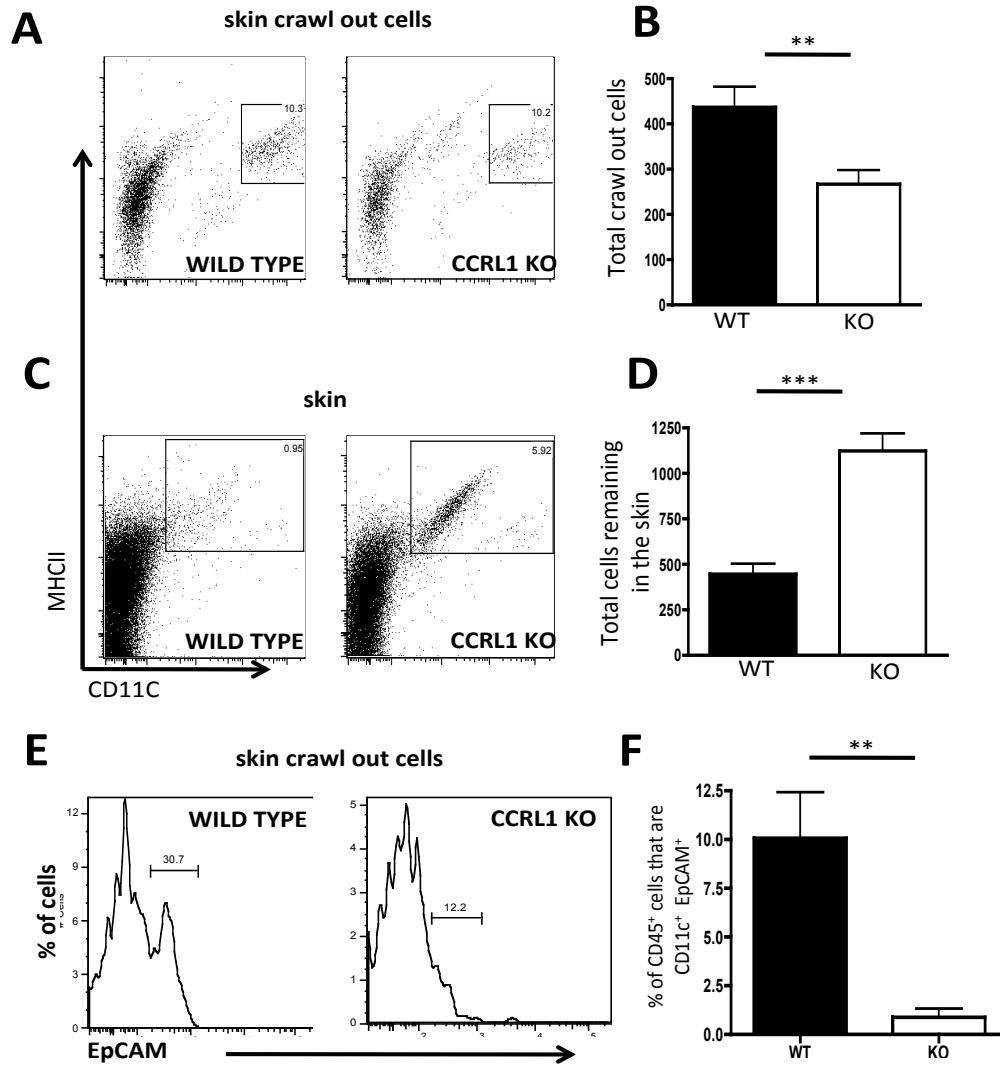


**Figure 3.20: Defective DC departure from CCRL1 KO skin.**

WT and CCRL1 KO dorsal skin was excised and cultured in complete media for three days to quantify the number of DCs that emigrate from the skin and accumulate in the medium. Crawl out cells were first classified as CD45<sup>+</sup> and CD45<sup>-</sup> cells by flow cytometry. Within the CD45<sup>+</sup> leukocyte population DC crawl out cells were identified (A). Skin preparations were analysed for DCs by staining for CD11c and MHCII expression (C). The total number of crawl out DCs is shown (B). Skin was harvested after the culture period and digested to give a single cell suspension. The number of DCs within this cell suspension was then calculated (D). Crawl out DCs were further analysed by examining expression of EpCAM (E) and the total number of CD11c<sup>+</sup> EpCAM<sup>+</sup> DCs was enumerated (F). Data are presented as the mean + SEM with 4-5 mice per group. Data were analysed using Student's t-test with  $p < 0.01$  \*\*,  $p < 0.001$  \*\*\*.

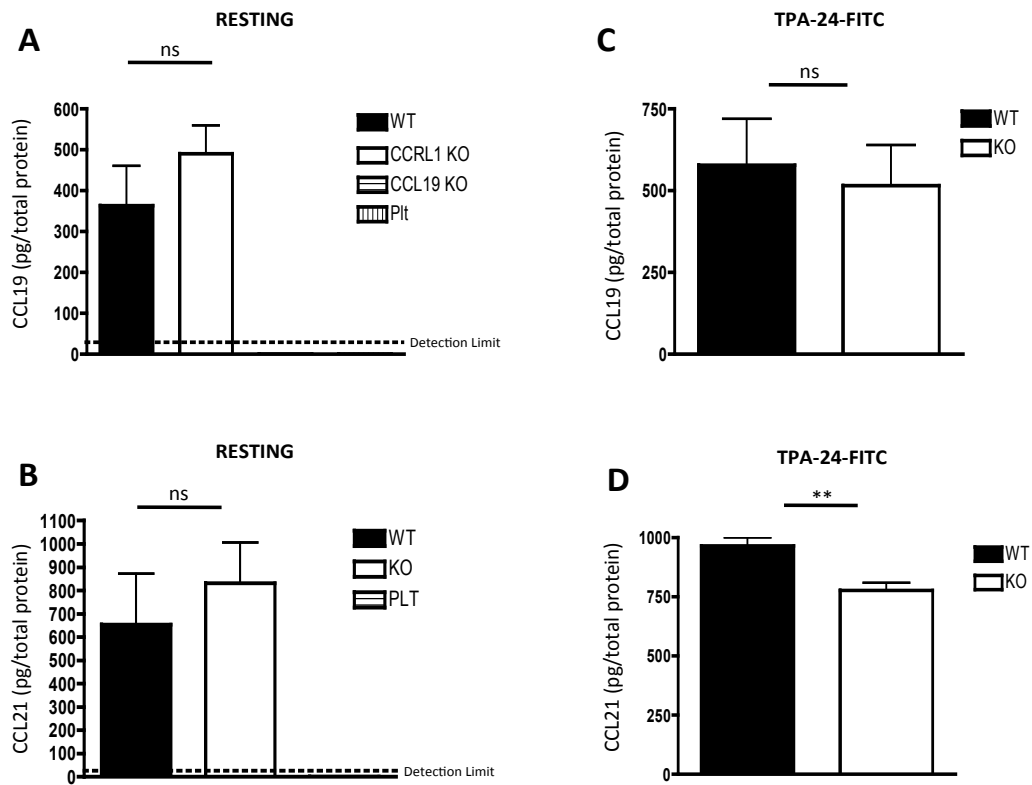
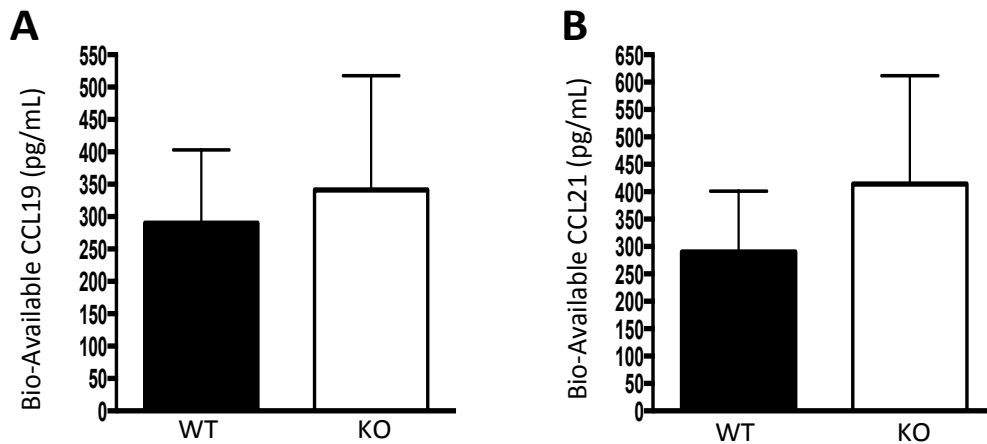


**Figure 3.21: CCL19 and CCL21 protein in resting and inflamed inguinal lymph nodes.**

Resting inguinal lymph nodes were harvested from WT, CCL19-deficient and CCRL1 KO mice and chemokine levels assessed by ELISA. Lysates of lymph nodes from plt mice were provided by Prof A.Rot, University of Birmingham, UK. Levels of CCL19 protein (A) and CCL21 protein (B) in the inguinal lymph nodes. The dorsal skin of WT and CCRL1 KO mice were challenged with TPA and then 24 hours later challenged again with FITC. 24 hours after FITC challenge inguinal lymph nodes were harvested, homogenates made, and levels of CCL19 protein (C) and CCL21 protein (D) quantified by ELISA. Data are representative of one of 2 independent experiments and show the mean + SEM. Statistical analyses was undertaken using Student's t-test with  $P < 0.01$  \*\* and ns= not significant.

## RESTING SKIN



## TPA-24-FITC SKIN

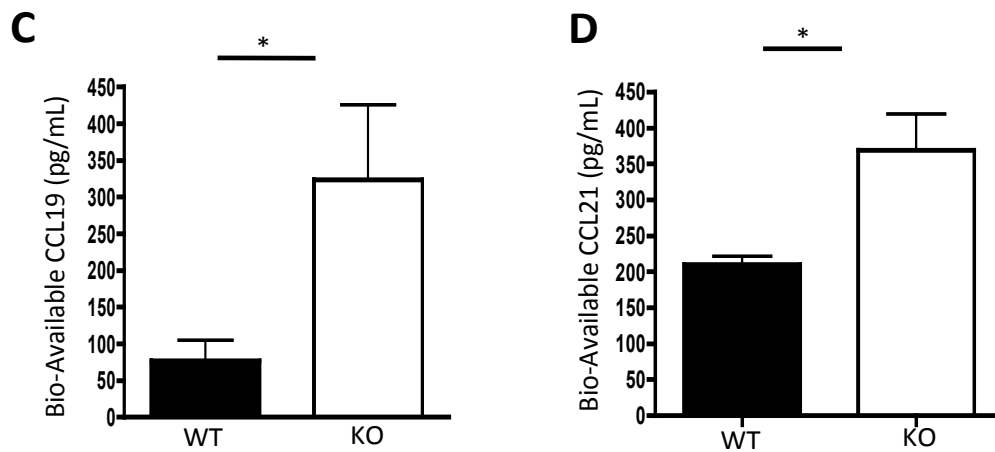


**Figure 3.22: Bio-available CCL19 and CCL21 levels are increased in the inflamed skin of CCRL1 KO mice.**

The dorsal skin of resting WT and CCRL1 KO mice was harvested. Alternatively the back skin of WT and CCRL1-deficient mice was shaved, challenged with TPA, rested for 24 hours and then painted with FITC. 24 hours after FITC challenge the skins were excised. 10x5mm diameter circular punch biopsies were excised from resting and TPA-inflamed skins and then incubated for 5 hours in PBS + protease inhibitor to allow chemokine to leach from the skin. After 5 hours the total CCL19 (A and C) and CCL21 (B and D) was quantified by ELISA. Data are representative of the mean + SEM from 1 of 2 independent experiments with 5 mice per genotype. Data were analysed using a Student's t-test with  $p < 0.05^*$ .

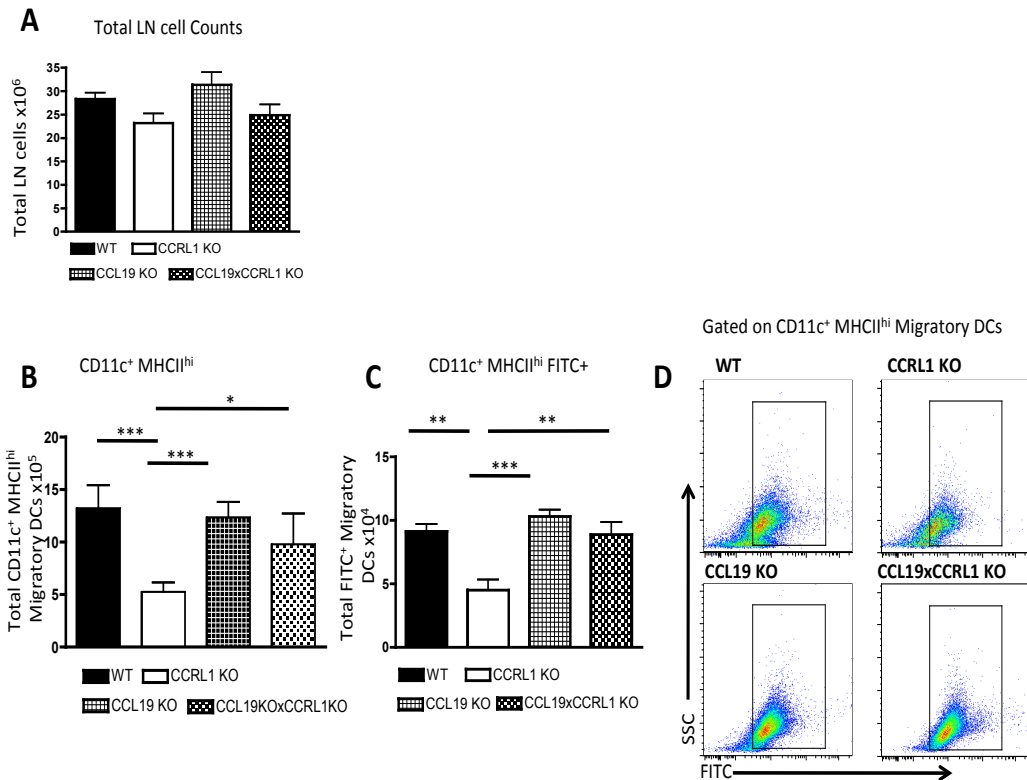


**Figure 3.23: Deletion of CCL19 rescues the migratory DC defect seen at rest in CCRL1 KO mice.**

WT, CCRL1 KO, CCL19 KO and CCL19<sup>-/-</sup> x CCRL1<sup>-/-</sup> mice were shaved on the dorsal skin and then 24 hours later painted with TPA. 24 hours later the back skin was painted with FITC and after a further 24 hours the inguinal lymph nodes were harvested to make single cell suspensions. The total lymph node cellularity was calculated from these cell suspensions (A). Samples were then stained using antibodies CD11c and MHCII to identify CD11c<sup>+</sup> MHCII<sup>hi</sup> migratory DCs across all four genotypes. The number of migratory DCs was then enumerated (B). To confirm that these cells are skin derived, FITC<sup>+</sup> migratory cells were then identified (D) and the total number of these cells enumerated (C). Data are representative of the mean + SEM from 5 mice per genotype. Statistical analysis was performed using one-way ANOVA with Tukey's post-test. p<0.05\* p<0.01\*\* and p<0.001\*\*\*.

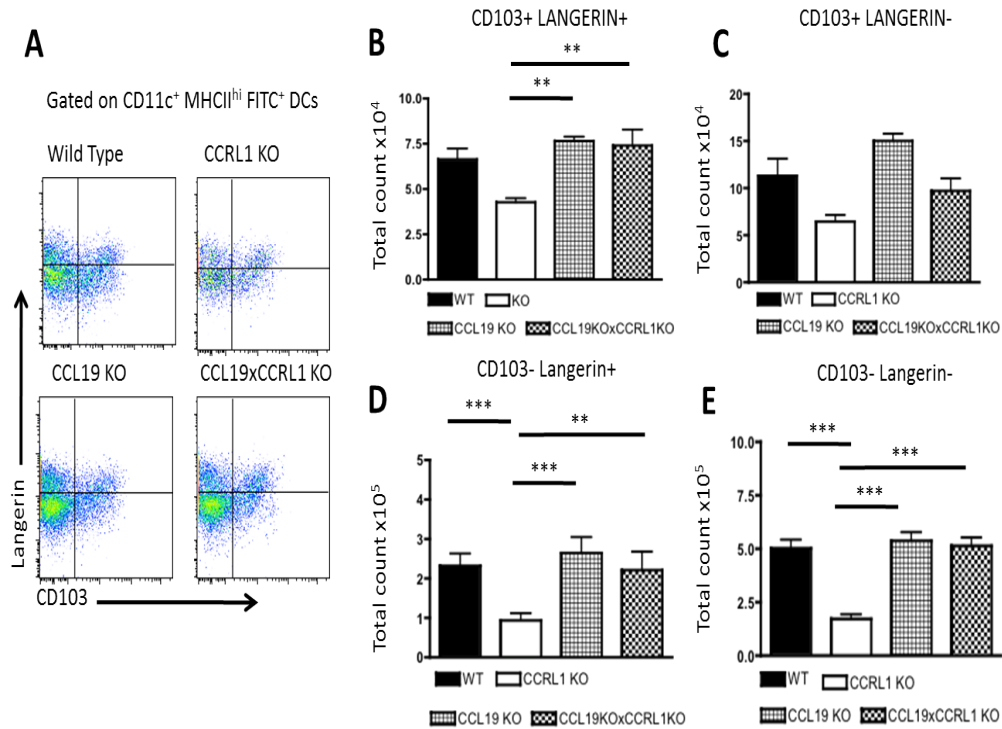


**Figure 3.24: Deletion of CCL19 rescues the migratory DC defects seen in CCRL1 KO mice.**

WT, CCRL1 KO, CCL19 KO and CCL19<sup>-/-</sup> x CCRL1<sup>-/-</sup> mice were shaved on the lower back and then 24 hours later painted with TPA. 24 hours later the back skin was painted with FITC and after a further 24 hours the inguinal lymph nodes were harvested to make single cell suspensions. Cells were stained and analysed by flow cytometry. Firstly cells were pre-gated on FITC<sup>+</sup> migratory DCs and then stained with CD103 and Langerin antibodies to reveal 4 skin-derived DC sub-populations (A). The total number of CD103<sup>+</sup> Langerin<sup>+</sup> (B) CD103<sup>+</sup> Langerin<sup>-</sup> (C) CD103<sup>-</sup> Langerin<sup>+</sup> (D) and CD103<sup>-</sup> Langerin<sup>-</sup> (E) DCs were enumerated. Data are representative of the mean + SEM from 5 mice per genotype. Statistical analysis was performed using one-way ANOVA with Tukey's post-test with p<0.01\*\* and p<0.001\*\*\*.

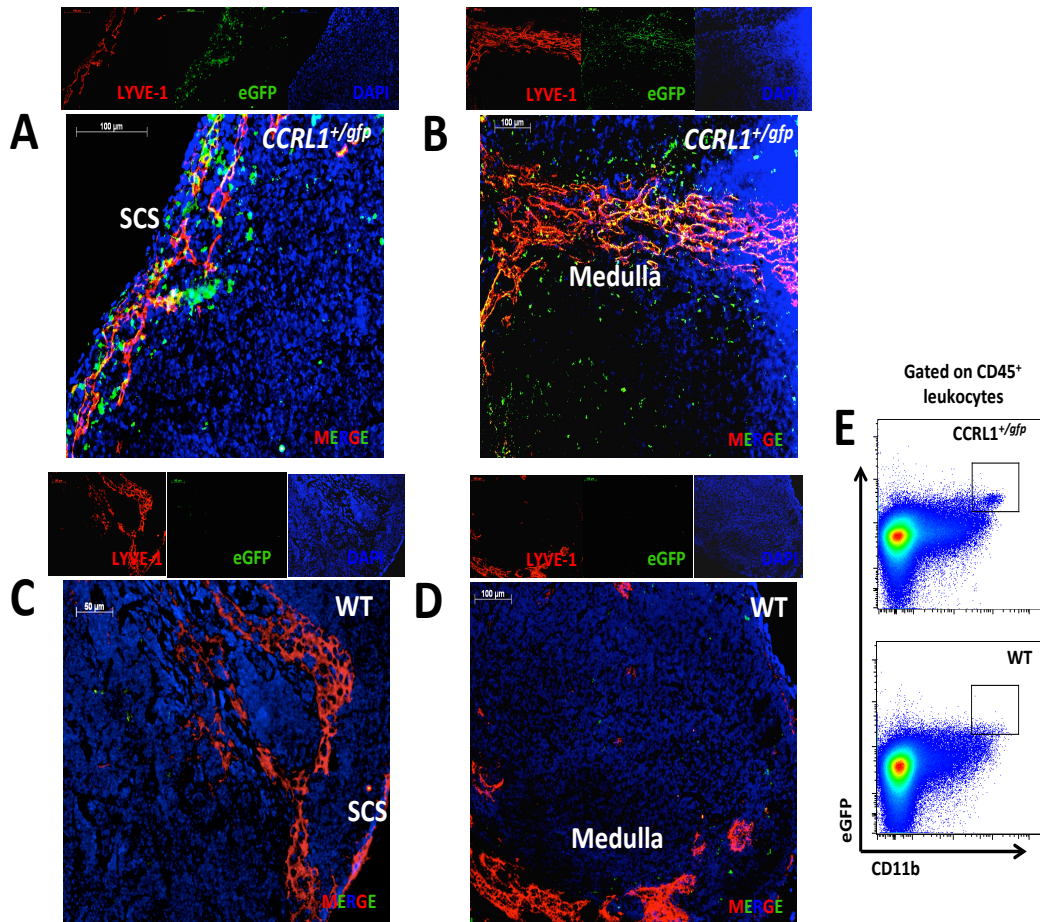


**Figure 3.25: eGFP is expressed on LYVE-1+ lymphatic endothelial cells and cells associated with these vessels in the inguinal lymph nodes of  $CCRL1^{gfp/+}$  mice.**

Resting inguinal lymph nodes from  $CCRL1^{gfp/+}$  and WT mice were harvested, placed in OCT compound and then frozen on dry ice. 8-10 $\mu$ m frozen sections were cut using a cryotome in preparation for antibody staining. Sections were stained with DAPI (blue) and anti-LYVE-1 antibody (red). eGFP is shown in green.  $CCRL1^{gfp/+}$  inguinal lymph nodes, showing the SCS region (A) and medullary region (B) of the lymph node are shown. WT inguinal lymph nodes showing the SCS region (C) and the medullary region (D) are shown. Non-LYVE-1<sup>+</sup> eGFP<sup>+</sup> cells in the lymph node of  $CCRL1^{gfp/+}$  mice were then analysed further by flow cytometry using anti-CD45 and anti-CD11b antibodies. WT mice were used as controls for eGFP expression (E). For each immunofluorescent image, single coloured images and merged coloured images are shown (A-D). Images are representative of 4 mice per genotype. For flow cytometry data, pseudocolour dot plots are representative of 3 mice per genotype.

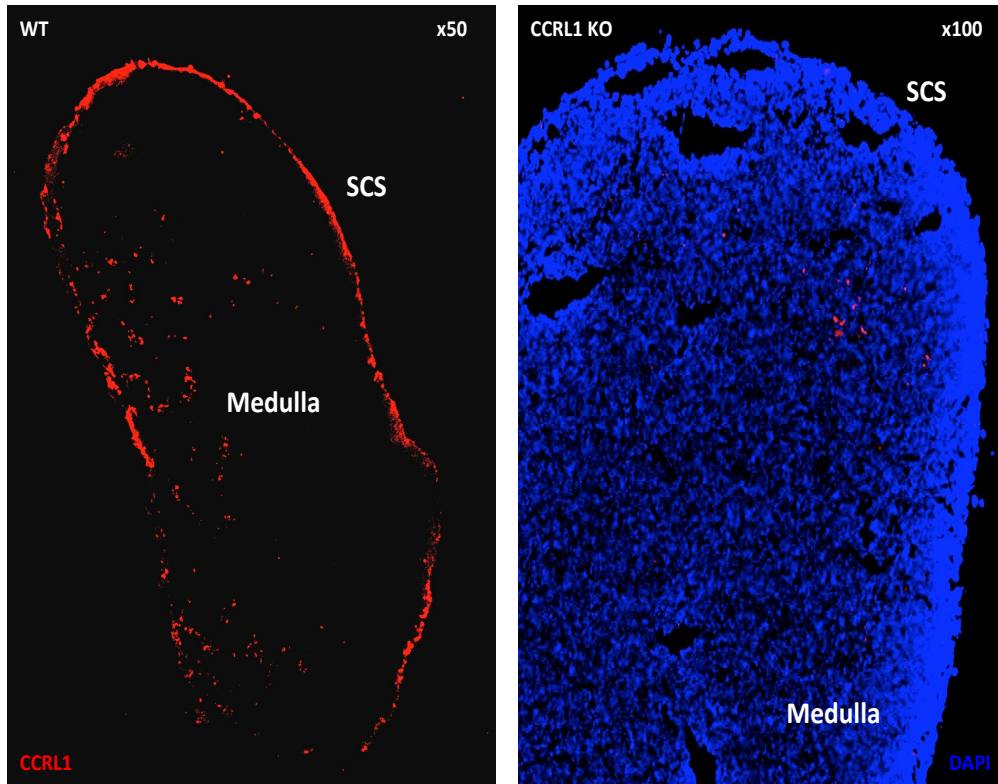


**Figure 3.26: CCRL1 protein is expressed by cells residing at the SCS and medullary regions of inguinal lymph nodes.**

Resting inguinal lymph nodes were harvested from WT and CCRL1 KO mice, placed in OCT compound and frozen on dry ice. 8-10 $\mu$ m frozen sections were cut using a cryotome in preparation for antibody staining. Representative image of WT resting inguinal lymph node stained with anti-CCRL1 antibody (red) (left panel). Representative image of CCRL1 KO resting inguinal lymph node stained with anti-CCRL1 antibody (red) and DAPI (blue) (right hand panel). Images are representative of at least 3 mice per genotype.

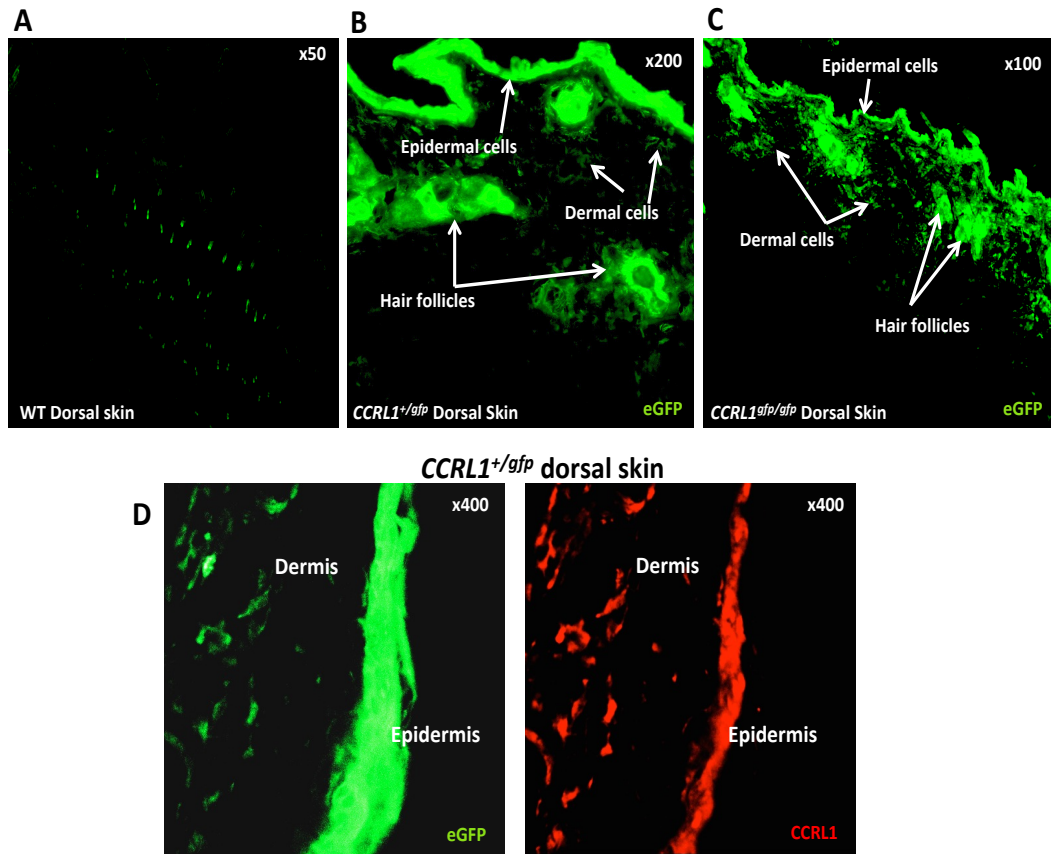


**Figure 3.27: CCRL1-eGFP is expressed by hair follicles and cells in the epidermis and dermis.**

Dorsal skin from resting WT (A) *CCRL1<sup>+/gfp</sup>* (B and D) and *CCRL1<sup>gfp/gfp</sup>* (C) mice was excised, placed in OCT compound and then frozen on dry ice. 8-10 $\mu$ m sections were then cut using a cryotome and directly imaged using a fluorescent microscope to localize eGFP expression. To localize CCRL1 protein expression, *CCRL1<sup>+/gfp</sup>* sections were stained with anti-CCRL1 antibody (red) (D right hand panel) and staining compared with eGFP expression (D left hand panel). Images are representative of 3-4 mice per genotype.

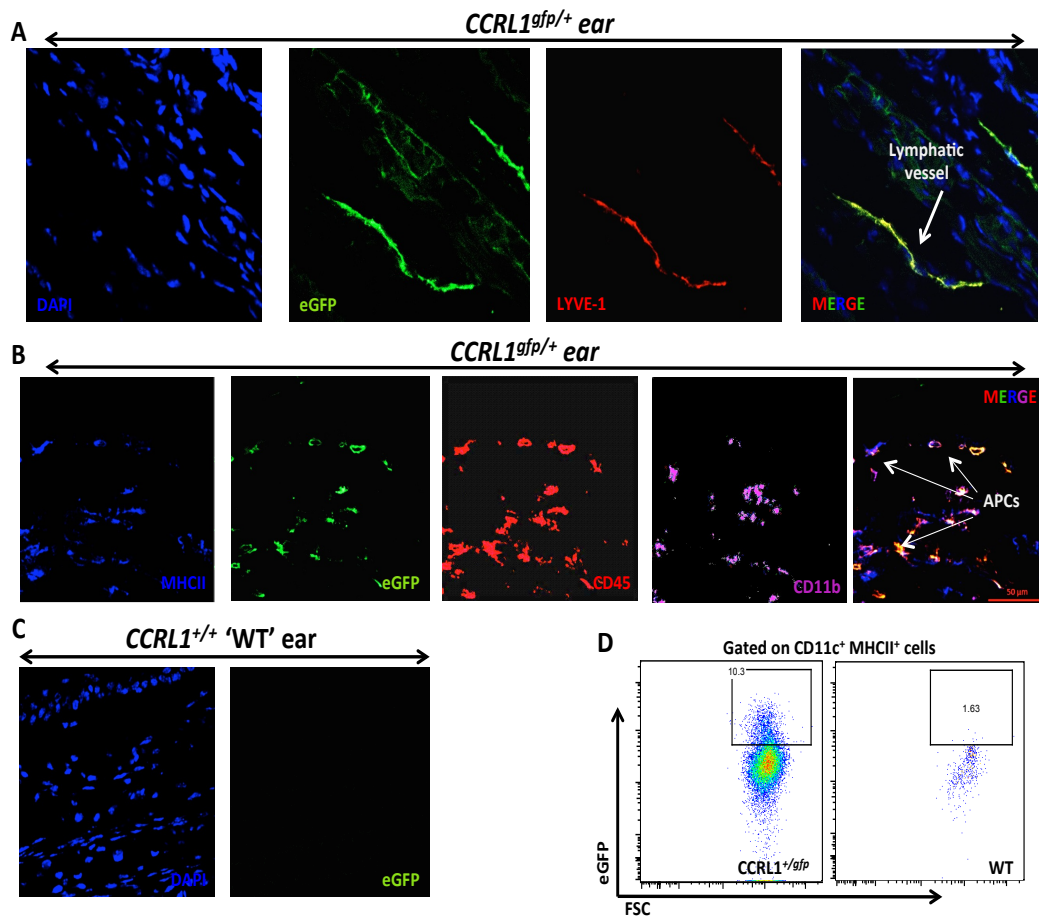


**Figure 3.28: CCRL1-eGFP is expressed on lymphatic vessels and APCs in the ear.**

Ears were harvested from  $CCRL1^{gfp/+}$  and WT mice and placed in 4% PFA for 4 hours. Ears were then washed twice in PBS, placed in OCT compound and frozen on dry ice. 8-10 $\mu$ m sections were then cut using a cryotome and sections stained with DAPI and anti-LYVE1 antibody (A). Sections were also stained for anti-CD11b, anti-MHCII and anti-CD45 antibodies (B). WT sections were used as controls throughout for eGFP expression (C). eGFP<sup>+</sup> cells in the skin were further analysed by flow cytometry by using anti-CD11c and anti-MHCII antibodies (D). WT mice were used as controls to confirm eGFP expression. Serial sections were imaged using a confocal microscope. Images are representative of 7  $CCRL1^{+/gfp}$  and 5 WT mice. Flow cytometry data are representative of 4 mice per genotype.

# Chapter Four

## The Role of CCRL1<sup>+</sup> Cells and CD169<sup>+</sup> Macrophages at the SCS Region of the Lymph Node

## **4 CCRL1 and CD169<sup>+</sup> macrophages at the SCS Region of the Lymph Node**

### **4.1 Introduction**

The experiments described in Chapter 3, explored the affect that deletion of CCRL1 had on the ability of CCR7<sup>+</sup> cells to migrate from one anatomical location to another, both of which were shown to harbour CCRL1-expressing cells. These experiments demonstrated that deletion of CCRL1 results in loss of CCL19 regulation that leads to defective migration of DCs out of the skin, culminating in fewer skin DCs arriving at the draining inguinal lymph nodes. Cells such as T cells and DCs also require CCR7 for intranodal migration and positioning. It has been shown here (Chapter 3), and by others, that CCRL1 expression in the lymph node is restricted to the SCS region. Therefore, in the next set of experiments, the focus shifted to investigating the role of CCRL1 in regulating the abundance and positioning of cells within the lymph node itself. The main focus was on cells known to be located near or adjacent to, CCRL1<sup>+</sup> cells in the lymph node. In particular, these experiments investigated the effect that deletion of CCRL1 had on LECs and innate-like leukocytes found in SCS and interfollicular regions, respectively. In addition, CD169<sup>+</sup> macrophages were studied in WT and CCRL1-deficient lymphoid tissues. These cells are positioned on the floor of the SCS where they are intimately associated with LECs<sup>85,86,151,158</sup>. The functional significance of this close physical interaction was also explored.

### **4.2 The Localisation of CD169 Macrophages in WT Inguinal Lymph Nodes**

First, the positioning of CD169<sup>+</sup> macrophages in the lymph node was investigated. In order to optimise staining techniques, the positioning of these cells in the inguinal lymph nodes was examined relative to LYVE-1<sup>+</sup> cells (predominantly LECs), MHCII<sup>+</sup> APCs and B220<sup>+</sup> B cells. As expected, this showed that CD169<sup>+</sup> macrophages are positioned on, or adjacent to the floor of

the SCS above B cell follicles and interfollicular regions of the lymph node (Figure 4.1). Some macrophages were also observed within the interfollicular areas at a distance from the SCS; and occasionally found within the B cell follicles themselves. Other sinuses deeper in the lymph node were also populated with CD169<sup>+</sup> macrophages. Throughout the lymph node, the large majority of CD169<sup>+</sup> macrophages were found amongst, or adjacent to, LYVE-1<sup>+</sup> LECs.

### **4.3 CCRL1 is Expressed Adjacent to CD169<sup>+</sup> Macrophages**

I previously demonstrated that CCRL1 is expression at the SCS region of the lymph node<sup>360</sup>. Furthermore, a post-doc in our lab has shown that ~60% of LECs in the inguinal lymph nodes of CCRL1<sup>gfp/+</sup> mice express CCRL1. Also located at this region, is a population of CD169<sup>+</sup> macrophages that extend processes into the SCS itself but remain anchored on the floor of the SCS by their “tails”. As such, these macrophages lie on or adjacent to CCRL1<sup>+</sup> cells. To confirm that CCRL1 is not expressed by CD169<sup>+</sup> macrophages, WT inguinal lymph nodes were stained with anti-CD169 and anti-CCRL1 antibodies and analysed by immunofluorescence. Whilst CCRL1 expressing cells and CD169 expressing macrophages are positioned at the SCS, there was no obvious co-expression of these markers on the same cell (Figure 4.2). It was apparent that macrophages are positioned underneath CCRL1<sup>+</sup> cells, however to confirm that macrophages do not express CCRL1, functional uptake assays involving CCL19<sup>AF647</sup> were undertaken.

### **4.4 CD169<sup>+</sup> Macrophages Express CCL19 Receptors, Probably CCR7**

As mentioned previously (Section 3.7), detection of CCR7 and CCRL1 by flow cytometry using conventional antibody staining is not sensitive enough to reliably detect CCR7<sup>+</sup> or CCRL1<sup>+</sup> cells. Instead, expression of CCL19 receptors on CD169 macrophages was examined by using fluorescently tagged CCL19, and culturing cells with the chemokine at 37°C. CD169<sup>+</sup> macrophages in inguinal lymph nodes of WT and CCRL1-deficient mice were identified as CD11b<sup>+</sup> CD169<sup>+</sup> cells. In both WT and CCRL1-deficient lymph nodes, there was

a subset of CD11b<sup>+</sup> CD169<sup>+</sup> cells that was capable of internalising CCL19<sup>AF647</sup> (Figure 4.3 A). Uptake of CCL19<sup>AF64</sup> was comparable between WT and CCRL1-deficient macrophages, suggesting that CCRL1 is not expressed by these cells and was in keeping with previous findings (Figure 4.2). The uptake of CCL19<sup>AF647</sup> was reduced after the addition of a 10-fold excess of unlabeled CCL19 competitor (Figure 4.3 B). This was encouraging as macrophages can non-specifically internalise extracellular material, including chemokines, by pinocytosis, thus, the knock-down in CCL19<sup>AF647</sup> uptake demonstrates the reliability and specificity of this assay in detecting CCL19 receptors. The CCL19 receptors expressed by a population of CD169<sup>+</sup> macrophages is in all likelihood, CCR7, as CCRL1 and CCR7 are the only known receptors for CCL19.

In summary, the results presented in these sections show that:

1. CD169<sup>+</sup> macrophages are found associated with LECs at the SCS region and also in deeper lymph node sinuses.
2. CD169<sup>+</sup> macrophages can be found in the interfollicular areas of the lymph node, above B cells follicles and more rarely, within B cell follicles.
3. CCRL1<sup>+</sup> cells are found adjacent to CD169<sup>+</sup> cells as the SCS region of the lymph node, and macrophages form close contacts with CCRL1<sup>+</sup> cells.
4. Macrophages lack expression of CCRL1.
5. CD169<sup>+</sup> macrophages express CCL19 receptors, probably CCR7.

#### **4.5 CD169<sup>+</sup> Macrophage Distribution and Number in Inguinal Lymph Nodes is Unaffected by CCRL1 Deficiency**

As CD169<sup>+</sup> macrophages are situated within the area of the lymph node known to express CCRL1 (the SCS), the positioning and numbers of CD169 macrophages was compared in WT and CCRL1-deficient inguinal lymph nodes. There was however, no gross defect in the positioning of CD169<sup>+</sup> macrophages in CCRL1-deficient lymph nodes (Figure 4.4 A-B). Similarly, when these cells were enumerated it was found that their abundance in WT and CCRL1-deficient mice was comparable (Figure 4.4 C). Therefore, the absence of CCRL1 in the

inguinal lymph node does not result in aberrant CD169<sup>+</sup> macrophage positioning or abundance at rest.

#### **4.6 Expansion of CD169<sup>+</sup> Macrophages and LYVE-1<sup>+</sup> Cells in Mesenteric Lymph Nodes of CCRL1-deficient Mice**

Next, CD169<sup>+</sup> macrophages were studied in the mesenteric lymph nodes of WT and CCRL1-deficient mice. Mesenteric lymph nodes lie downstream of the small intestine, so they are likely to be in a more constant state of immune activity. Moreover, the small intestine is a dominant site of CCL25 expression which may conceivably be dysregulated in CCRL1-deficient mice. Thus, I reasoned that this unique environment might be particularly susceptible to regulation by CCRL1.

First, the positioning of CD169<sup>+</sup> macrophages in the mesenteric lymph nodes of WT and CCRL1-deficient mice was investigated by immunofluorescent staining (Figure 4.5 A-B). Strikingly, in the mesenteric lymph nodes of CCRL1-deficient mice, CD169<sup>+</sup> macrophages were mislocalised and appeared more abundant (Figure 4.5 B). By using confocal microscopy along with tiling software, I was able to generate whole images of WT and CCRL1-deficient mesenteric lymph nodes (appendix). From these images, ImageJ software was used to enumerate the percentage of the total lymph node section occupied by CD169<sup>+</sup> macrophages. Compared with WT mice, a far greater proportion of CCRL1-deficient mesenteric lymph nodes were occupied by CD169<sup>+</sup> cells (Figure 4.5 C). Immunofluorescent analysis of mesenteric lymph nodes also included a LYVE-1 antibody to quantify the area occupied by LECs. As described in the Introduction, macrophages can support the expansion of lymphatic vessels by various means, particularly during inflammation. Therefore, LYVE-1 antibody staining was included to investigate whether macrophage expansion correlates with an expansion in LYVE-1<sup>+</sup> cells. To this end, it was found that the expansion in CD169<sup>+</sup> macrophages coincided with an increase in LYVE-1<sup>+</sup> cells in the mesenteric lymph nodes of CCRL1-deficient mice. As such, the area of the lymph node occupied by LYVE-1<sup>+</sup> cells was greater in CCRL1-deficient mice than in WT animals (Figure 4.5 D).

Flow cytometry was then used to examine if mesenteric lymph nodes of CCRL1-deficient mice had increased numbers of CD169<sup>+</sup> macrophages. At the time of conducting these experiments it was conventional to identify CD169<sup>+</sup> macrophages as CD11b<sup>+</sup> CD169<sup>+</sup> cells as described previously for inguinal lymph nodes. However, an article published at this time described a more precise method for detecting these cells by flow cytometry<sup>369</sup>. In this publication, it was reported that T cells acquire membrane blebs from CD169<sup>+</sup> macrophages during the preparation of single cell suspensions for flow cytometry. T cells can therefore masquerade as CD169<sup>+</sup> macrophages making it difficult to differentiate between the two cell populations in post-acquisition analysis. Therefore, it is necessary to include T cell markers in the staining panel in order to exclude T cells from the analysis of CD169 macrophages. Using this approach, the total number of CD169<sup>+</sup> macrophages in the mesenteric lymph nodes of WT and CCRL1-deficient mice was enumerated after exclusion of contaminating T cells (Figure 4.6 A). This revealed a statistically significant increase in the number of macrophages present in the mesenteric lymph nodes of CCRL1-deficient mice compared with WT animals (Figure 4.6 B) and supports the conclusions made from immunofluorescent analysis of mesenteric lymph nodes.

In summary, the data show that:

- 1) CD169<sup>+</sup> macrophages are mislocalised in the mesenteric lymph nodes of CCRL1-deficient mice.
- 2) The abundance of CD169<sup>+</sup> macrophages is increased in the mesenteric lymph nodes of CCRL1-deficient mice.
- 3) CD169<sup>+</sup> macrophage mislocalisation and expansion coincides with an expansion of LYVE-1<sup>+</sup> cells in the mesenteric lymph nodes.

#### **4.7 CCL19 Receptor Expression on CD169<sup>+</sup> Macrophages Revisited**

Previously, CCL19 receptor expression on CD169<sup>+</sup> macrophages isolated from inguinal lymph nodes was shown. However, as discussed, the correct identification of these macrophages requires the exclusion of T cells when

analysing results from flow cytometry. Therefore, to attempt to validate CCR7 expression by CD169<sup>+</sup> macrophages from mesenteric lymph nodes, CCL19<sup>AF647</sup> uptake by macrophages in the mesenteric lymph node was analysed after T cell exclusion. As T cells express high levels of CCR7 it was important to confirm that previous characterisation of CD169 macrophages as having functional CCL19 receptors was not a result of contamination by T cells. To this end, TcRβ<sup>+</sup> cells were excluded before CD11b<sup>+</sup> CD169<sup>+</sup> cells were identified by flow cytometry (Figure 4.7 A). MHCII<sup>+</sup> CCL19<sup>+</sup> cells in the macrophage gates were then identified amongst samples containing CCL19<sup>AF647</sup> alone and competition samples containing CCL19<sup>AF647</sup> + 10-fold excess of unlabeled CCL19 competitor (Figure 4.7 B-C). In contrast to previous findings, only a small level of CCL19 uptake by CD169<sup>+</sup> macrophages was found (Figure 4.7 B). Although samples containing unlabeled CCL19 had slightly less CCL19<sup>AF647</sup> uptake, results from this experiment would suggest that CD169<sup>+</sup> macrophages isolated from mesenteric lymph nodes have little, if any, CCL19 receptor expression. To confirm the sensitivity and specificity of the assay, CCL19<sup>AF647</sup> uptake by TcRβ<sup>+</sup> T cells in the samples was also analysed. As expected, T cells showed a high level of CCL19<sup>AF647</sup> uptake that was reduced when a 10-fold excess of unlabeled CCL19 was added (Figure 4.7 D) consistent with CCR7 expression by these cells. At the same time, mesenteric lymph node cells were analysed for CCR9 expression using conventional antibody staining. CD169 macrophages were identified after exclusion of contaminating T cells and were found to lack expression of CCR9 (Figure 4.7 E).

These data show that CD169<sup>+</sup> macrophages do not express CCR9 or CCL19 receptors. These observations emphasise the importance of the findings by Gray *et al* with regards to the correct identification of CD169 macrophages by flow cytometry<sup>369</sup>. These data also suggest that it is unlikely that the macrophage/LEC expansion seen in CCRL1-deficient mice is driven by excess chemokines activating CCR7 or CCR9 on the macrophages.

## 4.8 Characterisation of NK, iNKT and $\gamma\delta$ T cells in Mesenteric Lymph Nodes

As CD169<sup>+</sup> macrophages were dramatically affected by loss of CCRL1 in the mesenteric lymph node, I moved on to characterising populations of innate-like cells positioned close to the SCS within the interfollicular areas. Specifically, I was interested in cells known to interact with CD169<sup>+</sup> macrophages, namely, T cells,  $\gamma\delta$  T cells, iNKT cells and NK cells.

First, I was interested in enumerating conventional T cells and  $\gamma\delta$  T cells. Single cell suspensions of mesenteric lymph nodes were stained with antibodies against CD3, TcR $\beta$  and TcR $\gamma\delta$  (Figure 4.8 A). In agreement with work from others in the lab, there was no difference in the absolute number of TcR $\beta$ <sup>+</sup> CD3<sup>+</sup> T cells in the mesenteric lymph nodes of CCRL1-deficient mice compared with WT counterparts (Figure 4.8 B). However, when the total number of  $\gamma\delta$  T cells (TcR $\beta$ <sup>-</sup> TcR $\gamma\delta$ <sup>+</sup>) was enumerated (Figure 4.8 C), I found that they were significantly reduced in the mesenteric lymph nodes of CCRL1-deficient mice (Figure 4.8 D). The small intestine contains a large population of intra-epithelial  $\gamma\delta$  T cells and this phenotype may represent defective migration and/or entry of these cells into the mesenteric lymph node.

Next, the number of NK cells in the mesenteric lymph nodes was calculated. NK cells were identified by flow cytometry by their lack of CD3 and TcR $\beta$  expression and their expression of NK1.1 (Figure 4.10 A). Furthermore, NK cells could be divided into subsets based on expression of CCR6 and DX5 (Figure 4.10 A). Calculation of the total number of CCR6<sup>+</sup> DX5<sup>-</sup> NK cells and CCR6<sup>-</sup> DX5<sup>+</sup> NK cells revealed a small, but statistically significant reduction in the CCR6<sup>-</sup> DX5<sup>+</sup> population of cells in CCRL1-deficient mesenteric lymph nodes (Figure 4.10 B-C). However the other NK cell subsets identified in the mesenteric lymph node were of comparable abundance between WT and CCRL1-deficient mice (Figure 4.10 B).

To conclude the analysis of resting mesenteric lymph nodes, iNKT cells were enumerated. iNKT cells were identified as CD3<sup>+</sup> NK1.1<sup>+</sup> and within this population, four subsets of cells were identified based upon DX5 and CCR6 expression (Figure 4.10 A). There was a statistically significant reduction in the CCR6<sup>-</sup> DX5<sup>+</sup> iNKT cell population in CCRL1-deficient mice, however the other three iNKT cell populations were comparable between WT and CCRL1-deficient mice (Figure 4.10 B-E).

Thus, despite the evident expansion of LECs and CD169<sup>+</sup> macrophages, resting CCRL1-deficient mesenteric lymph nodes contain WT levels of TcRβ<sup>+</sup> T cells and only a small reduction in the size of the γδ T cell, NK1.1<sup>+</sup> CCR6<sup>-</sup> DX5<sup>+</sup> NK and CCR6<sup>-</sup> DX5<sup>+</sup> iNKT cell populations.

#### **4.9 Characterisation of NK, iNKT and γδT cells in the Inguinal Lymph Node**

Numbers of innate-like cells residing within the interfollicular regions of mesenteric lymph nodes from CCRL1-deficient mice was affected by loss of CCRL1 such that their numbers were significantly reduced compared to WT mice. Although it was previously shown that loss of CCRL1 in the inguinal lymph node did not affect numbers or distribution of CD169<sup>+</sup> macrophages, further investigation into innate-like cell numbers was undertaken.

Next, to investigate whether changes in innate-like cell numbers in the mesenteric lymph node was related to changes in macrophages/LECs, similar flow cytometry analysis was undertaken on inguinal lymph nodes (where macrophages and LECs are normal in CCRL1-deficient mice). First, CD3<sup>+</sup> TcRβ<sup>+</sup> conventional T cells were enumerated (Figure 4.11 A) with no differences found in the abundance between WT and CCRL1-deficient mice (Figure 4.11 B). Next, non-conventional T cells, specifically γδ T cells (TcRβ<sup>-</sup> TcRγδ<sup>+</sup>) and iNKT cells (CD3<sup>+</sup> NK1.1<sup>+</sup>) were investigated. (Figure 4.11 C and Figure 4.12 A). The absolute number of γδ T cells in the inguinal lymph nodes of CCRL1-deficient mice showed a statistically significant reduction at rest (Figure 4.11 D). This was similar to that seen in the mesenteric lymph node. Four populations of iNKT cells could be identified in the inguinal lymph nodes as in the previous

experiments with mesenteric lymph nodes (Figure 4.12 A). All iNKT cell subsets displayed a statistically significant reduction in the absence of CCRL1, except the CCR6<sup>-</sup> DX5<sup>-</sup> surface immunphenotype (Figure 4.12 B-E). Therefore, both innate-like T cell populations studied;  $\gamma\delta$  T cells and iNKT cells were reduced in the inguinal lymph nodes of CCRL1-deficient mice. Of the two populations of NK cells separated based on expression of CCR6 and DX5 (Figure 4.13 A), only the CD3<sup>-</sup> NK1.1<sup>+</sup> CCR6<sup>-</sup> NK cells were significantly reduced in CCRL1-deficient lymph nodes (Figure 4.13 B-C).

In conclusion, populations of NK cells,  $\gamma\delta$  T cells and iNKT cells are reduced in the inguinal lymph nodes of CCRL1-deficient mice at rest. This would suggest that changes in the abundance of innate-like cells in the lymph node are not linked to changes in the distribution and abundance of CD169<sup>+</sup> macrophages and LYVE-1<sup>+</sup> LECs. Innate-like cells may instead be more directly influenced by loss of CCRL1-mediated chemokine scavenging from LECs in lymph nodes. These possibilities are discussed in more depth in the Discussion (Chapter 6).

#### **4.10 CCRL1 Expression and Function in the Resting Spleen**

Alongside lymph node studies, I was also interested in examining if CCRL1 is expressed in other secondary lymphoid tissues. The spleen is a unique secondary lymphoid organ that performs an important function in filtering the blood and supporting B cell responses<sup>163</sup>. It is anatomically and functionally distinct from lymph nodes, particularly regarding the route of antigen delivery. In contrast to lymph nodes, the spleen is devoid of lymphatic vessels and antigen is transported to the spleen via blood that passes through the marginal sinus. The marginal zone is home to a variety of leukocyte subsets and importantly, contains a population of CD169<sup>+</sup> macrophages that are related to CD169<sup>+</sup> macrophages found in, and around, lymph node sinuses<sup>75,76,370-372</sup>. Thus, even though the spleen lacks the cells that express CCRL1 in lymph nodes (LECs), the anatomical and cellular similarities between lymph nodes and splenic white pulp lead us to consider whether other cells expressed CCRL1 in the spleen. Moreover, the positioning and number of CD169<sup>+</sup> macrophages in the spleen was of interest, particularly due to the observations made previously in mesenteric lymph nodes. At the same

time, the innate-like cells known to be affected by CCRL1 deficiency in lymph nodes were investigated in the spleens of WT and CCRL1-deficient mice.

Interestingly, analysis of frozen sections from WT mice by immunofluorescent staining revealed strong expression of CCRL1 by cells lining splenic venules situated in the red pulp region adjacent to regions of white pulp (Figure 4.14 A-B). Anti-CCRL1 staining was particularly strong in the endothelial cells lining venules located just outside the marginal zone. In many respects, this is anatomically similar to the expression of CCRL1 seen round the edges of lymph nodes. The expression of CCRL1 within this region does not directly co-localise with CD169<sup>+</sup> macrophages or SIGNR1<sup>+</sup> macrophages, although, as in the lymph nodes, these macrophages are found in close proximity to CCRL1 expressing cells. Weak staining with anti-CCRL1 antibody was found in cells present in the white pulp, however, their identity was not investigated further. Very little staining with anti-CCRL1 antibody was seen on frozen spleen sections from CCRL1-deficient mice showing the antibody to be specific (Figure 4.14 C). Unlike in the mesenteric lymph node, the positioning of CD169<sup>+</sup> macrophages appears normal in the spleen of CCRL1-deficient mice and these cells are localised in ring like structures in both WT and CCRL1-deficient mice (Figure 4.14 A-C). This was also the case for SIGNR1<sup>+</sup> marginal zone macrophages (Figure 4.14 A-C). Although the positioning of CD169<sup>+</sup> macrophages appeared normal in the spleens of CCRL1-deficient mice (Figure 4.14 A-C), their abundance in this organ was also investigated. Analysis by flow cytometry revealed that a higher percentage of cells in the spleens of CCRL1-deficient mice were CD169<sup>+</sup> macrophages (Figure 4.16 A-B). Therefore, as in the mesenteric lymph nodes, deletion of CCRL1 appears to affect CD169<sup>+</sup> macrophages abundance in the spleen.

Next, cells known to express CCR7 were quantified in WT and CCRL1-deficient spleens. No difference in the abundance of conventional TcRβ<sup>+</sup> T cells was found between WT and CCRL1-deficient spleens (Figure 4.17 A). Furthermore, when separated into CD4<sup>+</sup> (Figure 4.17 B) and CD8<sup>+</sup> (Figure 4.17 D) T cells there was no difference in the abundance of either T cell population between mouse strains (Figure 4.17 C and E). The same was true for B cells (Figure 4.17

F-G) and DCs (Figure 4.18 A-B). Therefore, the major CCR7<sup>+</sup> cells in the spleen appear unaffected by loss of CCRL1.

Next, the abundance of  $\gamma\delta$  T cells, NK cells and iNKT in WT and CCRL1-deficient spleens was investigated, cells that have previously been shown to be affected by deletion of CCRL1 in the lymph node. NK cells were identified by flow cytometry as NK1.1<sup>+</sup> TcR $\beta$ <sup>-</sup> (Figure 4.19 A). Although there was a trend towards a reduction in the percentage of these cells in CCRL1-deficient mice, this difference did not reach statistical significance (Figure 4.19 B). The same was true of  $\gamma\delta$  T cells (Figure 4.19 C-D) and iNKT cells (Figure 4.19 E-F).

With such high expression of CCRL1 at the gateway to the white pulp, it was hypothesised that CCRL1 may function to control the kinetics of entry and/or positioning of CCR7<sup>+</sup> leukocytes in the spleen. To test this,  $5 \times 10^6$  CMTPX labeled splenocytes from WT mice were injected intravenously into WT and CCRL1-deficient mice. 1 or 2 hours after injection, spleens were harvested and the positioning of adoptively transferred splenocytes was assessed by fluorescent microscopy. After 1 hour, there were few labeled splenocytes in B cell areas of the spleens of WT and CCRL1-deficient mice. In both WT and CCRL1-deficient spleens, adoptively transferred splenocytes were found in non-white pulp regions of the lymph node juxtaposed to B cells (Figure 4.15 A-B). However, at 2 hours, the white pulp of the spleens in WT and CCRL1-deficient mice contained labeled splenocytes. These cells localised in B cell areas of the white pulp and to non-B cell areas of the white pulp, which we can infer are T cell areas (Figure 4.15 C-D). However, as at the 1 hour time point, no gross differences in the localization of the transferred splenocytes was found between strains. Therefore, although these experiments were not developed further, they suggest that deletion of CCRL1 has no substantial affect on the positioning of adoptively transferred splenocytes in the spleen during the first few hours after transfer.

Collectively, these data show that CCRL1 is specifically expressed by endothelial cells lining venules in the red pulp of the spleen. CCRL1 deficiency does not affect the frequency of DCs, T cells or B cells in this tissue, and does not appear to regulate leukocyte recruitment to the spleen. Despite being less abundant in lymph nodes, splenic NK cell,  $\gamma\delta$  T cell and iNKT cell populations

appear unaffected by loss of CCRL1. In contrast, CD169<sup>+</sup> macrophages appear to be more abundant in the spleen of CCRL1-deficient mice than WT mice suggesting that CCRL1 regulates these cells both in both the mesenteric lymph node and the spleen.

#### **4.11 The Role of CD169<sup>+</sup> Macrophages in Regulating Lymphangiogenic Responses in Lymph Nodes**

The data generated in the experiments above stimulated an interest in the functional relationship between LECs and CD169<sup>+</sup> macrophages. These cells are intimately associated in lymph node sinuses, and macrophages are known to play key roles in regulating lymphangiogenic responses during inflammation in a variety of different tissues<sup>148,154,158,373</sup>. Thus, I wondered if lymph node macrophages contributed to the lymphangiogenic response that develops in lymph nodes in response to cutaneous inflammation induced by agents such as CFA. Moreover, the specific expression of CCRL1 by lymph node LECs led me to consider whether this atypical chemokine receptor could also contribute lymph node lymphangiogenesis. To explore these ideas, macrophages were to be specifically depleted in the popliteal lymph nodes by subcutaneous injection of clodronated liposomes into the footpad. Clodronated liposomes act as ‘Trojan horses’ that deliver aqueous clodronate to phagocytic cells. Macrophages ingest these liposomes by phagocytosis and subsequently clodronate is released inside the cell to induce apoptosis. Therefore, this reagent is a useful and widely used tool for the specific depletion of phagocytes. Several days after clodronated liposome injection, mice were to be challenged in the same footpad with CFA to drive the expansion of lymphatic vessels in draining lymph nodes. Popliteal lymph nodes and inguinal lymph nodes would then be analysed by flow cytometry and immunofluorescent staining using anti-LYVE-1 antibody to identify LECs and examine expansion of the lymphatic sinus network of the lymph node.

#### **4.11.1 CD169 Macrophages can be Depleted in the Popliteal Lymph Node by Administration of Clodronated Liposomes Into the Footpad**

First, to test the specificity and effectiveness of the clodronated liposomes for depletion of CD169<sup>+</sup> macrophages in the popliteal lymph node, clodronated liposomes were injected subcutaneously into the footpad of WT mice. One week later, macrophage depletion in popliteal and inguinal lymph nodes was assessed by flow cytometry and immunofluorescence. Encouragingly, it was found that TcRβ<sup>-</sup> CD11b<sup>+</sup> CD169<sup>+</sup> macrophages had virtually disappeared from popliteal lymph nodes after clodronated liposome injection but remained in PBS-injected control mice (Figure 4.20 A-D). CD169<sup>+</sup> macrophages also remained in the inguinal lymph nodes of clodronated liposome-treated animals and in the inguinal lymph nodes of PBS-treated mice (Figure 4.20 E-H), demonstrating that clodronated liposome injection into the footpad was useful for the specific and local depletion of CD169<sup>+</sup> macrophages from popliteal lymph nodes. Fluorescent liposomes containing PE dye instead of clodronate were specifically and only internalised by CD169<sup>+</sup> macrophages in popliteal lymph nodes, demonstrating the unique specificity of liposomes for macrophages in the lymph nodes (Figure 4.21 A-C).

Next, clodronated liposomes were injected into the footpad of WT mice and the presence of CD169<sup>+</sup> macrophages in the popliteal and inguinal lymph nodes assessed by flow cytometry and immunofluorescent staining 2 weeks post clodronate injection. In the inguinal lymph nodes, CD169<sup>+</sup> macrophages could be identified by flow cytometry and immunofluorescent staining (Figure 4.22 A and C). Few, if any, CD169<sup>+</sup> macrophages were found in the popliteal lymph node 2 weeks after clodronated liposome injection (Figure 4.22 B and D). This demonstrated that, in the absence of further challenge, CD169<sup>+</sup> macrophages are not regenerated from bone marrow progenitors entering the lymph node from the blood and differentiating into these cells. This would be in line with the ontogeny of these cells as yolk sac-derived self-renewing cells<sup>374</sup>. Indeed, previous work has shown that CD169<sup>+</sup> macrophages do not completely repopulate the popliteal

lymph node after clodronated liposome injection into the footpad until five months<sup>375</sup>.

#### **4.12 CD169 Macrophages are Required for Lymphatic Vessel Expansion During CFA-induced Inflammation in the Lymph Node.**

Having confirmed that CD169<sup>+</sup> macrophages in the popliteal lymph node are sensitive to depletion with clodronated liposomes and remain absent for at least 2 weeks after their depletion, investigations next focused on to characterising the impact of the depletion of macrophages on lymphangiogenic responses in the lymph node to challenge with CFA in the footpad. WT and CCRL1-deficient mice were injected with clodronated liposomes or PBS into the footpad and left to rest for 1 week, during which macrophages will be depleted from the clodronated liposome-treated group only. Then, mice were challenged in the same footpad with CFA. One week later, popliteal and inguinal lymph nodes were harvested and analysed by immunofluorescent staining to investigate the distribution of CD169<sup>+</sup> macrophages and lymphatic vessels.

As expected, the popliteal and inguinal lymph nodes of WT and CCRL1-deficient mice that had received PBS instead of clodronated liposomes developed a profound lymphatic vessel expression in response to CFA injection and lymphatic sinuses lined with LYVE-1<sup>+</sup> LECs were found throughout the lymph node parenchyma (Figure 4.23 A-B). Lymphatic vessel expansion was also seen in the inguinal lymph nodes of WT and CCRL1-deficient mice that had received clodronated liposomes, and no gross difference was observed between strains (Figure 4.25 A-B). As expected, at the dose of liposomes used, CD169<sup>+</sup> macrophages were not depleted from this lymph node (Figure 4.25 C-D) although again these cells appeared less firmly associated with LYVE-1<sup>+</sup> LECs in CCRL1-deficient mice than in WT counterparts.

In contrast, popliteal lymph nodes of mice that received clodronated liposomes lacked CD169<sup>+</sup> macrophages (data not shown) and appeared to have undergone far less expansion in their lymphatic sinus network (Figure 4.26 A-B) than animals that received PBS in place of the clodronated liposomes (Figure 4.23 C-

D.) In fact, these inflamed lymph nodes contained lymphatic sinus networks that were broadly similar to those seen in naïve lymph nodes (data not shown). As before, this apparent reduction in lymphangiogenesis appeared to be unaffected by CCRL1 deficiency.

Thus, although further work is required, these preliminary experiments indicate that depletion of lymph node macrophages can suppress inflammation-induced lymphangiogenesis in lymph nodes.

### 4.13 Summary

In this chapter I have shown that:

1. CD169<sup>+</sup> macrophages in the mesenteric lymph nodes of CCRL1-deficient mice are increased in abundance compared with WT counterparts and occupy more of the total lymph node area.
2. LYVE-1<sup>+</sup> cells are expanded in the mesenteric lymph nodes of CCRL1-deficient mice and occupy a greater volume of the total lymph node compared with WT mice.
3. In the mesenteric and inguinal lymph nodes, deletion of CCRL1 results in a small decrease in the size of the  $\gamma\delta$  T cell population, and reductions in the abundance of NK and iNKT cell subsets in the mesenteric lymph node.
4. CCRL1 is expressed by endothelial cells lining splenic venules in the red pulp, but deletion of the receptor does not affect the early trafficking of CCR7<sup>+</sup> cells into and within this organ
5. Deletion of CCRL1 results in a steady state increase in the abundance of CD169<sup>+</sup> macrophages in the spleen.
6. CD169<sup>+</sup> macrophages appear to be involved in lymphatic vessel expansion in the lymph node during CFA-induced inflammation.

These results will be discussed further in the Discussion (Chapter 6) and placed in the context of existing literature in this area.

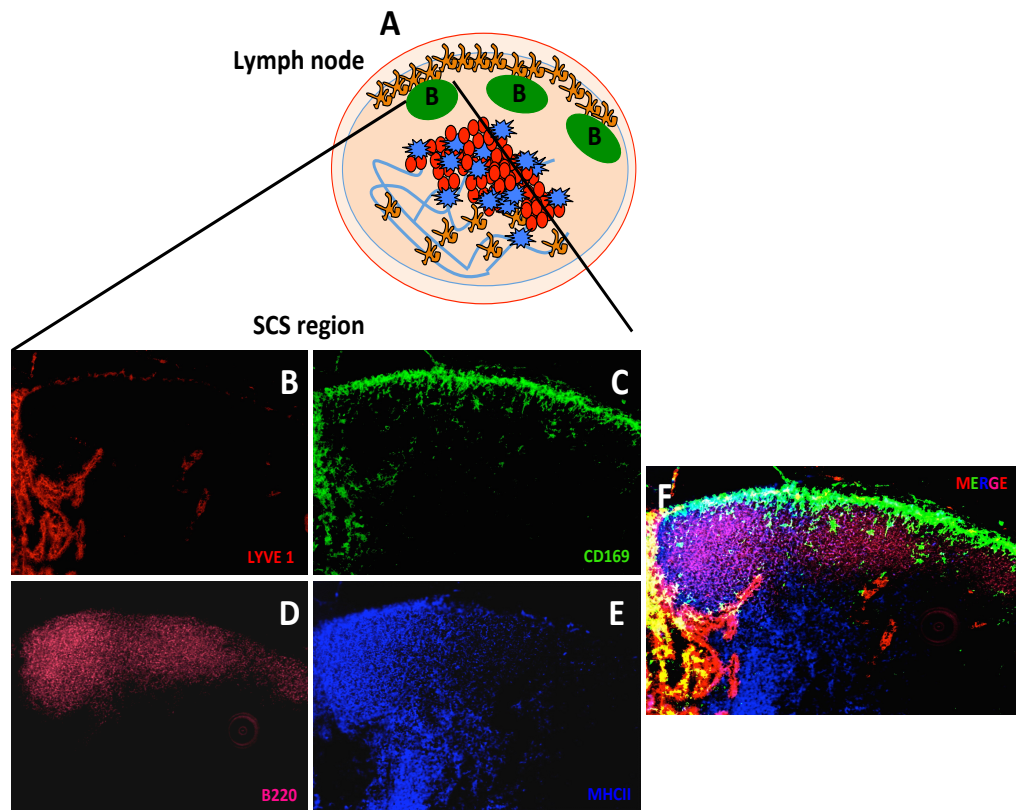


**Figure 4.1: CD169<sup>+</sup> macrophages are situated in the SCS region of the lymph.**

Naïve inguinal lymph nodes from WT mice were harvested, placed in OCT and frozen on dry ice. 8-10µm frozen sections were cut and sections were then stained with anti-CD169, anti-LYVE-1, anti-MHCII and anti-B220 antibodies to reveal the distribution of CD169<sup>+</sup> macrophages, LYVE-1<sup>+</sup> LECs, APCs and B cells respectively in WT lymph nodes. (A) Lymph node diagram indicating the region of the lymph node shown by immunofluorescent staining in (B-F). Individual images with each antibody stain are shown (B-E) and also as a merged image (F). Images are representative of lymph nodes from 10 mice.

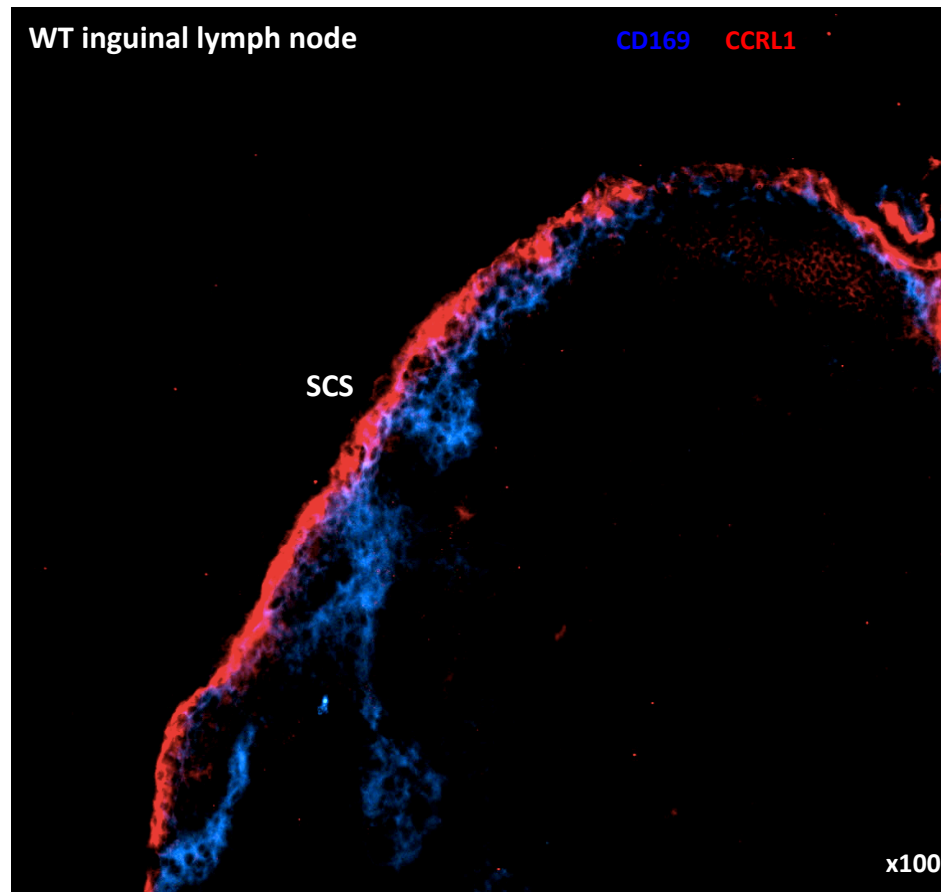


**Figure 4.2: CCRL1 is not expressed by CD169<sup>+</sup> SCS macrophages.**

WT inguinal lymph nodes were harvested, placed in OCT, frozen on dry ice and then 8-10 $\mu$ m sections cut. Sections were stained with anti-CCRL1 (red) and anti-CD169 (blue) antibodies then imaged using a fluorescent Zeiss Axio Imager microscope. Images are representative of 4 mice.

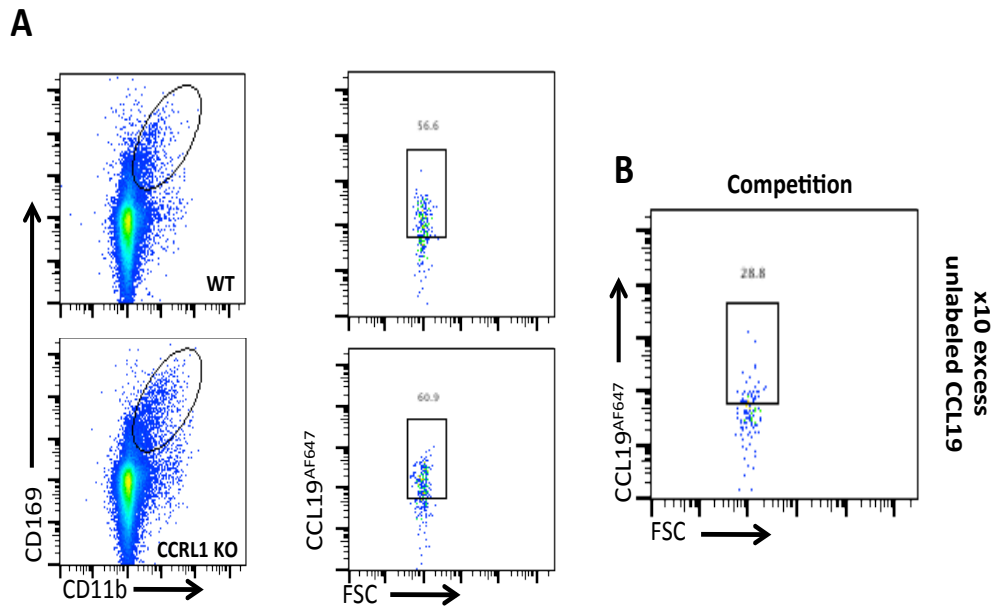


**Figure 4.3: CD169<sup>+</sup> macrophages express CCL19 receptors.**

Single cell suspensions were prepared from resting inguinal lymph nodes harvested from WT and CCRL1-deficient mice. Cells were incubated with CCL19<sup>AF647</sup> at 37°C in order to identify active CCL19 receptors. At the same time, cells were incubated at 37°C with a 10 molar excess of unlabelled CCL19 competitor to compete for fluorescent CCL19<sup>AF647</sup> uptake and are shown above as “competition”. Cells were stained with anti-CD169 and anti-CD11b antibodies to identify macrophages and then analysed by flow cytometry. Data are representative of 1 from 2 independent experiments with at least 3 mice per experiment.

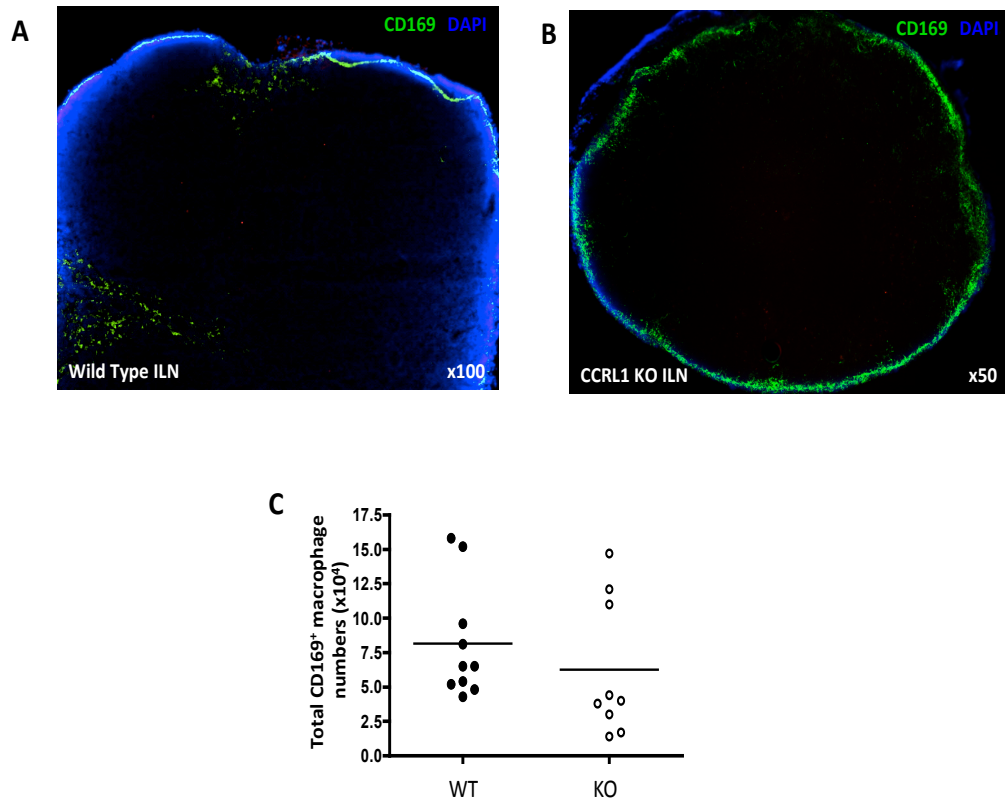


**Figure 4.4: CD169<sup>+</sup> macrophage distribution and abundance is normal in the inguinal lymph nodes of CCRL1-deficient mice.**

Naïve inguinal lymph nodes from WT and CCRL1-deficient mice were harvested, placed in OCT and frozen on dry ice. 8-10 $\mu$ m frozen sections were then cut using a cryotome. Sections were stained with DAPI and anti-CD169 antibody to reveal the distribution of CD169<sup>+</sup> macrophages in WT (A) and CCRL1-deficient (B) inguinal lymph nodes. The total number of CD11b<sup>+</sup> CD169<sup>+</sup> macrophages was calculated in WT and CCRL1-deficient inguinal lymph nodes after analysis by flow cytometry (C). Images are representative of at least 4 mice per genotype. Flow cytometry analysis was undertaken on 10 WT and 9 CCRL1-deficient mice, and data show the mean (horizontal lines) for each genotype. Statistical analysis was undertaken using an unpaired Student's t-test with no statistical significance found between genotypes.

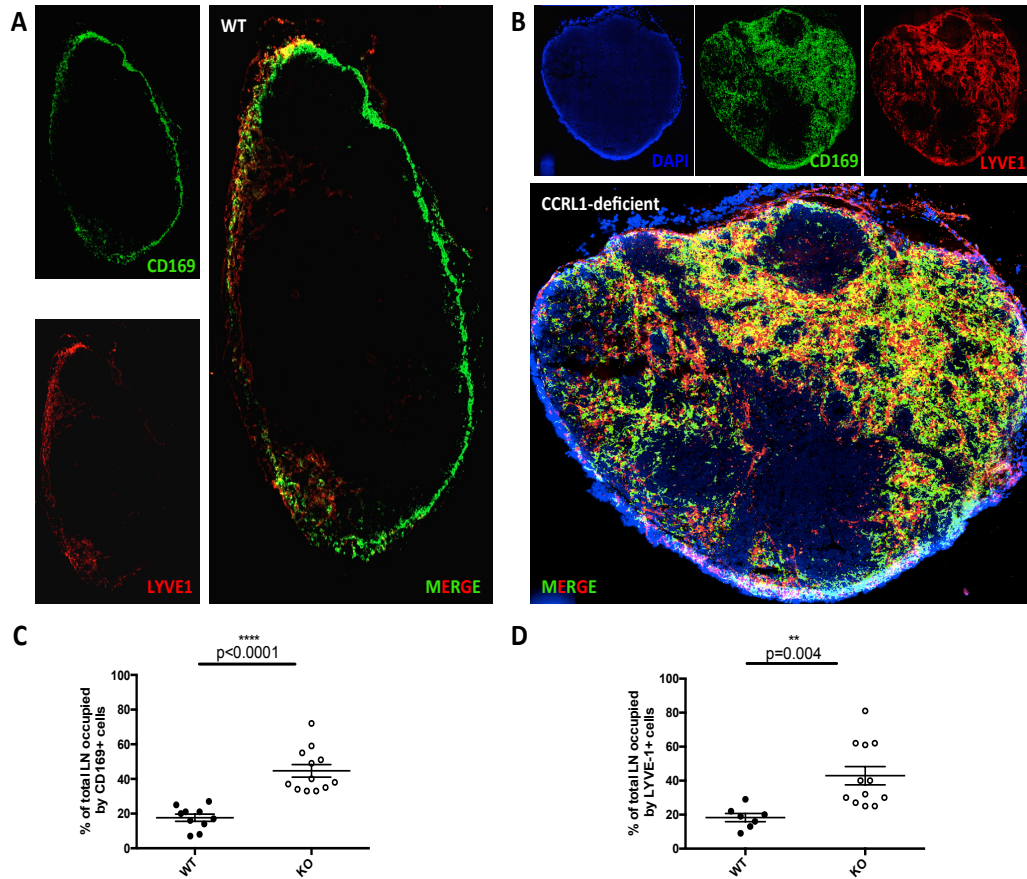


**Figure 4.5: Deletion of CCRL1 leads to an expansion of CD169<sup>+</sup> macrophages and LYVE-1<sup>+</sup> lymphatic vessels in the mesenteric lymph node.**

Mesenteric lymph nodes from resting WT and CCRL1-deficient mice were harvested into OCT and frozen on dry ice. 8-10 $\mu$ m sections were then cut and stained with DAPI, anti-CD169, and anti-LYVE-1 antibodies. Sections were then imaged using a fluorescent Zeiss confocal microscope. Single coloured images are shown for each antibody stain along with merged images of all antibody stains (A-B). Lymph nodes were analysed using ImageJ software to calculate the proportion of the total lymph node occupied by CD169<sup>+</sup> cells (C) and LYVE-1<sup>+</sup> cells (D). Each individual lymph node analysed for CD169 and LYVE-1 distribution is shown in appendix. Data are represented as the mean (horizontal lines)  $\pm$ SEM amongst individual data points (circles). Statistical analysis was undertaken using an unpaired Student's t-test with  $p < 0.001$ \*\*\* and  $p < 0.01$ \*\* . Data are representative of at least 7 mice per genotype.

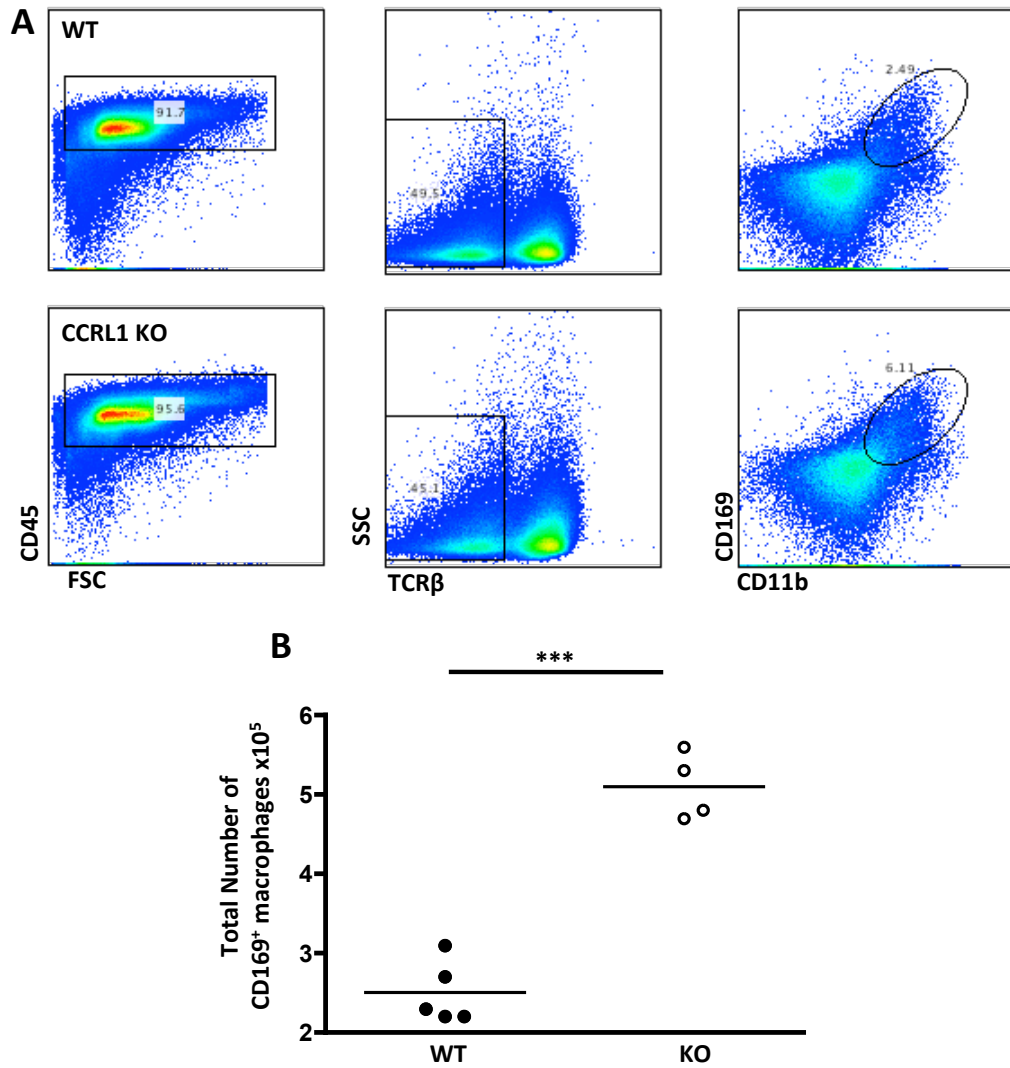


**Figure 4.6: CCRL1 deficiency is associated with an increase in CD169<sup>+</sup> macrophage abundance in the mesenteric lymph node.**

Single cell suspensions were prepared from resting mesenteric lymph nodes harvested from WT and CCRL1-deficient mice. Cells were stained with anti-CD45, anti-TcR $\beta$ , anti-CD11b and anti-CD169 antibodies and then analysed by flow cytometry (A). After identification of SSC macrophages, the total number of these cells was then calculated (B). Data represent the mean (horizontal lines) amongst individual data points (circles) and are from n=5 WT and n=4 CCRL1-deficient mice. Statistical analysis was performed using unpaired Student's t-test with  $p < 0.001$ \*\*\*.

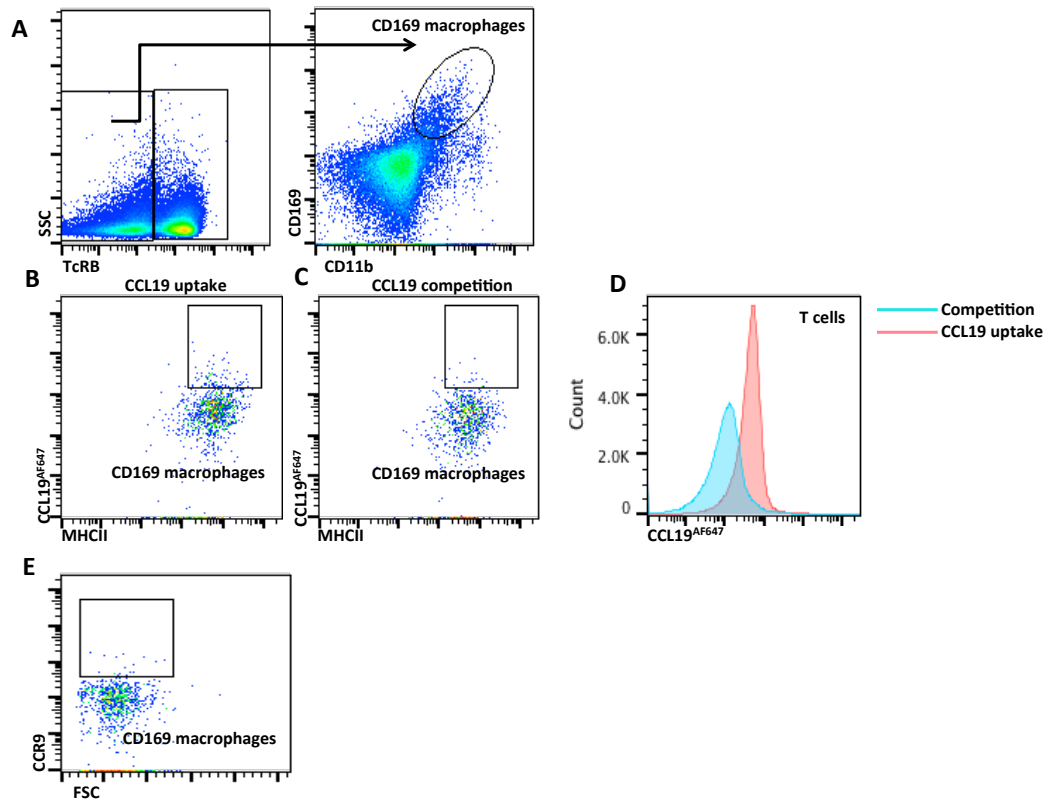


**Figure 4.7: CD169<sup>+</sup> macrophages do not express CCL19 receptors or CCR9.**

Lymph node single cell suspensions were prepared from resting mesenteric lymph nodes harvested from WT mice. Cells were stained with anti-CD11b, anti-CD169 and anti-TcR $\beta$  antibodies to identify SCS macrophages and then analysed by flow cytometry (A). Cells were incubated with CCL19<sup>AF647</sup> at 37°C in order to identify active CCL19 receptors (B). At the same time, cells were incubated with 10 molar excess of unlabelled CCL19 competitor to compete for fluorescent CCL19<sup>AF647</sup> uptake and are shown above as “CCL19 competition” (C). Control samples were included to look for uptake of CCL19<sup>AF647</sup> with and without competition on CCR7<sup>+</sup> T cells to assess the sensitivity and specificity of the assay (D). CCR9 expression was also assessed on CD169 macrophages by using conventional antibody staining and analysis by flow cytometry (E). Data are from 1 experiment with 5 WT mice.

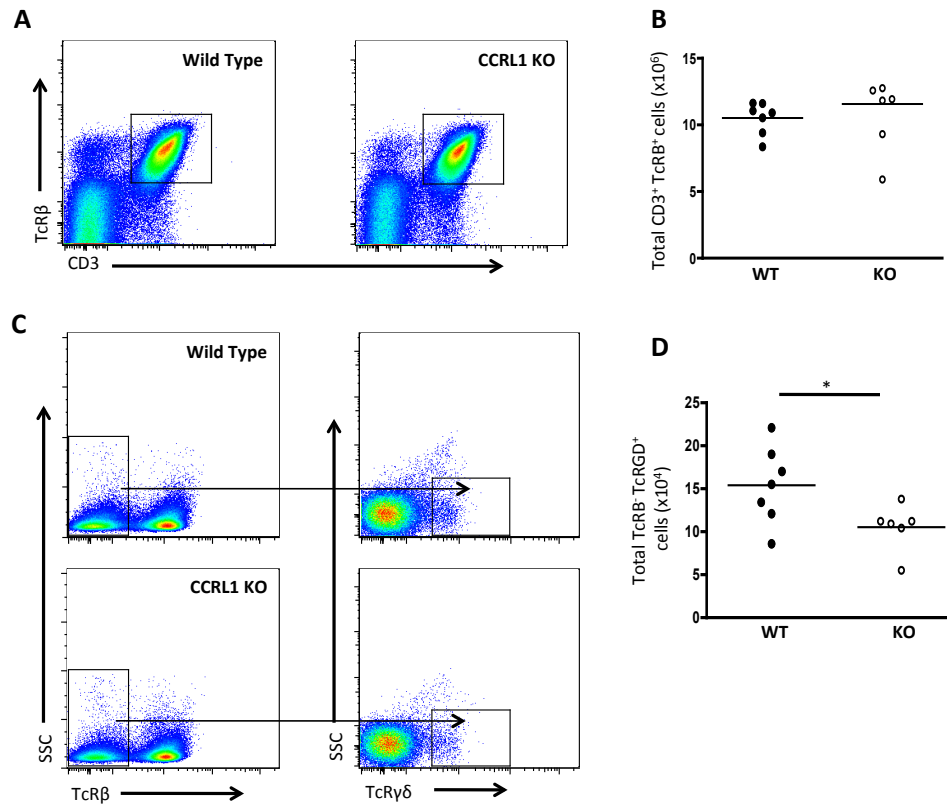


**Figure 4.8: Deletion of CCRL1 results in fewer  $\gamma\delta$  T cells in the mesenteric lymph node.**

Single cell suspensions were prepared from resting WT and CCRL1-deficient mesenteric lymph nodes. Cells were stained with anti-TcR $\beta$ <sup>+</sup> anti-CD3 and anti-TcR $\gamma\delta$  antibodies and analysed by flow cytometry (A and C). The total number of TcR $\beta$ <sup>+</sup> CD3<sup>+</sup> conventional T cells and TcR $\beta$ <sup>+</sup> TcR $\gamma\delta$ <sup>+</sup>  $\gamma\delta$  T cells were then enumerated (B and D). Data represent the mean (horizontal lines) amongst individual data points (circles) and are from 1 experiment with 7 WT mice and 6 CCRL1-deficient mice. Statistical analysis was performed using unpaired Student's t-test with

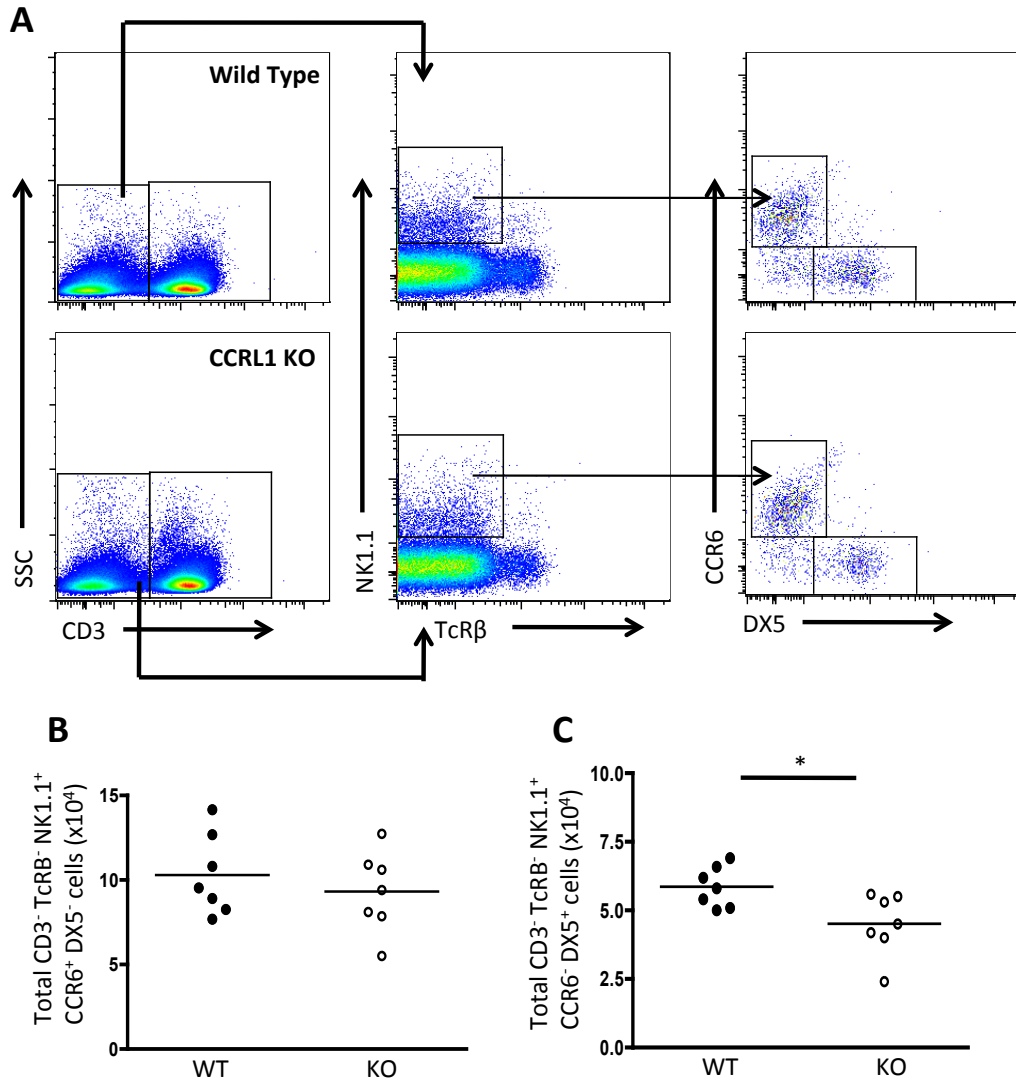


**Figure 4.9: Deletion of CCRL1 leads to a reduction in NK1.1<sup>+</sup> CCR6<sup>+</sup> DX5<sup>+</sup> NK cells in the mesenteric lymph node.** Single cell suspensions were prepared from resting WT and CCRL1-deficient mesenteric lymph nodes. Cells were stained with anti-CD3, anti-NK1.1, anti TcR $\beta$ , anti-CCR6 and anti-DX5 antibodies and analysed by flow cytometry (A). The total number of cells in the two dominant NK cell populations was then enumerated (B and C). Data represent the mean (horizontal lines) amongst individual data points (circles) and are from 1 experiment with 7 mice per genotype. Statistical analysis was performed using unpaired Students t-test with  $p < 0.05^*$ .

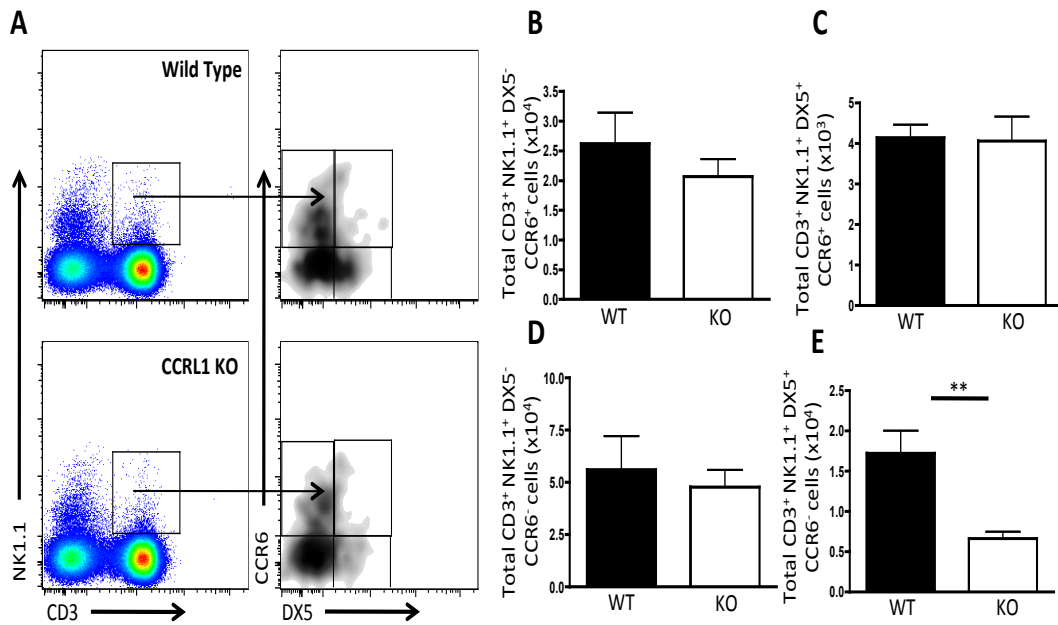


**Figure 4.10: Deletion of CCRL1 leads to a reduction in NK1.1<sup>+</sup> CCR6<sup>-</sup> DX5<sup>+</sup> iNKT cells in the mesenteric lymph node.**

Single cell suspensions were prepared from resting WT and CCRL1-deficient mesenteric lymph nodes. Cells were stained with anti-CD3, anti-NK1.1, anti-CCR6 and anti-DX5 antibodies then analysed by flow cytometry (A). The total number of iNKT cells in each of the four populations defined by CCR6/DX5 were then enumerated (B, C, D and E). Data represent the mean + SEM from 1 experiment with 7 mice per genotype. Statistical analysis was performed using unpaired Student's t-test with  $p < 0.01^{**}$ .

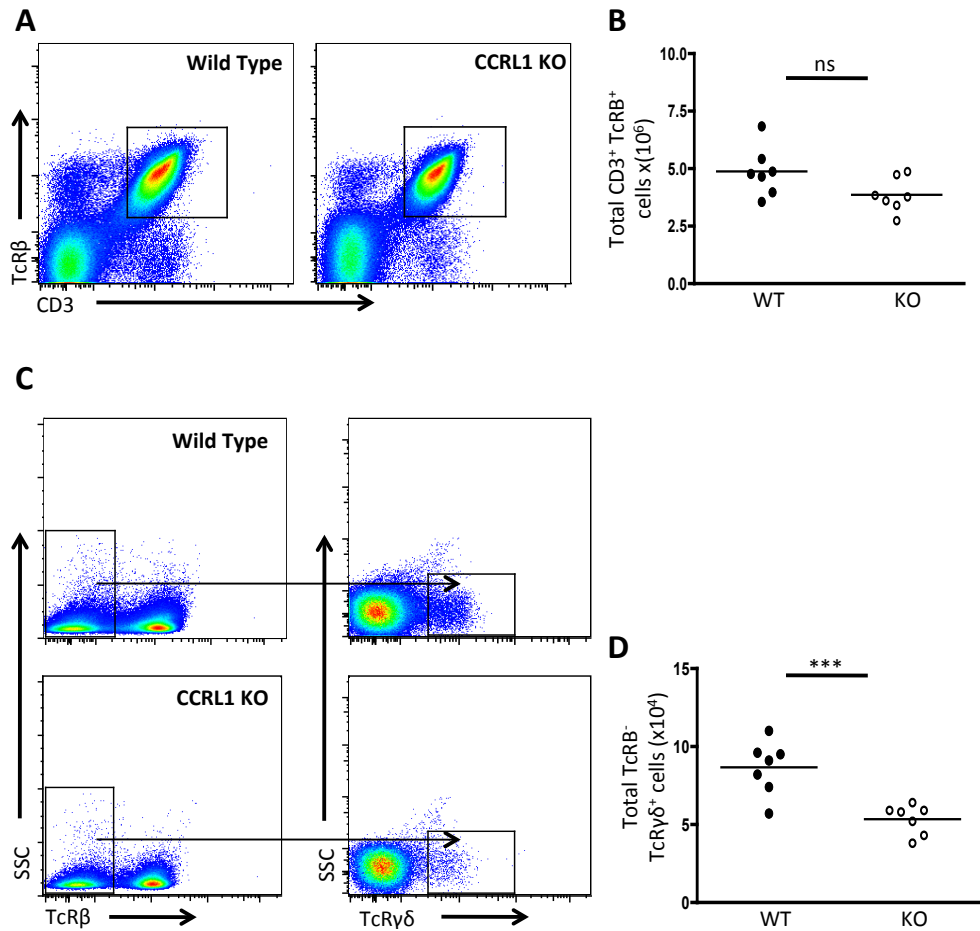


**Figure 4.11: Deletion of CCRL1 results in fewer  $\gamma\delta$  T cells in the inguinal lymph node.**

Single cell suspensions were prepared from resting WT and CCRL1-deficient inguinal lymph nodes. Cells were stained with anti-TcR $\beta$ , anti-CD3 and anti-TcR $\gamma\delta$  antibodies then analysed by flow cytometry (A and C). The total number of TcR $\beta$ <sup>+</sup> CD3<sup>+</sup> conventional T cells and TcR $\beta$ <sup>-</sup> TcR $\gamma\delta$ <sup>+</sup> T cells were then enumerated (B and D). Data represent the mean (horizontal lines) amongst individual data points (circles) and are from 1 experiment with 7 mice per genotype. Statistical analysis was performed using unpaired Student's t-test with  $p < 0.001$  \*\*\* and ns = not significant.

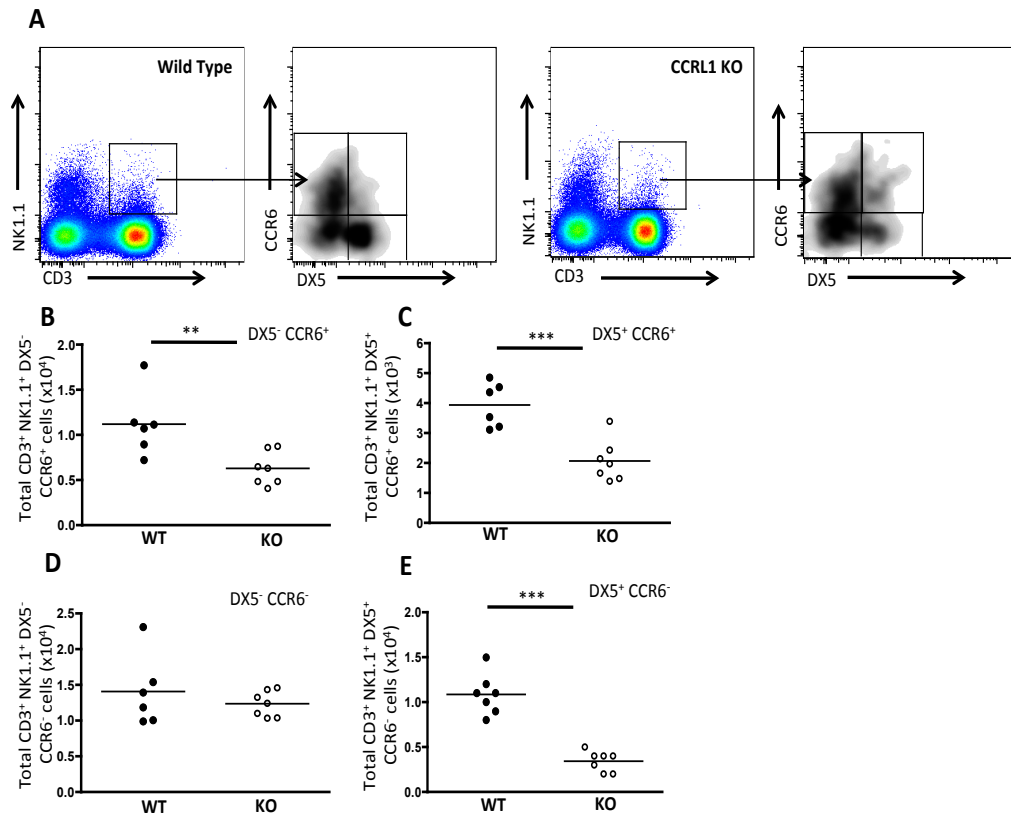


**Figure 4.12: Deletion of CCRL1 leads to a reduction in subsets of iNKT cells in the inguinal lymph node.**

Single cell suspensions were prepared from resting WT and CCRL1-deficient inguinal lymph nodes. Cells were stained with anti-NK1.1, anti-CD3, anti-CCR6 and anti-DX5 antibodies then analysed by flow cytometry (A). The total number of each iNKT cell population was then calculated (B, C, D and E). Data represent the mean (horizontal lines) amongst individual data points (circles) and are from 1 experiment with 7 mice per genotype. Statistical analysis was performed using unpaired Student's t-test with  $p < 0.01$  \*\* and  $p < 0.001$  \*\*\*.

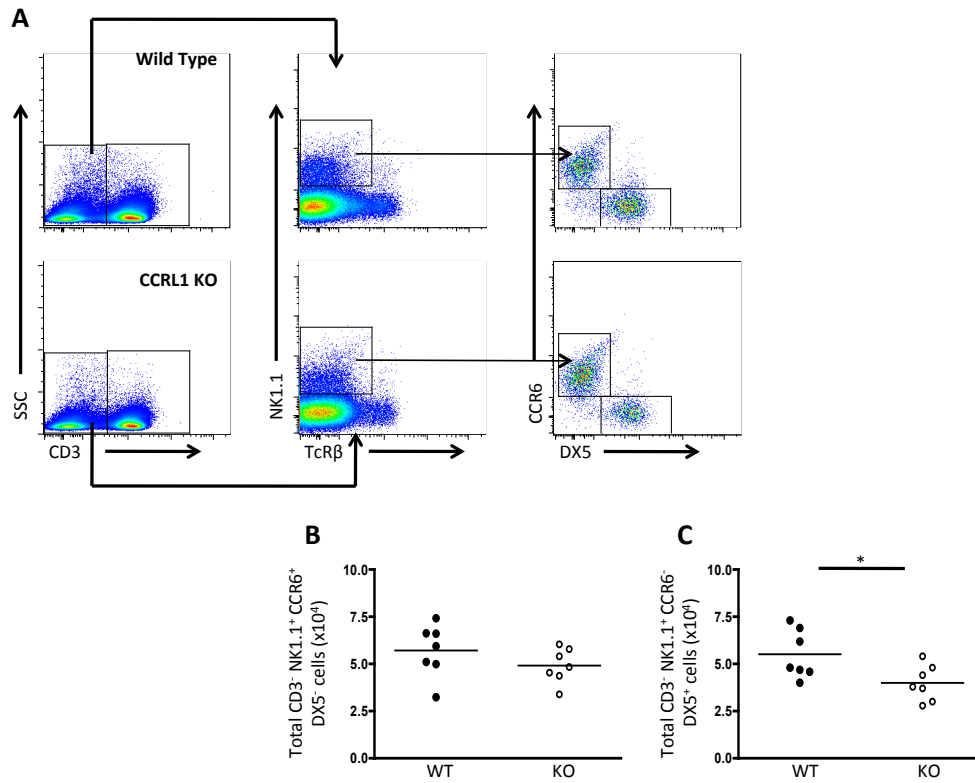


**Figure 4.13: Deletion of CCRL1 leads to a reduction in NK1.1<sup>+</sup> CCR6<sup>-</sup> DX5<sup>+</sup> NK cells in the inguinal lymph node**

Single cell suspensions were prepared from resting WT and CCRL1-deficient inguinal lymph nodes. Cells were stained with anti-CD3, anti-NK1.1, anti-Tcrβ, anti-CCR6 and anti-DX5 antibodies then analysed by flow cytometry (A). The total number of NK cells was then enumerated (B-C). Data represent the mean (horizontal lines) amongst individual data points (circles) and are from 1 experiment with 7 mice per genotype. Statistical analysis was performed using unpaired Student's t-test with  $p < 0.05^*$ .

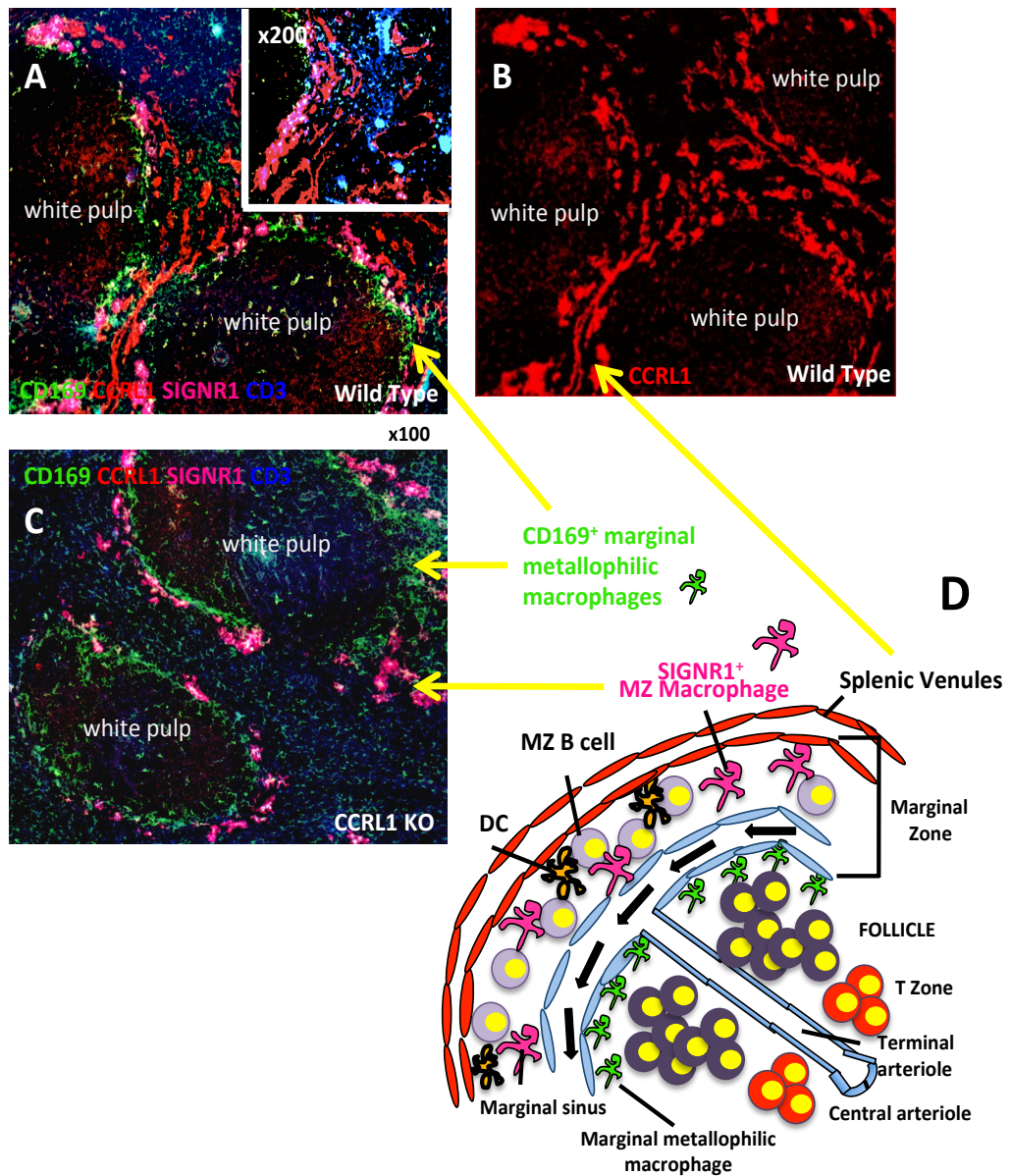


**Figure 4.14: CCRL1 is expressed on splenic venules.**

Resting spleens were harvested from WT and CCRL1 KO mice, placed in OCT and frozen on dry ice. 8-10µm sections were then cut and stained with antibodies against CD169, CCRL1, SIGNR1 and CD3. Representative images from WT (A-B) and CCRL1-deficient (C) spleens are shown. A and B are identical images except that only anti-CCRL1 staining is shown in B. A diagram of the spleen is shown in (D) to help orient the positioning of structures and cells within the spleen. Sections were imaged using a fluorescent Zeiss Axio Imager microscope. Images are representative of 4 mice per genotype.

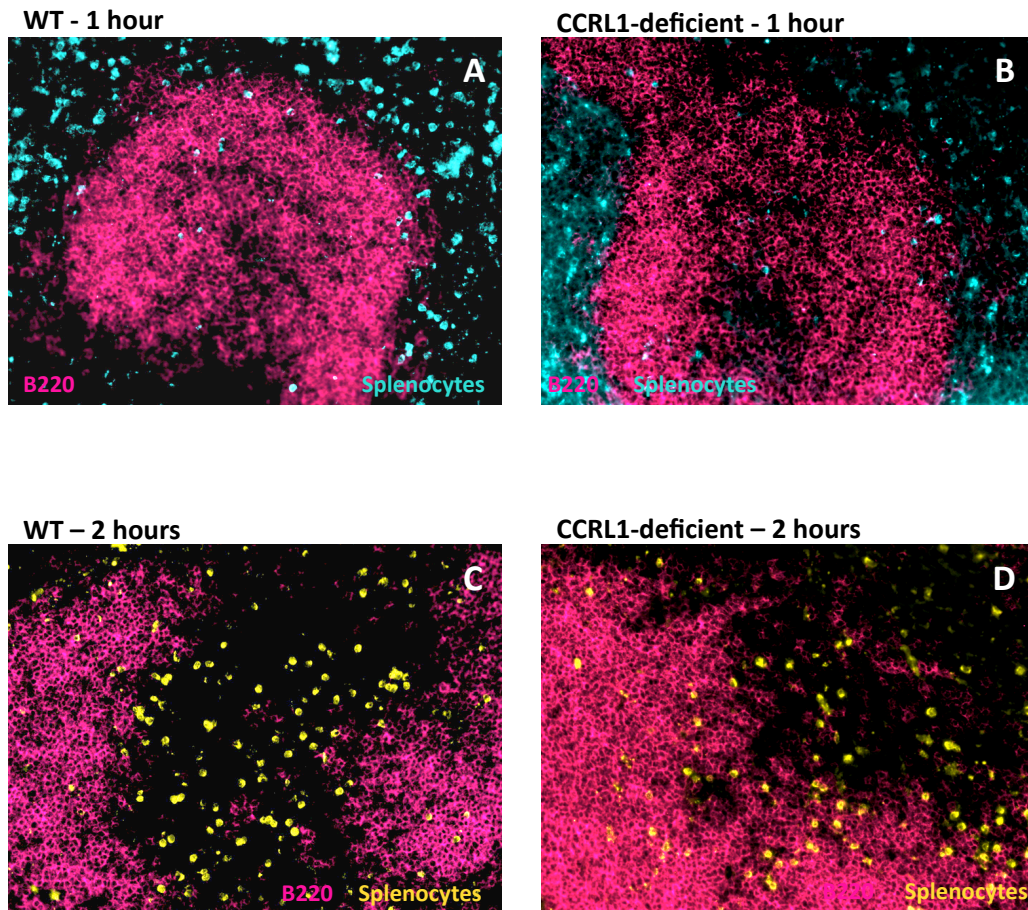


**Figure 4.15: Adoptively transferred WT splenocytes localise comparably in WT and CCRL1-deficient spleens.**

Splenocytes were isolated from WT spleens, labeled with CMTX and  $5 \times 10^6$  labeled cells in 100 $\mu$ l of PBS were injected intravenously in the tail vein of WT and CCRL1-deficient mice. Spleens were then harvested 1 hour (A-B) and 2 hours (C-D) after injection, snap frozen in OCT compound and 8-10 $\mu$ m sections cut using a cryotome. Spleens were then stained with anti-B220 antibody (pink) for the identification of B cells. CMTX labeled splenocytes are shown in blue (A-B) for the 1 hour time point and yellow (C-D) for the two hour time point. Sections were imaged using a fluorescent Zeiss Axio Imager microscope. Images are representative of 3 mice per genotype per timepoint.

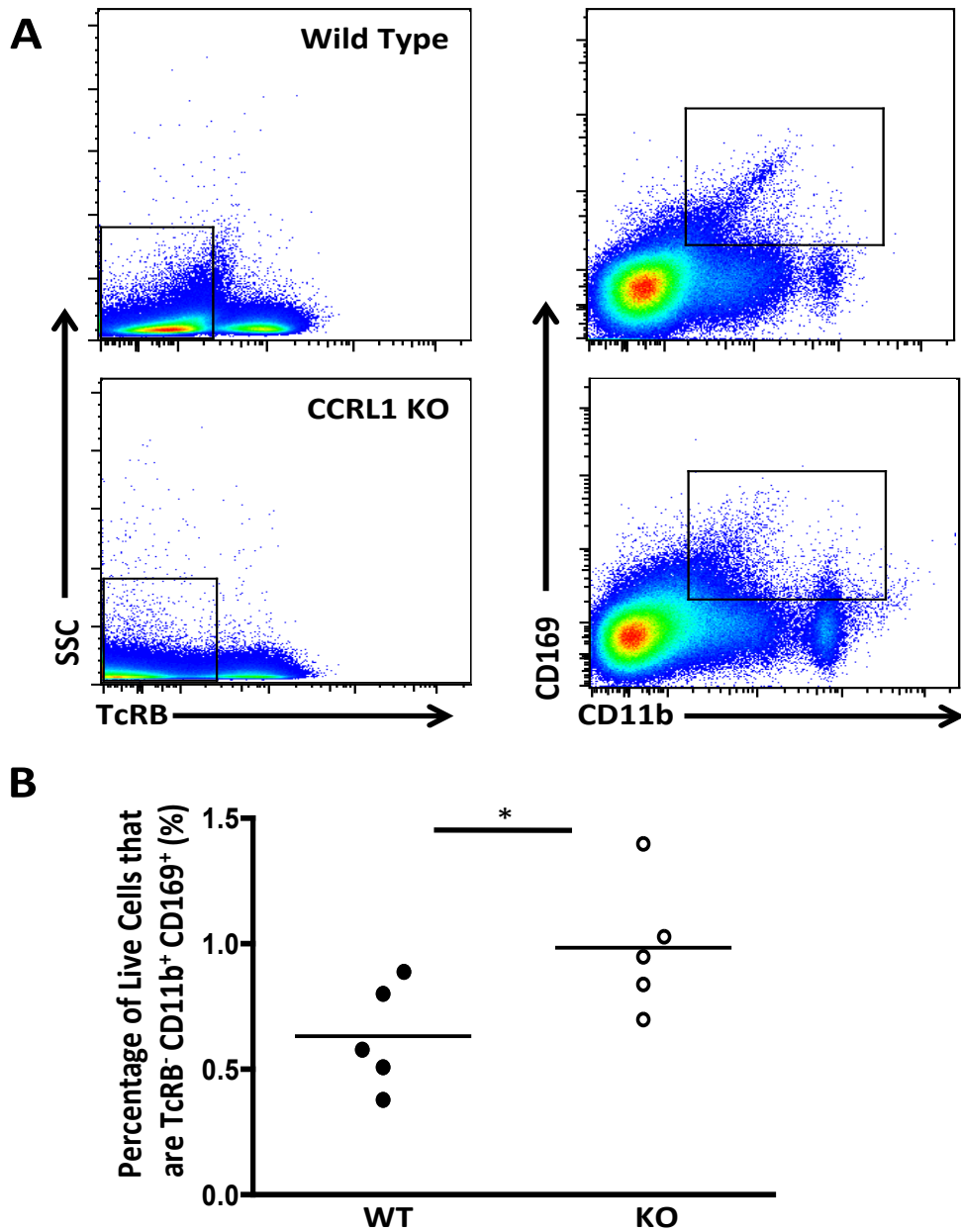


**Figure 4.16: The percentage of CD169 macrophages is increased in the spleens of CCRL1-deficient mice.**

Single cell suspensions were prepared from resting WT and CCRL1-deficient spleens. Cells were stained with anti-TcR $\beta$ , anti-CD11b and anti-CD169 antibodies then analysed by flow cytometry (A). The percentage of CD169<sup>+</sup> macrophages was then enumerated (B). Data represent the mean (horizontal lines) amongst individual data points (circles) and are from one experiment with 5 mice per genotype. Statistical analysis was performed using an unpaired Student's t-test with  $p < 0.05^*$ .

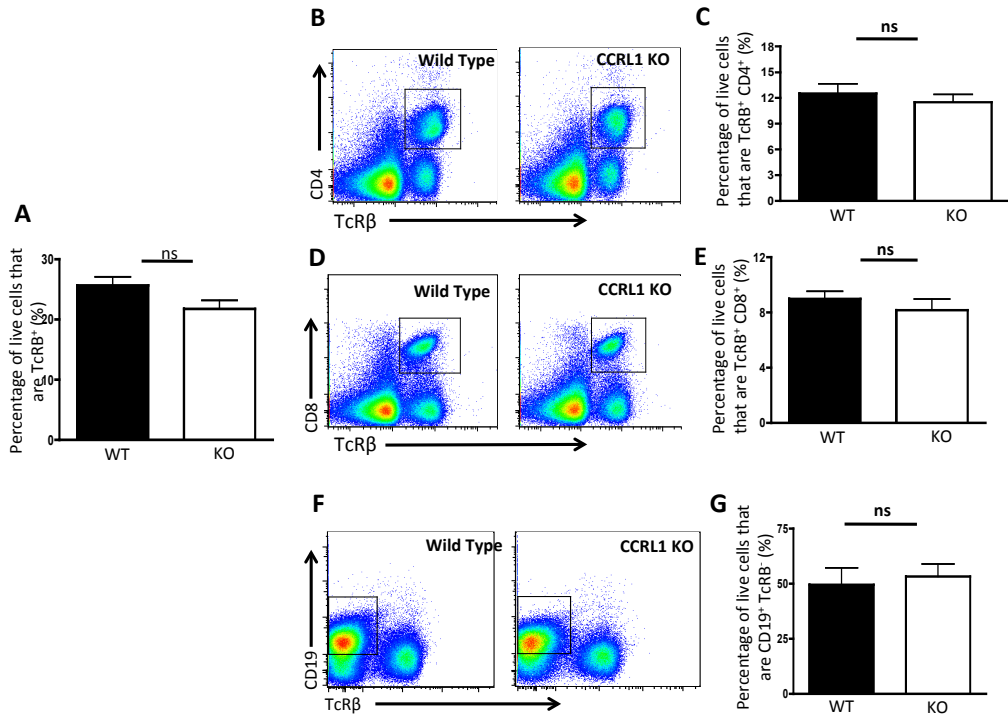


**Figure 4.17: Deletion of CCRL1 does not affect the abundance of T cells or B cells in the spleen.**

Single cell suspensions were prepared from resting WT and CCRL1-deficient spleens. Cells were stained with anti-CD4, anti-TcRβ, anti-CD8 and anti-CD19 antibodies then analysed by flow cytometry (B, D and G). The percentage of conventional T cells was then enumerated (A). The percentage of CD4 (C) and CD8 (E) T cells was calculated. The percentage of CD19<sup>+</sup> B cells was calculated and is represented in (F). Data represent the mean +SEM from 1 experiment with 4 mice per genotype. Statistical analysis was performed using unpaired Student's t-test with ns = not significant.

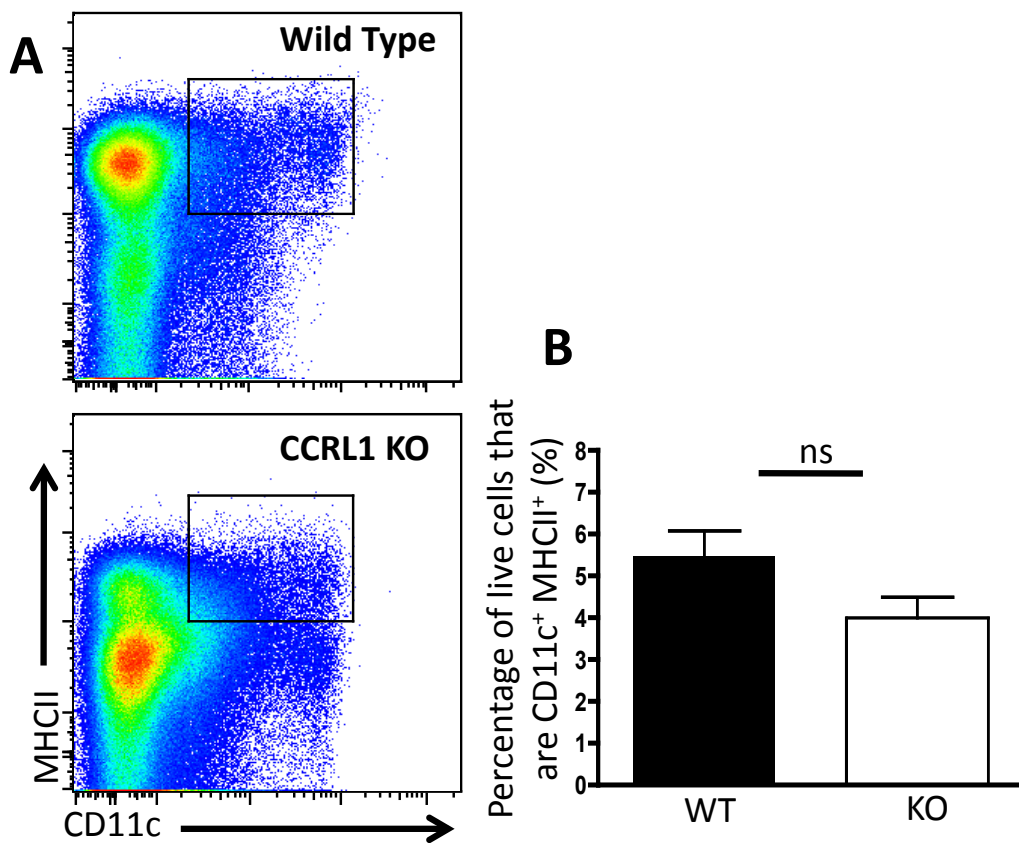


**Figure 4.18: Loss of CCRL1 does not affect the frequency of DCs in the spleen.**

Single cell suspensions were prepared from resting WT and CCRL1-deficient spleens. Cells were stained with anti-CD11c and anti-MHCII antibodies then analysed by flow cytometry (A). The percentage of CD11c<sup>+</sup> MHCII<sup>+</sup> DCs was then calculated (B). Data represents the mean + SEM from one experiment with 4 mice per genotype. Statistical analysis was performed using unpaired Student's t-test with ns = not significant.

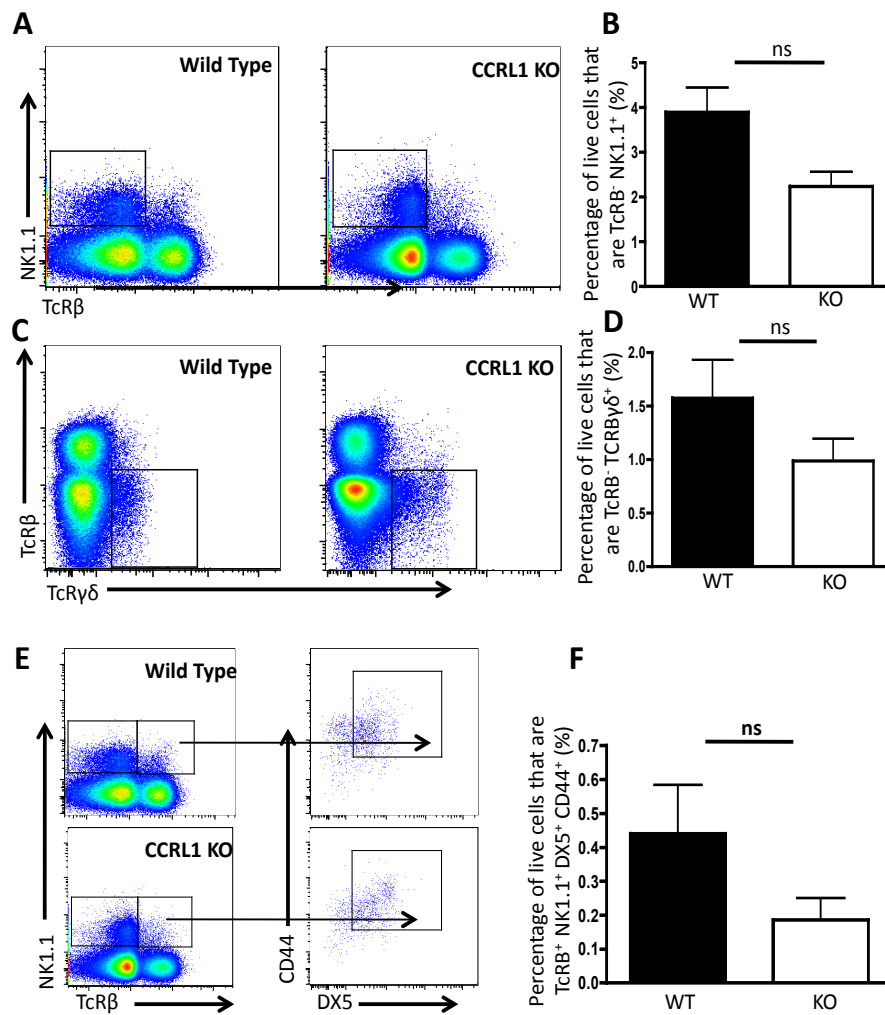


**Figure 4.19: The percentage of NK cells and iNKT cells is unaffected by loss of CCRL1 in the spleen.**

Single cell suspensions were prepared from resting WT and CCRL1-deficient spleens. Cells were stained with anti-NK1.1, anti-TcRβ, anti-TcRγδ anti-CD44 and anti-DX5 antibodies then analysed by flow cytometry (A, C and E). The percentage of NK cells (B) γδ T cells (D) and iNKT cells (F) was then calculated. Data represent the mean +SEM from one experiment with 4 mice per genotype. Statistical analysis was performed using unpaired Student's t-test with ns = not significant.

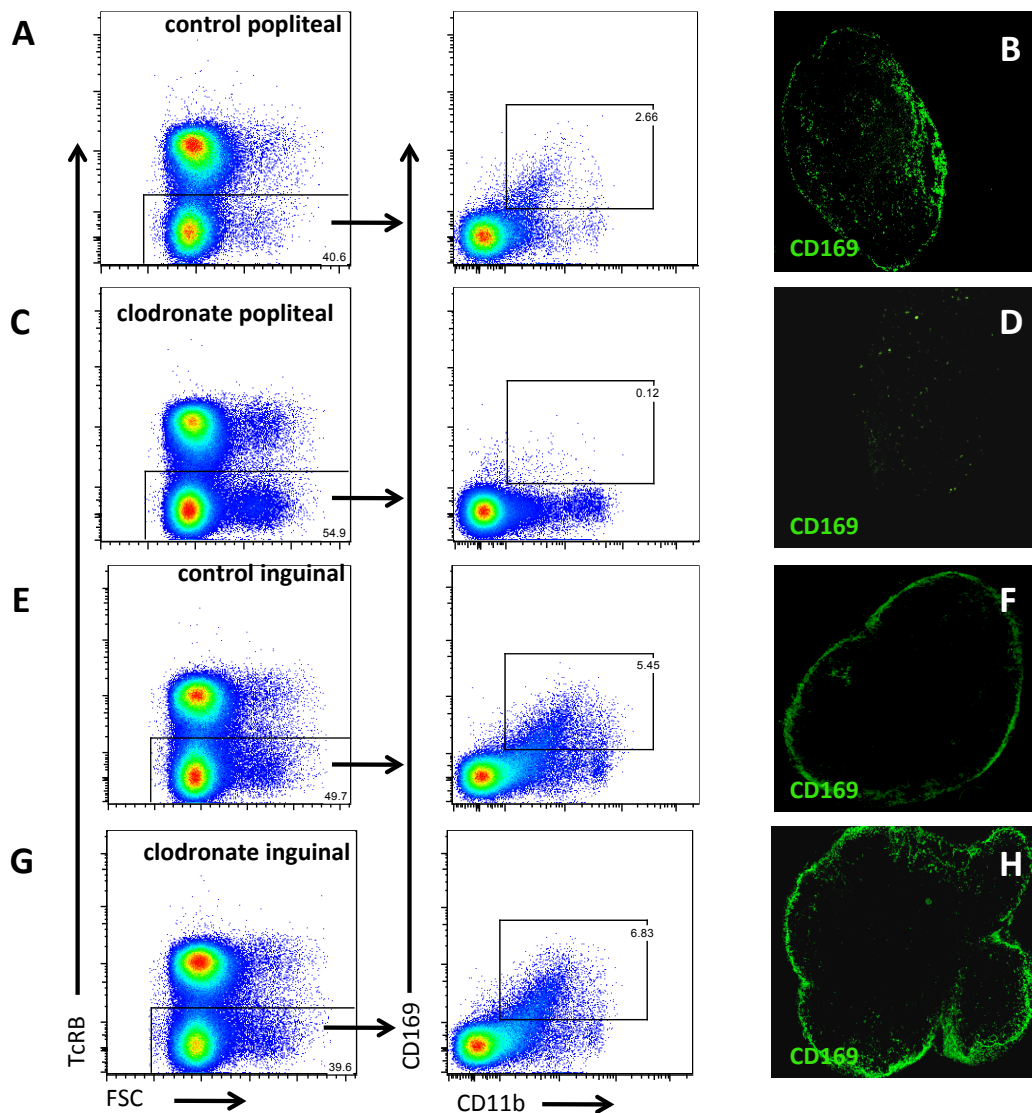


**Figure 4.20: CD169<sup>+</sup> macrophages are sensitive to local depletion in the lymph node by injection of clodronated liposomes.**

WT mice were injected with 30 $\mu$ l of clodronated liposomes into the right hind footpad and 30 $\mu$ l of PBS into the left hind footpad. 1 week later, draining popliteal and inguinal lymph nodes were harvested for flow cytometry (A,C,E and G) and immunofluorescent analysis (B,D,F and H). Popliteal and inguinal lymph nodes from PBS-injected footpads are labeled ‘control popliteal’ and ‘control inguinal’, respectively. Clodronate injected lymph nodes are termed ‘clodronate popliteal’ and ‘clodronate inguinal’, respectively. Single cell suspensions were made from inguinal and popliteal lymph nodes, stained with antibodies and analysed by flow cytometry for the presence of CD169<sup>+</sup> macrophages (A,C,E and G). Expression of CD11b and CD169 was examined on TcRB<sup>-</sup> cells. Alternatively, lymph nodes were snap frozen in OCT, cut using a cryotome to give 8-10 $\mu$ m sections and then stained with anti-CD169 antibody. Sections were then imaged using a fluorescent Zeiss Axio Imager microscope (B,D,F and H). Data are representative of results from 3 individual mice.

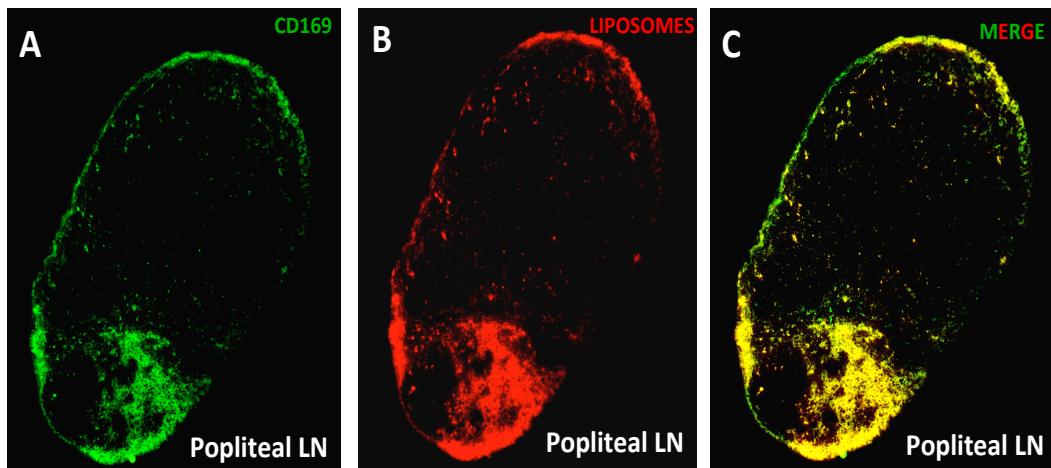


**Figure 4.21: Fluorescently labeled liposomes injected into the footpad are acquired by CD169<sup>+</sup> macrophages in the popliteal lymph.**

WT mice were injected with 30 $\mu$ l of fluorescently-labeled liposomes into the right footpad. 1 week later popliteal lymph nodes in the right leg were harvested into OCT compound and snap frozen. 8-10 $\mu$ m sections were then cut and stained with anti-CD169 antibody. Sections were imaged using a fluorescent Zeiss Axio Imager microscope. Images show CD169<sup>+</sup> stained macrophages in green (A) and the localisation of the fluorescent liposomes in red (B). The merged image of (A) and (B) is shown in (C). Images are representative of at least 3 individuals.

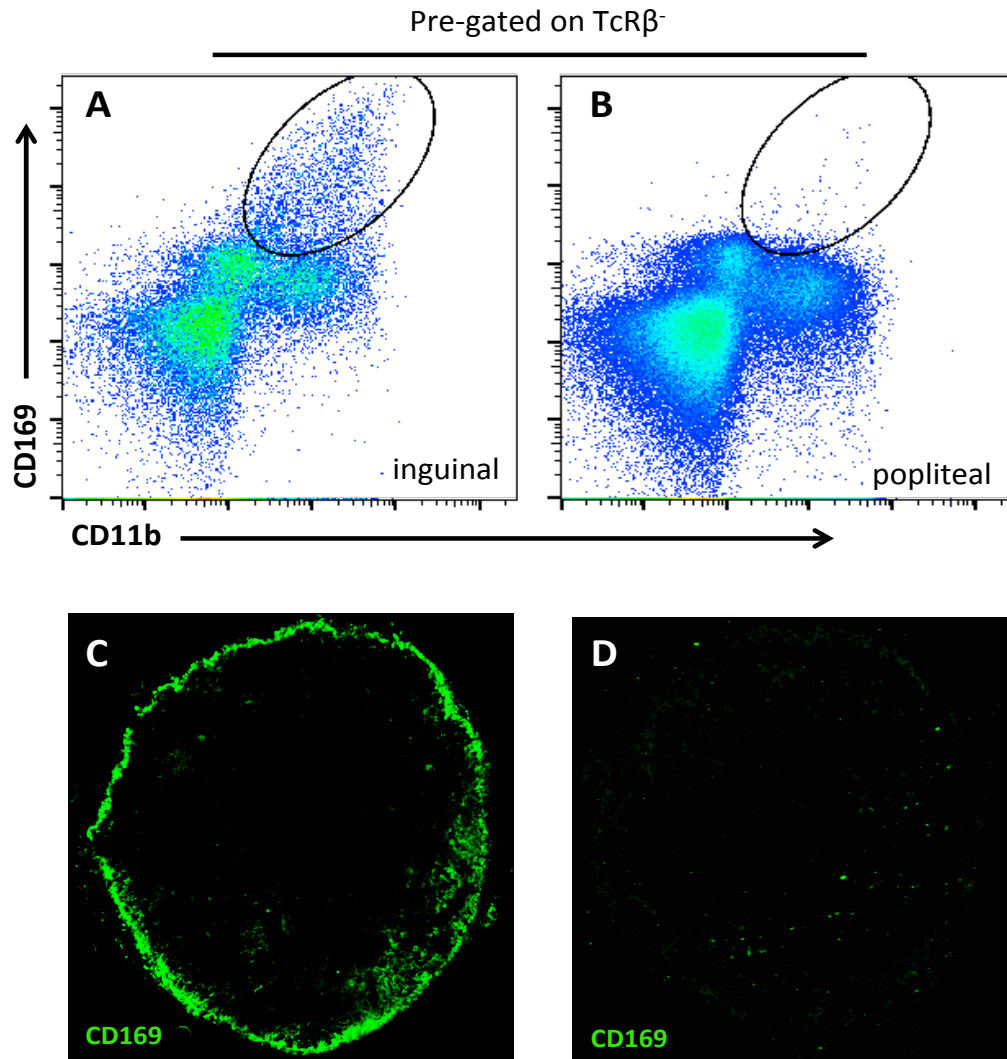


**Figure 4.22: CD169<sup>+</sup> macrophages are absent from popliteal lymph nodes two weeks after injection with clodronated liposomes into the footpad.**

WT mice were injected with 30 $\mu$ l of clodronated liposomes into the right hind footpad. 2 weeks later, popliteal lymph nodes and inguinal lymph nodes from the right leg were harvested for flow cytometry (A-B) and immunofluorescent analysis (C-D). Single cell suspensions were made from inguinal and popliteal lymph nodes, stained with antibodies and analysed by flow cytometry for the presence of CD169<sup>+</sup> macrophages (A-B). Expression of CD169 and CD11b were examined on TcR $\beta$ <sup>-</sup> cells. Alternatively, lymph nodes were snap frozen in OCT, cut using a cryotome to give 8-10 $\mu$ m sections and then stained with anti-CD169 antibody. Sections were then imaged using a fluorescent Zeiss Axio Imager microscope. Data are representative of results obtained from 3 individuals.

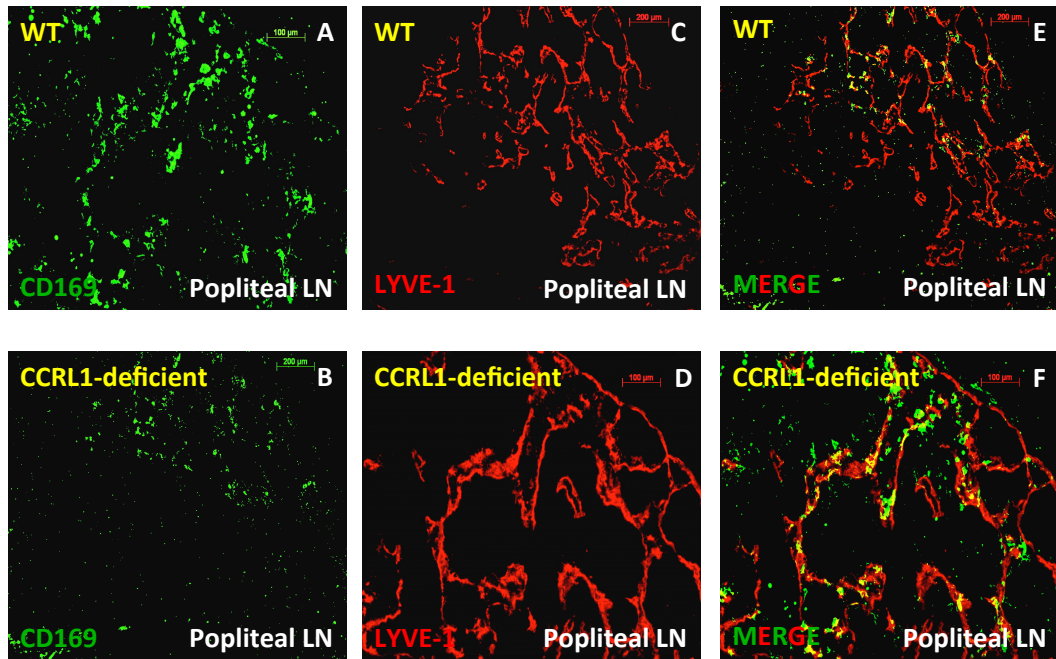


**Figure 4.23: CFA injection into the footpad drives lymphangiogenesis in WT and CCRL1-deficient popliteal lymph nodes.**

WT and CCRL1-deficient mice were injected with 30 $\mu$ l of PBS into the right footpad. 1 week later mice were then injected with 50 $\mu$ l of 4mg/mL CFA into the same footpad and animals allowed to rest for 1 week. Popliteal lymph nodes from the right leg of WT and CCRL1-deficient mice were harvested into OCT compound and snap frozen. 8-10 $\mu$ m sections were then cut and stained with anti-CD169 (green) and anti-LYVE1 (red) antibodies (A-D). Merged images showing CD169 and LYVE-1 on the same image are shown in E and F. Sections were imaged using a fluorescent Zeiss Axio Imager microscope. Images are representative of at least 3 mice per genotype.

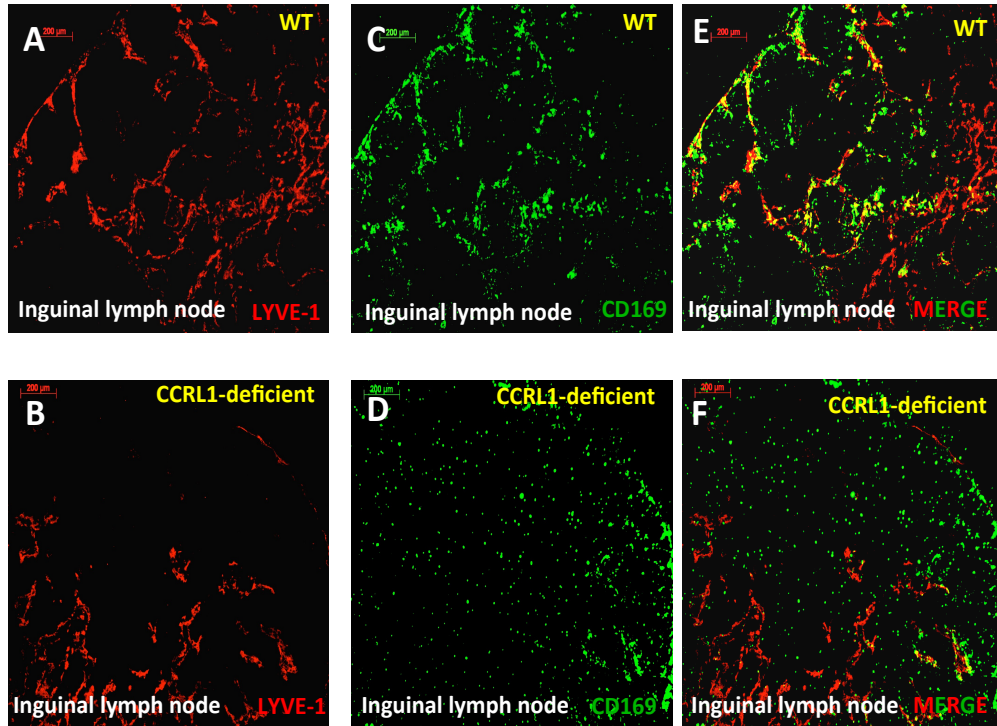


**Figure 4.24: CFA injection into the footpad drives lymphangiogenesis in WT and CCRL1-deficient inguinal lymph nodes.**

WT and CCRL1-deficient mice were injected with 30 $\mu$ l of PBS into the right footpad. 1 week later mice were injected with 50 $\mu$ l of 4mg/mL CFA into the same footpad and animals allowed to rest for 1 week. Inguinal lymph nodes from the right leg of WT and CCRL1-deficient mice were harvested into OCT compound and snap frozen. 8-10 $\mu$ m sections were then cut and stained with anti-CD169, and anti-LYVE1 antibodies (A-D). Images A-D represent each individual antibody stain and images E and F show the merged stains on a single image. Sections were imaged using a fluorescent Zeiss Axio Imager microscope. Images are representative of at least 3 mice per genotype.

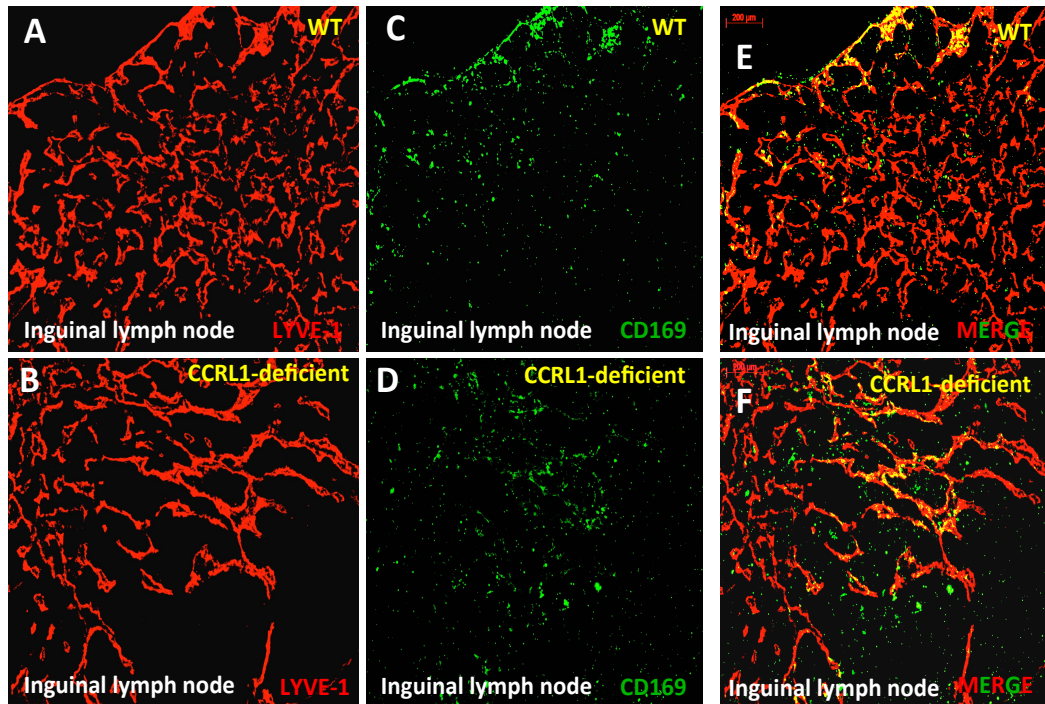


**Figure 4.25: Clodronated liposome and CFA injection into the footpad induces lymphangiogenesis in the inguinal lymph nodes of WT and CCRL1-deficient mice.**

WT and CCRL1-deficient mice were injected with 30 $\mu$ l of clodronated liposomes into the right footpad. 1 week later, mice were injected with 50 $\mu$ l of 4mg/mL CFA into the same footpad and animals allowed to rest for 1 week. Inguinal lymph nodes from the right leg WT and CCRL1-deficient mice were harvested into OCT compound and snap frozen. 8-10 $\mu$ m sections were cut and stained with anti-LYVE1 (A-B) and anti-CD169 (C-D) antibodies. Images E and F show the merged antibody stains on one single image. Sections were imaged using a fluorescent Zeiss Axio Imager microscope. Images are representative of at least 3 mice per genotype.

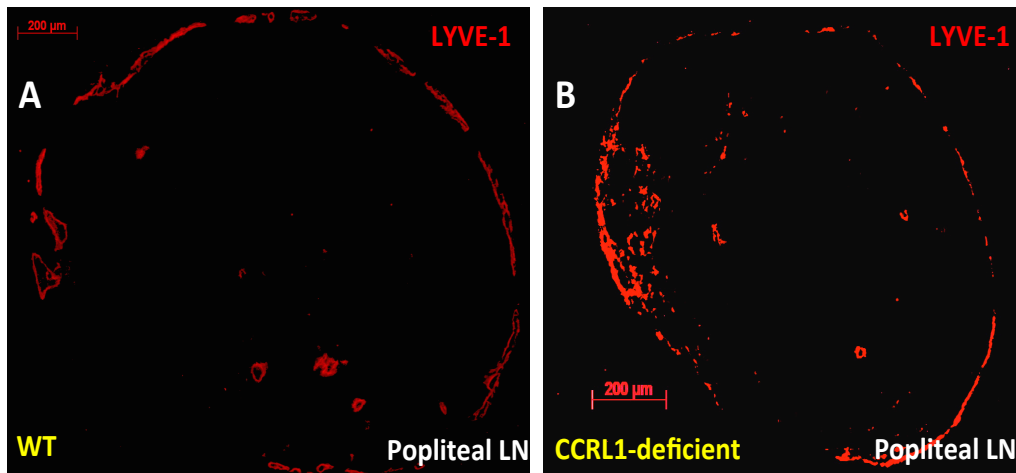


**Figure 4.26: Macrophages are required for lymphangiogenesis in the popliteal lymph node of WT and CCRL1-deficient mice after CFA injection into the footpad.**

WT and CCRL1-deficient mice were injected with 30 $\mu$ l of clodronated liposomes into the right footpad to deplete macrophages in the draining popliteal lymph node. 1 week later, mice were then injected with 50 $\mu$ l of 4mg/mL CFA into the same footpad and animals allowed to rest for 1 week. Popliteal lymph nodes from the right leg of WT (A) and CCRL1-deficient (B) mice were harvested into OCT compound and snap frozen. 8-10 $\mu$ m sections were cut and stained with anti-LYVE-1 antibody. Sections were imaged using a fluorescent Zeiss Avio Imager microscope. Images are representative of at least 3 individuals per genotype.

# Chapter Five

## Leukocyte-Mediated Truncation of C-terminus Extended Chemokines

## 5 Leukocyte-Mediated C-terminal Truncation of Chemokines

### 5.1 Introduction

Chemokines vary in size, charge, structure and function. Some chemokines are extended at the C terminus, facilitating their interactions with GAG molecules that decorate the surface of cells and the extracellular matrix. GAGs anchor chemokines on the surface of cells to facilitate leukocyte extravasation and interstitial haptotaxis and haptokinesis. A growing body of work has focused on characterising the post-translational modification of chemokines, including those modifications mediated by proteases released by leukocytes, cancer cells and other non-hematopoietic cells<sup>214,376-380</sup>. Processing of the N-terminal region of chemokines leads to the production of variants that have altered receptor specificity, affinity and activation properties<sup>213,376,381,382</sup>. Protease activity directed to the C-terminus of chemokines leads to the generation of chemotactically active, truncated forms of the native chemokine protein that have altered interactions with GAGs. One such chemokine, CCL21, has been studied by Schumann and colleagues and shown to be truncated *in vitro* by DCs<sup>383</sup>. The truncation of full length CCL21 (fCCL21) produces a soluble chemotactic fragment with reduced affinity for GAGs that is capable of inducing the chemotactic migration of CCR7<sup>+</sup> cells. Soluble truncated CCL21 protein, referred to hereafter as truncated CCL21 (tCCL21), can also be found *in vivo*, although the mechanism underpinning its production remains unclear. Similarly, it is yet to be shown how DCs truncate fCCL21 *in vitro*.

The biological significance of CCL21 cleavage is important to understand as the orchestration of adaptive immune responses relies heavily on the ability of CCR7<sup>+</sup> cells to migrate in response to CCL21. Furthermore, understanding how tCCL21 is regulated by CCRL1 will help us to appreciate the full extent of the relationship between CCR7 and CCRL1. Moreover, as this receptor is able to bind to fCCL21, it is conceivable that this binding in some way facilitates chemokine truncation. Similarly, the binding of CCR7 to fCCL21 may be involved in mediating the truncation of this chemokine.

In this chapter, the focus of my investigations was to understand DC-mediated chemokine truncation. This body of work can be viewed as a continuation of the work published by Schuman and colleagues<sup>383</sup>. In this chapter I explore the truncation of other C-terminally extended chemokines by DCs of mouse and human origin, and look for the existence of truncated chemokines *in vivo*. Of direct relevance to investigations into the biological role of CCRL1, DC mediated truncation of CCL25 was explored. Possible mechanisms for the truncation of chemokine by DCs are investigated, as well as the kinetics of CCL21 cleavage *in vivo* over the course of an inflammatory response. The ability of other leukocyte subsets to mediate CCL21 truncation is examined, and the presence of tCCL21 in various lymphoid tissues is also explored.

Collectively, these data shed new light on the truncation of C-terminus extended chemokines, and the role of leukocytes in mediating this process.

## **5.2 Truncation of Full Length CCL21 Chemokine by DCs *in vitro***

Following on from published research by Schumann and colleagues<sup>383</sup>, the initial aim was to confirm that *in vitro*-derived DCs have the ability to cleave fCCL21 chemokine to produce tCCL21. As mentioned previously and demonstrated in Chapter 3, a small population of DCs expresses CCRL1, therefore, to investigate the truncation of fCCL21 by CCRL1<sup>+</sup> DCs, bone marrow-derived DCs (BMDCs) were generated from WT and CCRL1-deficient animals and cultured with fCCL21. BMDCs were generated by culturing bone marrow with GM-CSF for 7 days as described in the Materials and Methods section. These cells were then cultured with recombinant CCL21 and truncation assessed by Western blotting (Figure 5.1). From the results it was clear that both WT and CCRL1-deficient BMDCs have the capacity to truncate CCL21 chemokine to produce a smaller ~8kDa protein from the 12kDa fCCL21 protein. The size of the tCCL21 corresponds to the size of the tCCL21 seen in Schuman's study<sup>383</sup>. Interestingly WT and CCRL1-deficient BMDCs were unable to truncate all of the recombinant fCCL21 to produce the ~8kDa fragment, and consistently a ~1:1 ratio of fCCL21 to tCCL21 was observed (Figure 5.1). This ~1:1 ratio agrees with previous published data from Schumann and colleagues<sup>383</sup>.

Therefore, GMCSF-matured BMDCs have the ability to cleave CCL21, and CCRL1 is dispensable for DC-mediated cleavage of CCL21. BMDCs were unable to cleave all of the full-length CCL21 to produce the soluble fragment after 16 hours in culture.

### **5.3 Chemokine Truncation - Non-Activated vs. Activated DCs**

As described in the Introduction, DCs undergo morphological and transcriptional changes upon activation with TLR ligands, such as LPS. Upon activation, DCs upregulate costimulatory molecules such as CD80/CD86, antigen presentation molecules such as MHCII and chemokine receptors such as CCR7. I was interested in assessing the impact that the maturation of BMDCs had on the cleavage of fICCL21 chemokine by BMDCs. To explore this, GMCSF-matured DCs were cultured with and without LPS for 24 hours, and 150ng of fICCL21 was added to these cells and left to culture overnight. The next day, supernatants were harvested for assessment of chemokine truncation and the cells were examined by flow cytometry. As expected, LPS activation of BMDCs drove their maturation as determined by their higher expression of CD86 and MHCII compared with unstimulated BMDCs (Figure 5.2 A-B). However, this difference in activation did not affect the ability of BMDCs to cleave fICCL21 (Figure 5.2 C). Both unactivated and LPS activated BMDCs cleave fICCL21 to produce tCCL21. Again, a substantial proportion of the fICCL21 remained uncleaved resulting in a ratio of ~1:1 fICCL21:tCCL21.

### **5.4 Chemokine Truncation - GMCSF vs. Flt3-L Matured BMDCs**

It is commonly accepted that the generation of DCs from bone marrow cells by culturing with GMCSF or Flt3L can drive the formation of phenotypically distinct BMDCs. Furthermore, Flt3L is commonly used to generate pDCs *in vitro*. To investigate the different possible cleavage capabilities of DCs matured in both of the aforementioned conditions, Flt3L matured BMDCs were cultured with fICCL21 and its cleavage assessed by Western blotting.

BMDCs were generated by culturing bone marrow cells with Flt3L for 9 days, giving rise to CD11c<sup>+</sup> MHCII<sup>hi</sup> BMDCs with ~83% purity (Figure 5.3 A). These Flt3-L matured BMDCs were able to cleave flCCL21 (Figure 5.3 B). The cleavage of flCCL21 by Flt3L matured DCs mirrors that of GMCSF matured DCs, producing a ~1:1 mix of flCCL21:tCCL21. However, some lanes did appear to have more tCCL21 than flCCL21 therefore this ~1:1 ratio was only an approximation and not found within each replicate. Therefore, BMDCs generated by GMCSF or Flt3L are able to cleave CCL21 to the same degree.

## 5.5 CCL21 Truncation by Human DCs

Next, the ability of human DCs to truncate flCCL21 was examined. Human DCs were generated by culturing peripheral blood mononuclear cells from buffy coats with 100ng/mL GMCSF and 20ng/mL IL-4. Human flCCL21 was added to these cultures and its truncation assessed by Western blotting. As for the experiments involving mouse bone marrow-derived DCs, I compared flCCL21 cleavage with and without DC activation using LPS. Activation of DCs was assessed by flow cytometry, and LPS treatment was shown to upregulate CD86 expression although “media alone” DCs also showed high expression of CD86 (Figure 5.4 A and C). flCCL21 cleavage was assessed at two different time points, 7 hours and 16 hours. As for mouse DCs, human DCs have the capacity to cleave flCCL21 into tCCL21 (Figure 5.4 B and D). Furthermore, as seen previously for mouse DC cultures, LPS activation of DCs did not result in more CCL21 cleavage (Figure 5.4 B and D). Furthermore, longer incubation of DCs with CCL21 did not appear to lead to the generation of more tCCL21. Thus, by 7 hours, DCs had truncated much of the flCCL21 to produce tCCL21, and do not appear to truncate any more flCCL21 over the next 9 hours (Figure 5.4 C-D). Notably, a very small amount of tCCL21 is present in the ‘CCL21 alone’ sample (Figure 5.4 D).

In summary, human DCs, like mouse DCs, fail to completely cleave flCCL21 to generate tCCL21.

## 5.6 Leukocyte-Mediated Chemokine Processing

Although Schumann and colleagues have previously explored the ability of T cells, macrophages and B cells to cleave recombinant fCCL21 *in vitro*<sup>383</sup> it was necessary to confirm this definitively before investigating the mechanism that is unique to DCs for the truncation of chemokine. To this end, the ability of other leukocyte populations to cleave fCCL21 was investigated by enriching T cells and B cells from the spleens of WT mice (**Figure 5.5 A-B**) and by generating bone marrow-derived macrophages (BMDMs) by culturing bone marrow cells with 40ng/mL M-CSF for 7 days (**Figure 5.5 D**). These cells were then cultured separately with 150ng of fCCL21 *in vitro* and their ability to cleave fCCL21 was assessed by Western blot. Additionally, at the same time, BMDCs were cultured with fCCL21 as a positive control. Compared to BMDCs, B cells and T cells were unable to effectively cleave fCCL21 to produce tCCL21 although there was a faint secondary band that is smaller than fCCL21 in samples from T cells cultured with fCCL21 (**Figure 5.5 C**). This band correlated with the size of the tCCL21 fragment observed when fCCL21 was cultured without cells (**Figure 5.1, Figure 5.2 C, Figure 5.4 D**). This band was clearer with longer exposure times of the film (data not shown) but the film had to be exposed for a long time and affected the clarity of the other protein bands. Notably, B cells and T cells appear to deplete fCCL21 from the medium, possibly via CCR7-mediated scavenging. BMDMs, when cultured with fCCL21, appear to convert fCCL21 to tCCL21, but also appear to consume the CCL21 (**Figure 5.5 E**). On the same blot, fCCL21 and tCCL21 can be seen from samples of DCs + CCL21. Collectively, the data demonstrate that while BMDCs cleave fCCL21 to tCCL21, lymphocytes do not but can consume the chemokine, while macrophages appear to cleave fCCL21 and consume CCL21. This experiment was undertaken in parallel with controls including culturing CCL21 in complete media alone and running a sample of CCL21 directly from the vial without culturing in media or with cells. The CCL21 sample that was ran on the gel without incubation with media or cells showed only the presence of the full length 12kDa fragment however chemokine that was cultured in complete media did show the presence of a faint CCL21

band the corresponded to the ~8kDa fragment found after DC culturing with CCL21 (data not shown).

## 5.7 CCL21 Truncation by Lymph Node Cells

*In vitro* work is useful for understanding processes such as chemokine cleavage in simplified systems as investigations are conducted in a readily controlled environment. However, GM-CSF matured BMDCs does not fully represent the complete repertoire of DCs that are found *in vivo*. Therefore, to build on *in vitro* studies, single cell suspensions of lymph nodes were made and  $6 \times 10^5$  cells in 100  $\mu$ l cultured with fCCL21. This population of cells will include a variety of different lymph node resident cells including various DC subsets, and the results from this experiment will reveal if fCCL21 has the capacity to be truncated by primary cells derived directly from lymph nodes. First, the presence of DCs (CD11c<sup>+</sup> MHCII<sup>+</sup>) in the lymph node cell suspensions was determined by flow cytometry (Figure 5.6 A). As expected, they account for a relatively small population of lymph node cells at rest. *In vitro* culture with CCL21, revealed that inguinal lymph node cells were able to cleave full length recombinant CCL21 *in vitro* generating a ratio of ~1:1 fCCL21:tCCL21 (Figure 5.6 B). Cells isolated from different secondary lymphoid tissues were also assessed for their ability to cleave fCCL21. In all samples from the 6 WT lymphoid tissues analysed the tCCL21 band was generated (Figure 5.6 C).

Therefore, CCL21 can be cleaved by cells isolated from a variety of different WT lymphoid tissues.

## 5.8 CCL21 Truncation *in vivo*

Next, the presence of tCCL21 was examined *in vivo*. Schumann and colleagues previously reported the presence of tCCL21 *in vivo*<sup>383</sup>, however, they had to immunoprecipitate lymph node lysates in order to detect this protein. In the next set of experiments, mesenteric lymph nodes, axillary lymph nodes and spleen were harvested and the lysates analysed by Western blotting without immunoprecipitating. Due to the solubility of tCCL21, I reasoned that tCCL21 may be more prone to regulation by CCRL1 compared with fCCL21, therefore,

WT and CCRL1-deficient tissues were prepared for analysis. I was able to detect a smaller chemokine fragment in a variety of tissues by preparing samples in this way (Figure 5.7 A). This fragment was of low abundance, and with longer exposures became more evident although background signal also increased (data not shown). No obvious difference in the abundance of tCCL21 was apparent between WT and CCRL1-deficient lymphoid tissues. However, there did not appear to be more fCCL21 in CCRL1-deficient samples from mesenteric and axillary lymph nodes compared to WT counterparts. Interestingly, the size of the tCCL21 protein found *in vivo* did not correspond to the size of *in vitro*-derived CCL21 produced by DC cleavage. *In vitro* derived tCCL21 had a molecular weight of ~8kDa, whereas the tCCL21 detectable in secondary lymphoid tissue lysates had a molecular weight of ~10kDa.

## **5.9 CCL21 Truncation *in vivo* After the Induction of Inflammation**

During homeostasis, DCs represent a small proportion of total lymph node cells, however, inflammation drives the migration of these cells from peripheral tissues and leads to an increase in DC numbers in lymph nodes. This was described in Chapter 3 for DC migration from the skin during TPA inflammation whereby DC numbers in the lymph node were shown to peak at ~24 hours post TPA paint. Therefore, this model of skin inflammation was adopted in order to investigate whether more DCs in the lymph node correlates with increased truncation of fCCL21 to tCCL21. WT and CCRL1-deficient mice were painted on the dorsal skins with TPA to induce skin inflammation. 6, 24, and 48 hours after topical application of TPA, the skin-draining inguinal lymph nodes of WT and CCRL1-deficient mice were harvested. Lymph node lysates were prepared from these samples and analysed for the presence of fCCL21 and tCCL21 by Western blotting anti probing with anti-CCL21 antibody (Figure 5.8 A-B). From the results it was clear that tCCL21 was present in WT and CCRL1-deficient inguinal lymph nodes. However, as at rest, the size of this protein did not correspond to the molecular weight of DC-generated tCCL21. Moreover, the presence of tCCL21 at each time point appeared unaffected by CCRL1 deficiency or by inflammation.

Thus, a truncated form of CCL21 is found in skin-draining inguinal lymph nodes but appears unaffected by skin inflammation, the number of DCs in the lymph node, or the deletion of CCRL1.

### **5.10 Truncation of CCL21 Cannot be Mediated by DC-Conditioned Medium or Competed by CCL19**

Next, the mechanism of DC-mediated truncation was investigated. Specifically, investigations were carried out to test whether truncation can be mediated by DC-conditioned medium. This may suggest that these cells secrete a soluble factor that mediates the truncation of flCCL21 to tCCL21. To test this, DCs were cultured in media for 16 hours and DC conditioned media then harvested. 100µl of BMDC conditioned media was added to each well of a 96-well plate, and to this was added 150ng of flCCL21. The samples were then left at 37°C for 16 hours, and chemokine truncation was assessed by Western blotting to detect flCCL21 and tCCL21. flCCL21 cultured with BMDC conditioned media was not substantially cleaved to produce the smaller ~8kDa fragment seen previously for flCCL21 + BMDCs (**Figure 5.8 A**). This would suggest the BMDC contact with flCCL21 is required for its cleavage. To investigate whether this contact-dependent truncation was mediated by CCR7, GM-CSF-matured BMDCs were pre-incubated with 1.5µg of CCL19 (10 fold excess) for 16 hours to block CCR7 binding sites. BMDCs were then incubated with flCCL21 for 16 hours and the presence of flCCL21 and tCCL21 detected by Western blot. From the results it was determined that DC truncation of flCCL21 is not mediated by CCR7 as tCCL21 was found in each of the 3 triplicate samples (**Figure 5.8 B**). However, to confirm this conclusively, it would be necessary to culture CCR7-deficient BMDCs with flCCL21 as it is likely that a 10-fold excess of CCL19 will not completely abrogate the binding of CCL21 to CCR7.

### **5.11 Truncation of Other Chemokines With Extended C-terminal Domains**

To explore the possible truncation of other C-terminally extended chemokine by BMDCs, we analysed the amino acid sequences of the chemokine family to

identify suitable candidates. Two possible chemokines were identified, CCL2 and CCL25, both of which are extended at the C-terminus in mice. Interestingly, although CCL2 is extended at the C-terminus in mice, it is not in humans. Recombinant mouse CCL2 is commercially available as either flCCL21 or tCCL2. The full length version is available from PeproTech and the shorter form from R&D Systems (Figure 5.9 A). Full length PeproTech CCL2 corresponds to the sequence of mature CCL2 without the 23 amino acid signal peptide. R&D Systems CCL2 is 73 amino acids long and lacks the signal peptide as well as residues 96-148. 150ng of R&D Systems CCL2 and 100ng of PeproTech CCL2 were analysed by Western blot using anti-CCL2 antibody and their molecular weights estimated by running molecular weight markers in a lane adjacent to the samples. From this experiment, it was shown that R&D Systems CCL2 has a molecular weight of ~8.5kDa and PeproTech CCL2 has a molecular weight of ~13.8kDa (Figure 5.9 B).

CCL25 with an extended C-terminus was purchased from R&D Systems. The amino acid sequence of this protein was the same as that encoded for by CCL25 cDNA minus the 23 amino acid signal peptide (Figure 5.10).

First, to assess BMDC mediated cleavage of flCCL2, flCCL2 from PeproTech was utilized.  $6 \times 10^5$  GM-CSF-matured BMDCs were cultured overnight in 100 $\mu$ l of complete media with 150ng of flCCL2 and the next day supernatants were harvested and assessed for the presence of flCCL2 and tCCL2. Results show that when cultured with BMDCs, virtually all the flCCL2 from PeproTech was cleaved to produce tCCL2 and was approximately the same molecular weight of ~8kDa that was around the same molecular weight as CCL2 from R&D Systems (Figure 5.11 A).

Next, the ability of GM-CSF-matured BMDCs and M-CSF-matured BMDMs to truncate CCL25 was explored. BMDCs and BMDMs were generated as before.  $6 \times 10^5$  BMDCs or BMDMs were incubated in 100 $\mu$ l of complete media overnight with 150ng of CCL25. The next day supernatants were harvested and analysed by Western blotting. When running the blots, a sample of recombinant CCL25 that had not been incubated in complete media or with cells, was ran at the same time to compare the size of any product observed. It was found that

BMDCs, when cultured with CCL25 do not cleave the protein to produce a truncated form of CCL25 detectable by Western blotting (Figure 5.9 A). Culturing of BMDMs also resulted in no detectable chemokine cleavage, but in fact the BMDMs appeared to consume the CCL25 as no chemokine was detected in the three triplicate wells (Figure 5.11 A). The samples were run a second time on a new gel with the same result (data not shown).

## 5.12 Summary

The results shown in this chapter demonstrate that:

1. flCCL21 can be truncated by mouse BMDCs to produce a ~8kDa tCCL21
2. Both immature and mature BMDCs can truncate flCCL21.
3. Human DCs are able to truncate flCCL21 to produce a ~8kDa tCCL21 protein *in vitro*.
4. Mouse B cells, T cells and BMDMs are ineffective at truncating flCCL21 *in vitro* and are able to consume extracellular CCL21.
5. Cells isolated from mouse spleen and lymph nodes of WT mice can truncate CCL21 *in vitro*.
6. A truncated version of CCL21 is present at low levels in the spleen and lymph nodes of WT and CCR1-deficient mice
7. flCCL21 appears to be differentially truncated *in vitro* and *in vivo* producing a ~8kDa fragment *in vitro* and ~10kDa fragment *in vivo*.
8. BMDC-conditioned medium is unable to truncate flCCL21 *in vitro* and the generation of tCCL21 is probably not mediated by CCR7.
9. Mouse BMDCs can truncate flCCL2 *in vitro* to produce a ~8kDa tCCL2 protein but neither BMDCs nor Bone marrow-derived macrophages do not truncate CCL25.

These observations are discussed in greater depth in the Discussion (Chapter 6).

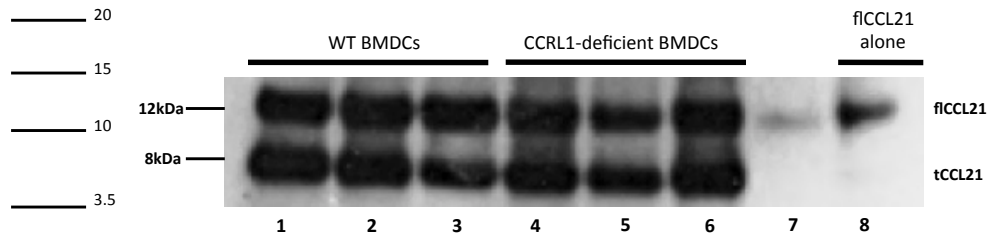


**Figure 5.1: WT and CCRL1-deficient BMDCs cleave full length CCL21 to produce a soluble CCL21 fragment.**

WT and CCRL1-deficient BMDCs were generated by culturing bone marrow cells with 40ng/mL GMCSF for 7 days.  $6 \times 10^5$  BMDCs in 100 $\mu$ l of complete media were cultured with 150ng of mouse fCCL21 for 16 hours. Supernatants were harvested and the presence of tCCL21 examined by Western blotting. Molecular weight was determined by electrophoresing molecular weight markers in a lane adjacent to the test samples (representative molecular weight markers are shown on the left hand side of the blot). Lanes 1-3 show WT BMDCs cultured in triplicate from 3 individual mice and lanes 4-6 represents show CCRL1-deficient BMDCs cultured in triplicate from 3 individual mice. Lane 7 is blank (but contains some spillover from Lane 8) and lane 8 “CCL21 alone” represents a sample of fCCL21 ran without prior incubation in complete media or with cells. The approximate molecular weight of the two protein bands detected is indicated on the right hand side of the blot.

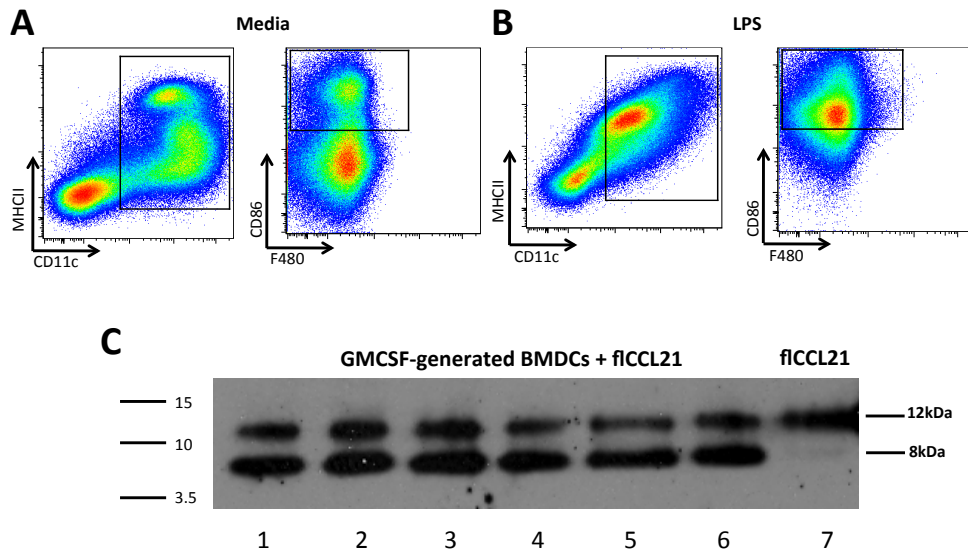


**Figure 5.2: Unactivated and LPS-matured BMDCs truncate ficCLL21 to the same degree.**

BMDCs were generated by culturing bone marrow cells with 40ng/mL of GMCSF for 7 days, after which they were treated with or without 1 $\mu$ g/mL of LPS for 24 hours. 150ng/mL of mouse ficCLL21 was then added to each culture containing 6 $\times$ 10<sup>5</sup> BMDCs in 100 $\mu$ L of complete media and supernatants and cells harvested 16 hours later. Flow cytometry was used to analyse unactivated (A) or LPS-activated (B) BMDCs. Western blot of supernatants from these cultures probed with anti-CCL21 antibody (C). Molecular weight was determined by electrophoresing molecular weight markers in a lane adjacent to the test samples (representative molecular weight markers are shown on the left hand side of the blot). The approximate molecular weight of the two protein bands detected is indicated on the right hand side of the blot. Lanes 1-3 represent experimental triplicates from BMDCs + ficCLL21, 4-6 represent LPS-matured BMDCs + ficCLL21 and lane 7 represent ficCLL21 only.

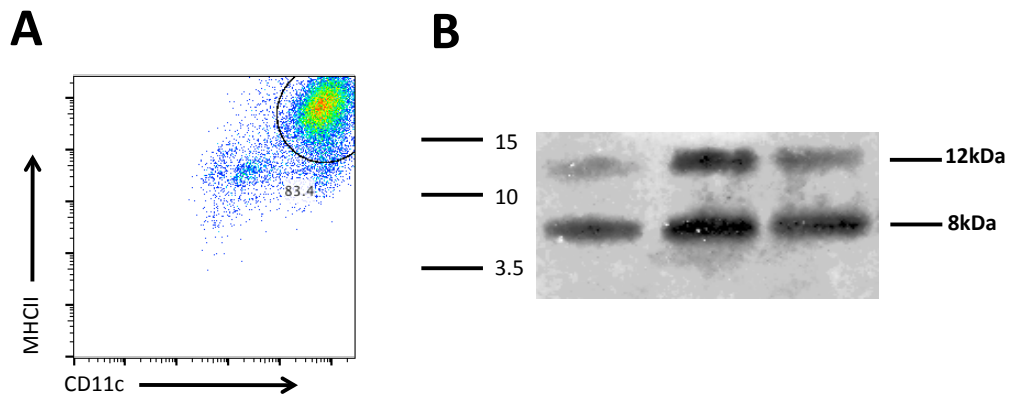


**Figure 5.3: FIt3L-matured BMDCs mediate CCL21 truncation *in vitro*.**

BMDCs were generated by culturing bone marrow cells from WT mice for 9 days with FIt3L. The presence of CD11c<sup>+</sup> MHCII<sup>hi</sup> BMDCs was assessed by flow cytometry (A).  $6 \times 10^5$  BMDCs in 100 $\mu$ L of complete media were cultured with 150ng of mouse fCCL21 for 16 hours. Supernatants were harvested from three biological replicates and the presence of fCCL21 and tCCL21 assessed by Western blot (B). Molecular weight was determined by electrophoresing molecular weight markers in a lane adjacent to the test samples (representative molecular weight markers are shown on the left hand side of the blot). The approximate molecular weight of the two protein bands detected is indicated on the right hand side of the blot.

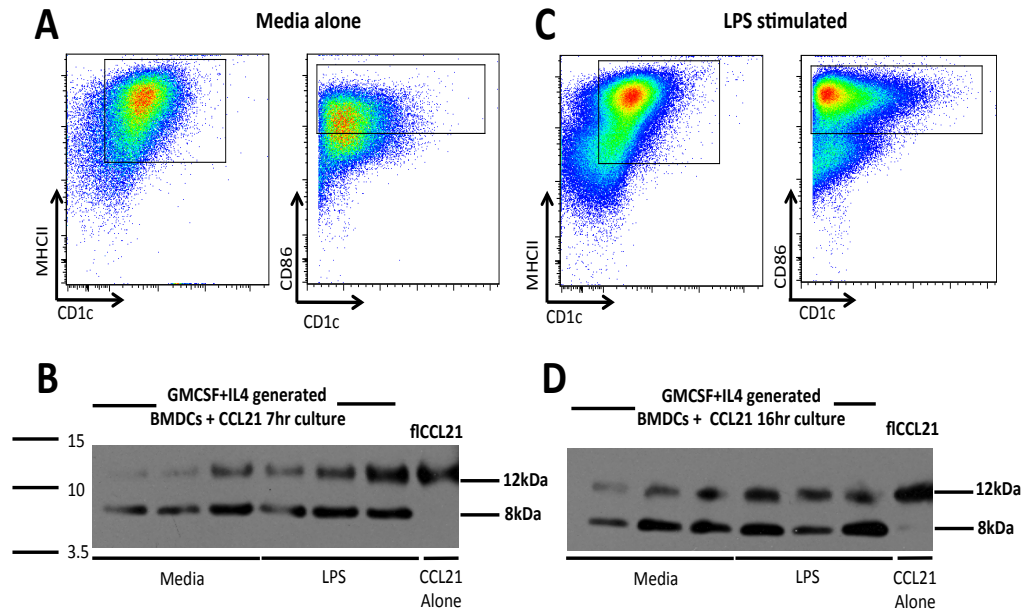


**Figure 5.4: fICCL21 chemokine is cleaved by human DCs, and this is unaffected by LPS activation.**

(A) Human PBMCs were incubated for 9 days with 100ng/mL of GMCSF and 40ng/mL of IL-4 to drive the maturation of DCs.  $6 \times 10^5$  DCs in 100 $\mu$ L of complete media were placed in each well of a 96 well plate, treated with or without 1mg/mL LPS for 24 hours and then 150ng of human fICCL21 was added. Supernatant was harvested 7 and 16 hours after fICCL21 addition. (A and C) Flow cytometry was used to analyse cultured cells grown in the absence (A) or presence (C) of LPS. Western blots, probed with anti-CCL21 antibodies, of supernatant taken 7 hours (B) or 16 hours (D) after CCL21 addition. 'fICCL21 alone' samples represents recombinant fICCL21 loaded onto the gel without prior incubation in complete media or complete media containing cells. For each condition, samples were done in triplicate representing three individual humans. Molecular weight was determined by electrophoresing molecular weight markers in a lane adjacent to the test samples (representative molecular weight markers are shown on the left hand side of the blots). The approximate molecular weight of the two protein bands detected is indicated on the right hand side of the blot.

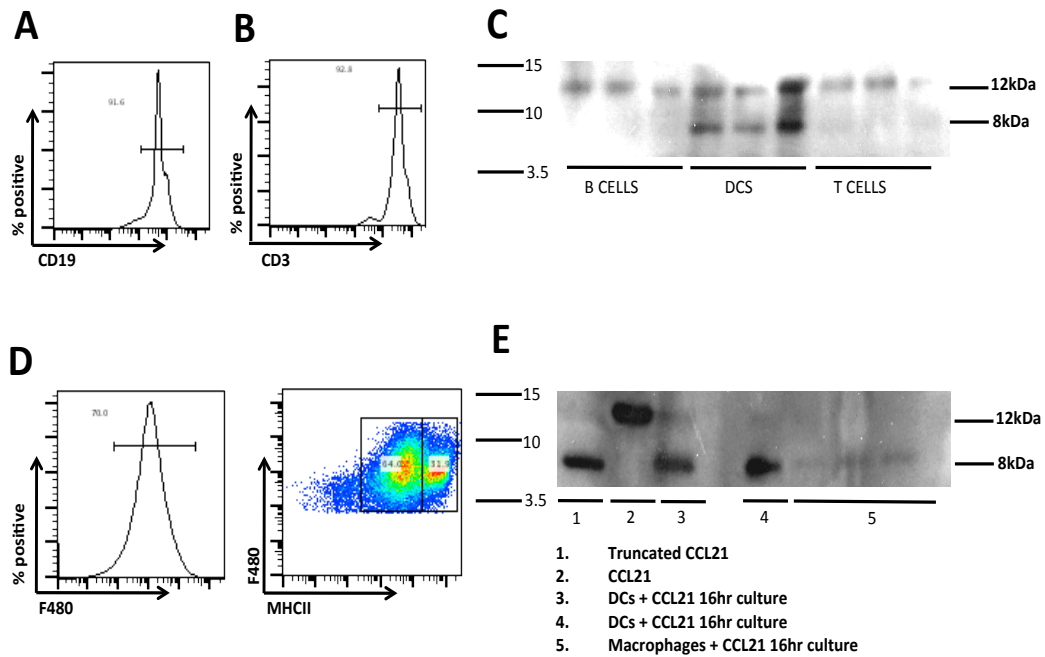


**Figure 5.5: ficCCL21 can be truncated by DCs, T cells and macrophages.**

Flow cytometry plots showing B cells (A) and T cells (B) enriched from WT mouse spleens using magnetically-labeled bead isolation kits specific for CD19<sup>+</sup> and CD3<sup>+</sup> cells respectively. Macrophages and DCs were generated by culturing bone marrow cells for 7 days with MCSF or GMCSF respectively. (C) 6x10<sup>5</sup> T cells, B cells or DCs were individually cultured in the presence of 150ng of recombinant ficCCL21 for 16 hours and the presence of ficCCL21 and tCCL21 assessed by Western blot. For each cell type, samples were done in triplicate representing 3 individual donor mice. (D) Representative flow cytometry profile of cells from M-CSF treated bone marrow cultures. BMDMs were first identified as F480<sup>+</sup>, and within this population, MHCII<sup>+</sup> and MHCII<sup>hi</sup> BMDMs were present (E). Western blot analysis of supernatants from BMDC cultures (lanes 3 and 4) and BMDMs (lanes 5,6 and 7) probed with anti-CCL21 antibody. Lane 1 shows purified tCCL21 and lane 2 shows ficCCL21 straight from the tube. 2 lanes for DC cultures + ficCCL21 and 3 lanes for BMDMs + ficCCL21 are shown representing 2 and 3 donor mice, respectively. Molecular weight was determined by electrophoresing molecular weight markers in a lane adjacent to the test samples (representative molecular weight markers are shown on the left hand side of the blots). The approximate molecular weight of the two protein bands detected is indicated on the right hand side of the blot.

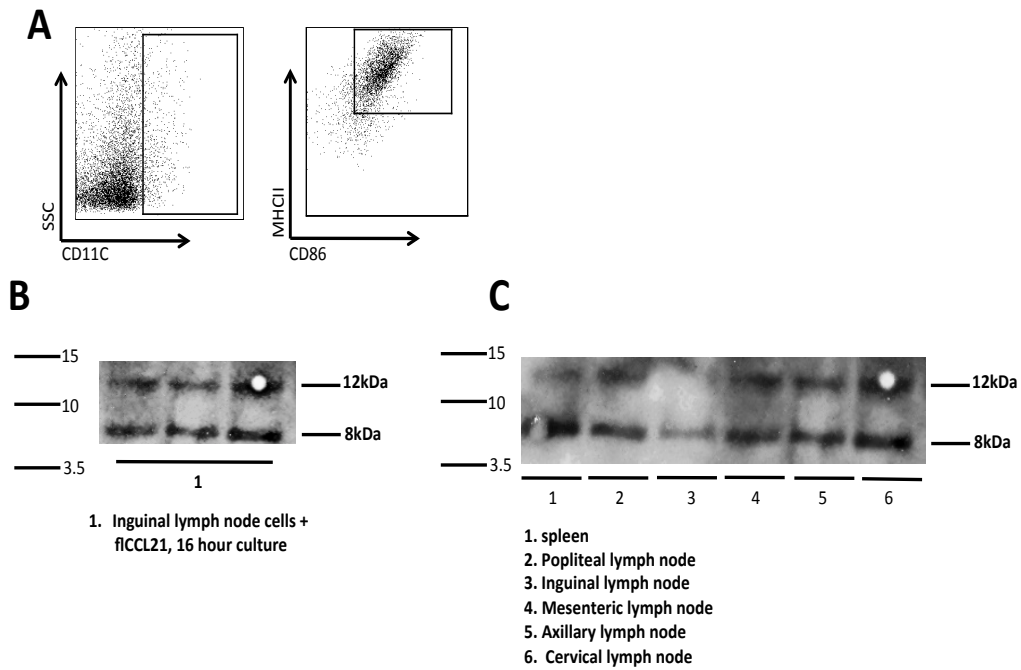


**Figure 5.6: tCCL21 is generated from fCCL21 by culture with cells from WT secondary lymphoid tissues.**

(A) Single cell suspensions were made from WT inguinal lymph nodes. Cells were stained with anti-CD11c, anti-MHCII and anti-CD86 antibodies and the presence of CD11c<sup>+</sup> MHCII<sup>+</sup> CD86<sup>+</sup> DCs identified by flow cytometry. (B)  $6 \times 10^5$  inguinal lymph node cells were cultured with 150ng of fCCL21 chemokine for 16 hours. The presence of fCCL21 and tCCL21 was assessed by Western blotting using anti-CCL21 antibody (B). 3 lanes for inguinal lymph node cell cultures + fCCL21 are shown representing 3 individual donor mice. (C)  $6 \times 10^5$  cells from the spleen, popliteal, inguinal, mesenteric, axillary and cervical lymph nodes of WT mice were isolated and cultured with 150ng of fCCL21 for 16 hours. The presence of fCCL21 and tCCL21 was assessed by Western blot using anti-CCL21 antibody. Molecular weight was determined by electrophoresing molecular weight markers in a lane adjacent to the test samples (representative molecular weight markers are shown on the left hand side of the blots). The approximate molecular weight of the two protein bands detected is indicated on the right hand side of the blot.

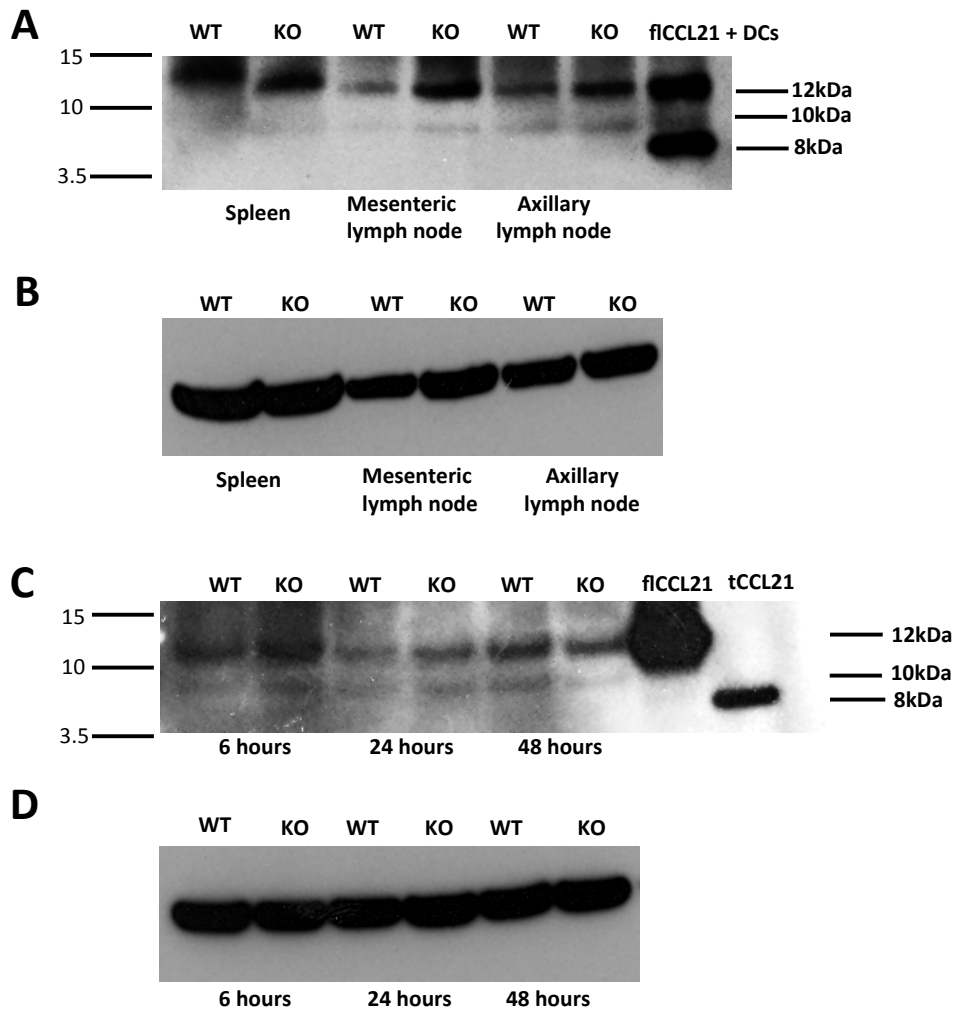


**Figure 5.7: tCCL21 is found in the spleen, mesenteric and axillary lymph nodes of WT and CCRL1-deficient mice and its abundance is unaffected by CCRL1-deficiency at rest or during skin inflammation.**

Spleen, mesenteric and axillary lymph nodes were harvested from WT and CCRL1-deficient mice and tissue homogenates were prepared. These homogenates were then assessed for the presence of ficCCL21 and tCCL21 by Western blot using anti-CCL21 antibody. Lane 7 represents a sample from BMDCs+ficCCL21 (A). Blots were stripped and re-probed for  $\beta$ -actin to assess protein loading (B). (C-D) Inguinal lymph nodes from WT and CCRL1-deficient (KO) mice were harvested 6, 24 and 48 hours after topical application of TPA on the dorsal flank. Lymph node homogenates were made and assessed for the presence of ficCCL21 and tCCL21 by Western blot (C). Blots were stripped and re-probed for  $\beta$ -actin to assess protein loading (D). Molecular weight was determined by electrophoresing molecular weight markers in a lane adjacent to the test samples (representative molecular weight markers are shown on the left hand side of the blots). The approximate molecular weight of the three protein bands detected is indicated on the right hand side of the blot.

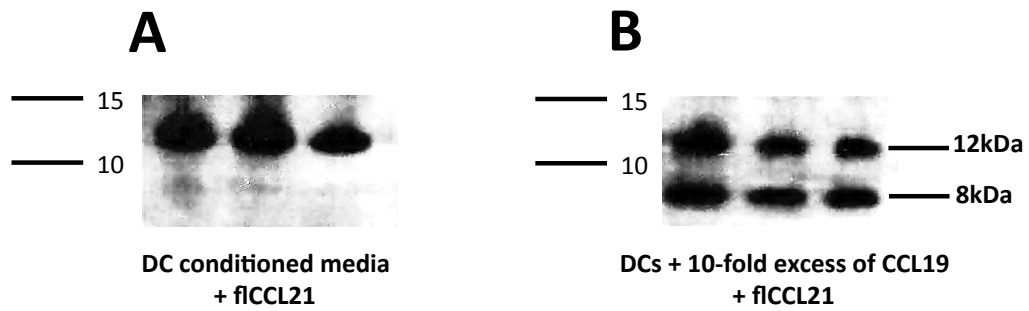


**Figure 5.8: Cleavage of CCL21 is not mediated by CCR7 or DC-conditioned medium.**

BMDCs were generated by culturing bone marrow cells with GMCSF for 7 days.  $6 \times 10^5$  BMDCs were cultured in 100 $\mu$ l of complete media for 16 hours in order to generate “BMDC conditioned media”. 100 $\mu$ l of BMDC conditioned media was cultured with 150ng of flCCL21 for 16 hours. The presence of flCCL21 and tCCL21 was assessed by Western blot using anti-CCL21 antibody (A).  $6 \times 10^5$  DCs were cultured for 16 hours with (1.5 $\mu$ g) ‘10-fold excess’ of CCL19 to block CCR7 binding sites. These BMDCs were then cultured with 150ng of flCCL21 in 100 $\mu$ l of complete media for 16 hours and the presence of flCCL21 and tCCL21 detected by Western blot using anti-CCL21 antibody (B). Molecular weight was determined by electrophoresing molecular weight markers in a lane adjacent to the test samples (representative molecular weight markers are shown on the left hand side of the blots). The approximate molecular weight of the two protein bands detected is indicated on the right hand side of the blot.

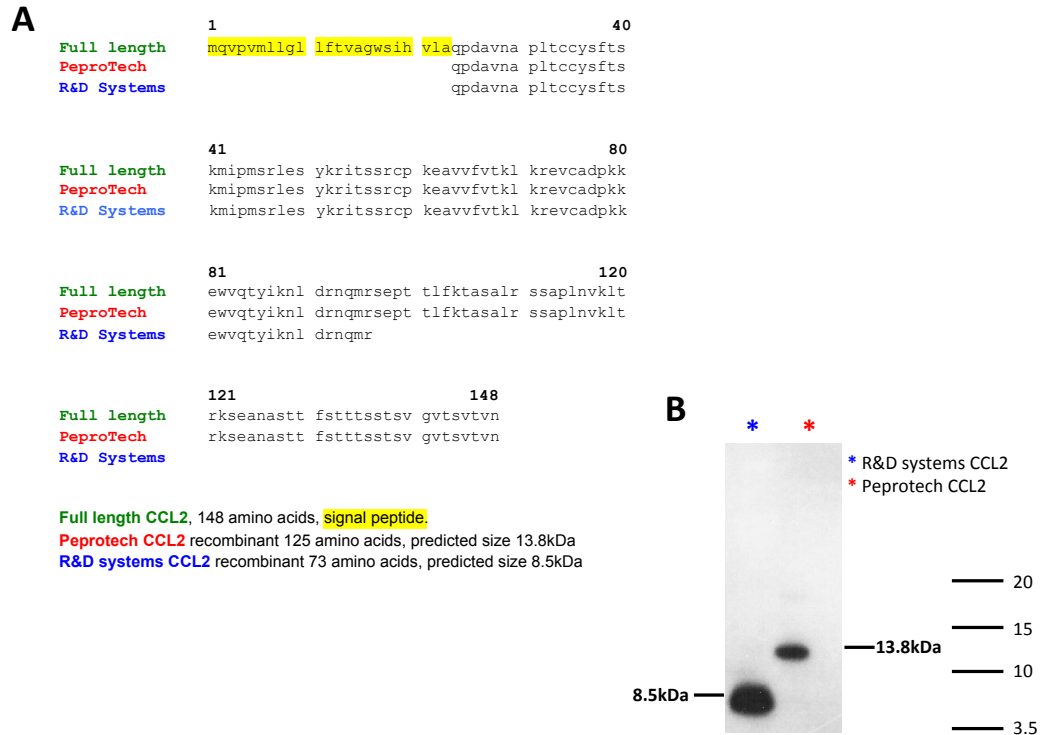


**Figure 5.9: There are two commercially available mouse CCL2 chemokines with different molecular weights.**

Recombinant CCL2 chemokine is commercially available from PeprTech and a C-terminally truncated form is available from R&D systems. (A) The amino acid sequence of “full length” CCL2, indicating the location of the signal peptide. CCL2 cDNA encodes a 148 amino acid precursor protein, and after cleavage of the signal peptide, yields a 125 amino acid mature protein. PeprTech CCL2 corresponds to the mature 125 amino acid protein without the signal peptide (A). CCL2 from R&D is 73 amino acids in length and lacks residues 96 – 148 (A). 100ng of recombinant CCL2 from PeprTech and 200ng of recombinant CCL2 from R&D were analysed by Western blot, probed with anti-CCL2 antibody. Molecular weight was determined by electrophoresing molecular weight markers in a lane adjacent to the test samples (representative molecular weight markers are shown on the right hand side of the blot). The approximate molecular weight of the two protein bands detected is indicated on the left and right hand side of the blot.

	1								50
<b>Full length</b>		mklwlfacly	acfv	gawmpv	vhaqqafedc	clgyqhrikw	nvlrharnyh		
<b>R&amp;D Systems</b>					vhaqqafedc	clgyqhrikw	nvlrharnyh		
	51								100
<b>Full length</b>		qqevsgscnl	ravr	fyfrqk	vvcgnpedmn	vkramrilta	rkrlvhwk	sa	
<b>R&amp;D Systems</b>		qqevsgscnl	ravr	fyfrqk	vvcgnpedmn	vkramrilta	rkrlvhwk	sa	
	101								144
<b>Full length</b>		sdsqterkks	nhmkskvenp	nstsvrsatl	ghprmvmmpr	ktnn			
<b>R&amp;D Systems</b>		sdsqterkks	nhmkskvenp	nstsvrsatl	ghprmvmmpr	ktnn			
<b>Full length,</b>	<b>144 amino acids,</b>	<b>23 aa</b>	<b>signal peptide</b>						
<b>R&amp;D Systems,</b>	<b>121 amino acids,</b>	<b>predicted size:</b>	<b>14kDa</b>						

**Figure 5.10: The amino acid sequence of full length mouse CCL25 and recombinant mouse CCL25 from R&D systems.**

Recombinant CCL25 chemokine is commercially available from R&D Systems. The amino acid sequence of “full length” CCL25, indicating the location of the signal peptide. CCL25 cDNA encodes a 144 amino acid precursor protein, and after cleavage of the signal peptide, yields a 121 amino acid mature protein. R&D Systems CCL25 corresponds to the mature 121 amino acid protein without the signal peptide.

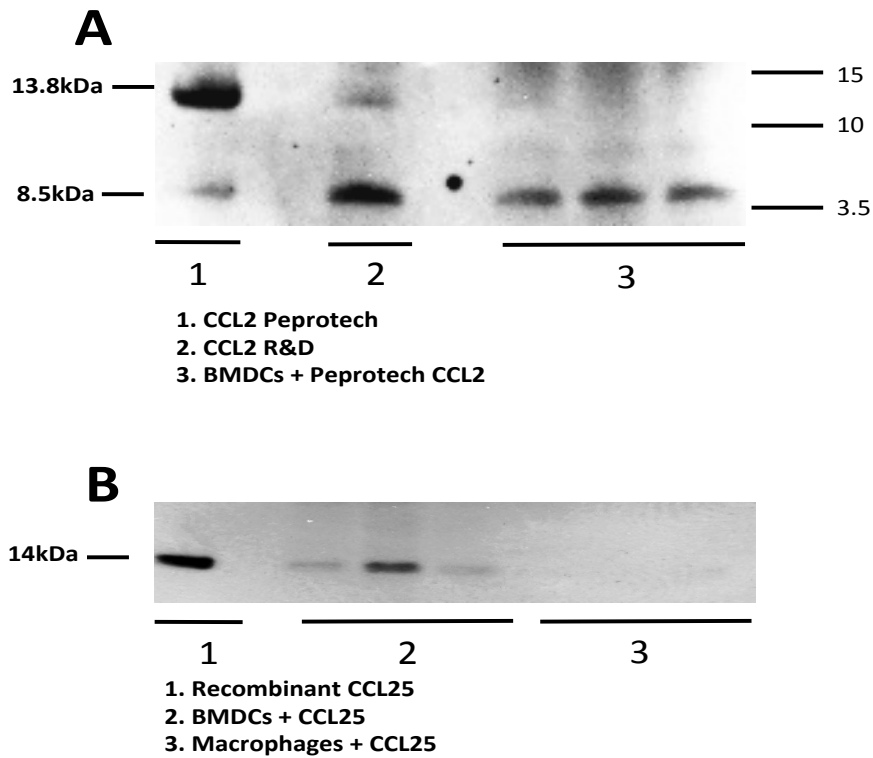


**Figure 5.11: BMDCs cleave full length CCL2 but DCs and macrophages are unable to cleave CCL25.**

150ng of PeproTech CCL2 and 150ng of R&D Systems CCL2 was cultured in 100 $\mu$ l of complete media for 16 hours. Supernatant was then harvested and the presence of CCL2 detected by Western Blot using anti-CCL2 antibody (A Lanes 1-2). DCs were generated by culturing bone marrow cells with GMCSF for 7 days.  $6 \times 10^5$  BMDCs were cultured with 150ng of PeproTech CCL2 for 16 hours and the presence of fCCL2 and tCCL2 was assessed by Western blot using anti-CCL2 antibody (A lanes 3). DC cultures are shown in triplicate representing 3 individual donor mice (B). CCL25 from R&D Systems was cultured for 16 hours in 100 $\mu$ l of complete media, supernatant harvested and then analysed by Western blot using anti-CCL25 antibody (B lane 1). BMDCs and macrophages were generated by culturing bone marrow cells with 40ng/mL GMCSF or 40ng/mL MCSF respectively, for 7 days.  $6 \times 10^5$  BMDCs and  $6 \times 10^5$  BMDMs were cultured separately with 100ng of CCL25 and the presence of fCCL25 and tCCL25 detected by Western blot using anti-CCL25 antibody (B 2 and 3). BMDC and BMDMs cultures are shown in triplicate representing 3 individual donor mice (B 2 and 3) Molecular weight was determined by electrophoresing molecular weight markers in a lane adjacent to the test samples.

# Chapter Six

## Discussion

## 6 Discussion

As the location of any immune cell is a critical component of its function, it is important to understand how immune cells move. To do so, we must have a firm understanding of chemokines and chemokine receptors, the main facilitators and regulators of cellular movement. Chemokines must be tightly controlled in order to prevent the aberrant localisation of immune cells that could be harmful to the host. The induction of cell movement is not the only function of chemokines. They can induce degranulation<sup>384,385</sup>, regulate cell survival<sup>231,341</sup> and direct angiogenesis<sup>346,355</sup> and these processes must also be properly regulated. Uncontrolled chemokine bioavailability could have a profound impact on the immune system. To prevent immune dysregulation, there is, within this highly heterogeneous network of chemokines and receptors, a family of atypical chemokine receptors that regulate the chemokine family and the immune system as a whole. These receptors are unified by their apparent inability to induce intracellular signaling after chemokine binding. One member of this family is CCRL1, which, like CCR7, is able to bind CCL19 and CCL21. CCRL1 also binds to the CCR9 ligand CCL25. *In vitro* and *in vivo* studies have led to the proposal that CCRL1 represents a novel way that CCL19, CCL21 and CCL25 can be controlled at a post-translational level.

When I began this thesis, much of our understanding of the scavenging capability of CCRL1 was derived from *in vitro* studies. However, from studies using *in vivo* models of disease, it is becoming clear that CCRL1 modulates adaptive immune responses. In the EAE model, CCRL1-deficient mice were shown to develop a more rapid onset of CNS pathology compared to WT counterparts<sup>361</sup>. Interestingly, CCRL1-deficient mice had also been described as having fewer migratory DCs in their skin-draining lymph nodes during homeostasis<sup>360</sup>. DCs are critical for the initiation of adaptive immune responses, and the maintenance of peripheral tolerance. Taking this into account, the initial aim of this project was to explore the impact of genetic deletion of CCRL1 on the migration of specific DC subsets. With the skin identified as one of the main peripheral sites of CCRL1 expression<sup>360</sup>, I focused on investigating the migration of skin-derived DCs to lymph nodes. In parallel, I also investigated the role of CCRL1 in the lymph node. Earlier studies involving CCRL1<sup>+gfp</sup> reporter mice identified the

SCS of lymph nodes as an area of CCRL1 expression<sup>360</sup> and this expression appears to be restricted primarily to LECs. This important lymph node gateway acts as an entry point for leukocytes, including DCs, that traverse the floor of the SCS in a CCR7-dependent manner to gain entry into the lymph node, and finally, to migrate towards the parenchyma. I investigated the impact that deletion of CCRL1 had on cells resident within the lymph node. Specifically, I examined the positioning and abundance of tissue-resident CD169<sup>+</sup> macrophages, that position within the SCS, medulla and interfollicular regions of the lymph node. As these macrophages form close contacts with CCRL1<sup>+</sup> cells, I explored the abundance and positioning of CD169<sup>+</sup> SCS macrophages and other cells that are located at or adjacent to the SCS region of lymph nodes.

Whilst *in vitro* studies have shown that CCRL1 is capable of scavenging CCL21, at the beginning of this thesis, a paper was published describing the post-translational truncation of fCCL21 by DCs to produce a tCCL21 protein<sup>383</sup>. This paper was the first to describe a dual role for CCL21 as being able to exert its chemotactic cues in both an insoluble and soluble form. The truncation of fCCL21 by leukocytes represents another way that bioavailable CCL21 can be controlled at a post-translational level. Thus, efforts were made to understand the mechanism of leukocyte-mediated truncation of fCCL21, and to compare truncation between mice and humans. These studies also extended to encompass the investigation into truncation of other C-terminus extended chemokines.

## **6.1 Basal DC trafficking in CCRL1-deficient mice**

As mentioned previously, a study by Heinzl and colleagues published in 2007 reported that, CCRL1-deficient mice have fewer migratory DCs in their skin-draining lymph nodes than WT mice at rest<sup>360</sup>. However, their characterisation of DCs was limited to CD11c and MHCII expression with migratory DCs defined as CD11c<sup>+</sup> MHCII<sup>hi</sup><sup>360</sup>. To expand on these findings, I employed a series of markers known to identify specific populations of DCs that emanate from the skin<sup>172,183,185,386</sup>. Surprisingly, and in contrast to reports by Heinzl, I found no difference in the total number of migratory CD11c<sup>+</sup> MHCII<sup>hi</sup> DCs in skin-draining inguinal lymph nodes at rest, although I consistently found a trend

towards lower numbers in the CCRL1-deficient mice. Notably, the difference seen by Heinzl and colleagues, although significant, was subtle, and the use of a larger group size in my studies may have resulted in a significant difference between strains. However, of note, a former PhD student from our lab was also unable to find any impact of CCRL1 deficiency on CD11c<sup>+</sup> MHCII<sup>hi</sup> cell abundance in skin-draining lymph nodes (C.Hurson 2010). Furthermore, the mouse strain used in the Heinzl study (FVB) was different to the strain I used (C57Bl6/J) and so this is another explanation for the inconsistency in results. However, when I fractionated migratory DCs based on expression of CD103 and Langerin, I found that there was a specific reduction in two DC populations; Langerhans cells and CD103<sup>+</sup> Langerin<sup>+</sup> dermal DCs. This was accompanied by an increase in CD11c<sup>+</sup> MHCII<sup>+</sup> DCs in the skin of CCRL1-deficient mice. As there was no difference in the percentage of live cells or CD45<sup>+</sup> cells in the skin between WT and CCRL1-deficient strains, this showed that there was no gross changes in the cellularity or cell death in the skin. CD103<sup>+</sup> Langerin<sup>+</sup> dermal DCs were increased in abundance on the skin of CCRL1-deficient mice, indicating that their reduced abundance in the inguinal lymph nodes may be at least due in part to defective egress from the skin. This is possibly due to the loss of gradient formation in the skin, as CCL21 gradients in the skin have been shown to be instrumental for the guidance of DCs into lymphatic vessels<sup>266</sup>. All other DC subsets in the skin were unaffected by deletion of CCRL1 at rest, including Langerhans cells, which are under-represented in the inguinal lymph node at rest. Others have shown that Langerhans cells have a normal distribution and abundance in the epidermis of CCRL1-deficient mice compared with WT counterparts<sup>360</sup>. These cells are a self-renewing population of skin-resident DCs, therefore, it is possible that they are defective in their egress from the skin but their numbers are controlled locally. However, it is possible that these cells depart the skin normally, but they fail to enter the lymph nodes. The possible mechanisms at play during rest is represented in (Figure 6.1).

A paper published towards the end of my studies demonstrated that CCRL1 is expressed by ceiling LECs (cLECs) in lymph nodes. These cells line the roof of the SCS, and were shown to support CCL21 gradient formation that emanates from the SCS and protrudes into lymph node interfollicular regions. This

gradient was shown to be required for the migration of DCs into the lymph node and towards T cell areas. Deletion of CCRL1 resulted in higher levels of bioavailable CCL21 at the SCS and interfollicular regions. When intralymphatically injected BMDCs were enumerated in the lymph nodes of CCRL1-deficient mice, they were found to be held up within the SCS region of these mice, whereas they localised in T cell zones in WT mice. Furthermore, endogenous Langerin<sup>+</sup> DCs were found to localise in the SCS region whereas these cells were virtually absent from the SCS of WT mice. This shows that CCRL1 expression at the SCS region of the lymph node guides the entry of skin-derived DCs into the lymph node parenchyma. However, in the same study, the lymph node cellularity of CCRL1-deficient mice was found to be lower than WT animals. There was also less total B cells and T cells in the lymph nodes of CCRL1-deficient mice although the proportions of these cells were comparable to WT mice. These findings have not been reproduced in our lab, thus, these discrepancies require further investigation. It is possible that the animal facility that the mice are housed effects of the number of these cells. In any case, we must resolve the differences in the findings between the two labs.

## **6.2 The Role of CCRL1 in Regulating DC trafficking during inflammation**

CCR7 drives the migration of DCs from the periphery during homeostasis but is also important during inflammation<sup>58,387</sup>. DCs up regulate CCR7 expression during activation in order to facilitate their migration towards lymph nodes<sup>189,366</sup>. To investigate DC migration during inflammation, a variety of simple models of skin inflammation were used, and in each model, defects in DC trafficking could be inferred from the data. Furthermore, I was able to show that CCR7 is required for the migration of DCs from the skin to the lymph node during these models, as genetic deletion of CCR7 resulted in very few DCs in the lymph nodes compared with WT mice. The first model undertaken involved painting the dorsal skin with FITC to induce DC mobilisation, and to track the migration of skin-derived DCs to the lymph node. The total number of FITC<sup>+</sup> migratory DCs was reduced in the skin draining inguinal lymph nodes of CCRL1-deficient mice 48 hours after the application of FITC. Thus, mild skin inflammation results in a lower abundance

of skin-derived migratory DCs in the draining lymph nodes. This experimental set-up was also undertaken by Heinzl and colleagues, but lymph nodes were harvested 24 hours after the application of FITC. They found no difference in the number of migratory CD11c<sup>+</sup> MHCII<sup>hi</sup> DCs in the skin-draining lymph nodes. This shows that CCRL1 can control the migration of DCs from the skin during models of skin inflammation but only within a defined period of time. As there was a large number of skin-derived migratory DCs in WT and CCRL1-deficient mice, it can be inferred that the reduction in FITC<sup>+</sup> DCs in CCRL1-deficient animals after painting with FITC is unlikely to be attributed to there being fewer DCs in the skins of these animals. This is substantiated by the fact that I have demonstrated how, at rest, both strains contain comparable frequencies of DCs in the skin. Further work should be done to characterise FITC<sup>+</sup> DCs in the lymph node based on Langerin and CD103 expression, as this staining combination was adopted in subsequent experiments involving TPA painting. By including these markers it would be possible to identify specific DC populations and determine whether all subsets are reduced after FITC painting or if the defect in DC migration is subset specific. Furthermore, analysis of the DCs in the skin during this model will help to relate any possible defects in DC subsets found in the skin-draining lymph nodes.

Next, I investigated DC migration during a non-invasive, self-resolving, skin inflammation model involving the painting of the back skin with TPA. TPA painting induces an acute inflammatory reaction resulting in edema, erythema and infiltration of inflammatory leukocytes<sup>388</sup>. This is a common model of skin inflammation used both in the literature and in our lab and it has been used previously to explore skin inflammation in D6-deficient mice<sup>306</sup>. FITC was also painted onto the skin to identify DCs in the lymph node that had originated in the skin. 24 hours after TPA, a far greater number of migratory DCs were present in the lymph nodes of WT and CCRL1-deficient mice compared with numbers seen at rest. However, no difference in the abundance of CD11c<sup>+</sup> MHCII<sup>hi</sup> migratory DCs or FITC<sup>+</sup> skin-derived migratory DCs was found when comparing CCRL1-deficient mice with WT animals. One population of dermal DCs (CD103<sup>+</sup> Langerin<sup>-</sup>) amongst the FITC<sup>+</sup> migratory DC population, was found to be less abundant in the lymph nodes of CCRL1-deficient mice compared to WT

animals. Unsurprisingly, there were very few Langerhans cells in the lymph nodes of both mice strains. These cells take longer to migrate from the skin to lymph nodes after the induction of inflammation due to their positioning in the epidermis and the time it takes for them to migrate towards lymphatic vessels and to travel to the lymph node. Langerhans are present in the lymph node of WT and CCRL1-deficient mice at rest, but during the TPA model, as cells were pre-gated first on FITC<sup>+</sup> cells, no Langerhans cells were detected in the lymph nodes of either strain. This is because FITC labeling identifies cells that migrate during inflammation and not cells that migrate constitutively.

As Langerhans cells were reduced at rest, we were interested to explore the migration of these cells during inflammation. A period of 24 hours was placed between TPA and FITC application in an effort to allow sufficient time for Langerhans cells to migrate from the skin. FITC<sup>+</sup> Langerhans cells were present in the lymph nodes of WT and CCRL1-deficient mice during this model. Moreover, this approach revealed much more striking phenotypes in CCRL1-deficient mice than those observed when TPA and FITC were co-applied. The total number of migratory DCs in the lymph nodes of both WT and CCRL1-deficient mice was significantly higher than at rest, but less than when TPA&FITC were painted on the same day. The reduction in total migratory DCs was probably a result of cells dying after their activation, something that occurs to limit disproportionate immune responses<sup>56</sup>. Furthermore, CCRL1-deficient DCs were ~60% reduced whereas WT DCs were only ~20% reduced. This led me to hypothesise that CCRL1-deficient DCs were hindered in their ability to migrate out of the skin during this model, were less able to acquire FITC or were more susceptible to apoptosis. Using kaede mice, I demonstrated that DCs did not have differential antigen uptake capabilities between WT and CCRL1-deficient strains. I also showed that there was no difference in cell death between strains in cells examined from the skin or lymph nodes. However, the total number of migratory DCs, as well as each of the four skin-derived DC subpopulations was specifically reduced in the lymph node of CCRL1-deficient mice during the TPA-24-FITC model. This coincided with an increase in CD11c<sup>+</sup> MHCII<sup>+</sup> DCs in the skin at this timepoint. Within this population, only Langerhans cells were found to be increased in abundance in the skin with other

DC subsets unaffected by genetic deletion of CCRL1. Similarly, in another model of skin inflammation induced by injection of CFA, migratory DCs were also reduced in the lymph node of CCRL1-deficient mice coinciding with a specific reduction in Langerhans cells and CD103<sup>+</sup> Langerin<sup>+</sup> dermal DCs. These results demonstrate that CCRL1 controls the migration of DCs during different models of skin inflammation but within a defined period of time. These results also show that Langerhans cells are particularly prone to regulation by CCRL1 during inflammation resulting in their impaired localisation in skin-draining lymph nodes. This is because these cells are trapped in the skin and do not egress properly from this tissue by way of the lymphatic vessels. Further analysis of the skin involving *ex vivo* skin-crawl out assays showed that DCs have a reduced propensity to crawl out from skin explants of CCRL1-deficient mice with significantly less DCs accumulating in the culture medium compared with WT counterparts. At the same time, CD11c<sup>+</sup> DCs showed a higher abundance in the skin after the crawl out assay. Furthermore, there was a specific reduction in the egress of cells expressing markers of Langerhans cells. Taken together, these data would indicate that Langerhans cells have an impaired ability to egress the skin during inflammation.

There are several theories to explain why CCRL1 is only able to control DC migration from the skin within a defined period of time. The induction of skin inflammation with TPA induces the production of CCL19 and CCL21 by stromal cells and DCs in the skin. However, this takes time, and so, when TPA and FITC are painted at the same time, there is only a moderate increase in the bioavailability of these chemokines. In contrast, in the TPA-24-FITC model, bioavailable levels of CCL19 and CCL21 are increased, and are higher in CCRL1-deficient mice than WT counterparts. In WT mice, CCRL1 can control levels of these chemokines and maintain gradients, thus, cells are guided directionally towards lymphatic vessels in the skin. In CCRL1-deficient mice, CCL19 and CCL21 scavenging capabilities are lost, bioavailable chemokine levels increase, and gradient formation is diminished. As a consequence, DCs meander in the skin, moving in a non-directed fashion and possibly downregulate CCR7 expression due to receptor desensitisation coupled with the extended length of time spent in the skin. Together, these possibilities would account for

the accumulation of DCs in the skin (Figure 6.2). At the later timepoints, bioavailable levels of CCL19 and CCL21 were found to be comparable between WT and CCRL1-deficient mice (data not shown). This would indicate that CCRL1-independent mechanisms control the bioavailability of these chemokines at later timepoints. Furthermore, chemokines have a short half-life, and so 24 hours after TPA painting may represent the peak of chemokine production, after which, chemokine protein is degraded. At rest, CCRL1 has been shown to be expressed by cLECs in the lymph node. Therefore, it is possible that the DC subsets that were found to be unaffected in their abundance in the skin of CCRL1-deficient mice during inflammation may be affected by deletion of CCRL1 at the SCS of the lymph node. Further work that focuses on the migration of skin-derived DC populations into the lymph node during inflammation are required to understand the effect of CCRL1 deletion on their entry into lymph nodes.

It was unsurprising that Langerhans cell should be specifically affected by the loss of CCRL1 in the skin due to their positioning within the epidermis, as it is within this region that CCRL1 is expressed. We can make a firm ascertain that CCRL1, by virtue of its described role *in vitro* and from the data I have presented, functions within this region to control the proper and timely migration of Langerhans cells out of the skin. For future experiments, it would be informative to look at the level of CCR7 expression on Langerhans cells from the skin. It is possible that the increase in CCL19 and CCL21 bioavailability in this tissue leads to receptor desensitisation and so in CCRL1-deficient mice Langerhans cells may express less surface CCR7. These cells are known to take longer to depart the skin during inflammation<sup>187</sup>, so in the models used they are exposed to excessive bioavailable CCL19 and CCL21 for longer which could conceivably lead to CCR7 desensitisation and downregulation. It would also be interesting to investigate the positioning of these cells in the skin. We would expect that in CCRL1-deficient mice these cells will be positioned at or close to the epidermis, whereas in WT mice they may be closer to the lymphatic vessels in the dermis. This would provide further evidence that CCRL1 functions in the epidermis to establish chemokine gradients, guiding Langerhans cells towards lymphatic vessels in the dermis.

The fact that Langerhans cells show a specific migratory defect from the skin during models of skin inflammation is useful for the design of future experiments. Langerhans cells are known to initiate inflammatory immune responses to bacteria<sup>389</sup> and regulate contact hypersensitivity (CHS)<sup>181,390</sup>. Furthermore, these cells have been shown to play a crucial role in anti-viral immune responses whilst maintaining tolerance to commensal bacteria<sup>51,114,391-394</sup>. Therefore, in future experiments, it would be interesting to employ different models to investigate the affect that the aberrant migration of Langerhans cells from the skin has on the adaptive immune response. Specifically, mice could be challenged in the skin with viruses such as herpes simplex virus (HSV), human immunodeficiency virus (HIV) or varicella zoster virus (VZV) as these viruses have been used and described by others<sup>180,190,393,395</sup>. As Langerhans cells are described as playing a role in the initiation of the immune response to all these viruses, we would expect that the adaptive immune response would be affected by loss of CCRL1, and thus Langerhans cell migration from the skin. Similarly, as Langerhans cells regulate CHS, we could sensitise mice with dinitrofluorobenzene (DNFB) and then measure ear swelling after challenge with DNFB as a read out of the elicitation phase of CHS. We may expect that, as Langerhans cells have been described as negatively regulating CHS, that CCRL1-deficient mice would have exaggerated ear swelling over WT mice. In the TPA-24-FITC model, FITC<sup>+</sup> migratory DCs were reduced in the inguinal lymph nodes of CCRL1-deficient mice by ~50%. Therefore, as these cells are not completely absent in CCRL1-deficient mice, it would be interesting to investigate how a reduction in the abundance of these cells in the lymph node correlated with T cell responses. To answer this, we could transfer OT-I or OT-II transgenic T cells into WT and CCRL1-deficient mice and challenge in the skin with cutaneous OVA painting, after painting with TPA for 24 hours. We would expect that due to the fewer numbers of DCs in CCRL1-deficient mice, that these animals would undergo less T cell priming and thus we would expect to see less T cell proliferation in CCRL1-deficient animals. These types of experiments are planned for the future to help give us a functional read out of aberrant DC migration in CCRL1-deficient mice. It is hoped that these experiments will paint a clearer picture of the affect that deletion of CCRL1 has on the adaptive immune response.

Finally, these models represent acute inflammatory responses, however, it would be interesting to investigate the migration of DCs from the skin during a model of chronic inflammation. We can assume that chronic inflammation may drive the sustained production of CCL19 and CCL21, and in mice lacking CCRL1, this may lead to an exaggerated defect in DC migration than that seen during the short-term skin inflammation models used here.

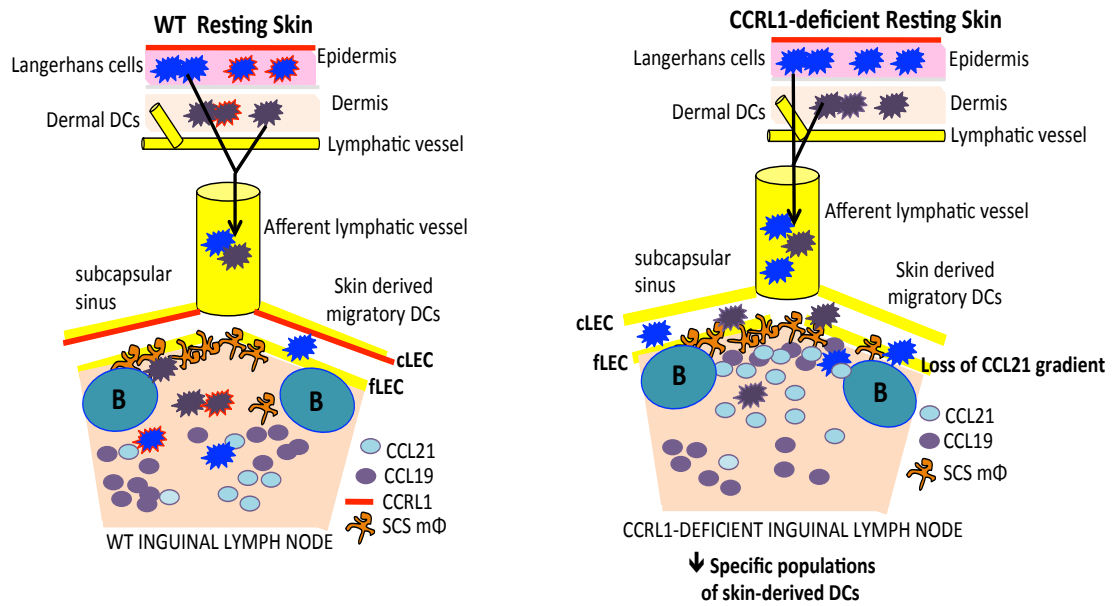


**Figure 6.1. Proposed mechanism of DC migration from the resting skin of WT and CCRL1-deficient mice.** CCRL1 is expressed by keratinocytes and LECs and coordinates the migration of DCs from the skin to the lymph node. At rest, specific populations of skin-derived DCs are held up in the SCS in CCRL1-deficient mice and their abundance in the lymph node is reduced. CCRL1 scavenges CCL21 at the SCS to coordinate the migration of DCs across the floor of the SCS. Loss of CCRL1 expression at the SCS results in accumulation of CCL21 leading to the loss of CCL21 gradients. This may also be true for CCL19.

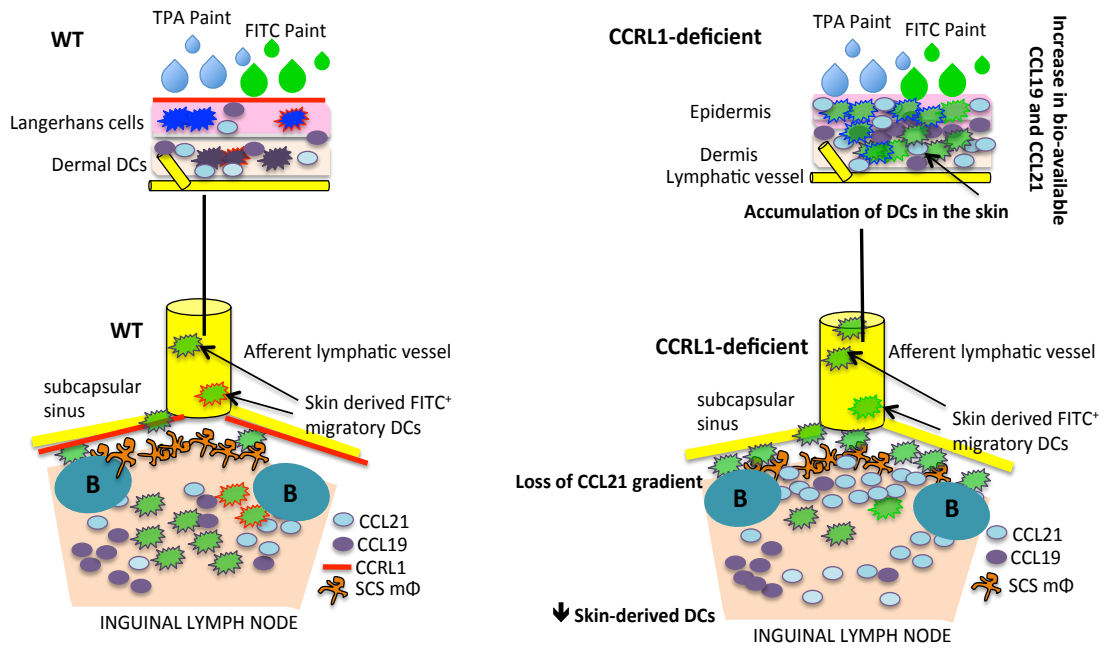


**Figure 6.2: Proposed mechanism of CCRL1-guided DC exit from the skin during inflammation.** CCRL1 is expressed by keratinocytes and LECs and coordinates the migration of all DC subsets from the skin to the lymph node during inflammation. TPA&FITC painting induces the production of CCL19 and CCL21 in the skin. These chemokines are not scavenged in CCRL1-deficient mice leading to an increase in their bioavailability. In CCRL1-deficient mice, skin DCs are exposed to high levels of CCL19 and CCL21 which desensitises CCR7 on these cells. DCs that reach the SCS do not enter the lymph node properly due to dysregulated gradients of CCL21, and possibly CCL19. The result is fewer migratory DC subsets in the lymph nodes of CCRL1-deficient animals.

## 6.3 The Role of CCRL1 at the SCS

In Chapter 4, I focused on characterising the affect that deletion of CCRL1 had on the abundance and positioning of cells within the lymph node. CCRL1 was shown by others<sup>360,368</sup>, and in Chapter 3, to be expressed by LECs lining the SCS of the lymph node. A population of lymph node resident CD169<sup>+</sup> macrophages closely associate with CCRL1 expressing cells in these tissues. Due to the close relationship between these cells, the functional consequences of CCRL1 deletion were explored, specifically in relation to these macrophages. This chapter also examined the affect of CCRL1 deficiency on innate-like T cells that are often found in the interfollicular regions of lymph nodes, as well as characterising CCRL1 expression in the spleen and the recruitment of CCR7<sup>+</sup> cells to this organ. Finally, due to their intimate association with LECs in lymph nodes, macrophage-driven lymphangiogenesis during inflammation was explored in CCRL1-deficient mice and WT animals.

### 6.3.1 CD169<sup>+</sup> SCS macrophages

First, the expression of CCRL1 in lymph nodes was explored using anti-CCRL1 antibody, and colocalisation with CD169 assessed. I found no CCRL1<sup>+</sup> CD169<sup>+</sup> cells, leading me to conclude that CD169 macrophages are CCRL1<sup>-</sup>. This agrees with published observations<sup>360</sup> and data from Immgen ([www.Immgen.org](http://www.Immgen.org)). I reasoned that CCRL1 may function in the lymph node to control the positioning and and/or the abundance of CD169<sup>+</sup> macrophages. This led us to explore if these cells express CCR7. If they do, then CCRL1-mediated regulation of CCL19 and CCL21 at the SCS might be involved in preventing the aberrant localisation of macrophages, keeping them anchored at this microanatomical region. Indeed, initial chemokine uptake assays with fluorescent CCL19 suggested that CD169<sup>+</sup> macrophages express CCR7. However, subsequent to these experiments, a paper was published describing a new method for identifying these cells by flow cytometry. In the paper, the authors describe how T cells acquire membrane blebs from macrophages during the digestion of lymphoid tissues to obtain single cell suspensions. Therefore, flow cytometry

analysis requires the inclusion of T cell specific markers to exclude contaminating T cells from macrophage gates in post acquisition analysis. When we revisited this experiment and included T cell exclusion markers, we found few, if any macrophages internalised CCL19, suggesting that these cells are not in fact CCR7<sup>+</sup>. Moreover, there was no difference in CD169<sup>+</sup> macrophage positioning or abundance in inguinal lymph nodes from WT and CCRL1-deficient mice. However, to our surprise, we found an obvious defect in macrophage abundance in the mesenteric lymph nodes of CCRL1-deficient mice. Absence of CCRL1 resulted in more CD169<sup>+</sup> macrophages in the mesenteric lymph node compared with WT counterparts, as determined by immunofluorescent staining and flow cytometry. Furthermore, this coincided with an expansion in the abundance of LYVE-1<sup>+</sup> LECs. Although the mechanisms remains unclear, it is possible that, because mesenteric lymph nodes drain the small intestine, in which CCL25 chemokine is highly expressed, dysregulated CCL25 draining into the mesenteric lymph node from the small intestine in CCRL1-deficient mice is the cause of this defect. It is possible that excess CCL25 from the small intestine travels in the lymph and arrives in the mesenteric lymph node driving the expansion of CD169<sup>+</sup> macrophages. However, we would then perhaps expect macrophages to express CCR9, but analysis by flow cytometry using anti-CCR9 antibody did not substantiate this. Furthermore, evidence for CCL25 dysregulation in the small intestine of CCRL1-deficient mice, is lacking, although it would merit future analysis. However, commercially available ELISA kits fail to reliably detect CCL25 protein, as confirmed by a comparison of WT and CCL25 deficient mice (Prof. Rob Nibbs, personal communication). Therefore, with lack of any clear evidence to suggest involvement of CCR7 or CCR9 expression on these cells, and lack of tools to quantify CCL25 protein, there was no obvious mechanism to explain why CD169<sup>+</sup> macrophages were affected by deletion of CCRL1. It would be interesting to explore whether macrophage expansion in the mesenteric lymph nodes was seen in mice doubly deficient for CCL25 and CCRL1. These mice have not been engineered but this may be something that our group explores in the future.

Another theory to explain these observations is that there may be a lymph-borne factor that specifically drives the proliferation of CD169<sup>+</sup> macrophages. To address this, we could cannulate lymph draining from the mesenteric lymph nodes of CCRL1-deficient mice and then inject this into the footpad of WT mice. We could then assess whether injected lymph drives CD169<sup>+</sup> macrophage expansion in the draining popliteal lymph node, which, at rest, has normal numbers and positioning of CD169<sup>+</sup> macrophages in WT and CCRL1-deficient mice. In future experiments, it would also be interesting to explore whether this defect in CD169<sup>+</sup> macrophages is present during development or if it is only present in the adult mouse. In adults, the gut flora may drive the mislocalisation of these cells by affecting the small intestine environment to alter the mesenteric lymph nodes. If this were the case, we could examine the mesenteric lymph nodes of WT and CCRL1-deficient germ-free mice. In fact, we considered whether the microflora in our animal facility may specifically drive this defect in mesenteric lymph node macrophages. However, CCRL1-deficient mice rederived at the Beatson Institute, and housed in SPF conditions, also exhibited this phenotype (data not shown).

Inguinal lymph nodes appeared normal in terms of macrophage localisation and number, and this was also true of popliteal and axillary lymph nodes (data not shown). Therefore, the results demonstrate that a facet of the gut immune system appears to specifically drive macrophage expansion in CCRL1-deficient mice. A previous PhD student in the lab explored the role of CCRL1 in the gut. She found that in the mesenteric lymph nodes of CCRL1-deficient mice there are few/if any pDCs. Moreover, she found that CCRL1-deficient mice could not be orally tolerised (E.Anderson, 2010). It would be interesting to explore if this defect in pDCs is related to defects I observed in CD169<sup>+</sup> macrophages. Interestingly, I also found in a small study that pDCs were significantly reduced in the liver of CCRL1-deficient mice, and that eGFP expression was detectable by flow cytometry on a liver stromal cell population in CCRL1<sup>+gfp</sup> mice (data not shown). Therefore, there is clear evidence to suggest that CCRL1 expression in the gastro-intestinal tract regulates leukocyte abundance and positioning.

Coinciding with the expansion of CD169<sup>+</sup> macrophages in the mesenteric lymph nodes of CCRL1-deficient mice, was an expansion of LYVE-1<sup>+</sup> LECs. Although

it is difficult to ascertain the mechanism underpinning the expansion of these cells, macrophages probably play a large part in this. Macrophages are known to produce large quantities of VEGF which drives lymphangiogenesis<sup>147,148</sup>. Furthermore, these cells have been described as playing roles in promoting vascularisation in tumors<sup>85,87,150</sup> and driving lymphangiogenesis during models of inflammation<sup>85,86,158,373</sup>. As CD169<sup>+</sup> macrophages are more abundant in the mesenteric lymph nodes of CCRL1-deficient mice, this could predispose these animals to an expansion in LYVE-1<sup>+</sup> LECs. It would be interesting to explore the gene expression profile of CCRL1-deficient and WT CD169<sup>+</sup> macrophages to look for differential expression of proangiogenic factors. Due to their prominent role in lymphangiogenesis during inflammation, this may explain why these cells have a specific effect in mesenteric lymph nodes. These lymph nodes, as mentioned previously, are constantly exposed to antigen, commensal bacteria and soluble inflammatory mediators draining from the small intestine. This is in contrast to other lymph nodes such as inguinal lymph nodes and popliteal lymph nodes that are only exposed to transient inflammation in response to insult in the skin. An alternative explanation is that chemokine dysregulation plays a direct role in driving the expansion of LECs in the mesenteric lymph node of CCRL1-deficient mice. Chemokines CXCL12 and CXCL1 have been shown by others to drive angiogenesis of endothelial cell precursors<sup>396</sup>. Furthermore, tumour conditioned Gr1<sup>+</sup> CD11b<sup>+</sup> myeloid cells have been shown to promote angiogenesis by secreting CCL2 and CXCL16<sup>397</sup>. This highlights the role of leukocytes and chemokines in driving lymphangiogenesis. Furthermore, chemokines and chemokine receptors that are of direct relevance to this thesis, CCL21 and CCR7, have been shown to play a direct role in the process of lymphatic vessel expansion. In a model of pancreatic cancer, this receptor ligand pairing has been described as playing a role in mediating microvessel density and microlymphatic vessel density in tumours<sup>398</sup>. Thus, chemokine dysregulation in CCRL1 deficient mice may directly enhance LEC expansion and this may even precede the increase in CD169<sup>+</sup> macrophages in mesenteric lymph nodes. It is possible that CD169<sup>+</sup> macrophages secrete these chemokines and support the expansion of LYVE-1<sup>+</sup> lymphatic vessels in CCRL1-deficient mice. Gene expression could also be investigated in LECs isolated from WT and CCRL1-deficient mesenteric lymph nodes. It is possible that deletion of CCRL1 affects

the gene expression profile of mesenteric lymph node LECs. Microarray analysis of FACS sorted LECs would help us to study this.

Collectively these data show that gastro-intestinal tract appears to be particularly permissive to regulation by CCRL1. Currently, a post-doc in our lab is working to characterise the relationship and consequences of the previously described observations. It is hoped that these preliminary findings, together with her findings, will help to shed new light on the role of CCRL1 in the immune system of the gut.

## 6.4 Innate-like lymphocytes

Recent publications have detailed the interplay between NK cells, CD169 macrophages, gamma delta T cells and innate like CD8<sup>+</sup> T cells at the SCS during infection<sup>83,124</sup>. I was therefore interested to see how the absence of CCRL1 affected these cells.

Compared to WT mice, the inguinal lymph node of resting CCRL1-deficient mice contained fewer NK cells, iNKT cells and  $\gamma\delta$  T cells, although only specific populations of iNKT cells were affected by the deletion of CCRL1. In the mesenteric lymph nodes of CCRL1 deficient mice, I found a reduction in the frequency of  $\gamma\delta$  T cells and subsets of iNKT cells. Therefore, cells known to reside within the SCS of lymph nodes appear to be affected by deletion of CCRL1. It would be interesting to investigate the expression of CCR7 or CCR9 on all of these cell populations and examine whether deletion of CCRL1 ligands, such as CCL19, corrects this defect in CCRL1-deficient mice. It would also be interesting to challenge CCRL1 deficient mice with bacteria or virus that is specifically targeted to reach mesenteric lymph nodes. As there is a profound degree of CD169 macrophage expansion in these lymph nodes, alongside reduced numbers of innate like cells involved in the restriction and clearance of virus and bacteria, it would be interesting to investigate the response mounted in these mice to challenge compared to WT mice. We would assume that these mice would show aberrant responses to virus or bacteria challenge, as CD169<sup>+</sup> macrophages and innate-like lymphocytes have been shown to be critical for the clearance of bacteria and viruses<sup>17,77,83,124</sup>.

## 6.5 The Spleen

The spleen is a unique lymphoid tissue both in terms of its architecture and its primary role within the immune system. The function of the spleen is to monitor and respond to foreign antigen and pathogens in the blood and is instrumental in the filtration of the blood<sup>163,165,166,399</sup>. It is anatomically distinct from lymph nodes as it contains no afferent lymphatic vessels and thus it senses and acquires antigen in the marginal zone region<sup>164,165,370</sup>. In my anatomical mapping of CCRL1 expression, I found strong anti-CCRL1 immunoreactivity on cells lining vessels in the red pulp of the spleen. Staining for CD169 macrophages and CCRL1 expressing cells revealed a very close pattern of staining with regards to both markers, although there was no colocalisation. Thus, as in the lymph node, CCRL1<sup>+</sup> cells lie closely apposed to CD169<sup>+</sup> macrophages in the spleen. Moreover, deletion of CCRL1 results in a small increase in the proportion of CD169<sup>+</sup> macrophages in the spleen. Consistent with earlier findings by members of our group, no other differences in leukocyte populations were found at rest in the spleen of WT and CCRL1-deficient mice. Furthermore, I found that the absence of CCRL1 did not affect the early recruitment of CCR7<sup>+</sup> leukocytes into the spleen. Therefore, with the exception of CD169<sup>+</sup> macrophage numbers, the cellularity of the spleen appeared comparable with WT animals. Similarly, the gross anatomy of the spleen in CCRL1-deficient mice was similar to WT animals. These data demonstrate that at rest, CCRL1 deficiency in the spleen leads to no gross abnormalities in cell number or positioning. It would now be interesting to investigate immune responses in the spleen after challenge, as preliminary data from our lab suggests that the spleens of CCRL1-deficient mice become excessively enlarged during a model of lung inflammation (Dr Asquith, personal communication). Similarly, elevated levels of IL-23 transcripts were found in the spleen of CCRL1-deficient mice in the EAE model, and attributed to the earlier onset of disease<sup>361</sup>.

## 6.6 Macrophage driven lymphangiogenesis

Macrophages are important in the propagation of lymphatic vessel expansion in a variety of contexts, including inflammation<sup>147,162</sup>. Other studies have detailed

how macrophages can contribute to lymphatic vessel expansion by integrating within newly forming vessel walls<sup>86</sup>. To investigate the role that CD169<sup>+</sup> macrophages play in mediating the expansion of LECs, I depleted macrophages in the popliteal lymph node by injection of clodronated liposomes into the footpad. I then injected CFA into the footpad 1 week after clodronated liposome depletion in order drive lymphatic vessel expansion. Mice depleted of macrophages did not undergo lymphatic vessel expansion in the popliteal lymph nodes whereas in the same mice, inguinal lymph nodes, which are not depleted of macrophages, undergo a massive expansion in lymphatic vessel density. Mice that did not undergo clodronated liposome-mediated macrophage depletion underwent expansion of lymphatic vessels in the popliteal lymph node. This would suggest that macrophages are needed to drive the expansion of lymphatic vessels in lymph nodes during inflammation. In future experiments, whole images of lymph nodes could be generated using this software which would allow us to quantify the area occupied by LYVE-1<sup>+</sup> LECs using image j software, as done in previous experiments.

The mechanisms that mediate macrophage-driven lymphangiogenesis in response to inflammation still need further investigation. Results from preliminary experiments suggest that CCRL1 deletion does not affect LEC expansion in the popliteal lymph node after injection of CFA into the footpad. Enumeration of LECs by flow cytometry would help to substantiate these preliminary findings. The functional consequences of exaggerated lymph node lymphangiogenesis also needs further investigation. We may expect that an increase in antigen delivery might coincide with an increase in lymphatic vessels in these lymph nodes, which may lead to an increase in T cell priming. This could be examined by studying T cell proliferation in mice challenged with OVA after adoptively transferring OTII T cells, and in which the extent of lymphangiogenesis in the lymph node has been altered by macrophage depletion or perhaps by CCRL1 deletion, as is the case in mesenteric lymph nodes.

## **6.7 Chemokine Truncation by DCs**

The basis of my investigations into chemokine cleavage by DCs stems from an earlier paper published in 2010 by Michael Sixt's group who describe how

BMDCs are able to cleave fCCL21<sup>268</sup>. This paper showed for the first time the presence of tCCL21 that retained its ability to induce chemotaxis in CCR7<sup>+</sup> cells. Furthermore, since the publication of this paper it is appreciated that CCL21 has a dual role in mediating cellular movement by inducing haptotaxis and haptokinesis. tCCL21 is free from GAG binding domains and so acts like CCL19 in that it can diffuse from the source of production to attract CCR7<sup>+</sup> cells. Together, tCCL21 and CCL19 mediate chemotaxis whereas fCCL21 induces haptotaxis, haptokinesis and adhesion in CCR7<sup>+</sup> cells.

Importantly, these data looking directly at chemokine function are linked to the behaviour of DCs of which a significant proportion of this thesis is dedicated. As the ability to truncate fCCL21 was shown to be a feature unique to DCs<sup>383</sup>, there is a direct link between DCs and the shaping of the chemokine network. As my characterisation of DC migration in CCRL1-deficient mice revealed a defect in DC trafficking during rest and inflammation, it was conceivable that this may coincide with a reduction in the truncation of CCL21 *in vivo*.

I showed that BMDCs are able to cleave fCCL21 chemokine *in vitro* to produce a smaller tCCL21 protein. This was not a new finding but it confirmed the earlier report by Schuman and colleagues<sup>268</sup>. There was no detectable difference in the ability of GM-CSF and Flt3L matured BMDCs to cleave fCCL21, showing that phenotypically different DCs share the ability to cleave fCCL21.

I explored the ability of BMDCs to cleave chemokine after LPS-induced activation. DCs adopt a less dendritic morphology whilst upregulating costimulatory molecules and chemokine receptors, including CCR7, upon stimulation with LPS. However, I found that activation does not affect the ability of BMDCs to cleave fCCL21 and does not result in more or less production of the tCCL21 fragment. It is possible that other TLR ligands or inflammatory agents such as TNF may promote the truncation of fCCL21 by BMDCs by inducing different changes in the DC. Furthermore, it is difficult to generate truly 'immature BMDCs' *in vitro*. This was clear when comparing the activation markers of LPS-stimulated and unstimulated BMDCs. Whilst LPS stimulation upregulated the expression of activation markers MHCII and CD86, expression of these markers was relatively high on unstimulated BMDCs. Taking this into

account, it may be that LPS stimulation leads to a subtle increase in BMDC-mediated CCL21 cleavage that is not detectable due to the difficulties in preparing genuinely immature BMDC cultures as comparisons.

To test whether CCR7 is involved in the recognition of fCCL21 chemokine and facilitates subsequent truncation, I incubated BMDCs with an excess of CCL19 chemokine in order to saturate CCR7 binding domains and to induce receptor desensitisation. I then cultured BMDCs with fCCL21 chemokine and found that BMDCs retain their ability to cleave fCCL21 to produce tCCL21. Therefore, I concluded that cleavage was probably occurring independently of CCR7. It would be useful to confirm these findings by culturing CCR7-deficient BMDCs with fCCL21 and quantifying the presence of tCCL21. Unfortunately the CCR7-deficient mouse strain was only available during my summer placement at MGH. However, as we had generated data to suggest that BMDCs truncate fCCL21 independent of CCR7, we did not pursue this further. It is known that cells are able to secrete proteases that act to cleave chemokines to produce soluble chemokine fragments<sup>378,379,400,401</sup>. However, I was able to demonstrate that truncation of fCCL21 chemokine requires direct contact with DCs and fCCL21 rather than a protease released by the DCs.

## **6.8 Leukocyte-Mediated Chemokine truncation**

I was interested to discover whether the ability to cleave fCCL21 chemokine was a feature unique to BMDCs. Surprisingly, I found the presence of a faint tCCL21 band from cultures of purified splenic T cells and B cells incubated with fCCL21. However, it was clear that T cells and B cells are unable to cleave fCCL21 chemokine to the same degree as BMDCs. I also cultured MCSF matured BMDMs with fCCL21 and then compared chemokine truncation with that of BMDCs. I found that BMDMs are able to cleave fCCL21 to produce a smaller tCCL21 fragment. Interestingly, macrophages appeared to consume CCL21 from the culture media. This is possibly mediated by phagocytosis, although direct evidence for this is lacking.

## 6.9 *In vivo* Truncation

Having shown that cells matured *in vivo* have the capacity to cleave fCCL21, I moved on to quantifying the presence of tCCL21 in lymph node homogenates. I was able to detect a truncated version of CCL21 in popliteal, inguinal, axillary, mesenteric and cervical lymph nodes as well as the spleen from WT mice. It was unsurprising to find tCCL21 in all lymphoid tissues investigated as in each of these tissues there are resident DCs, migratory DCs, and high levels of fCCL21. However, the size of the CCL21 fragment found in lymphoid tissues, including lymph nodes, was different to that produced *in vitro* in BMDC cultures. The reason for this is not clear, but suggested that BMDCs do not recapitulate the CCL21 processing that occurs *in vivo*. I found that levels of tCCL21 *in vivo* appear to be unaffected by deletion of CCRL1 in lymph nodes or in the spleen suggesting that CCRL1 cannot regulate tCCL21 abundance. Furthermore, the presence of tCCL21 was unaffected by TPA-induced skin inflammation between WT and CCRL1-deficient mice or by the number of DCs in the lymph node. Although DCs are the most potent cells at truncating fCCL21, it is possible that other factors mediate this *in vivo*. T cells and B cells were shown to truncate fCCL21 *in vitro*, and as these cells comprise the majority of cells in lymphoid tissues, it is possible that they are principally responsible for fCCL21 truncation *in vivo*. Similarly, not all of the fCCL21 *in vivo* or from *in vitro* cultures is converted to tCCL21. Therefore, there is a factor that limits the truncation of fCCL21 to tCCL21, however, this remains to be elucidated. There are fewer migratory DCs in CCRL1-deficient inguinal lymph nodes during TPA-induced inflammation, however this reduction was not be sufficient to reveal detectable differences in the presence of tCCL21. It would be interesting to explore the presence of tCCL21 in lymph nodes of CCR7-deficient mice, which have a more profound migratory DC defect during rest and inflammation<sup>189</sup>. Furthermore, DCs can be specifically depleted in CD11c-DTR transgenic mice<sup>402-405</sup>, and these mice would be useful to explore the loss of DCs in the lymph node and how this impacts the abundance of tCCL21. As other leukocyte subsets have the capacity to truncate fCCL21, albeit to a lesser extent than DCs, we would expect that there would be less tCCL21 in CD11c-DTR mice, but that fCCL21 truncation would not be completely ablated in these animals.

DCs were also shown to be able to truncate CCL2. However, both BMDCs and BMDMs were not able to truncate CCL25. Interestingly, when incubated with recombinant CCL25, macrophages appeared to consume CCL25 and degrade the chemokine from the culture medium. The truncation of fCCL2 to produce a tCCL2 fragment is interesting, and has implications for other members of the atypical chemokine receptor family. D6, a member of this family, is known to bind to fCCL2, however, as yet, it is not known whether D6 can recognise tCCL2. Similarly, post-translational modifications of chemokines can change their receptor affinity. Therefore, when characterising the binding of chemokine receptors and atypical chemokine receptors to chemokines, we must consider the binding of shortened truncated forms of the full length chemokines.

My description of DC-mediated chemokine truncation has revealed some important observations. I have shown the presence of tCCL21 *in vitro* and *in vivo*. Furthermore I have shown that truncation of fCCL21 is mediated largely by DCs, although T cells, B cells and macrophages are able to truncate fCCL21 to a lesser extent. I have also shown that fCCL2 can be cleaved by BMDCs to produce tCCL2. Although I investigated various possible mechanisms for DC-mediated chemokine truncation, I was unable to elucidate the mechanism by which DCs truncate chemokine. It still remains to be seen if CCRL1 scavenges tCCL21. However, there were no differences in the abundance of tCCL21 in lymphoid tissue lysates from CCRL1-deficient mice compared with WT animals. It is important to answer this question in future experiments, and this may be achieved by *in vitro* assays involving CCRL1-transfected cells. Demonstration of the presence of tCCL2 chemokine in tissues would also be important to show in order to demonstrate that these findings had implications *in vivo*. To answer this question, it would be necessary to look during inflammation as levels of fCCL2 are low in lymphoid tissues at rest, and presumably levels of tCCL2 would be low also.

## 6.10 Future Directions

Future experiments are necessary to provide insight into the function of CCRL1 *in vivo*. CCRL1 clearly facilitates DC migration from the skin to the lymph node

under certain circumstances, and ongoing experiments in our lab are attempting to characterise the movement of DCs in the skin and their entry into lymphatic vessels, as well as assessing T cell priming in CCRL1-deficient mice. The successful completion of these experiments will help to generate a clearer picture of the *in vivo* role of CCRL1 during adaptive immunity. The functional consequence of CD169<sup>+</sup> macrophage and LEC expansion in mesenteric lymph nodes of CCRL1-deficient mice is another aspect of this study requiring further investigation. Experiments are being designed that will target delivery of bacteria or antigen to the mesenteric lymph node to measure the response mounted by innate like T cells and macrophages. Finally, the ability of CCRL1 to scavenge tCCL21 needs to be addressed. Assays involving CCRL1-transfected cells for the assessment of extracellular tCCL21 scavenging could be used to study this. The successful completion of all these studies will greatly enhance our understanding of CCRL1 function, and the regulation of bioavailable chemokine, and may provide opportunities to effectively target aspects of CCRL1-controlled chemokine networks for therapeutic purposes.

# Chapter Seven

## Appendix

## 7 Appendix

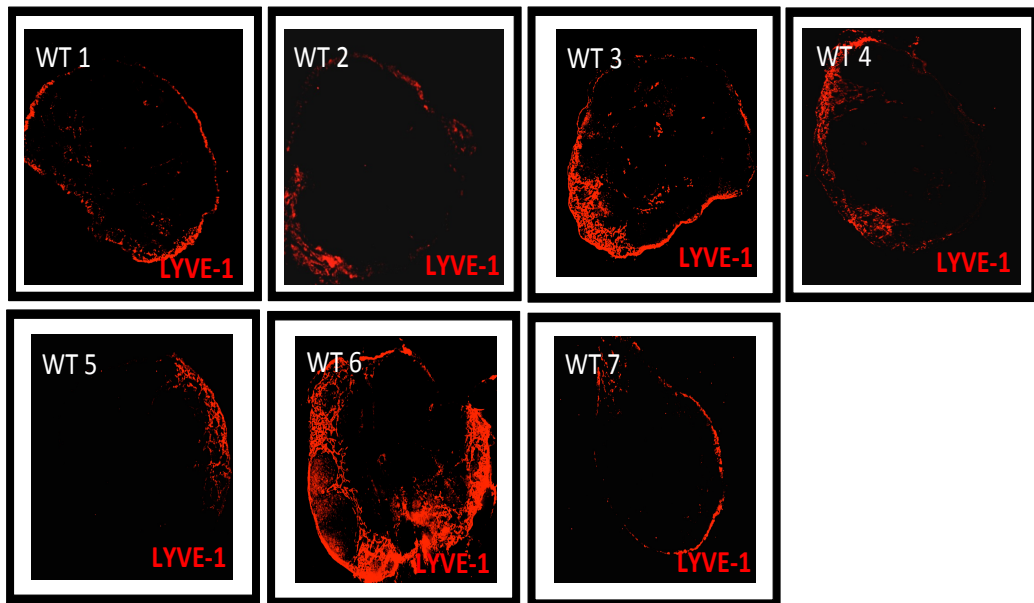


**Figure 7.1: LYVE-1 distribution in WT mesenteric lymph nodes.**

Mesenteric lymph nodes from resting wild type (WT) mice were harvested into OCT and frozen on dry ice. 8-10 $\mu$ m sections were cut and then stained with anti-LYVE-1 antibody. Sections were imaged using a fluorescent Zeiss confocal microscope.

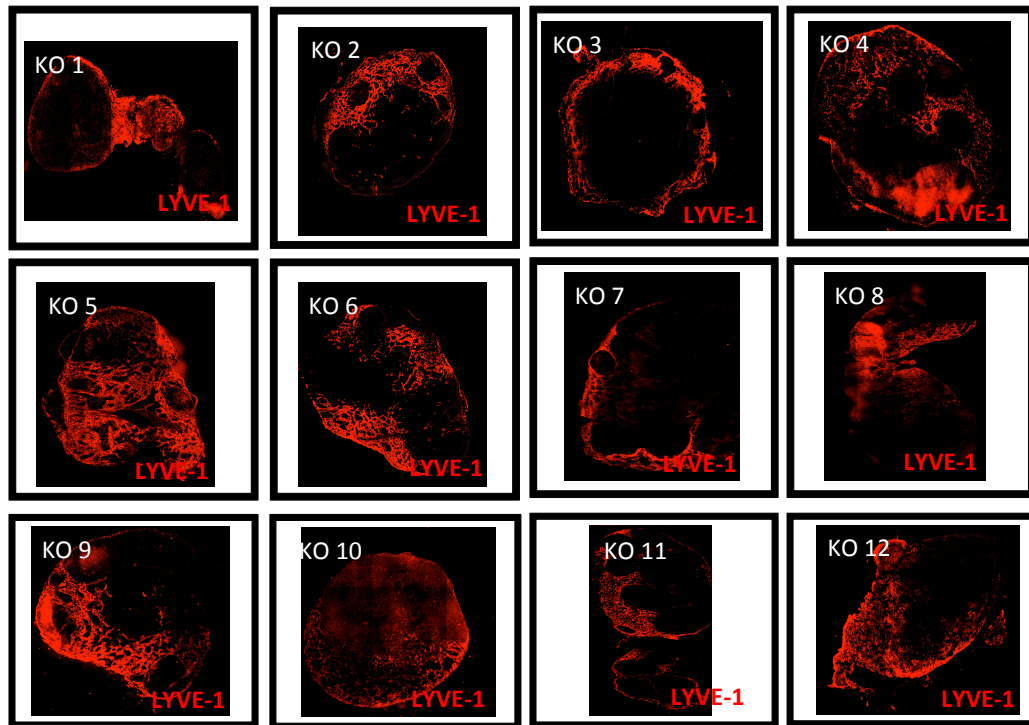


**Figure 7.2: LYVE-1 distribution in CCRL1-deficient mesenteric lymph nodes.**

Mesenteric lymph nodes from resting CCRL1-deficient (KO) mice were harvested into OCT and frozen on dry ice. 8-10 $\mu$ m sections were then cut and stained with anti-LYVE-1 antibody. Sections were then imaged using a fluorescent Zeiss confocal microscope.

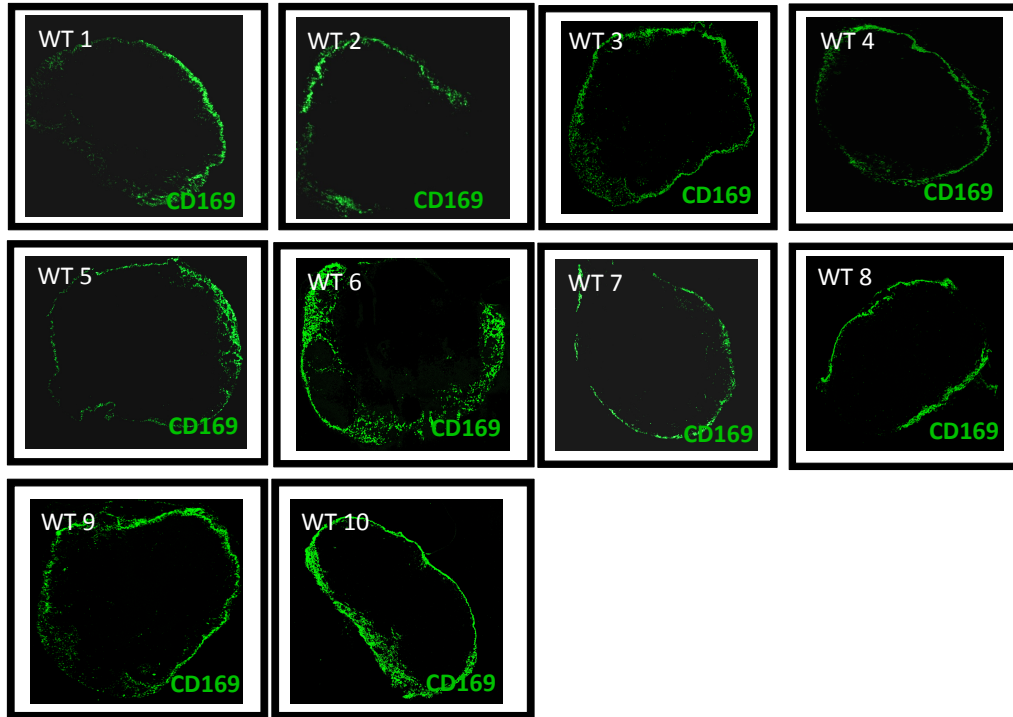


**Figure 7.3: CD169<sup>+</sup> macrophage distribution in WT mesenteric lymph nodes.**

Mesenteric lymph nodes from resting wild type (WT) mice were harvested into OCT and frozen on dry ice. 8-10 $\mu$ m sections were then cut and stained with anti-CD169 antibody. Sections were then imaged using a fluorescent Zeiss confocal microscope.

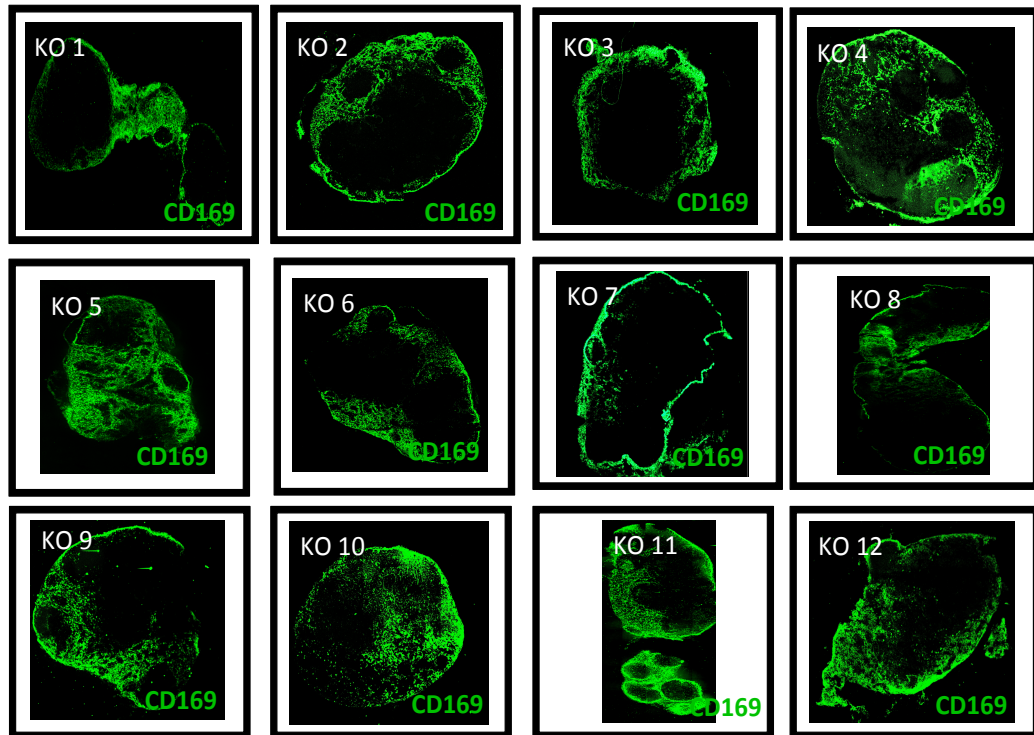


**Figure 7.4: CD169<sup>+</sup> macrophage distribution in CCRL1-deficient lymph nodes.**

Mesenteric lymph nodes from resting CCRL1-deficient (KO) mice were harvested into OCT and frozen on dry ice. 8-10 $\mu$ m sections were then cut and stained with anti-CD169 antibody. Sections were then imaged using a fluorescent Zeiss confocal microscope.

# References

1. Ohtani, O. & Ohtani, Y. Structure and function of rat lymph nodes. *Arch. Histol. Cytol.* **71**, 69–76 (2008).
2. Willard-Mack, C. L. Normal structure, function, and histology of lymph nodes. *Toxicol Pathol* **34**, 409–424 (2006).
3. van de Pavert, S. A. & Mebius, R. E. Development of secondary lymphoid organs in relation to lymphatic vasculature. *Adv Anat Embryol Cell Biol* **214**, 81–91 (2014).
4. Randall, T. D., Carragher, D. M. & Rangel-Moreno, J. Development of secondary lymphoid organs. *Annu. Rev. Immunol.* **26**, 627–650 (2008).
5. van de Pavert, S. A. & Mebius, R. E. New insights into the development of lymphoid tissues. *Nat. Rev. Immunol.* **10**, 664–674 (2010).
6. Roozendaal, R. *et al.* Conduits mediate transport of low-molecular-weight antigen to lymph node follicles. *Immunity* **30**, 264–276 (2009).
7. Luther, S. A., Tang, H. L., Hyman, P. L., Farr, A. G. & Cyster, J. G. Coexpression of the chemokines ELC and SLC by T zone stromal cells and deletion of the ELC gene in the plt/plt mouse. *Proc. Natl. Acad. Sci. U.S.A.* **97**, 12694–12699 (2000).
8. Buettner, M., Pabst, R. & Bode, U. Lymph node stromal cells strongly influence immune response suppression. *Eur. J. Immunol.* **41**, 624–633 (2011).
9. Khan, O. *et al.* Regulation of T cell priming by lymphoid stroma. *PLoS ONE* **6**, e26138 (2011).
10. Fletcher, A. L. *et al.* Lymph node fibroblastic reticular cells directly present peripheral tissue antigen under steady-state and inflammatory conditions. *J. Exp. Med.* **207**, 689–697 (2010).
11. Lukacs-Kornek, V. *et al.* Regulated release of nitric oxide by nonhematopoietic stroma controls expansion of the activated T cell pool in lymph nodes. *Nat. Immunol.* **12**, 1096–1104 (2011).
12. Shikh, El, M. E. M., Sayed, El, R. M., Sukumar, S., Szakal, A. K. & Tew, J. G. Activation of B cells by antigens on follicular dendritic cells. *Trends Immunol.* **31**, 205–211 (2010).
13. Aydar, Y., Sukumar, S., Szakal, A. K. & Tew, J. G. The influence of immune complex-bearing follicular dendritic cells on the IgM response, Ig class switching, and production of high affinity IgG. *J. Immunol.* **174**, 5358–5366 (2005).
14. Denzer, K. *et al.* Follicular dendritic cells carry MHC class II-expressing microvesicles at their surface. *J. Immunol.* **165**, 1259–1265 (2000).
15. Heesters, B. A. *et al.* Endocytosis and recycling of immune complexes by follicular dendritic cells enhances B cell antigen binding and activation. *Immunity* **38**, 1164–1175 (2013).
16. Gray, E. E. & Cyster, J. G. Lymph node macrophages. *J. Innate Immun* **4**, 424–436 (2012).
17. Junt, T. *et al.* Subcapsular sinus macrophages in lymph nodes clear lymph-borne viruses and present them to antiviral B cells. *Nature* **450**, 110–114 (2007).
18. Carrasco, Y. R. & Batista, F. D. B cells acquire particulate antigen in a macrophage-rich area at the boundary between the follicle and the subcapsular sinus of the lymph node. *Immunity* **27**, 160–171 (2007).
19. Barral, P. *et al.* CD169(+) macrophages present lipid antigens to mediate early activation of iNKT cells in lymph nodes. *Nat. Immunol.* **11**, 303–

- 312 (2010).
20. Hadeiba, H. *et al.* CCR9 expression defines tolerogenic plasmacytoid dendritic cells able to suppress acute graft-versus-host disease. *Nat. Immunol.* **9**, 1253–1260 (2008).
  21. Scheinecker, C., McHugh, R., Shevach, E. M. & Germain, R. N. Constitutive presentation of a natural tissue autoantigen exclusively by dendritic cells in the draining lymph node. *J. Exp. Med.* **196**, 1079–1090 (2002).
  22. Belz, G. T. *et al.* The CD8alpha(+) dendritic cell is responsible for inducing peripheral self-tolerance to tissue-associated antigens. *J. Exp. Med.* **196**, 1099–1104 (2002).
  23. Baekkevold, E. S. *et al.* The CCR7 ligand elc (CCL19) is transcytosed in high endothelial venules and mediates T cell recruitment. *J. Exp. Med.* **193**, 1105–1112 (2001).
  24. Pham, T. H. M., Okada, T., Matloubian, M., Lo, C. G. & Cyster, J. G. S1P1 receptor signaling overrides retention mediated by G alpha i-coupled receptors to promote T cell egress. *Immunity* **28**, 122–133 (2008).
  25. Yopp, A. C. *et al.* Sphingosine 1-phosphate receptors regulate chemokine-driven transendothelial migration of lymph node but not splenic T cells. *J. Immunol.* **175**, 2913–2924 (2005).
  26. Steinman, R. M. & Witmer, M. D. Lymphoid dendritic cells are potent stimulators of the primary mixed leukocyte reaction in mice. *Proc. Natl. Acad. Sci. U.S.A.* **75**, 5132–5136 (1978).
  27. Steinman, R. M., Kaplan, G., Witmer, M. D. & Cohn, Z. A. Identification of a novel cell type in peripheral lymphoid organs of mice. V. Purification of spleen dendritic cells, new surface markers, and maintenance in vitro. *J. Exp. Med.* **149**, 1–16 (1979).
  28. Asselin-Paturel, C. *et al.* Type I interferon dependence of plasmacytoid dendritic cell activation and migration. *J. Exp. Med.* **201**, 1157–1167 (2005).
  29. Chan, C. W. *et al.* Interferon-producing killer dendritic cells provide a link between innate and adaptive immunity. *Nat. Med.* **12**, 207–213 (2006).
  30. Huber, C. *et al.* Lymphotoxin-beta receptor-dependent genes in lymph node and follicular dendritic cell transcriptomes. *J. Immunol.* **174**, 5526–5536 (2005).
  31. Schnizlein, C. T., Szakal, A. K. & Tew, J. G. Follicular dendritic cells in the regulation and maintenance of immune responses. *Immunobiology* **168**, 391–402 (1984).
  32. Cyster, J. G. *et al.* Follicular stromal cells and lymphocyte homing to follicles. *Immunol. Rev.* **176**, 181–193 (2000).
  33. Wang, X. *et al.* Follicular dendritic cells help establish follicle identity and promote B cell retention in germinal centers. *J. Exp. Med.* **208**, 2497–2510 (2011).
  34. Szakal, A. K., Holmes, K. L. & Tew, J. G. Transport of immune complexes from the subcapsular sinus to lymph node follicles on the surface of nonphagocytic cells, including cells with dendritic morphology. *J. Immunol.* **131**, 1714–1727 (1983).
  35. Vremec, D. The isolation of mouse dendritic cells from lymphoid tissues

- and the identification of dendritic cell subtypes by multiparameter flow cytometry. *Methods Mol. Biol.* **595**, 205–229 (2010).
36. Lemos, M. P., Fan, L., Lo, D. & Laufer, T. M. CD8 $\alpha$ <sup>+</sup> and CD11b<sup>+</sup> dendritic cell-restricted MHC class II controls Th1 CD4<sup>+</sup> T cell immunity. *J. Immunol.* **171**, 5077–5084 (2003).
  37. Segura, E. *et al.* Characterization of resident and migratory dendritic cells in human lymph nodes. *J. Exp. Med.* **209**, 653–660 (2012).
  38. Bachem, A. *et al.* Superior antigen cross-presentation and XCR1 expression define human CD11c<sup>+</sup>CD141<sup>+</sup> cells as homologues of mouse CD8<sup>+</sup> dendritic cells. *J. Exp. Med.* **207**, 1273–1281 (2010).
  39. Petersen, T. R., Knight, D. A., Tang, C.-W., Osmond, T. L. & Hermans, I. F. Batf3-independent langerin- CX3CR1- CD8 $\alpha$ <sup>+</sup> splenic DCs represent a precursor for classical cross-presenting CD8 $\alpha$ <sup>+</sup> DCs. *J. Leukoc. Biol.* (2014). doi:10.1189/jlb.1A0314-130R
  40. Segura, E. & Amigorena, S. Cross-presentation by human dendritic cell subsets. *Immunol. Lett.* **158**, 73–78 (2014).
  41. Lorenzi, S. *et al.* Type I IFNs control antigen retention and survival of CD8 $\alpha$ (<sup>+</sup>) dendritic cells after uptake of tumor apoptotic cells leading to cross-priming. *J. Immunol.* **186**, 5142–5150 (2011).
  42. Thacker, R. I. & Janssen, E. M. Cross-presentation of cell-associated antigens by mouse splenic dendritic cell populations. *Front Immunol* **3**, 41 (2012).
  43. Farrand, K. J. *et al.* Langerin<sup>+</sup> CD8 $\alpha$ <sup>+</sup> dendritic cells are critical for cross-priming and IL-12 production in response to systemic antigens. *J. Immunol.* **183**, 7732–7742 (2009).
  44. Joffre, O. P., Segura, E., Savina, A. & Amigorena, S. Cross-presentation by dendritic cells. *Nat. Rev. Immunol.* **12**, 557–569 (2012).
  45. Hennies, C. M. *et al.* Selective expansion of merocytic dendritic cells and CD8DCs confers anti-tumour effect of Fms-like tyrosine kinase 3-ligand treatment in vivo. *Clin. Exp. Immunol.* **163**, 381–391 (2011).
  46. Macho-Fernandez, E. *et al.* Targeted delivery of  $\alpha$ -galactosylceramide to CD8 $\alpha$ <sup>+</sup> dendritic cells optimizes type I NKT cell-based antitumor responses. *J. Immunol.* **193**, 961–969 (2014).
  47. Domínguez, P. M. & Ardavin, C. Differentiation and function of mouse monocyte-derived dendritic cells in steady state and inflammation. *Immunol. Rev.* **234**, 90–104 (2010).
  48. Cavanagh, L. L. & Andrian, von, U. H. Travellers in many guises: the origins and destinations of dendritic cells. *Immunol. Cell Biol.* **80**, 448–462 (2002).
  49. Chu, C.-C. *et al.* Resident CD141 (BDCA3)<sup>+</sup> dendritic cells in human skin produce IL-10 and induce regulatory T cells that suppress skin inflammation. *J. Exp. Med.* **209**, 935–945 (2012).
  50. Hintzen, G. *et al.* Induction of tolerance to innocuous inhaled antigen relies on a CCR7-dependent dendritic cell-mediated antigen transport to the bronchial lymph node. *J. Immunol.* **177**, 7346–7354 (2006).
  51. van der Aar, A. M. G. *et al.* Langerhans cells favor skin flora tolerance through limited presentation of bacterial antigens and induction of regulatory T cells. *J. Invest. Dermatol.* **133**, 1240–1249 (2013).
  52. Tal, O. *et al.* DC mobilization from the skin requires docking to immobilized CCL21 on lymphatic endothelium and intralymphatic

- crawling. *J. Exp. Med.* **208**, 2141–2153 (2011).
53. Braun, A. *et al.* Afferent lymph-derived T cells and DCs use different chemokine receptor CCR7-dependent routes for entry into the lymph node and intranodal migration. *Nat. Immunol.* **12**, 879–887 (2011).
  54. Saeki, H., Moore, A. M., Brown, M. J. & Hwang, S. T. Cutting edge: secondary lymphoid-tissue chemokine (SLC) and CC chemokine receptor 7 (CCR7) participate in the emigration pathway of mature dendritic cells from the skin to regional lymph nodes. *J. Immunol.* **162**, 2472–2475 (1999).
  55. Robbiani, D. F. *et al.* The leukotriene C(4) transporter MRP1 regulates CCL19 (MIP-3beta, ELC)-dependent mobilization of dendritic cells to lymph nodes. *Cell* **103**, 757–768 (2000).
  56. Kriehuber, E. *et al.* Balance between NF-kappaB and JNK/AP-1 activity controls dendritic cell life and death. *Blood* **106**, 175–183 (2005).
  57. Vigl, B. *et al.* Tissue inflammation modulates gene expression of lymphatic endothelial cells and dendritic cell migration in a stimulus-dependent manner. *Blood* **118**, 205–215 (2011).
  58. Ohl, L. *et al.* CCR7 governs skin dendritic cell migration under inflammatory and steady-state conditions. *Immunity* **21**, 279–288 (2004).
  59. Henri, S. *et al.* Mature DC from skin and skin-draining LN retain the ability to acquire and efficiently present targeted antigen. *Eur. J. Immunol.* **37**, 1184–1193 (2007).
  60. Allenspach, E. J., Lemos, M. P., Porrett, P. M., Turka, L. A. & Laufer, T. M. Migratory and lymphoid-resident dendritic cells cooperate to efficiently prime naive CD4 T cells. *Immunity* **29**, 795–806 (2008).
  61. Mempel, T. R., Henrickson, S. E. & Andrian, von, U. H. T-cell priming by dendritic cells in lymph nodes occurs in three distinct phases. *Nature* **427**, 154–159 (2004).
  62. Kohrgruber, N. *et al.* Survival, maturation, and function of CD11c- and CD11c+ peripheral blood dendritic cells are differentially regulated by cytokines. *J. Immunol.* **163**, 3250–3259 (1999).
  63. Yoneyama, H. *et al.* Evidence for recruitment of plasmacytoid dendritic cell precursors to inflamed lymph nodes through high endothelial venules. *Int. Immunol.* **16**, 915–928 (2004).
  64. Penna, G., Sozzani, S. & Adorini, L. Cutting edge: selective usage of chemokine receptors by plasmacytoid dendritic cells. *J. Immunol.* **167**, 1862–1866 (2001).
  65. Penna, G., Vulcano, M., Sozzani, S. & Adorini, L. Differential migration behavior and chemokine production by myeloid and plasmacytoid dendritic cells. *Hum. Immunol.* **63**, 1164–1171 (2002).
  66. Barchet, W. *et al.* Virus-induced interferon alpha production by a dendritic cell subset in the absence of feedback signaling in vivo. *J. Exp. Med.* **195**, 507–516 (2002).
  67. Krug, A. *et al.* Toll-like receptor expression reveals CpG DNA as a unique microbial stimulus for plasmacytoid dendritic cells which synergizes with CD40 ligand to induce high amounts of IL-12. *Eur. J. Immunol.* **31**, 3026–3037 (2001).
  68. Foster, G. R., Germain, C., Jones, M., Lechler, R. I. & Lombardi, G. Human T cells elicit IFN-alpha secretion from dendritic cells following cell to cell interactions. *Eur. J. Immunol.* **30**, 3228–3235 (2000).

69. Furlan, R. *et al.* Activation of invariant NKT cells by alphaGalCer administration protects mice from MOG35-55-induced EAE: critical roles for administration route and IFN-gamma. *Eur. J. Immunol.* **33**, 1830–1838 (2003).
70. Liu, C. *et al.* Plasmacytoid dendritic cells induce NK cell-dependent, tumor antigen-specific T cell cross-priming and tumor regression in mice. *J. Clin. Invest.* **118**, 1165–1175 (2008).
71. Chao, D. & MacPherson, G. G. Lymph node macrophage heterogeneity: the phenotypic and functional characterization of two distinct populations of macrophages from rat lymph node. *Eur. J. Immunol.* **19**, 1273–1281 (1989).
72. Xu, P., Gao, Y. M., Li, S. L. & Wang, Y. Morphological and functional investigations on macrophages with heterogeneous fluorescent staining. *Sci. Sin., Ser. B, Chem. Biol. Agric. Med. Earth Sci.* **28**, 707–714 (1985).
73. Kumamoto, Y. *et al.* Identification of sialoadhesin as a dominant lymph node counter-receptor for mouse macrophage galactose-type C-type lectin 1. *J Biol Chem* **279**, 49274–49280 (2004).
74. Kawasaki, N. *et al.* Targeted delivery of lipid antigen to macrophages via the CD169/sialoadhesin endocytic pathway induces robust invariant natural killer T cell activation. *Proc. Natl. Acad. Sci. U.S.A.* **110**, 7826–7831 (2013).
75. Crocker, P. R. & Gordon, S. Mouse macrophage hemagglutinin (sheep erythrocyte receptor) with specificity for sialylated glycoconjugates characterized by a monoclonal antibody. *J. Exp. Med.* **169**, 1333–1346 (1989).
76. van den Berg, T. K. *et al.* Sialoadhesin on macrophages: its identification as a lymphocyte adhesion molecule. *J. Exp. Med.* **176**, 647–655 (1992).
77. Iannaccone, M. *et al.* Subcapsular sinus macrophages prevent CNS invasion on peripheral infection with a neurotropic virus. *Nature* **465**, 1079–1083 (2010).
78. Crivellato, E. & Mallardi, F. Stromal cell organisation in the mouse lymph node. A light and electron microscopic investigation using the zinc iodide-osmium technique. *J. Anat.* **190 ( Pt 1)**, 85–92 (1997).
79. Girard, J.-P., Moussion, C. & Förster, R. HEVs, lymphatics and homeostatic immune cell trafficking in lymph nodes. *Nat. Rev. Immunol.* **12**, 762–773 (2012).
80. Phan, T. G., Green, J. A., Gray, E. E., Xu, Y. & Cyster, J. G. Immune complex relay by subcapsular sinus macrophages and noncognate B cells drives antibody affinity maturation. *Nat. Immunol.* **10**, 786–793 (2009).
81. Moseman, E. A. *et al.* B cell maintenance of subcapsular sinus macrophages protects against a fatal viral infection independent of adaptive immunity. *Immunity* **36**, 415–426 (2012).
82. Phan, T. G., Grigorova, I., Okada, T. & Cyster, J. G. Subcapsular encounter and complement-dependent transport of immune complexes by lymph node B cells. *Nat. Immunol.* **8**, 992–1000 (2007).
83. Kastenmüller, W., Torabi-Parizi, P., Subramanian, N., Lämmermann, T. & Germain, R. N. A spatially-organized multicellular innate immune response in lymph nodes limits systemic pathogen spread. *Cell* **150**, 1235–1248 (2012).

84. Hamada, S. *et al.* IL-17A produced by gammadelta T cells plays a critical role in innate immunity against listeria monocytogenes infection in the liver. *J. Immunol.* **181**, 3456–3463 (2008).
85. Maruyama, K. *et al.* Inflammation-induced lymphangiogenesis in the cornea arises from CD11b-positive macrophages. *J. Clin. Invest.* **115**, 2363–2372 (2005).
86. Attout, T. *et al.* Lymphatic vascularisation and involvement of Lyve-1+ macrophages in the human onchocerca nodule. *PLoS ONE* **4**, e8234 (2009).
87. Schledzewski, K. *et al.* Lymphatic endothelium-specific hyaluronan receptor LYVE-1 is expressed by stabilin-1+, F4/80+, CD11b+ macrophages in malignant tumours and wound healing tissue in vivo and in bone marrow cultures in vitro: implications for the assessment of lymphangiogenesis. *J. Pathol.* **209**, 67–77 (2006).
88. Förster, R. *et al.* CCR7 coordinates the primary immune response by establishing functional microenvironments in secondary lymphoid organs. *Cell* **99**, 23–33 (1999).
89. M'Rini, C. *et al.* A novel endothelial L-selectin ligand activity in lymph node medulla that is regulated by alpha(1,3)-fucosyltransferase-IV. *J. Exp. Med.* **198**, 1301–1312 (2003).
90. Lichtenstein, L. *et al.* Angptl4 protects against severe proinflammatory effects of saturated fat by inhibiting fatty acid uptake into mesenteric lymph node macrophages. *Cell Metab.* **12**, 580–592 (2010).
91. Steer, H. W. & Foot, R. A. Changes in the medulla of the parathyroid lymph nodes of the rat during acute gastro-intestinal inflammation. *J. Anat.* **152**, 23–36 (1987).
92. Paus, R., Hofmann, U., Eichmüller, S. & Czarnetzki, B. M. Distribution and changing density of gamma-delta T cells in murine skin during the induced hair cycle. *Br. J. Dermatol.* **130**, 281–289 (1994).
93. Ito, Y. *et al.* Gamma/delta T cells are the predominant source of interleukin-17 in affected joints in collagen-induced arthritis, but not in rheumatoid arthritis. *Arthritis Rheum.* **60**, 2294–2303 (2009).
94. Roark, C. L. *et al.* Exacerbation of collagen-induced arthritis by oligoclonal, IL-17-producing gamma delta T cells. *J. Immunol.* **179**, 5576–5583 (2007).
95. Roark, C. L., Simonian, P. L., Fontenot, A. P., Born, W. K. & O'Brien, R. L. gammadelta T cells: an important source of IL-17. *Curr. Opin. Immunol.* **20**, 353–357 (2008).
96. Al-Mossawi, M. H., Ridley, A., Kiedel, S. & Bowness, P. The role of natural killer cells, gamma delta T-cells and other innate immune cells in spondyloarthritis. *Curr Opin Rheumatol* **25**, 434–439 (2013).
97. Gray, E. E., Suzuki, K. & Cyster, J. G. Cutting edge: Identification of a motile IL-17-producing gammadelta T cell population in the dermis. *J. Immunol.* **186**, 6091–6095 (2011).
98. Cai, Y. *et al.* Pivotal role of dermal IL-17-producing  $\gamma\delta$  T cells in skin inflammation. *Immunity* **35**, 596–610 (2011).
99. Mölne, L., Corthay, A., Holmdahl, R. & Tarkowski, A. Role of gamma/delta T cell receptor-expressing lymphocytes in cutaneous infection caused by Staphylococcus aureus. *Clin. Exp. Immunol.* **132**, 209–215 (2003).

100. Caccamo, N. *et al.* gammadelta T cells condition dendritic cells in vivo for priming pulmonary CD8 T cell responses against Mycobacterium tuberculosis. *Eur. J. Immunol.* **36**, 2681–2690 (2006).
101. Brandes, M., Willimann, K. & Moser, B. Professional antigen-presentation function by human gammadelta T Cells. *Science* **309**, 264–268 (2005).
102. Cheng, L. *et al.* Mouse gammadelta T cells are capable of expressing MHC class II molecules, and of functioning as antigen-presenting cells. *J. Neuroimmunol.* **203**, 3–11 (2008).
103. Brandes, M. *et al.* Cross-presenting human gammadelta T cells induce robust CD8+ alphabeta T cell responses. *Proc. Natl. Acad. Sci. U.S.A.* **106**, 2307–2312 (2009).
104. Rahimpour, A. *et al.*  $\gamma\delta$  T cells augment rejection of skin grafts by enhancing cross-priming of CD8 T cells to skin-derived antigen. *J. Invest. Dermatol.* **132**, 1656–1664 (2012).
105. Xu, S. *et al.* IL-17A-producing gammadeltaT cells promote CTL responses against Listeria monocytogenes infection by enhancing dendritic cell cross-presentation. *J. Immunol.* **185**, 5879–5887 (2010).
106. Kinjo, Y. *et al.* Natural killer T cells recognize diacylglycerol antigens from pathogenic bacteria. *Nat. Immunol.* **7**, 978–986 (2006).
107. King, I. L. *et al.* The mechanism of splenic invariant NKT cell activation dictates localization in vivo. *J. Immunol.* **191**, 572–582 (2013).
108. Nieda, M. *et al.* Activation of human Valpha24NKT cells by alpha-glycosylceramide in a CD1d-restricted and Valpha24TCR-mediated manner. *Hum. Immunol.* **60**, 10–19 (1999).
109. Doisne, J.-M. *et al.* Cutting edge: crucial role of IL-1 and IL-23 in the innate IL-17 response of peripheral lymph node NK1.1- invariant NKT cells to bacteria. *J. Immunol.* **186**, 662–666 (2011).
110. Oh, S. J. & Chung, D. H. Invariant NKT cells producing IL-4 or IL-10, but not IFN-gamma, inhibit the Th1 response in experimental autoimmune encephalomyelitis, whereas none of these cells inhibits the Th17 response. *J. Immunol.* **186**, 6815–6821 (2011).
111. Mars, L. T. *et al.* Invariant NKT cells regulate experimental autoimmune encephalomyelitis and infiltrate the central nervous system in a CD1d-independent manner. *J. Immunol.* **181**, 2321–2329 (2008).
112. Kawano, T. *et al.* A novel recognition motif of human NKT antigen receptor for a glycolipid ligand. *Int. Immunol.* **11**, 881–887 (1999).
113. Mattarollo, S. R., Yong, M., Tan, L., Frazer, I. H. & Leggatt, G. R. Secretion of IFN-gamma but not IL-17 by CD1d-restricted NKT cells enhances rejection of skin grafts expressing epithelial cell-derived antigen. *J. Immunol.* **184**, 5663–5669 (2010).
114. Fukunaga, A. *et al.* Langerhans cells serve as immunoregulatory cells by activating NKT cells. *J. Immunol.* **185**, 4633–4640 (2010).
115. Balato, A. *et al.* CD1d-dependent, iNKT-cell cytotoxicity against keratinocytes in allergic contact dermatitis. *Exp. Dermatol.* **21**, 915–920 (2012).
116. Koguchi, Y. *et al.* Preformed CD40L is stored in Th1, Th2, Th17, and T follicular helper cells as well as CD4+ 8- thymocytes and invariant NKT cells but not in Treg cells. *PLoS ONE* **7**, e31296 (2012).
117. Trobonjaca, Z., Leithäuser, F., Möller, P., Schirmbeck, R. & Reimann, J.

- Activating immunity in the liver. I. Liver dendritic cells (but not hepatocytes) are potent activators of IFN-gamma release by liver NKT cells. *J. Immunol.* **167**, 1413–1422 (2001).
118. Matsuda, H. *et al.* Plasticity of invariant NKT cell regulation of allergic airway disease is dependent on IFN-gamma production. *J. Immunol.* **185**, 253–262 (2010).
  119. Doisne, J.-M. *et al.* Skin and peripheral lymph node invariant NKT cells are mainly retinoic acid receptor-related orphan receptor (gamma)t+ and respond preferentially under inflammatory conditions. *J. Immunol.* **183**, 2142–2149 (2009).
  120. Watarai, H. *et al.* Development and function of invariant natural killer T cells producing T(h)2- and T(h)17-cytokines. *PLoS Biol.* **10**, e1001255 (2012).
  121. Wang, H., Feng, D., Park, O., Yin, S. & Gao, B. Invariant NKT cell activation induces neutrophil accumulation and hepatitis: Opposite regulation by IL-4 and IFN- $\gamma$ . *Hepatology* **58**, 1474–1485 (2013).
  122. Herberman, R. B., Holden, H. T., Ting, C. C., Lavrin, D. L. & Kirchner, H. Cell-mediated immunity to leukemia virus- and tumor-associated antigens in mice. *Cancer Res* **36**, 615–621 (1976).
  123. Quinnan, G. V. & Manischewitz, J. E. The role of natural killer cells and antibody-dependent cell-mediated cytotoxicity during murine cytomegalovirus infection. *J. Exp. Med.* **150**, 1549–1554 (1979).
  124. Garcia, Z. *et al.* Subcapsular sinus macrophages promote NK cell accumulation and activation in response to lymph-borne viral particles. *Blood* **120**, 4744–4750 (2012).
  125. K uchler, A. M. *et al.* Development of the zebrafish lymphatic system requires VEGFC signaling. *Curr. Biol.* **16**, 1244–1248 (2006).
  126. Wigle, J. T. & Oliver, G. Prox1 function is required for the development of the murine lymphatic system. *Cell* **98**, 769–778 (1999).
  127. Boussaud, V., Soler, P., Moreau, J., Goodwin, R. G. & Hance, A. J. Expression of three members of the TNF-R family of receptors (4-1BB, lymphotoxin-beta receptor, and Fas) in human lung. *Eur. Respir. J.* **12**, 926–931 (1998).
  128. Rennert, P. D., Browning, J. L., Mebius, R., Mackay, F. & Hochman, P. S. Surface lymphotoxin alpha/beta complex is required for the development of peripheral lymphoid organs. *J. Exp. Med.* **184**, 1999–2006 (1996).
  129. Kim, D. *et al.* Regulation of peripheral lymph node genesis by the tumor necrosis factor family member TRANCE. *J. Exp. Med.* **192**, 1467–1478 (2000).
  130. Chappaz, S., G artner, C., Rodewald, H.-R. & Finke, D. Kit ligand and Il7 differentially regulate Peyer's patch and lymph node development. *J. Immunol.* **185**, 3514–3519 (2010).
  131. Kim, N., Odgren, P. R., Kim, D. K., Marks, S. C. & Choi, Y. Diverse roles of the tumor necrosis factor family member TRANCE in skeletal physiology revealed by TRANCE deficiency and partial rescue by a lymphocyte-expressed TRANCE transgene. *Proc. Natl. Acad. Sci. U.S.A.* **97**, 10905–10910 (2000).
  132. Cupedo, T. *et al.* Presumptive lymph node organizers are differentially represented in developing mesenteric and peripheral nodes. *J. Immunol.*

- 173**, 2968–2975 (2004).
133. Vondenhoff, M. F. *et al.* LTbetaR signaling induces cytokine expression and up-regulates lymphangiogenic factors in lymph node anlagen. *J. Immunol.* **182**, 5439–5445 (2009).
  134. Cuff, C. A., Sacca, R. & Ruddle, N. H. Differential induction of adhesion molecule and chemokine expression by LTalpha3 and LTalpha in inflammation elucidates potential mechanisms of mesenteric and peripheral lymph node development. *J. Immunol.* **162**, 5965–5972 (1999).
  135. Luther, S. A. *et al.* Differing activities of homeostatic chemokines CCL19, CCL21, and CXCL12 in lymphocyte and dendritic cell recruitment and lymphoid neogenesis. *J. Immunol.* **169**, 424–433 (2002).
  136. van de Pavert, S. A. *et al.* Chemokine CXCL13 is essential for lymph node initiation and is induced by retinoic acid and neuronal stimulation. *Nat. Immunol.* **10**, 1193–1199 (2009).
  137. Baluk, P. *et al.* Functionally specialized junctions between endothelial cells of lymphatic vessels. *J. Exp. Med.* **204**, 2349–2362 (2007).
  138. Martínez-Corral, I. *et al.* In vivo imaging of lymphatic vessels in development, wound healing, inflammation, and tumor metastasis. *Proc. Natl. Acad. Sci. U.S.A.* **109**, 6223–6228 (2012).
  139. Aranguren, X. L. *et al.* COUP-TFII orchestrates venous and lymphatic endothelial identity by homo- or hetero-dimerisation with PROX1. *J. Cell. Sci.* **126**, 1164–1175 (2013).
  140. Wilting, J. *et al.* The transcription factor Prox1 is a marker for lymphatic endothelial cells in normal and diseased human tissues. *FASEB J.* **16**, 1271–1273 (2002).
  141. Yang, Y. *et al.* Lymphatic endothelial progenitors bud from the cardinal vein and intersomitic vessels in mammalian embryos. *Blood* **120**, 2340–2348 (2012).
  142. Kreuger, J. *et al.* Early lymph vessel development from embryonic stem cells. *Arterioscler. Thromb. Vasc. Biol.* **26**, 1073–1078 (2006).
  143. Choi, I. *et al.* Visualization of lymphatic vessels by Prox1-promoter directed GFP reporter in a bacterial artificial chromosome-based transgenic mouse. *Blood* **117**, 362–365 (2011).
  144. Wilting, J., Tomarev, S. I., Christ, B. & Schweigerer, L. Lymphangioblasts in embryonic lymphangiogenesis. *Lymphat Res Biol* **1**, 33–40 (2003).
  145. Hogan, B. M. *et al.* Ccbe1 is required for embryonic lymphangiogenesis and venous sprouting. *Nat. Genet.* **41**, 396–398 (2009).
  146. Yaniv, K. *et al.* Live imaging of lymphatic development in the zebrafish. *Nat. Med.* **12**, 711–716 (2006).
  147. Oh, S. J. *et al.* VEGF and VEGF-C: specific induction of angiogenesis and lymphangiogenesis in the differentiated avian chorioallantoic membrane. *Dev. Biol.* **188**, 96–109 (1997).
  148. Shi, V. Y., Bao, L. & Chan, L. S. Inflammation-driven dermal lymphangiogenesis in atopic dermatitis is associated with CD11b<sup>+</sup> macrophage recruitment and VEGF-C up-regulation in the IL-4-transgenic mouse model. *Microcirculation* **19**, 567–579 (2012).
  149. Tan, K. W. *et al.* Neutrophils contribute to inflammatory lymphangiogenesis by increasing VEGF-A bioavailability and secreting

- VEGF-D. *Blood* (2013). doi:10.1182/blood-2012-11-466532
150. Kubota, Y. *et al.* M-CSF inhibition selectively targets pathological angiogenesis and lymphangiogenesis. *J. Exp. Med.* **206**, 1089–1102 (2009).
  151. Asano, K. *et al.* CD169-positive macrophages dominate antitumor immunity by crosspresenting dead cell-associated antigens. *Immunity* **34**, 85–95 (2011).
  152. Wang, Y. *et al.* Ephrin-B2 controls VEGF-induced angiogenesis and lymphangiogenesis. *Nature* **465**, 483–486 (2010).
  153. Cao, Y. *et al.* Vascular endothelial growth factor C induces angiogenesis in vivo. *Proc. Natl. Acad. Sci. U.S.A.* **95**, 14389–14394 (1998).
  154. Dellinger, M. T., Meadows, S. M., Wynne, K., Cleaver, O. & Brekken, R. A. Vascular endothelial growth factor receptor-2 promotes the development of the lymphatic vasculature. *PLoS ONE* **8**, e74686 (2013).
  155. Hall, K. L., Volk-Draper, L. D., Flister, M. J. & Ran, S. New model of macrophage acquisition of the lymphatic endothelial phenotype. *PLoS ONE* **7**, e31794 (2012).
  156. Kerjaschki, D. *et al.* Lymphatic endothelial progenitor cells contribute to de novo lymphangiogenesis in human renal transplants. *Nat. Med.* **12**, 230–234 (2006).
  157. Jiang, S. *et al.* Hematopoietic stem cells contribute to lymphatic endothelium. *PLoS ONE* **3**, e3812 (2008).
  158. Kim, K. E. *et al.* Role of CD11b+ macrophages in intraperitoneal lipopolysaccharide-induced aberrant lymphangiogenesis and lymphatic function in the diaphragm. *Am. J. Pathol.* **175**, 1733–1745 (2009).
  159. Yuan, Z., Rodela, H., Hay, J. B., Oreopoulos, D. & Johnston, M. G. Lymph flow and lymphatic drainage of inflammatory cells from the peritoneal cavity in a casein-peritonitis model in sheep. *Lymphology* **27**, 114–128 (1994).
  160. Kurahara, H. *et al.* M2-polarized tumor-associated macrophage infiltration of regional lymph nodes is associated with nodal lymphangiogenesis and occult nodal involvement in pN0 pancreatic cancer. *Pancreas* **42**, 155–159 (2013).
  161. Kobayashi, N. *et al.* Hyaluronan deficiency in tumor stroma impairs macrophage trafficking and tumor neovascularization. *Cancer Res* **70**, 7073–7083 (2010).
  162. Skobe, M. *et al.* Concurrent induction of lymphangiogenesis, angiogenesis, and macrophage recruitment by vascular endothelial growth factor-C in melanoma. *Am. J. Pathol.* **159**, 893–903 (2001).
  163. Brendolan, A., Rosado, M. M., Carsetti, R., Selleri, L. & Dear, T. N. Development and function of the mammalian spleen. *Bioessays* **29**, 166–177 (2007).
  164. Bajénoff, M., Glaichenhaus, N. & Germain, R. N. Fibroblastic reticular cells guide T lymphocyte entry into and migration within the splenic T cell zone. *J. Immunol.* **181**, 3947–3954 (2008).
  165. Aichele, P. *et al.* Macrophages of the splenic marginal zone are essential for trapping of blood-borne particulate antigen but dispensable for induction of specific T cell responses. *J. Immunol.* **171**, 1148–1155 (2003).
  166. Kang, Y.-S. *et al.* The C-type lectin SIGN-R1 mediates uptake of the

- capsular polysaccharide of *Streptococcus pneumoniae* in the marginal zone of mouse spleen. *Proc. Natl. Acad. Sci. U.S.A.* **101**, 215–220 (2004).
167. Eloranta, M. L. & Alm, G. V. Splenic marginal metallophilic macrophages and marginal zone macrophages are the major interferon-alpha/beta producers in mice upon intravenous challenge with herpes simplex virus. *Scand. J. Immunol.* **49**, 391–394 (1999).
  168. Weiss, L. W. & Zelickson, A. S. Embryology of the epidermis: ultrastructural aspects. 1. Formation and early development in the mouse with mammalian comparisons. *Acta Derm. Venereol.* **55**, 161–168 (1975).
  169. Byrne, C., Tainsky, M. & Fuchs, E. Programming gene expression in developing epidermis. *Development* **120**, 2369–2383 (1994).
  170. Sumaria, N. *et al.* Cutaneous immunosurveillance by self-renewing dermal gammadelta T cells. *J. Exp. Med.* **208**, 505–518 (2011).
  171. Jameson, J. *et al.* A role for skin gammadelta T cells in wound repair. *Science* **296**, 747–749 (2002).
  172. Bursch, L. S. *et al.* Identification of a novel population of Langerin+ dendritic cells. *J. Exp. Med.* **204**, 3147–3156 (2007).
  173. Ginhoux, F. *et al.* Blood-derived dermal langerin+ dendritic cells survey the skin in the steady state. *J. Exp. Med.* **204**, 3133–3146 (2007).
  174. Flacher, V. *et al.* Skin langerin+ dendritic cells transport intradermally injected anti-DEC-205 antibodies but are not essential for subsequent cytotoxic CD8+ T cell responses. *J. Immunol.* **188**, 2146–2155 (2012).
  175. Bromley, S. K., Yan, S., Tomura, M., Kanagawa, O. & Luster, A. D. Recirculating memory T cells are a unique subset of CD4+ T cells with a distinct phenotype and migratory pattern. *J. Immunol.* **190**, 970–976 (2013).
  176. Ariotti, S. *et al.* Tissue-resident memory CD8+ T cells continuously patrol skin epithelia to quickly recognize local antigen. *Proc. Natl. Acad. Sci. U.S.A.* **109**, 19739–19744 (2012).
  177. Kellersch, B. & Brocker, T. Langerhans cell homeostasis in mice is dependent on mTORC1 but not mTORC2 function. *Blood* **121**, 298–307 (2013).
  178. van de Ven, R. *et al.* Characterization of four conventional dendritic cell subsets in human skin-draining lymph nodes in relation to T-cell activation. *Blood* **118**, 2502–2510 (2011).
  179. Frugé, R. E., Krout, C., Lu, R., Matsushima, H. & Takashima, A. Real-time visualization of macromolecule uptake by epidermal Langerhans cells in living animals. *J. Invest. Dermatol.* **132**, 609–614 (2012).
  180. Puttur, F. K. *et al.* Herpes simplex virus infects skin gamma delta T cells before Langerhans cells and impedes migration of infected Langerhans cells by inducing apoptosis and blocking E-cadherin downregulation. *J. Immunol.* **185**, 477–487 (2010).
  181. Igyarto, B. Z. *et al.* Langerhans cells suppress contact hypersensitivity responses via cognate CD4 interaction and langerhans cell-derived IL-10. *J. Immunol.* **183**, 5085–5093 (2009).
  182. Olvera-Gomez, I. *et al.* Cholera toxin activates nonconventional adjuvant pathways that induce protective CD8 T-cell responses after epicutaneous vaccination. *Proc. Natl. Acad. Sci. U.S.A.* **109**, 2072–2077

- (2012).
183. Henri, S. *et al.* CD207+ CD103+ dermal dendritic cells cross-present keratinocyte-derived antigens irrespective of the presence of Langerhans cells. *J. Exp. Med.* **207**, 189–206 (2010).
  184. Flacher, V. *et al.* Epidermal Langerhans cells rapidly capture and present antigens from C-type lectin-targeting antibodies deposited in the dermis. *J. Invest. Dermatol.* **130**, 755–762 (2010).
  185. Valladeau, J. *et al.* Identification of mouse langerin/CD207 in Langerhans cells and some dendritic cells of lymphoid tissues. *J. Immunol.* **168**, 782–792 (2002).
  186. Takahara, K. *et al.* Identification and expression of mouse Langerin (CD207) in dendritic cells. *Int. Immunol.* **14**, 433–444 (2002).
  187. Kissenpfennig, A. *et al.* Dynamics and function of Langerhans cells in vivo: dermal dendritic cells colonize lymph node areas distinct from slower migrating Langerhans cells. *Immunity* **22**, 643–654 (2005).
  188. Cummings, R. J. *et al.* Exposure to ionizing radiation induces the migration of cutaneous dendritic cells by a CCR7-dependent mechanism. *J. Immunol.* **189**, 4247–4257 (2012).
  189. Ohl, L. *et al.* CCR7 governs skin dendritic cell migration under inflammatory and steady-state conditions. *Immunity* **21**, 279–288 (2004).
  190. Eidsmo, L. *et al.* Differential migration of epidermal and dermal dendritic cells during skin infection. *J. Immunol.* **182**, 3165–3172 (2009).
  191. Bedoui, S. *et al.* Cross-presentation of viral and self antigens by skin-derived CD103+ dendritic cells. *Nat. Immunol.* **10**, 488–495 (2009).
  192. Albanesi, C. *et al.* Chemerin expression marks early psoriatic skin lesions and correlates with plasmacytoid dendritic cell recruitment. *J. Exp. Med.* **206**, 249–258 (2009).
  193. Lande, R. *et al.* Plasmacytoid dendritic cells sense self-DNA coupled with antimicrobial peptide. *Nature* **449**, 564–569 (2007).
  194. Shibata, S. *et al.* IL-27 activates Th1-mediated responses in imiquimod-induced psoriasis-like skin lesions. *J. Invest. Dermatol.* **133**, 479–488 (2013).
  195. Ekman, A.-K. *et al.* Systemically elevated Th1-, Th2- and Th17-associated chemokines in psoriasis vulgaris before and after ultraviolet B treatment. *Acta Derm. Venereol.* **93**, 527–531 (2013).
  196. Zhang, P. *et al.* Analysis of Th1/Th2 response pattern for erythrodermic psoriasis. *J. Huazhong Univ. Sci. Technol. Med. Sci.* **34**, 596–601 (2014).
  197. He, R. *et al.* TSLP acts on infiltrating effector T cells to drive allergic skin inflammation. *Proc. Natl. Acad. Sci. U.S.A.* **105**, 11875–11880 (2008).
  198. Vestergaard, C., Deleuran, M., Gesser, B. & Grønhøj Larsen, C. Expression of the T-helper 2-specific chemokine receptor CCR4 on CCR10-positive lymphocytes in atopic dermatitis skin but not in psoriasis skin. *Br. J. Dermatol.* **149**, 457–463 (2003).
  199. Elloso, M. M., Gomez-Angelats, M. & Fourie, A. M. Targeting the Th17 pathway in psoriasis. *J. Leukoc. Biol.* **92**, 1187–1197 (2012).
  200. Gray, E. E. *et al.* Deficiency in IL-17-committed V $\gamma$ 4(+)  $\gamma\delta$  T cells in a spontaneous Sox13-mutant CD45.1(+) congenic mouse substrain

- provides protection from dermatitis. *Nat. Immunol.* **14**, 584–592 (2013).
201. Girardi, M. *et al.* Regulation of cutaneous malignancy by gammadelta T cells. *Science* **294**, 605–609 (2001).
  202. Girardi, M. *et al.* The distinct contributions of murine T cell receptor (TCR)gammadelta+ and TCRalphabeta+ T cells to different stages of chemically induced skin cancer. *J. Exp. Med.* **198**, 747–755 (2003).
  203. Gilhar, A. *et al.* Psoriasis is mediated by a cutaneous defect triggered by activated immunocytes: induction of psoriasis by cells with natural killer receptors. *J. Invest. Dermatol.* **119**, 384–391 (2002).
  204. Bonish, B. *et al.* Overexpression of CD1d by keratinocytes in psoriasis and CD1d-dependent IFN-gamma production by NK-T cells. *J. Immunol.* **165**, 4076–4085 (2000).
  205. Luster, A. D. Chemokines - Chemotactic cytokines that mediate inflammation. *New Engl J Med* **338**, 436–445 (1998).
  206. Zou, Y. R., Kottmann, A. H., Kuroda, M., Taniuchi, I. & Littman, D. R. Function of the chemokine receptor CXCR4 in haematopoiesis and in cerebellar development. *Nature* **393**, 595–599 (1998).
  207. Lim, J. K. *et al.* Chemokine receptor Ccr2 is critical for monocyte accumulation and survival in West Nile virus encephalitis. *J. Immunol.* **186**, 471–478 (2011).
  208. Nomiya, H., Osada, N. & Yoshie, O. A family tree of vertebrate chemokine receptors for a unified nomenclature. *Dev. Comp. Immunol.* **35**, 705–715 (2011).
  209. Zlotnik, A. & Yoshie, O. Chemokines: a new classification system and their role in immunity. *Immunity* **12**, 121–127 (2000).
  210. Rot, A. & Andrian, von, U. H. Chemokines in innate and adaptive host defense: basic chemokine grammar for immune cells. *Annu. Rev. Immunol.* **22**, 891–928 (2004).
  211. Wintges, K. *et al.* Impaired bone formation and increased osteoclastogenesis in mice lacking chemokine (C-C motif) ligand 5 (Ccl5). *J. Bone Miner. Res.* **28**, 2070–2080 (2013).
  212. Serbina, N. V. & Pamer, E. G. Monocyte emigration from bone marrow during bacterial infection requires signals mediated by chemokine receptor CCR2. *Nat. Immunol.* **7**, 311–317 (2006).
  213. Guan, E., Wang, J. & Norcross, M. A. Amino-terminal processing of MIP-1beta/CCL4 by CD26/dipeptidyl-peptidase IV. *J. Cell. Biochem.* **92**, 53–64 (2004).
  214. Guan, E., Wang, J., Roderiquez, G. & Norcross, M. A. Natural truncation of the chemokine MIP-1 beta /CCL4 affects receptor specificity but not anti-HIV-1 activity. *J Biol Chem* **277**, 32348–32352 (2002).
  215. Ali, S., Fritchley, S. J., Chaffey, B. T. & Kirby, J. A. Contribution of the putative heparan sulfate-binding motif BBXB of RANTES to transendothelial migration. *Glycobiology* **12**, 535–543 (2002).
  216. Ali, S., Palmer, A. C., Banerjee, B., Fritchley, S. J. & Kirby, J. A. Examination of the function of RANTES, MIP-1alpha, and MIP-1beta following interaction with heparin-like glycosaminoglycans. *J Biol Chem* **275**, 11721–11727 (2000).
  217. Ali, S. *et al.* A non-glycosaminoglycan-binding variant of CC chemokine ligand 7 (monocyte chemoattractant protein-3) antagonizes

- chemokine-mediated inflammation. *J. Immunol.* **175**, 1257–1266 (2005).
218. Severin, I. C. *et al.* Characterization of the chemokine CXCL11-heparin interaction suggests two different affinities for glycosaminoglycans. *J. Biol. Chem.* **285**, 17713–17724 (2010).
  219. Kuschert, G. S. *et al.* Glycosaminoglycans interact selectively with chemokines and modulate receptor binding and cellular responses. *Biochemistry* **38**, 12959–12968 (1999).
  220. Jen, C. H. & Leary, J. A. A competitive binding study of chemokine, sulfated receptor, and glycosaminoglycan interactions by nano-electrospray ionization mass spectrometry. *Anal Biochem* **407**, 134–140 (2010).
  221. Witt, D. P. & Lander, A. D. Differential binding of chemokines to glycosaminoglycan subpopulations. *Curr. Biol.* **4**, 394–400 (1994).
  222. Hoogewerf, A. J. *et al.* Glycosaminoglycans mediate cell surface oligomerization of chemokines. *Biochemistry* **36**, 13570–13578 (1997).
  223. Proudfoot, A. E. I. *et al.* Glycosaminoglycan binding and oligomerization are essential for the in vivo activity of certain chemokines. *Proc. Natl. Acad. Sci. U.S.A.* **100**, 1885–1890 (2003).
  224. Murphy, P. M. *et al.* International union of pharmacology. XXII. Nomenclature for chemokine receptors. *Pharmacol Rev* **52**, 145–176 (2000).
  225. Mueller, S. G., White, J. R., Schraw, W. P., Lam, V. & Richmond, A. Ligand-induced desensitization of the human CXC chemokine receptor-2 is modulated by multiple serine residues in the carboxyl-terminal domain of the receptor. *J. Biol. Chem.* **272**, 8207–8214 (1997).
  226. Schraufstatter, I. U., Burger, M., Hoch, R. C., Oades, Z. G. & Takamori, H. Importance of the carboxy-terminus of the CXCR2 for signal transduction. *Biochem. Biophys. Res. Commun.* **244**, 243–248 (1998).
  227. Huttenrauch, F., Nitzki, A., Lin, F. T., Honing, S. & Oppermann, M. Beta-arrestin binding to CC chemokine receptor 5 requires multiple C-terminal receptor phosphorylation sites and involves a conserved Asp-Arg-Tyr sequence motif. *J Biol Chem* **277**, 30769–30777 (2002).
  228. Kim, K. M. & Caron, M. G. Complementary roles of the DRY motif and C-terminus tail of GPCRS for G protein coupling and beta-arrestin interaction. *Biochem. Biophys. Res. Commun.* **366**, 42–47 (2008).
  229. Lagane, B. *et al.* Mutation of the DRY motif reveals different structural requirements for the CC chemokine receptor 5-mediated signaling and receptor endocytosis. *Mol Pharmacol* **67**, 1966–1976 (2005).
  230. Rovati, G. E., Capra, V. & Neubig, R. R. The highly conserved DRY motif of class A G protein-coupled receptors: beyond the ground state. *Mol Pharmacol* **71**, 959–964 (2007).
  231. Fang, W. B. *et al.* CCL2/CCR2 chemokine signaling coordinates survival and motility of breast cancer cells through Smad3 protein- and p42/44 mitogen-activated protein kinase (MAPK)-dependent mechanisms. *J. Biol. Chem.* **287**, 36593–36608 (2012).
  232. Banas, B. *et al.* Binding of the chemokine SLC/CCL21 to its receptor CCR7 increases adhesive properties of human mesangial cells. *Kidney Int* **66**, 2256–2263 (2004).
  233. Kuipers, H. F. *et al.* CC chemokine receptor 5 gene promoter activation by the cyclic AMP response element binding transcription factor. *Blood*

- 112**, 1610–1619 (2008).
234. Zigmond, S. H., Levitsky, H. I. & Kreel, B. J. Cell polarity: an examination of its behavioral expression and its consequences for polymorphonuclear leukocyte chemotaxis. *J. Cell Biol.* **89**, 585–592 (1981).
  235. Lusche, D. F., Wessels, D. & Soll, D. R. The effects of extracellular calcium on motility, pseudopod and uropod formation, chemotaxis, and the cortical localization of myosin II in *Dictyostelium discoideum*. *Cell Motil Cytoskeleton* **66**, 567–587 (2009).
  236. Stepanovic, V., Wessels, D., Daniels, K., Loomis, W. F. & Soll, D. R. Intracellular role of adenylyl cyclase in regulation of lateral pseudopod formation during *Dictyostelium* chemotaxis. *Eukaryot Cell* **4**, 775–786 (2005).
  237. Soriano, S. F. *et al.* In vivo analysis of uropod function during physiological T cell trafficking. *J. Immunol.* **187**, 2356–2364 (2011).
  238. Vicker, M. G. The regulation of chemotaxis and chemokinesis in *Dictyostelium* amoebae by temporal signals and spatial gradients of cyclic AMP. *J. Cell. Sci.* **107 ( Pt 2)**, 659–667 (1994).
  239. Bialkowska, K. *et al.* Evidence that beta3 integrin-induced Rac activation involves the calpain-dependent formation of integrin clusters that are distinct from the focal complexes and focal adhesions that form as Rac and RhoA become active. *J. Cell Biol.* **151**, 685–696 (2000).
  240. Moratz, C. *et al.* Regulator of G protein signaling 1 (RGS1) markedly impairs Gi alpha signaling responses of B lymphocytes. *J. Immunol.* **164**, 1829–1838 (2000).
  241. Moratz, C., Hayman, J. R., Gu, H. & Kehrl, J. H. Abnormal B-cell responses to chemokines, disturbed plasma cell localization, and distorted immune tissue architecture in *Rgs1*<sup>-/-</sup> mice. *Mol. Cell. Biol.* **24**, 5767–5775 (2004).
  242. Agenès, F., Bosco, N., Mascarell, L., Fritah, S. & Ceredig, R. Differential expression of regulator of G-protein signalling transcripts and in vivo migration of CD4<sup>+</sup> naïve and regulatory T cells. *Immunology* **115**, 179–188 (2005).
  243. Oldham, W. M., Van Eps, N., Preininger, A. M., Hubbell, W. L. & Hamm, H. E. Mapping allosteric connections from the receptor to the nucleotide-binding pocket of heterotrimeric G proteins. *Proc. Natl. Acad. Sci. U.S.A.* **104**, 7927–7932 (2007).
  244. Mueller, A., Kelly, E. & Strange, P. G. Pathways for internalization and recycling of the chemokine receptor CCR5. *Blood* **99**, 785–791 (2002).
  245. Borroni, E. M., Mantovani, A., Locati, M. & Bonecchi, R. Chemokine receptors intracellular trafficking. *Pharmacol. Ther.* **127**, 1–8 (2010).
  246. Vroon, A., Heijnen, C. J. & Kavelaars, A. GRKs and arrestins: regulators of migration and inflammation. *J. Leukoc. Biol.* **80**, 1214–1221 (2006).
  247. Claing, A., Laporte, S. A., Caron, M. G. & Lefkowitz, R. J. Endocytosis of G protein-coupled receptors: roles of G protein-coupled receptor kinases and beta-arrestin proteins. *Prog. Neurobiol.* **66**, 61–79 (2002).
  248. Shenoy, S. K. & Lefkowitz, R. J. Receptor-specific ubiquitination of beta-arrestin directs assembly and targeting of seven-transmembrane receptor signalosomes. *J Biol Chem* **280**, 15315–15324 (2005).

249. Chaudhuri, A. *et al.* Detection of Duffy antigen in the plasma membranes and caveolae of vascular endothelial and epithelial cells of nonerythroid organs. *Blood* **89**, 701–712 (1997).
250. Comerford, I., Milasta, S., Morrow, V., Milligan, G. & Nibbs, R. The chemokine receptor CCX-CKR mediates effective scavenging of CCL19 in vitro. *Eur. J. Immunol.* **36**, 1904–1916 (2006).
251. Pruenster, M. *et al.* The Duffy antigen receptor for chemokines transports chemokines and supports their promigratory activity. *Nat. Immunol.* **10**, 101–108 (2009).
252. Baumhater, S. *et al.* Binding of L-selectin to the vascular sialomucin CD34. *Science* **262**, 436–438 (1993).
253. Puri, K. D., Finger, E. B. & Springer, T. A. The faster kinetics of L-selectin than of E-selectin and P-selectin rolling at comparable binding strength. *J. Immunol.* **158**, 405–413 (1997).
254. Möhle, R., Moore, M. A., Nachman, R. L. & Rafii, S. Transendothelial migration of CD34+ and mature hematopoietic cells: an in vitro study using a human bone marrow endothelial cell line. *Blood* **89**, 72–80 (1997).
255. van Zante, A. *et al.* Lymphocyte-HEV interactions in lymph nodes of a sulfotransferase-deficient mouse. *J. Exp. Med.* **198**, 1289–1300 (2003).
256. Simon, S. I. *et al.* L-selectin (CD62L) cross-linking signals neutrophil adhesive functions via the Mac-1 (CD11b/CD18) beta 2-integrin. *J. Immunol.* **155**, 1502–1514 (1995).
257. Nagamatsu, H. *et al.* Regulation of T-lymphocyte trafficking by ICAM-1, MAdCAM-1, and CCR7 in microcirculation of appendicular and intestinal lymphoid tissues. *Microcirculation* **11**, 493–502 (2004).
258. Green, C. E. *et al.* Dynamic shifts in LFA-1 affinity regulate neutrophil rolling, arrest, and transmigration on inflamed endothelium. *Blood* **107**, 2101–2111 (2006).
259. Schenkel, A. R. & Pauza, C. D. Pertussis toxin treatment in vivo reduces surface expression of the adhesion integrin leukocyte function antigen-1 (LFA-1). *Cell Adhes. Commun.* **7**, 183–193 (1999).
260. Im, S. Y. *et al.* Dual effects of pertussis toxin on murine neutrophils in vivo. I. Pertussis toxin inhibits extravasation potential of mature neutrophils while simultaneously stimulating granulopoiesis. *Inflammation* **13**, 707–726 (1989).
261. Weninger, W., Biro, M. & Jain, R. Leukocyte migration in the interstitial space of non-lymphoid organs. *Nat. Rev. Immunol.* **14**, 232–246 (2014).
262. McDonald, B. *et al.* Intravascular danger signals guide neutrophils to sites of sterile inflammation. *Science* **330**, 362–366 (2010).
263. Mempel, T. R., Junt, T. & Andrian, von, U. H. Rulers over randomness: stroma cells guide lymphocyte migration in lymph nodes. *Immunity* **25**, 867–869 (2006).
264. Bajénoff, M. *et al.* Stromal cell networks regulate lymphocyte entry, migration, and territoriality in lymph nodes. *Immunity* **25**, 989–1001 (2006).
265. Kastenmüller, W. *et al.* Peripheral prepositioning and local CXCL9 chemokine-mediated guidance orchestrate rapid memory CD8+ T cell responses in the lymph node. *Immunity* **38**, 502–513 (2013).
266. Weber, M. *et al.* Interstitial dendritic cell guidance by haptotactic

- chemokine gradients. *Science* **339**, 328–332 (2013).
267. Lämmermann, T. *et al.* Neutrophil swarms require LTB4 and integrins at sites of cell death in vivo. *Nature* **498**, 371–375 (2013).
268. Schumann, K. *et al.* Immobilized chemokine fields and soluble chemokine gradients cooperatively shape migration patterns of dendritic cells. *Immunity* **32**, 703–713 (2010).
269. Baggiolini, M., Walz, A. & Kunkel, S. L. Neutrophil-activating peptide-1/interleukin 8, a novel cytokine that activates neutrophils. *J. Clin. Invest.* **84**, 1045–1049 (1989).
270. Britschgi, M. R., Favre, S. & Luther, S. A. CCL21 is sufficient to mediate DC migration, maturation and function in the absence of CCL19. *Eur. J. Immunol.* **40**, 1266–1271 (2010).
271. Link, A. *et al.* Fibroblastic reticular cells in lymph nodes regulate the homeostasis of naive T cells. *Nat. Immunol.* **8**, 1255–1265 (2007).
272. Haessler, U., Pisano, M., Wu, M. & Swartz, M. A. Dendritic cell chemotaxis in 3D under defined chemokine gradients reveals differential response to ligands CCL21 and CCL19. *Proc. Natl. Acad. Sci. U.S.A.* **108**, 5614–5619 (2011).
273. Schneider, M. A., Meingassner, J. G., Lipp, M., Moore, H. D. & Rot, A. CCR7 is required for the in vivo function of CD4<sup>+</sup> CD25<sup>+</sup> regulatory T cells. *J. Exp. Med.* **204**, 735–745 (2007).
274. Worbs, T., Mempel, T. R., Bölter, J., Andrian, von, U. H. & Förster, R. CCR7 ligands stimulate the intranodal motility of T lymphocytes in vivo. *J. Exp. Med.* **204**, 489–495 (2007).
275. Nakano, H. *et al.* Genetic defect in T lymphocyte-specific homing into peripheral lymph nodes. *Eur. J. Immunol.* **27**, 215–221 (1997).
276. Gunn, M. D. *et al.* Mice lacking expression of secondary lymphoid organ chemokine have defects in lymphocyte homing and dendritic cell localization. *J. Exp. Med.* **189**, 451–460 (1999).
277. Nakano, H. *et al.* A novel mutant gene involved in T-lymphocyte-specific homing into peripheral lymphoid organs on mouse chromosome 4. *Blood* **91**, 2886–2895 (1998).
278. Zlotoff, D. A. *et al.* CCR7 and CCR9 together recruit hematopoietic progenitors to the adult thymus. *Blood* **115**, 1897–1905 (2010).
279. Ueno, T. *et al.* Role for CCR7 ligands in the emigration of newly generated T lymphocytes from the neonatal thymus. *Immunity* **16**, 205–218 (2002).
280. Misslitz, A. *et al.* Thymic T cell development and progenitor localization depend on CCR7. *J. Exp. Med.* **200**, 481–491 (2004).
281. Davalos-Misslitz, A. C. M., Worbs, T., Willenzon, S., Bernhardt, G. & Förster, R. Impaired responsiveness to T-cell receptor stimulation and defective negative selection of thymocytes in CCR7-deficient mice. *Blood* **110**, 4351–4359 (2007).
282. Calderón, L. & Boehm, T. Three chemokine receptors cooperatively regulate homing of hematopoietic progenitors to the embryonic mouse thymus. *Proc. Natl. Acad. Sci. U.S.A.* **108**, 7517–7522 (2011).
283. Stein, J. V. *et al.* The CC chemokine thymus-derived chemotactic agent 4 (TCA-4, secondary lymphoid tissue chemokine, 6Ckine, exodus-2) triggers lymphocyte function-associated antigen 1-mediated arrest of rolling T lymphocytes in peripheral lymph node high endothelial

- venules. *J. Exp. Med.* **191**, 61–76 (2000).
284. Krueger, A., Willenzon, S., Lyszkiewicz, M., Kremmer, E. & Förster, R. CC chemokine receptor 7 and 9 double-deficient hematopoietic progenitors are severely impaired in seeding the adult thymus. *Blood* **115**, 1906–1912 (2010).
285. Mori, S. *et al.* Mice lacking expression of the chemokines CCL21-ser and CCL19 (plt mice) demonstrate delayed but enhanced T cell immune responses. *J. Exp. Med.* **193**, 207–218 (2001).
286. Davalos-Misslitz, A. C. M. *et al.* Generalized multi-organ autoimmunity in CCR7-deficient mice. *Eur. J. Immunol.* **37**, 613–622 (2007).
287. Uehara, S., Grinberg, A., Farber, J. M. & Love, P. E. A role for CCR9 in T lymphocyte development and migration. *J. Immunol.* **168**, 2811–2819 (2002).
288. Papadakis, K. A. *et al.* The role of thymus-expressed chemokine and its receptor CCR9 on lymphocytes in the regional specialization of the mucosal immune system. *J. Immunol.* **165**, 5069–5076 (2000).
289. Wendland, M. *et al.* CCR9 is a homing receptor for plasmacytoid dendritic cells to the small intestine. *Proc. Natl. Acad. Sci. U.S.A.* **104**, 6347–6352 (2007).
290. Mizuno, S. *et al.* CCR9+ plasmacytoid dendritic cells in the small intestine suppress development of intestinal inflammation in mice. *Immunol. Lett.* **146**, 64–69 (2012).
291. Hadeiba, H. *et al.* Plasmacytoid dendritic cells transport peripheral antigens to the thymus to promote central tolerance. *Immunity* **36**, 438–450 (2012).
292. Seth, S. *et al.* CCR7 essentially contributes to the homing of plasmacytoid dendritic cells to lymph nodes under steady-state as well as inflammatory conditions. *J. Immunol.* **186**, 3364–3372 (2011).
293. Liu, X. *et al.* Tolerance induction towards cardiac allografts under costimulation blockade is impaired in CCR7-deficient animals but can be restored by adoptive transfer of syngeneic plasmacytoid dendritic cells. *Eur. J. Immunol.* **41**, 611–623 (2011).
294. Eksteen, B. *et al.* Gut homing receptors on CD8 T cells are retinoic acid dependent and not maintained by liver dendritic or stellate cells. *Gastroenterology* **137**, 320–329 (2009).
295. Hammerschmidt, S. I. *et al.* Retinoic acid induces homing of protective T and B cells to the gut after subcutaneous immunization in mice. *J. Clin. Invest.* **121**, 3051–3061 (2011).
296. Jang, M. H. *et al.* CCR7 is critically important for migration of dendritic cells in intestinal lamina propria to mesenteric lymph nodes. *J. Immunol.* **176**, 803–810 (2006).
297. Molenaar, R. *et al.* Lymph node stromal cells support dendritic cell-induced gut-homing of T cells. *J. Immunol.* **183**, 6395–6402 (2009).
298. Evans, T. I. & Reeves, R. K. All-trans-retinoic acid imprints expression of the gut-homing marker  $\alpha 4\beta 7$  while suppressing lymph node homing of dendritic cells. *Clin. Vaccine Immunol.* **20**, 1642–1646 (2013).
299. Marino, D., Dabouras, V., Brändli, A. W. & Detmar, M. A role for all-trans-retinoic acid in the early steps of lymphatic vasculature development. *J. Vasc. Res.* **48**, 236–251 (2011).
300. Wurbel, M. A. *et al.* Mice lacking the CCR9 CC-chemokine receptor

- show a mild impairment of early T- and B-cell development and a reduction in T-cell receptor gamma delta(+) gut intraepithelial lymphocytes. *Blood* **98**, 2626–2632 (2001).
301. Pabst, O. *et al.* Chemokine receptor CCR9 contributes to the localization of plasma cells to the small intestine. *J. Exp. Med.* **199**, 411–416 (2004).
  302. Nibbs, R. J., Wylie, S. M., Yang, J., Landau, N. R. & Graham, G. J. Cloning and characterization of a novel promiscuous human beta-chemokine receptor D6. *J. Biol. Chem.* **272**, 32078–32083 (1997).
  303. Madigan, J. *et al.* Chemokine scavenger D6 is expressed by trophoblasts and aids the survival of mouse embryos transferred into allogeneic recipients. *J. Immunol.* **184**, 3202–3212 (2010).
  304. Jamieson, T. *et al.* The chemokine receptor D6 limits the inflammatory response in vivo. *Nat. Immunol.* **6**, 403–411 (2005).
  305. Collins, C. B., McNamee, E. N., Wermers, J. D., Lebsack, M. D. P. & Rivera-Nieves, J. Chemokine decoy receptor D6 in inflammatory bowel disease (IBD) and IBD-associated colon cancer. *Gut* **59**, 151–152 (2010).
  306. Lee, K. M. *et al.* D6 facilitates cellular migration and fluid flow to lymph nodes by suppressing lymphatic congestion. *Blood* **118**, 6220–6229 (2011).
  307. Nibbs, R. J. *et al.* The beta-chemokine receptor D6 is expressed by lymphatic endothelium and a subset of vascular tumors. *Am. J. Pathol.* **158**, 867–877 (2001).
  308. McKimmie, C. S. *et al.* An analysis of the function and expression of D6 on lymphatic endothelial cells. *Blood* **121**, 3768–3777 (2013).
  309. Rot, A. *et al.* Cell-autonomous regulation of neutrophil migration by the D6 chemokine decoy receptor. *J. Immunol.* **190**, 6450–6456 (2013).
  310. McKimmie, C. S. *et al.* Hemopoietic cell expression of the chemokine decoy receptor D6 is dynamic and regulated by GATA1. *J. Immunol.* **181**, 8171–8181 (2008).
  311. Bonecchi, R. *et al.* Differential recognition and scavenging of native and truncated macrophage-derived chemokine (macrophage-derived chemokine/CC chemokine ligand 22) by the D6 decoy receptor. *J. Immunol.* **172**, 4972–4976 (2004).
  312. Savino, B. *et al.* Recognition versus adaptive up-regulation and degradation of CC chemokines by the chemokine decoy receptor D6 are determined by their N-terminal sequence. *J. Biol. Chem.* **284**, 26207–26215 (2009).
  313. Nibbs, R. J., Yang, J., Landau, N. R., Mao, J. H. & Graham, G. J. LD78beta, a non-allelic variant of human MIP-1alpha (LD78alpha), has enhanced receptor interactions and potent HIV suppressive activity. *J Biol Chem* **274**, 17478–17483 (1999).
  314. Hansell, C. A. H. *et al.* Universal expression and dual function of the atypical chemokine receptor D6 on innate-like B cells in mice. *Blood* **117**, 5413–5424 (2011).
  315. Nibbs, R. J., Wylie, S. M., Pragnell, I. B. & Graham, G. J. Cloning and characterization of a novel murine beta chemokine receptor, D6. Comparison to three other related macrophage inflammatory protein-1alpha receptors, CCR-1, CCR-3, and CCR-5. *J. Biol. Chem.* **272**, 12495–12504 (1997).

316. Weber, M. *et al.* The chemokine receptor D6 constitutively traffics to and from the cell surface to internalize and degrade chemokines. *Mol. Biol. Cell* **15**, 2492–2508 (2004).
317. Weber, M. *et al.* The chemokine receptor D6 constitutively traffics to and from the cell surface to internalize and degrade chemokine. *Mol. Biol. Cell* **15**, 2492–2508 (2004).
318. Malhotra, D. *et al.* Transcriptional profiling of stroma from inflamed and resting lymph nodes defines immunological hallmarks. *Nat. Immunol.* **13**, 499–510 (2012).
319. Ford, L. B., Hansell, C. A. H. & Nibbs, R. J. B. Using fluorescent chemokine uptake to detect chemokine receptors by fluorescent activated cell sorting. *Methods Mol. Biol.* **1013**, 203–214 (2013).
320. Ford, L. B. *et al.* Characterization of Conventional and Atypical Receptors for the Chemokine CCL2 on Mouse Leukocytes. *J. Immunol.* **193**, 400–411 (2014).
321. Bazzan, E. *et al.* Expression of the atypical chemokine receptor D6 in human alveolar macrophages in COPD. *Chest* **143**, 98–106 (2013).
322. McKimmie, C. S. *et al.* Hemopoietic cell expression of the chemokine decoy receptor D6 is dynamic and regulated by GATA1. *J. Immunol.* **181**, 3353–3363 (2008).
323. Savino, B. *et al.* Control of murine Ly6C(high) monocyte traffic and immunosuppressive activities by atypical chemokine receptor D6. *Blood* **119**, 5250–5260 (2012).
324. Vetrano, S. *et al.* The lymphatic system controls intestinal inflammation and inflammation-associated Colon Cancer through the chemokine decoy receptor D6. *Gut* **59**, 197–206 (2010).
325. Nibbs, R. J. *et al.* The atypical chemokine receptor D6 suppresses the development of chemically induced skin tumors. *J. Clin. Invest.* **117**, 1884–1892 (2007).
326. Nibbs, R. J. B. *et al.* The atypical chemokine receptor D6 suppresses the development of chemically induced skin tumors. *J. Clin. Invest.* **117**, 1884–1892 (2007).
327. Martinez de la Torre, Y. *et al.* Increased inflammation in mice deficient for the chemokine decoy receptor D6. *Eur. J. Immunol.* **35**, 1342–1346 (2005).
328. Di Liberto, D. *et al.* Role of the chemokine decoy receptor D6 in balancing inflammation, immune activation, and antimicrobial resistance in Mycobacterium tuberculosis infection. *J. Exp. Med.* **205**, 2075–2084 (2008).
329. Berres, M.-L. *et al.* The chemokine scavenging receptor D6 limits acute toxic liver injury in vivo. *Biol. Chem.* **390**, 1039–1045 (2009).
330. Whitehead, G. S. *et al.* The chemokine receptor D6 has opposing effects on allergic inflammation and airway reactivity. *Am. J. Respir. Crit. Care Med.* **175**, 243–249 (2007).
331. Madigan, J. *et al.* Chemokine scavenger D6 is expressed by trophoblasts and aids the survival of mouse embryos transferred into allogeneic recipients. *J. Immunol.* **184**, 3202–3212 (2010).
332. Demogines, A., Truong, K. A. & Sawyer, S. L. Species-specific features of DARC, the primate receptor for Plasmodium vivax and Plasmodium knowlesi. *Mol. Biol. Evol.* **29**, 445–449 (2012).

333. Tournamille, C., Colin, Y., Cartron, J. P. & Le Van Kim, C. Disruption of a GATA motif in the Duffy gene promoter abolishes erythroid gene expression in Duffy-negative individuals. *Nat. Genet.* **10**, 224–228 (1995).
334. Grann, V. R. *et al.* Duffy (Fy), DARC, and neutropenia among women from the United States, Europe and the Caribbean. *Br. J. Haematol.* **143**, 288–293 (2008).
335. Ramsuran, V. *et al.* Duffy-null-associated low neutrophil counts influence HIV-1 susceptibility in high-risk South African black women. *Clin. Infect. Dis.* **52**, 1248–1256 (2011).
336. Thobakgale, C. F. & Ndung'u, T. Neutrophil counts in persons of African origin. *Curr. Opin. Hematol.* **21**, 50–57 (2014).
337. Peiper, S. C. *et al.* The Duffy antigen/receptor for chemokines (DARC) is expressed in endothelial cells of Duffy negative individuals who lack the erythrocyte receptor. *J. Exp. Med.* **181**, 1311–1317 (1995).
338. Kashiwazaki, M. *et al.* A high endothelial venule-expressing promiscuous chemokine receptor DARC can bind inflammatory, but not lymphoid, chemokines and is dispensable for lymphocyte homing under physiological conditions. *Int. Immunol.* **15**, 1219–1227 (2003).
339. Dawson, T. C. *et al.* Exaggerated response to endotoxin in mice lacking the Duffy antigen/receptor for chemokines (DARC). *Blood* **96**, 1681–1684 (2000).
340. Reutershan, J., Harry, B., Chang, D., Bagby, G. J. & Ley, K. DARC on RBC limits lung injury by balancing compartmental distribution of CXC chemokines. *Eur. J. Immunol.* **39**, 1597–1607 (2009).
341. Burns, J. M. *et al.* A novel chemokine receptor for SDF-1 and I-TAC involved in cell survival, cell adhesion, and tumor development. *J. Exp. Med.* **203**, 2201–2213 (2006).
342. Sierro, F. *et al.* Disrupted cardiac development but normal hematopoiesis in mice deficient in the second CXCL12/SDF-1 receptor, CXCR7. *Proc. Natl. Acad. Sci. U.S.A.* **104**, 14759–14764 (2007).
343. Décaillot, F. M. *et al.* CXCR7/CXCR4 heterodimer constitutively recruits beta-arrestin to enhance cell migration. *J. Biol. Chem.* **286**, 32188–32197 (2011).
344. Levoye, A., Balabanian, K., Baleux, F., Bachelerie, F. & Lagane, B. CXCR7 heterodimerizes with CXCR4 and regulates CXCL12-mediated G protein signaling. *Blood* **113**, 6085–6093 (2009).
345. Gerrits, H. *et al.* Early postnatal lethality and cardiovascular defects in CXCR7-deficient mice. *Genesis* **46**, 235–245 (2008).
346. Miao, Z. *et al.* CXCR7 (RDC1) promotes breast and lung tumor growth in vivo and is expressed on tumor-associated vasculature. *Proc. Natl. Acad. Sci. U.S.A.* **104**, 15735–15740 (2007).
347. Wang, J. *et al.* The role of CXCR7/RDC1 as a chemokine receptor for CXCL12/SDF-1 in prostate cancer. *J Biol Chem* **283**, 4283–4294 (2008).
348. Mazzinghi, B. *et al.* Essential but differential role for CXCR4 and CXCR7 in the therapeutic homing of human renal progenitor cells. *J. Exp. Med.* **205**, 479–490 (2008).
349. Odemis, V. *et al.* The presumed atypical chemokine receptor CXCR7 signals through G(i/o) proteins in primary rodent astrocytes and human glioma cells. *Glia* **60**, 372–381 (2012).

350. Donà, E. *et al.* Directional tissue migration through a self-generated chemokine gradient. *Nature* (2013). doi:10.1038/nature12635
351. Venkiteswaran, G. *et al.* Generation and Dynamics of an Endogenous, Self-Generated Signaling Gradient across a Migrating Tissue. *Cell* (2013). doi:10.1016/j.cell.2013.09.046
352. Cubedo, N., Cerdan, E., Sapede, D. & Rossel, M. CXCR4 and CXCR7 cooperate during tangential migration of facial motoneurons. *Mol. Cell. Neurosci.* **40**, 474–484 (2009).
353. Lipfert, J., Ödemis, V., Wagner, D.-C., Boltze, J. & Engele, J. CXCR4 and CXCR7 form a functional receptor unit for SDF-1/CXCL12 in primary rodent microglia. *Neuropathol. Appl. Neurobiol.* **39**, 667–680 (2013).
354. Memi, F. *et al.* CXC Chemokine Receptor 7 (CXCR7) Affects the Migration of GnRH Neurons by Regulating CXCL12 Availability. *J. Neurosci.* **33**, 17527–17537 (2013).
355. Wang, J. *et al.* The role of CXCR7/RDC1 as a chemokine receptor for CXCL12/SDF-1 in prostate cancer. *J Biol Chem* **283**, 4283–4294 (2008).
356. Tarnowski, M. *et al.* Regulation of expression of stromal-derived factor-1 receptors: CXCR4 and CXCR7 in human rhabdomyosarcomas. *Mol. Cancer Res.* **8**, 1–14 (2010).
357. Maksym, R. B. *et al.* The role of stromal-derived factor-1--CXCR7 axis in development and cancer. *Eur. J. Pharmacol.* **625**, 31–40 (2009).
358. Gosling, J. *et al.* Cutting edge: identification of a novel chemokine receptor that binds dendritic cell- and T cell-active chemokines including ELC, SLC, and TECK. *J. Immunol.* **164**, 2851–2856 (2000).
359. Townson, J. R. & Nibbs, R. J. B. Characterization of mouse CCX-CKR, a receptor for the lymphocyte-attracting chemokines TECK/mCCL25, SLC/mCCL21 and MIP-3 beta/mCCL19: comparison to human CCX-CKR. *Eur. J. Immunol.* **32**, 1230–1241 (2002).
360. Heinzl, K., Benz, C. & Bleul, C. C. A silent chemokine receptor regulates steady-state leukocyte homing in vivo. *Proc. Natl. Acad. Sci. U.S.A.* **104**, 8421–8426 (2007).
361. Comerford, I. *et al.* The atypical chemokine receptor CCX-CKR scavenges homeostatic chemokines in circulation and tissues and suppresses Th17 responses. *Blood* **116**, 4130–4140 (2010).
362. Bunting, M. D. *et al.* CCX-CKR deficiency alters thymic stroma impairing thymocyte development and promoting autoimmunity. *Blood* **121**, 118–128 (2013).
363. Zeng, X.-H. *et al.* Coexpression of atypical chemokine binders (ACBs) in breast cancer predicts better outcomes. *Breast Cancer Res. Treat.* **125**, 715–727 (2011).
364. Comerford, I. *et al.* The atypical chemokine receptor CCX-CKR scavenges homeostatic chemokines in circulation and tissues and suppresses Th17 responses. *Blood* **116**, 4130–4140 (2010).
365. Tomura, M. *et al.* Monitoring cellular movement in vivo with photoconvertible fluorescence protein ‘Kaede’ transgenic mice. *Proc. Natl. Acad. Sci. U.S.A.* **105**, 10871–10876 (2008).
366. Johnson, L. A. & Jackson, D. G. Inflammation-induced secretion of CCL21 in lymphatic endothelium is a key regulator of integrin-mediated dendritic cell transmigration. *Int. Immunol.* **22**, 839–849 (2010).

367. Platt, A. M. *et al.* Normal dendritic cell mobilization to lymph nodes under conditions of severe lymphatic hypoplasia. *J. Immunol.* **190**, 4608–4620 (2013).
368. Ulvmar, M. H. *et al.* The atypical chemokine receptor CCRL1 shapes functional CCL21 gradients in lymph nodes. *Nat. Immunol.* (2014). doi:10.1038/ni.2889
369. Gray, E. E., Friend, S., Suzuki, K., Phan, T. G. & Cyster, J. G. Subcapsular sinus macrophage fragmentation and CD169<sup>+</sup> bleb acquisition by closely associated IL-17-committed innate-like lymphocytes. *PLoS ONE* **7**, e38258 (2012).
370. Oehen, S. *et al.* Marginal zone macrophages and immune responses against viruses. *J. Immunol.* **169**, 1453–1458 (2002).
371. Geijtenbeek, T. B. H. *et al.* Marginal zone macrophages express a murine homologue of DC-SIGN that captures blood-borne antigens in vivo. *Blood* **100**, 2908–2916 (2002).
372. Ito, S. *et al.* Roles of a macrophage receptor with collagenous structure (MARCO) in host defense and heterogeneity of splenic marginal zone macrophages. *Arch. Histol. Cytol.* **62**, 83–95 (1999).
373. Utrera-Barillas, D. *et al.* The role of macrophages and mast cells in lymphangiogenesis and angiogenesis in cervical carcinogenesis. *Exp. Mol. Pathol.* **89**, 190–196 (2010).
374. Epelman, S., Lavine, K. J. & Randolph, G. J. Origin and Functions of Tissue Macrophages. *Immunity* **41**, 21–35 (2014).
375. Delemarre, F. G., Kors, N., Kraal, G. & van Rooijen, N. Repopulation of macrophages in popliteal lymph nodes of mice after liposome-mediated depletion. *J. Leukoc. Biol.* **47**, 251–257 (1990).
376. Proost, P. *et al.* Truncation of macrophage-derived chemokine by CD26/dipeptidyl-peptidase IV beyond its predicted cleavage site affects chemotactic activity and CC chemokine receptor 4 interaction. *J Biol Chem* **274**, 3988–3993 (1999).
377. Struyf, S. *et al.* Natural truncation of RANTES abolishes signaling through the CC chemokine receptors CCR1 and CCR3, impairs its chemotactic potency and generates a CC chemokine inhibitor. *Eur. J. Immunol.* **28**, 1262–1271 (1998).
378. Yao, Y. & Tsirka, S. E. Truncation of monocyte chemoattractant protein 1 by plasmin promotes blood-brain barrier disruption. *J. Cell. Sci.* **124**, 1486–1495 (2011).
379. Denney, H., Clench, M. R. & Woodroffe, M. N. Cleavage of chemokines CCL2 and CXCL10 by matrix metalloproteinases-2 and -9: implications for chemotaxis. *Biochem. Biophys. Res. Commun.* **382**, 341–347 (2009).
380. Van den Steen, P. E., Proost, P., Wuyts, A., Van Damme, J. & Opdenakker, G. Neutrophil gelatinase B potentiates interleukin-8 tenfold by aminoterminal processing, whereas it degrades CTAP-III, PF-4, and GRO-alpha and leaves RANTES and MCP-2 intact. *Blood* **96**, 2673–2681 (2000).
381. Mortier, A. *et al.* Posttranslational modification of the NH<sub>2</sub>-terminal region of CXCL5 by proteases or peptidylarginine Deiminases (PAD) differently affects its biological activity. *J. Biol. Chem.* **285**, 29750–29759 (2010).

382. Richter, R. *et al.* Significance of N-terminal proteolysis of CCL14a to activity on the chemokine receptors CCR1 and CCR5 and the human cytomegalovirus-encoded chemokine receptor US28. *J. Immunol.* **183**, 1229–1237 (2009).
383. Schumann, K. *et al.* Immobilized chemokine fields and soluble chemokine gradients cooperatively shape migration patterns of dendritic cells. *Immunity* **32**, 703–713 (2010).
384. Kampen, G. T. *et al.* Eotaxin induces degranulation and chemotaxis of eosinophils through the activation of ERK2 and p38 mitogen-activated protein kinases. *Blood* **95**, 1911–1917 (2000).
385. Fujisawa, T. *et al.* Chemokines induce eosinophil degranulation through CCR-3. *J. Allergy Clin. Immunol.* **106**, 507–513 (2000).
386. King, I. L., Kroenke, M. A. & Segal, B. M. GM-CSF-dependent, CD103<sup>+</sup> dermal dendritic cells play a critical role in Th effector cell differentiation after subcutaneous immunization. *J. Exp. Med.* **207**, 953–961 (2010).
387. Wendland, M. *et al.* Lymph node T cell homeostasis relies on steady state homing of dendritic cells. *Immunity* **35**, 945–957 (2011).
388. Stanley, P. L., Steiner, S., Havens, M. & Tramposch, K. M. Mouse skin inflammation induced by multiple topical applications of 12-O-tetradecanoylphorbol-13-acetate. *Skin Pharmacol.* **4**, 262–271 (1991).
389. Hitzler, M. *et al.* Human Langerhans cells control Th cells via programmed death-ligand 1 in response to bacterial stimuli and nickel-induced contact allergy. *PLoS ONE* **7**, e46776 (2012).
390. Wang, L. *et al.* Langerin expressing cells promote skin immune responses under defined conditions. *J. Immunol.* **180**, 4722–4727 (2008).
391. Said, A., Bock, S., Müller, G. & Weindl, G. Inflammatory conditions distinctively alter immunological functions of Langerhans-like cells and dendritic cells in vitro. *Immunology* (2014). doi:10.1111/imm.12363
392. Epaulard, O. *et al.* Macrophage- and Neutrophil-Derived TNF- $\alpha$  Instructs Skin Langerhans Cells To Prime Antiviral Immune Responses. *J. Immunol.* **193**, 2416–2426 (2014).
393. Nasr, N. *et al.* Inhibition of Two Temporal Phases of HIV-1 Transfer from Primary Langerhans Cells to T Cells: The Role of Langerin. *J. Immunol.* **193**, 2554–2564 (2014).
394. Liard, C. *et al.* Intradermal immunization triggers epidermal Langerhans cell mobilization required for CD8 T-cell immune responses. *J. Invest. Dermatol.* **132**, 615–625 (2012).
395. Cunningham, A. L., Abendroth, A., Jones, C., Nasr, N. & Turville, S. Viruses and Langerhans cells. *Immunol. Cell Biol.* **88**, 416–423 (2010).
396. Kanzler, I. *et al.* Differential roles of angiogenic chemokines in endothelial progenitor cell-induced angiogenesis. *Basic Res. Cardiol.* **108**, 310 (2013).
397. Han, E. C., Lee, J., Ryu, S.-W. & Choi, C. Tumor-conditioned Gr-1(+)CD11b(+) myeloid cells induce angiogenesis through the synergistic action of CCL2 and CXCL16 in vitro. *Biochem. Biophys. Res. Commun.* **443**, 1218–1225 (2014).
398. Zhao, B. *et al.* The chemotactic interaction between CCL21 and its receptor, CCR7, facilitates the progression of pancreatic cancer via induction of angiogenesis and lymphangiogenesis. *J Hepatobiliary*

- Pancreat Sci* (2011). doi:10.1007/s00534-011-0395-4
399. Nagy, T. A., Moreland, S. M., Andrews-Polymenis, H. & Detweiler, C. S. The Ferric Enterobactin Transporter Fep Is Required for Persistent *Salmonella enterica* Serovar Typhimurium Infection. *Infect. Immun.* **81**, 4063–4070 (2013).
  400. McQuibban, G. A. *et al.* Matrix metalloproteinase activity inactivates the CXC chemokine stromal cell-derived factor-1. *J Biol Chem* **276**, 43503–43508 (2001).
  401. Mortier, A. *et al.* Biological activity of CXCL8 forms generated by alternative cleavage of the signal peptide or by aminopeptidase-mediated truncation. *PLoS ONE* **6**, e23913 (2011).
  402. Bar-On, L. & Jung, S. Defining in vivo dendritic cell functions using CD11c-DTR transgenic mice. *Methods Mol. Biol.* **595**, 429–442 (2010).
  403. Probst, H. C. *et al.* Histological analysis of CD11c-DTR/GFP mice after in vivo depletion of dendritic cells. *Clin. Exp. Immunol.* **141**, 398–404 (2005).
  404. Hochweller, K., Striegler, J., Hämmerling, G. J. & Garbi, N. A novel CD11c.DTR transgenic mouse for depletion of dendritic cells reveals their requirement for homeostatic proliferation of natural killer cells. *Eur. J. Immunol.* **38**, 2776–2783 (2008).
  405. Bennett, C. L. & Clausen, B. E. DC ablation in mice: promises, pitfalls, and challenges. *Trends Immunol.* **28**, 525–531 (2007).